An Electrochemical and Catalytic Investigation of Catalysis by Gold

by

Patrick L. Jenkins

Ph.D. Thesis

Department of Chemistry

Cardiff University

September 2005

ProQuest LLC
789 East Eisenhower Parkway
P.O. Box 1346
Ann Arbor, MI 48106-1346

Abstract

The performance of gold/graphite as an oxidation catalyst has been investigated in an electrochemical cell (electrooxidation at ambient temperature and pressure) and in a high pressure reactor (conventional catalytic oxidation typically at 3 bar and 333 K).

A range of gold/graphite catalysts having various metal loadings were prepared and characterised by cyclic voltammetry (CV), X-ray photoelectron spectroscopy (XPS), and transmission electron microscopy (TEM). The technique of lead underpotential deposition (Pb_{UPD}) was used to reveal the presence of {111}, {100}, and {110} facets in the surfaces of the gold microcrystals.

Oxidation of 1-propanol to propionic acid, of 2-propanol to acetone, and of glycerol to wide range of products was investigated both in electrooxidation and in conventional catalytic oxidation.

Variation of the surface morphology of the gold active phase was achieved by (i) thermal annealing and sintering of the catalysts under air and under hydrogen, (ii) deposition of bismuth onto the gold surface, and (iii) preparation of further catalysts in which Au was deposited onto Pt/graphite.

Conventional catalytic oxidation of the 1-propanol, 2-propanol, and glycerol over the full range of gold-containing catalysts is reported. Variations in catalyst structure were accompanied by changes in activity and selectivity, indicating that these reactions were indeed structure sensitive. However, few correlations of these experimental outcomes with the surface states identified by the voltammetric techniques were evident.

Acknowledgments

I would like to thank my supervisors, Prof. Gary Attard, Prof. Peter Wells and Prof. Graham Hutchings for their continuous support and guidance over the course of this work. In addition I would like to thank Laura Prati for providing me with the catalysts used in section 3.4 and contributing to the glycerol oxidation study.

I would also like to thank my parents, David and Mary, who have supported me throughout the course of this research.

Finally I thank the EPSRC and Johnson Matthey for funding this research.

Contents

Chapter One

Introduction

1.1 A Brief History of Catalysis

1.1.1 Definition of catalysis

Early in human history, it was recognised that the rate of fermentation could be considerably enhanced by the addition of yeast [1]. This process of rate enhancement has become known as *catalysis*. One of the earliest industrial scale *homogeneous catalytic* reactions for the production of sulphuric acid (the Bell process) was well underway in the 1740s [2]. Further recognition of catalytic phenomenon came in 1814 in the context of the hydrolysis of starch, when Kirchhoff noted that acids enabled the process. In 1817 Humphry Davy observed that a hot platinum wire would glow when in contact with coal gas and air, the platinum remaining unchanged. This discovery led to the invention of the Davy safety lamp [2]. Oxidation catalysts dominated in this early era of catalysis and probably the earliest catalytic oxidation was carried out in 1820 when Davy used platinum to catalyse the oxidation of ethanol to acetic acid [3].

Even though there was much interest in these new reactions, their true importance went unappreciated until the early nineteenth century when Berzeluis published a paper concerning the decomposition of hydrogen peroxide. The words "catalytic" and "catalysis" were used for the first time by him in 1836:

> *"The substances that cause the decomposition of H_2O_2 do not achieve this goal by being incorporated into the new compounds (H_2O and O_2); in each case they remain unchanged and hence act by means of an inherent force whose nature is still unknown... So long as the nature of the new force remains hidden, it will help our researches and discussions about it if we have a special name for it. I hence will name it the catalytic force of the substances, and I will name decomposition by this force catalysis. The catalytic force is reflected in the capacity that some substances have, by their mere presence and not by their own reactivity, to awaken activities that are slumbering in molecules at a given temperature." [4]*

This is the earliest definition of catalysis and included the idea that a catalyst could aid a reaction but was overall unaffected by the reaction that it aided. Since this early

definition was proposed, a more detailed account of catalysis has been developed. A catalyst is now defined as a substance that increases the rate at which a reaction approaches equilibrium without itself being consumed in the process [5].

Figure 1.1 shows the reaction profile for both a catalysed and un-catalysed reaction. For reaction to occur, it is necessary for the reactants to collide with sufficient kinetic energy (and in the correct orientation) to overcome the activation barrier (E_a) of the reaction. The introduction of a catalyst to the system provides a faster "route" to product formation and hence an alternative mechanism for the reaction to follow. This results in a lower activation barrier.

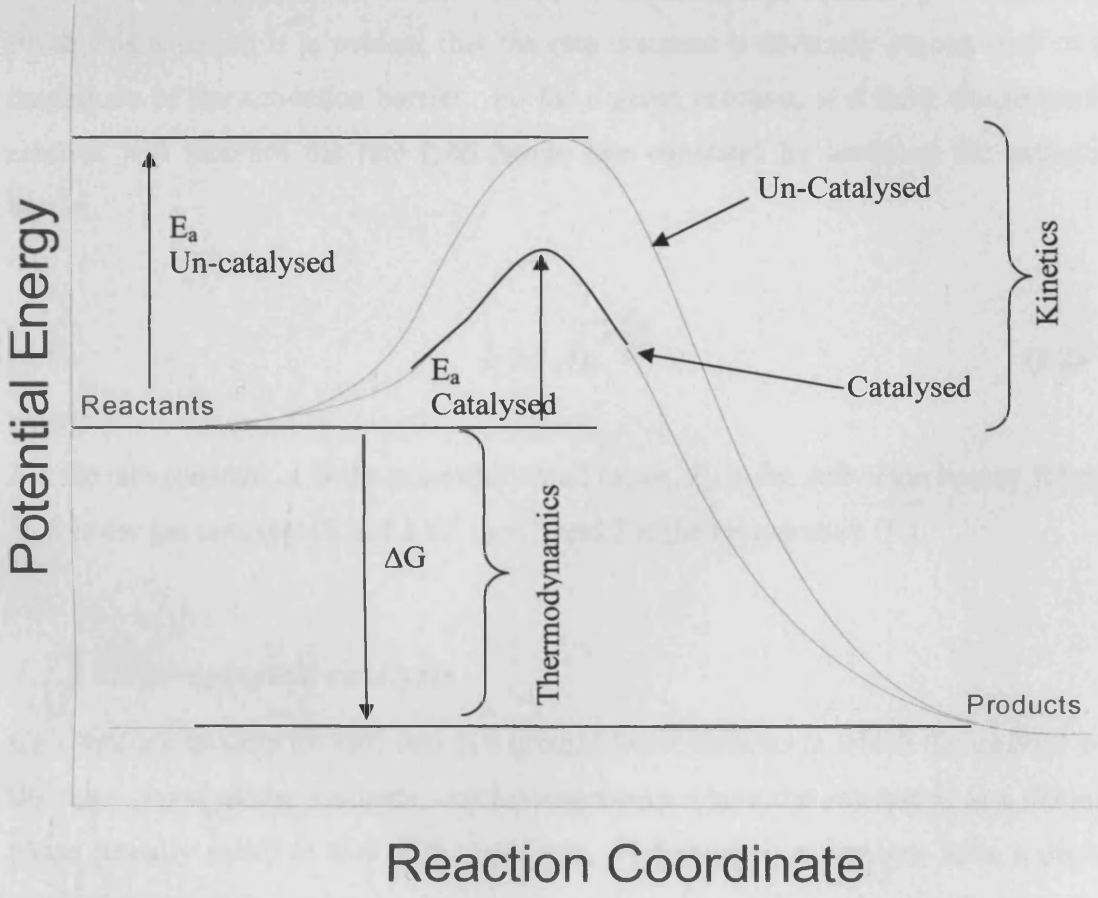

Figure 1.1: A reaction profile showing the effect of a catalyst on the activation barrier of a chemical reaction. The free energy change (ΔG) associated with the reaction is to be contrasted with the role of the activation barrier in determining kinetics.

As stated above, one of the predominant features of a catalyst is its ability to increase the rate of reaction. Shown below is a simple rate equation for the reaction of two

species. This equation shows that the rate of reaction is directly proportional to the rate constant and so an increased rate corresponds to a larger rate constant for a given reaction.

$$rate = k[A]^x[B]^y \tag{1.1}$$

where:

rate is the rate of reaction (mol l^{-1} s^{-1}), k is the rate constant, $[A]$ is the concentration of species A (mol l^{-1}), x is the order of reaction with respect to A, $[B]$ is the concentration of species B (mol l^{-1}) and y is the order of reaction with respect to B.

The rate constant, k, can be further defined by the Arrhenius equation presented below. From this equation it is evident that the rate constant is inversely proportional to the magnitude of the activation barrier. So for a given reaction, at a fixed temperature, a catalyst will increase the rate (and hence rate constant) by lowering the activation barrier.

$$k = Ae^{-\frac{E_a}{RT}} \tag{1.2}$$

where:

k is the rate constant, A is the pre-exponential factor, E_a is the activation barrier (kJ mol^{-1}), R is the gas constant (8.314 J K^{-1} mol^{-1}) and T is the temperature (K).

1.1.2 Heterogeneous catalysis

Catalysts are broadly divided into two groups; homogeneous in which the catalyst is in the same phase as the reactants, and heterogeneous where the catalyst is in a different phase (usually solid) to that of the reactants. Heterogeneous catalysts have a distinct advantage when it comes to large industrial scale catalysis due to their ease of separation from the reaction mixture.

All heterogeneous catalytic reactions follow the same basic steps. Firstly one or more species is adsorbed on to the surface of the catalyst. This may be followed by movement of the species across the surface of the catalyst. Next, reaction will occur

between different adsorbed species or between adsorbed species and reactants in the gas/liquid phase. Finally, the adsorbed products are released from the surface of the catalyst and the cycle can begin again.

When only one reactant is present in a catalytic reaction it has to become adsorbed onto the surface of the catalyst for reaction to occur. When two or more reactants are involved in the reaction, two different mechanisms become possible [6]. The Langmuir-Hinshelwood mechanism is one in which all reactants adsorb onto the surface of the catalyst and hence the reaction takes place solely on the catalyst surface. The Rideal-Eley mechanism assumes a mixed state where at least one of the reactants is adsorbed onto the catalyst surface, but other reactants interact with the adsorbed species from the gas/liquid phase. These differences are depicted schematically in figure 1.2.

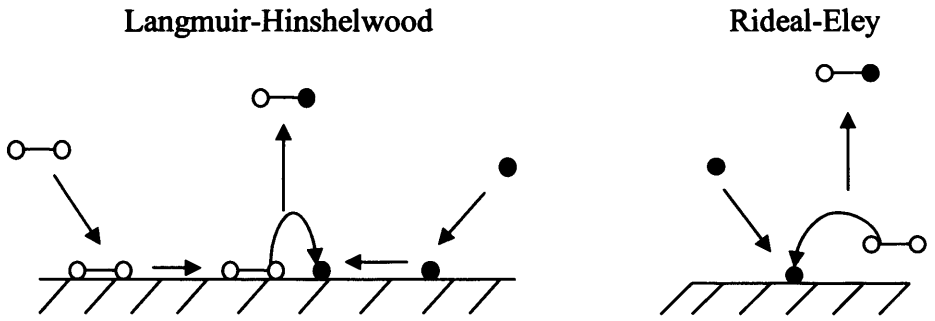

Figure 1.2: Representation of the heterogeneous catalytic reaction of a diatomic and monatomic species following the Langmuir-Hinshelwood and Rideal-Eley mechanisms respectively.

A good heterogeneous catalyst normally contains metal in a high state of division which is often supported on an inert support, such as alumina [7-9] or graphite [10-12]. The small particle size dramatically increases the available surface area of the active metal and so the surface to bulk ratio is increased dramatically. This can contribute to small particles (<2 nm) having a different chemical response to large particles (>4 nm) [13]. This behaviour may be explained by a decrease in the overlap of electron orbitals due to the decreased number of bonds between atoms in smaller particles. This results in a weakening of the band structure and hence the chemical properties of the surface atoms alter [14].

The nature of the adsorbed state is important and two distinct types of adsorption are possible, physisorption and chemisorption. There are two main differences between these processes - the strength of the adsorption and the mechanism by which it operates. These differences between the adsorbed states are outlined diagrammatically in figure 1.3 which is based on the Lennard-Jones style potential energy diagrams for the dissociation of a diatomic molecule [15]. Physisorption of the molecule from the gas phase is represented as a shallow minimum, a short distance away from the metal surface. On progressing closer to the surface, chemisorption may occur and is represented by a much deeper potential energy minimum situated at the metal-adsorbate equilibrium bond distance. The relative depth of the potential energy well in both cases illustrates the much stronger interactions of the molecule in its chemisorbed state.

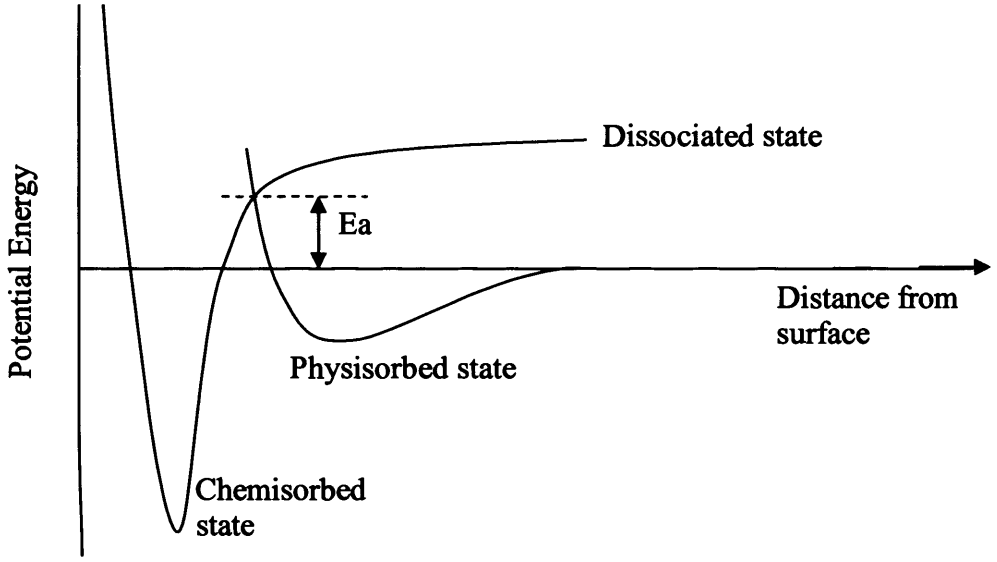

Figure 1.3: Lennard-Jones potential energy diagram for the physisorption and chemisorption of a diatomic species on to a surface.

Physisorption is a weak process exhibiting enthalpies of adsorption in the range of 10 - 40 kJ mol^{-1} and as such is commonly associated with long range van der Waals-type interactions. The distance between the surface and the physisorbed species is roughly equal to the sum of the covalent radii of the surface atoms and the physisorbed species, plus the van der Waals envelopes (0.3 – 0.4 nm) [16]. Bonding is characterised by changes in the electron charge density at both the surface and molecule giving rise to electrostatic interaction or induced dipoles depending on the system [17].

Chemisorption on the other hand tends to exhibit adsorption enthalpies in the range of 80 - 400 kJ mol^{-1} and is associated with the breaking and forming of chemical bonds. The distance between the surface and the chemisorbed species is smaller than that seen for physisorption due to the formation of chemical bonds (and hence overlap of electron orbitals) between the species (typical bond lengths are 0.15 – 0.3 nm) [16]. E_a is the activation barrier for chemisorption of the species on to the metal surface and its magnitude will depend upon the system under investigation (see figure 1.3).

When species are chemisorbed onto a surface they can undergo two forms of adsorption, associative adsorption or dissociative adsorption [18], as shown in figure 1.4. Associative adsorption is where the molecule adsorbs without fragmentation onto the surface (i.e. the species forms bonds with the surface without internal bonds being ruptured) whereas dissociative adsorption occurs when the adsorbed species dissociates on the surface into smaller adsorbed fragments. This is generally the more common scenario [19]. However the type of adsorption that occurs will depend on the surface used and the molecule being adsorbed, as well as the conditions under which the adsorption takes place. As such the mechanism of adsorption will vary from surface to surface.

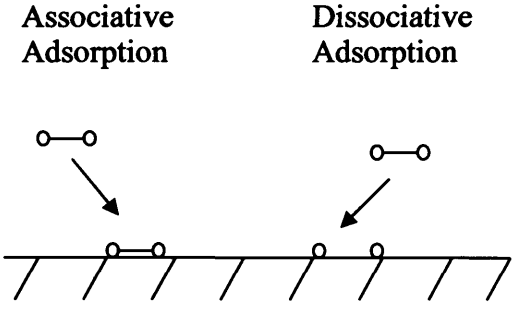

Figure 1.4: Associative and dissociative adsorption of a diatomic molecule onto a surface.

1.1.3 Types of catalyst

Table 1.1 shows some of the reactions that are promoted via heterogeneous catalysts. This is by no means a complete list, but does indicate the wide variety of reactions and catalysts that are available for study. As stated earlier, catalysts are broadly divided into two groups, homogeneous and heterogeneous. Heterogeneous catalysts can be further

sub-divided into smaller groups and some of the main groups of interest are briefly discussed.

Table 1.1: A selection of heterogeneous industrial processes showing the reaction and the catalyst used, reproduced from [20].

Process	Reaction	Catalyst
Steam reforming	$CH_4 + H_2O \rightarrow CO + 3H_2$	Ni/Al_2O_3
Methanol synthesis	$CO + 2H_2 \rightarrow CH_3OH$	$Cu/ZnO/Al_2O_3$
Fischer Tropsch	$nCO + 2nH_2 \rightarrow C_nH_{2n} + nH_2O$	Alkali-promoted Fe
Low temperature water gas shift	$CO + H_2O \rightarrow CO_2 + H_2$	Ni/Al_2O_3
Haber process	$N_2 + 3H_2 \rightarrow 2NH_3$	K-promoted Fe
Ammonia oxidation	$4NH_3 + 5O_2 \rightarrow 4NO + 6H_2O$	Pt-Rh gauze
Hydrodesulfurisation	$C_4H_4S + 2H_2 \rightarrow C_4H_6 + H_2S$	Co- or Ni-promoted MoS_2/Al_2O_3 or WS_2/Al_2O_3
Hydrodenitrogenation	$C_5H_5N + 5H_2 \rightarrow C_5H_{12} + NH_3$	As above
Hydrodemetallation	Ni-porphyrin $+nH_2 \rightarrow Ni\downarrow$ + hydrocarbons	As above
Alkane cracking	$C_nH_{2n} + H^+_{(ads)} \rightarrow [C_nH_{2n+1}]_{(ads)}$ $[C_nH_{2n+1}]_{(ads)} \rightarrow [C_{n-2}H_{2n-3}]_{(ads)} + C_2H_{4(g)}$	Type Y faujasitc
Reforming	$2C_6H_{14} \rightarrow C_6H_6 + C_6H_{12} + 5H_2$	Rh-promoted Pt supported on Cl-promoted Al_2O_3
Oxidative dehydrogenation	$C_2H_5CH{=}CH_2 + \frac{1}{2} O_2 \rightarrow CH_2{=}CHCH{=}CH_2 + H_2O$	Fe_2O_3; Cr_2O_3; $BiPO_4$
Oxidation	$CH_3CH{=}CH_2 + \frac{1}{2} O_2 \rightarrow CH_2{=}CHCHO$	Bismuth molybdate
Ethene Oxidation (epoxidation)	$C_2H_4 + \frac{1}{2} O_2 \rightarrow C_2H_4O$	(Cs + Cl)-promoted Ag/α-Al_2O_3
Claus reaction	$H_2S + \frac{1}{2} O_2 \rightarrow S\downarrow + H_2O$	Al_2O_3 unrefined $Al(OH)_3$
Enantioselective hydrogenation	$CH_3COCOOC_2H_5 + H_2 \rightarrow CH_3C^*H(OH)COOC_2H_5$	Chichona/Pt/Al_2O_3

1.1.3.1 Catalysis by metals

Metal catalysts are characterised by their adsorption processes which involve physisorption and chemisorption, as described above. Metal catalysts are used extensively in industry and a good example of this is in the Haber process used to manufacture ammonia from nitrogen and hydrogen [21, 22]. The ideal conditions for the process involve high pressures and low temperatures. Industrially however, a relatively low pressure of 150 - 350 bar has been used as the beneficial effects of higher pressure (i.e. driving the equilibrium towards ammonia formation) are countered by cost factors. Thermodynamically low temperatures are beneficial to the reaction, however a high temperature (~700 K) is used to overcome kinetic limitations [18].

To obtain the best results from the process, a careful choice of catalyst was needed. Originally an osmium catalyst was used for the process, but this was replaced by an iron catalyst promoted with several other components (such as metal oxides). Even though un-promoted iron was not the best catalyst found for the process [18] it was one of the cheapest and safest to use.

Scheme 1.1 shows the established mechanism for the production of ammonia over an iron catalyst. It is a typical mechanism for a metal catalyst and illustrates the dissociative chemisorption of hydrogen and the associative/dissociative adsorption of nitrogen on to the catalytic surface. The $N_{2(ads)(\gamma)}$ has been identified as a physisorbed state and the $N_{2(ads)(\alpha)}$ has been identified as a precursor state to the dissociation of N_2 [23]. Once the constituent atoms have been formed they are able to interact with each other forming new bonds and giving rise to adsorbed ammonia. This is then released from the surface as the final product.

$$H_2 \leftrightarrow 2H_{(ads)}$$

$$N_2 \leftrightarrow N_{2(ads)(\gamma)} \leftrightarrow N_{2(ads)(\alpha)} \leftrightarrow 2N_{(ads)}$$

$$N_{(ads)} + H_{(ads)} \leftrightarrow NH_{(ads)}$$

$$NH_{(ads)} + H_{(ads)} \leftrightarrow NH_{2(ads)}$$

$$NH_{2(ads)} + H_{(ads)} \leftrightarrow NH_{3(ads)} \leftrightarrow NH_3$$

Scheme 1.1: Mechanism for the formation of ammonia from nitrogen and hydrogen over an iron catalyst, reproduced from [18].

1.1.3.2 Catalysis by oxides

Oxide catalysts behave differently from metal catalysts in a number of ways. First, adsorbed species tend to undergo heterolytic splitting as a result of the ionic nature of the catalyst [24-26]. Adsorption often takes place in defects where the metal ion coordination is unsatisfied which generally results in a higher reactivity. Second, oxidations on oxide catalysts can be characterised by their consumption of oxygen from the surface of the catalyst during reaction, which is then replaced by dissociative adsorption of oxygen from the gas phase (commonly known as the Mars-van-Krevelen mechanism, shown in figure 1.5 [27]). Third, for transition metal oxides, the metal may be in one of a number of different oxidation states (i.e. FeO, Fe_3O_4 and Fe_2O_3 [28-30]) and this can be used to tailor the catalytic properties to the system of interest.

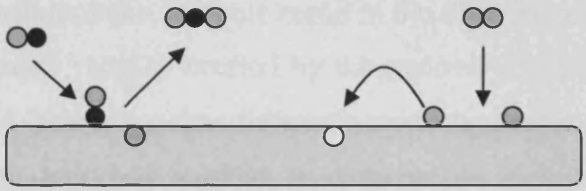

Figure 1.5: The Mars-van-Krevelen mechanism - adsorption and reaction of a diatomic molecule followed by the replacement of extracted oxygen from the gas phase.

Zeolites are crystalline alumino-silicates, alumino-phosphates or silico-alumino-phosphates. They are a group of oxide catalysts of particular interest due to their uniform pore size, high surface area and ability to be size-selective. The size-selectivity can be introduced by changes in the size of the zeolite cage [31], shown in figure 1.6. Zeolites are used in a wide range of situations as molecular sieves [32] and drying agents [33] as well as in catalysis [34-36].

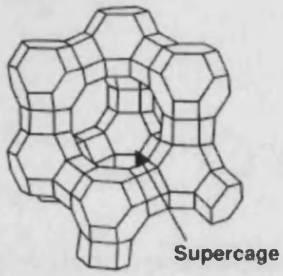

Figure 1.6: Representation of a faujasite zeolite, reproduced from [37].

1.1.3.3 Catalysis by sulphides

Sulphur has long been known to act as a poison to active catalysts such as platinum [38] and in the Fischer-Tropsch reaction [39, 40]. However sulphur has also been used as a catalyst component in various reactions. Sulphide catalysts are generally used for hydrodesulphurization and hydrodenitrogenation reactions [41-43].

Scheme 1.2 shows the proposed mechanism for hydrodesulphurization of dibenzothiophene over a sulphided TiO_2 catalyst. The catalyst was placed under a hydrogen atmosphere which resulted in hydrogen adsorbing on to the surface. This in turn led to the removal of some sulphur as H_2S. Left behind were anion vacancies that could be used to adsorb species. Two possible pathways were proposed for the adsorption of dibenzothiophene, but both result in the adsorption of the sulphur from the adsorbate into the anion vacancy created by the removal of H_2S. Cleavage of the CS bond then occurred releasing the different products produced by the respective mechanisms and the adsorbed sulphur is removed as H_2S regenerating the anion vacancy [44]:

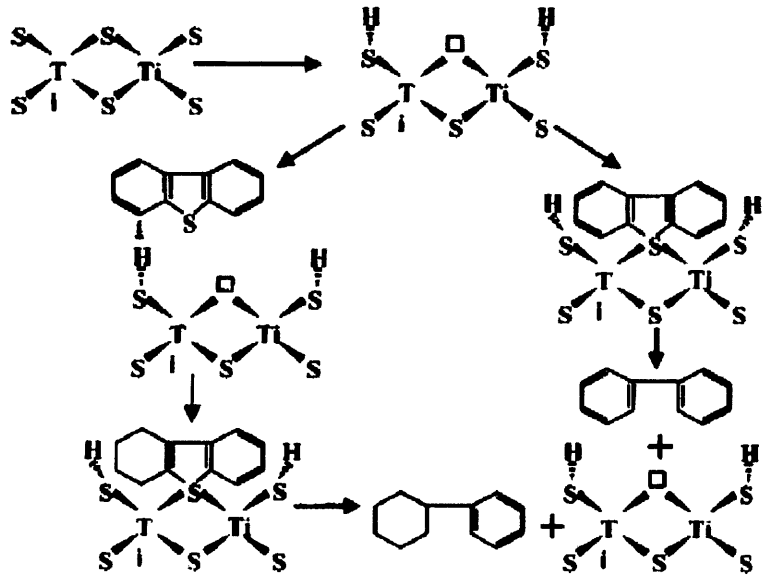

Scheme 1.2: Hydrodesulphurization mechanism on a TiO_2 catalyst, reproduced from [44].

1.1.3.4 Catalysis by supported enzymes

Enzymes are Nature's catalysts and are generally superior to heterogeneous catalysts in terms of selectivity [45]. They are large, complex proteins molecules, as illustrated by figure 1.7. However, only a small part of the molecule actually acts as a catalyst. This is referred to as the active site and often takes the form of a fissure that is highly shape-selective. If a species is to undergo reaction, then it must exactly match the shape of this active site, as illustrated in figure 1.8.

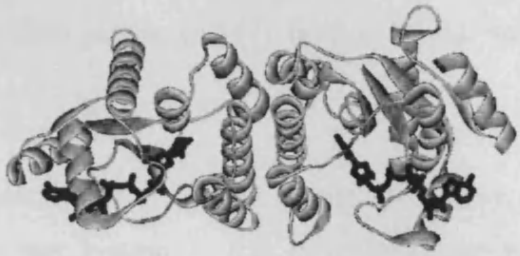

Figure 1.7: Modelled dimeric structure of thymidine monophosphate kinase, reproduced from [46].

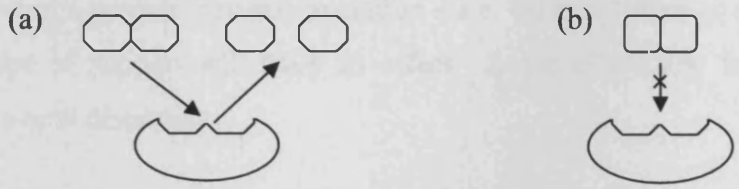

Figure 1.8: (a) Successful interaction and subsequent dissociation of a molecule on an active site and (b) no reaction occurring between an active site and a species of the wrong shape.

A heterogeneous aspect may be introduced by immobilizing an enzyme onto a support. This approach was first used in the 1920s by Nelson and Griffin [6]. Since then, supported enzyme catalysts have been used in a number of industrial-scale systems (e.g. optical resolution of α-amino acids, glucose isomerisation and steroid conversions [6]). However a drawback to enzyme catalysis is that enzymes are far more sensitive to reaction conditions than traditional heterogeneous catalysts. Heating can destroy an enzyme catalyst by breaking the weak bonds that hold the active site in its correct configuration [45]. Altering the pH can also have a detrimental effect on the catalyst. For example, decreasing the pH can result in carboxylate groups being converted to carboxylic acid groups [45]. Such changes in enzyme structure may result in the adsorbate no longer being 'recognised' by the enzyme.

1.1.4 Factors influencing the behaviour of a heterogeneous catalyst

The performance of a catalyst is defined by its activity and selectivity. In heterogeneous catalysis, activity can be defined as the ability of the catalyst to convert reactants to products [18]. In other words, it is a measure of the rate at which equilibrium is obtained under particular reaction conditions [16]. Selectivity can be defined as the ability of the catalyst to produce one product when multiple products are possible [18]. More precisely, the catalyst is able to follow one of a number of thermodynamically possible pathways [47] leading to the selective production of a product.

The performance of a catalyst will depend on the system that it is applied to and the conditions used within that system. But in addition, the performance (and hence activity and selectivity) will be dependent upon a number of different preparation parameters. For the catalyst, the most important features include the metal used, its loading, average particle size and oxidation state. Also, whether or not a support is used and the type of support will have an effect. Some of the key features that affect a catalyst are now discussed.

Compared with an unsupported catalyst, a supported catalyst will contain smaller, more dispersed particles resulting in a higher surface area. This, among other things, can lead to changes in the supported catalyst's properties (activity/selectivity) when compared with the unsupported equivalent. For example the partial oxidation of methane over $FePO_4$ and $FePO_4/SiO_2$ showed that the unsupported catalyst exhibited selectivity to formaldehyde, whereas the supported catalyst exhibited selectivity to both formaldehyde and methanol [48]. In addition the support can help to prevent sintering of the catalyst which would lead to its deactivation [1]. It has been suggested that the support may influence the catalytic properties of a metal or that metal particles may become active at the junction between them and the support. In the case of Pd/AlF_3 catalysts, used for the conversion of dichlorodifluoromethane, it was suggested that the support protected the metal from diffusion of fluorine into the bulk [49].

The more common methods for the preparation of supported metal catalysts are *(i) impregnation, (ii) incipient wetness, (iii) co-precipitation* and *(iv) deposition* [1, 16, 18].

(i) *Impregnation* occurs when the support is soaked in a solution of the metal salt. After the salt has been deposited onto the support, the material is dried and the salt calcined and reduced under hydrogen to form the metal.

(ii) *Incipient wetness* occurs when the metal salt solution is added to the dry support until the mixture becomes 'tacky' indicating that the pores of the support have become filled with the solution. The catalyst is then dried and calcined as necessary.

(iii) *Co-precipitation* occurs when the metal salt is placed in solution with another substance (the support precursor) and the catalyst forced out of solution by use of a precipitating agent such as sodium carbonate. This intimate mixture can then by dried and calcined as in the previous methods.

(iv) *Deposition* occurs when the metal is directly deposited onto the support in suspension. As before, the catalyst is dried, calcined and reduced as necessary.

The preparation method selected and small changes in the methodology used (such as pH, calcining temperature and reduction agent etc) can have large effects on the resultant activity and selectivity of the catalyst. An example of this selectivity by preparation methods is found in methane partial oxidation over supported platinum based catalysts prepared by precipitation and impregnation [50]. Here the catalysts prepared by the impregnation method showed significantly greater activity, greater CO / H_2 selectivity and longer life.

It is possible to alter a catalyst's activity/selectivity or extend its life by the addition of a promoter. There are several mechanisms by which the promoter may improve the catalyst. It may act by blocking sites within the catalyst and in so doing prevent the formation of poisons by secondary pathways, such as in the case of cinnamyl alcohol oxidation over supported platinum catalysts promoted by bismuth [51]. The promoter may increase the lifetime of the catalyst by preventing sintering from occurring, as has been seen for La promoted Ni/Al_2O_3 catalysts [52]. Alternatively the promoter may affect the electronic properties of the metal surface as has been suggested to occur for

alkali promoted platinum catalysts [53]. The promoter may also be directly involved in the reaction as has been seen for tartronic acid oxidation over bismuth-promoted platinum catalysts [54]. It has been proposed that a complex is formed between the bismuth promoter and the tartronic acid during reaction and this leads to preferential oxidation on the surrounding platinum surface.

An alloy can sometimes exhibit greater active or selective for a given reaction than an individual metal. Sinfelt investigated copper-nickel alloys in the 1970s and found that the activity for cyclohexane dehydrogenation on the alloys was greater than that seen on either of the two pure metals [55]. These changes in properties may be ascribed to changes in the electronic structure of the metals within the alloy, as has been observed for Ag-Pd and Cu-Ni alloys [56]. So in some cases it is possible to improve a catalyst by alloying it with another metal, however care must be taken in choosing metals of similar atomic size and bond energy to prevent segregation of the alloy into the individual elements [1].

As well as improving a catalyst by the addition of other materials, it is also possible for species to deactivate them. A poison is any species that reduces the activity or life of a catalyst. A wide-range of chemical species such as Cl, S, O or π-bonded molecules such as CO (as has been seen for methanol oxidation [57]) may be included in this category. Poisons are introduced as unwanted by-products or by impurities in the system. They prevent the catalyst from functioning by chemisorbing onto the surface of the catalyst and blocking its active sites, such as with the poisoning of Pt by SO_2 [58]. As well as geometric blocking, poisons can also reduce activity by altering the electronic structure of the metal, such as observed in fundamental surface science studies of CO poisoning on Pd{210} [59]. However species that are selective poisons can also become catalytic promoters in some instances. This is true in the case of sulphur (which is often regarded as a severe poison) for the hydrogenation of but-2-enal, where the controlled addition of sulphur to a silver catalyst significantly improved its activity and selectivity [60].

As well as poisoning, a catalyst can be deactivated in a number of other ways [61, 62]. Some of the more common methods include sintering, leaching and coking which will

all reduce the active lifetime of a catalyst. Sintering occurs when a catalyst is heated, causing small particles to agglomerate and form larger particles with a smaller surface area and hence fewer active sites. Leaching is the loss of the metal from the surface of the catalyst into solution which again results in a loss of active sites. Coking is a process whereby hydrocarbons form carbonaceous species which act to cover the catalyst's active sites either by physical blocking (in a porous catalyst) or by chemisorption.

1.2 Characterisation of metal catalysts

1.2.1 Introduction

At an atomic level metal catalysts exhibit a heterogeneous structure and the properties of the catalyst as a whole will depend upon the nature of this structure. So to fully characterise a metal catalyst, it is necessary to understand its surface structure. To minimise free energy, atoms in a metal take on an ordered structure which can be represented by a unit cell. There are three common unit cell types - face centred cubic (FCC), body centred cubic (BCC) and hexagonal close packed (HCP) [47, 63, 64] which are illustrated in figure 1.9. Gold, platinum and palladium all exhibit FCC packing (which has a packing efficiency of 74% - the highest possible) under normal conditions. Since these three metals are of importance in the work reported in this thesis, attention is focused on the FCC unit cell in the following discussion.

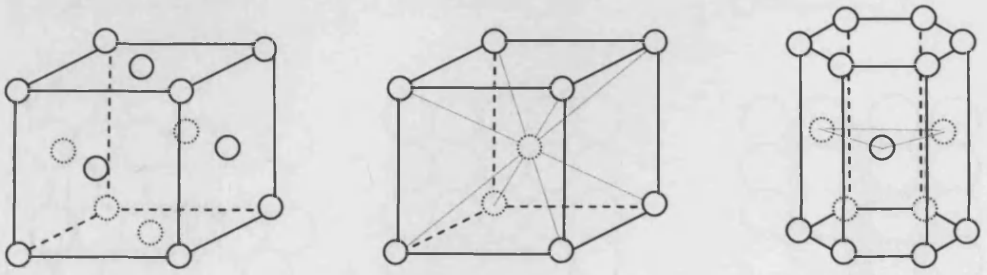

Figure 1.9: The three common metal unit cells - face centred cubic (FCC), body centred cubic (BCC) and hexagonal close packed (HCP).

The unit cell may be repeated along specific directions to generate a bulk metal crystal. Since catalyst particles consist of small metal crystals, it is important to understand and

be able to characterise the surface arrangement of atoms at the surface of such crystals. The distribution and types of individual surface sites will ultimately govern the overall catalysis exhibited by the system.

By cutting through the unit cell in different directions and positions, different crystal planes are exposed. So it is possible to define the surface structure of a metal by reference to the bulk and the position of the cut through it. The surfaces resulting from these cuts are identified by their Miller indices [63, 65]. Figure 1.10 shows three cuts through the FCC unit cell, the resultant planes exposed and the Miller indices for each plane. The Miller indices are assigned in the following way. The intercepts of the cut (shown as the grey area) with the axes of the base vectors $\bar{a}$, $\bar{b}$, $\bar{c}$ (which define the unit cell) are determined. Then the distances between the origin and the intercepts are defined as a, b, c respectively. From this, the Miller indices h, k, l are defined as $h = \bar{a}/a$, $k = \bar{b}/b$ and $l = \bar{c}/c$. So the notation used to define the crystal surface is {hkl} [5]. In the case of the {100} plain, it is so labelled because the cut crosses the $\bar{a}$ vector at a distance of one unit cell length from the origin, but the $\bar{b}$, $\bar{c}$ axes are never crossed. So from the above equations, $h = 1$, $k = 0$ and $l = 0$ or {100}.

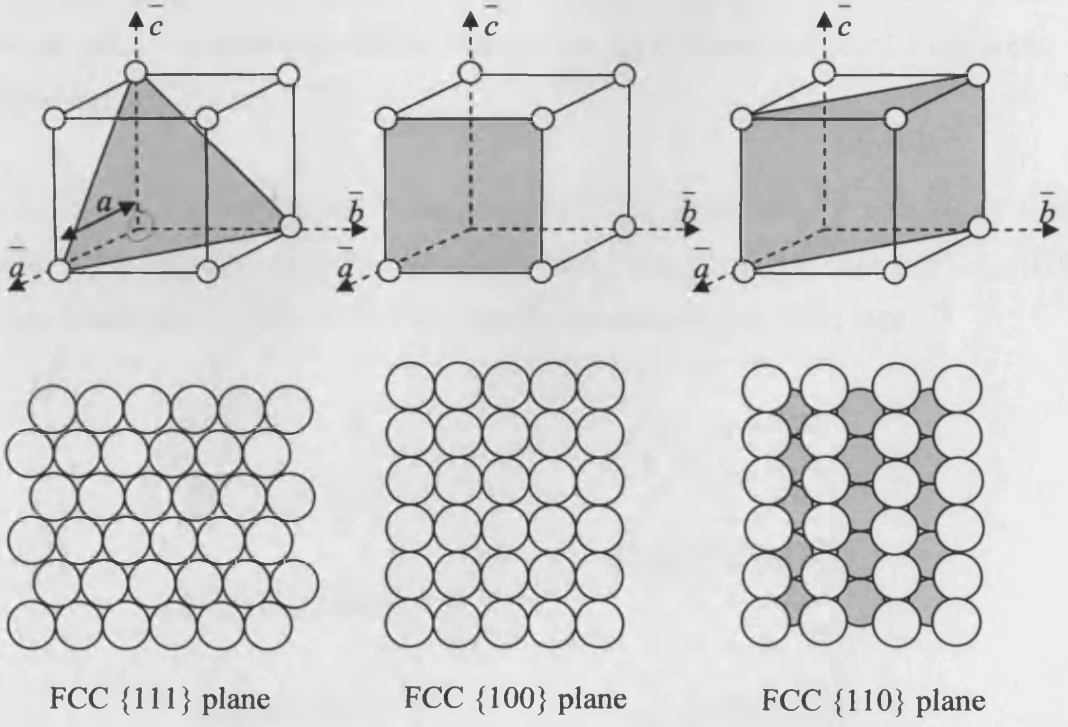

Figure 1.10: Three cuts through the FCC unit cell, the corresponding surfaces produced and the Miller indices for each plane.

If the calculation of *h*, *k* or *l* results in fractional values, then these are multiplied by a common factor to give the smallest integers. For example {1/4, 1/2, 4} would become {1, 2, 16} since the common multiple is four. If the intercept is negative then a bar is placed above the value to indicate this (e.g. $\{11\bar{2}\}$) [19].

The {100}, {110} and {111} are known as the low Miller index planes and are the simplest arrangements of surface atoms possible when cutting through a FCC crystal. As well as these low Miller index planes, it is also possible to produce high Miller index planes which can be "stepped" or "kinked". A stepped surface is obtained when the surface exhibits a contribution from two different basal planes and the kinked surface occurs when there is a surface comprising all three low Miller index planes.

Figure 1.11 shows the structure of two linear stepped surfaces containing {111} terraces separated by {100} steps. The Miller indices for these surfaces are {533} and {755} respectively. However a more 'descriptive' nomenclature can be employed. Lang proposed a procedure [66] where these structures could be defined by a 'microfacet' notation. In this method, a Miller index {hkl} can be presented in the form $n\{h_tk_tl_t\}x\{h_sk_sl_s\}$ where n represents the average terrace width in terms of surface atoms, $\{h_tk_tl_t\}$ represents the Miller index of the terrace itself and $\{h_sk_sl_s\}$ represents the Miller index of the step.

Using this procedure, the {533} becomes 4{111} x {100} since it consists of 4 atom wide {111} terraces separated by a {100} step. The {755} becomes 6{111} x {100} since it consists of 6 atom wide {111} terraces separated by a {100} step.

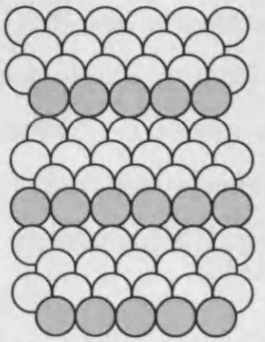

{533} or 4{111} x {100}

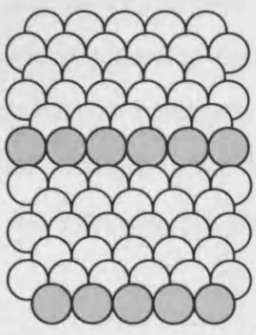

{755} or 6{111} x {100}

Figure 1.11: Two stepped surfaces described by the Miller and Lang nomenclature.

So far, this discussion has dealt with ideal surfaces with perfect structure. In reality surfaces have unsatisfied valances [16] (due to a loss of coordination) making them regions of high energy and of prime importance so far as "active sites" in catalysis are concerned. For example, surface atoms in the {100} plain have a coordination number of only 8 compared with a value of 12 for atoms in the bulk. To compensate for the 'excess' energy this produces, the plane may undergo 'surface relaxation', as illustrated in figure 1.12. This is where bond lengths between the atoms in the surface and the bulk undergo contraction or expansion. The atoms at the surface contract towards the second layer in order to increase their coordination and the third layer atoms expand away from the second layer to compensate for its over-coordination [19].

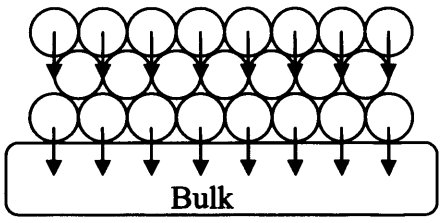

Figure 1.12: Mechanism of relaxation of a surface, reproduced from [19].

If the surface energy reduction is large enough, *reconstruction* of the surface may occur. This can result in an increase in the coordination number of the surface atoms so reducing the surface energy, but more importantly the surface may no longer reflect the symmetry expected from the Miller index plane derived from the bulk crystal. Surface reconstruction can either occur spontaneously [67] or be induced by the adsorption of surface species [68] and leads to significant changes in the surface properties. For example, Au{110} can reconstruct to form a (1x2) superstructure [69, 70] (so called because the periodicity is doubled in one direction) whereby each alternate row of atoms is 'removed', as shown in figure 1.13. Hence a surface must be carefully characterised before use to make certain that no changes have occurred, otherwise phenomenon experienced during catalysis may be wrongly attributed to a particular surface structure.

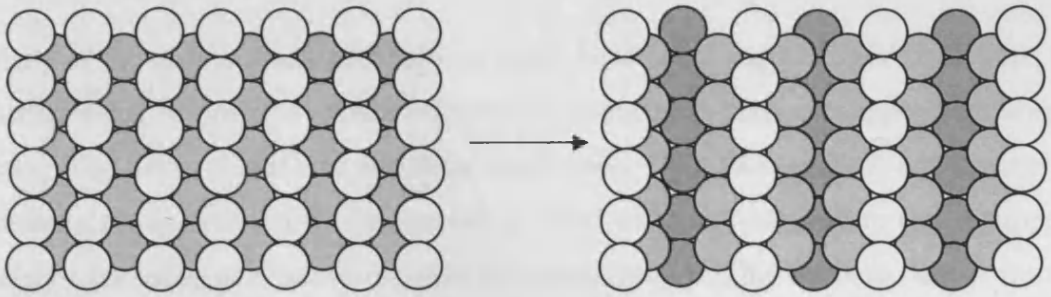

Figure 1.13: Schmatic representation of the reconstruction of Au{110} to the corresponding (1x2) superstructure.

1.2.2 Surface science

It is important to characterise as fully as possible any surface that is being investigated, especially in catalysis where minor changes in surface structure can have a large effect on catalytic properties. There are a variety of different methods available for the investigation of both the surface and bulk properties of catalysts. Some of the more common surface science techniques are listed in table 1.2.

Table 1.2: Surface science techniques used to characterise catalysts and the properties that they can determine, reproduced from [18].

Technique	Properties determined
Photoelectron spectroscopy (UPS, XPS)	Chemical identity of surface layers
Auger spectroscopy	Chemical identity of surface layers
SIMS	Chemical identity of surface layers
Temperature programmed desorption	Chemical identity of adsorbed surface species
Physisorption of gases	Total surface area
Chemisorption of CO, H_2 or O_2	Surface area of metal components
Chemisorption of bases	Surface concentration of acidic sites
Chemisorption of acidic gases	Surface concentration of basic sites
IR, Visible, UV spectroscopy	Types of chemical bond present
HREELS	Type of chemical bond present
EXAFS	Atomic structure of surfaces and adsorbates
NMR	Chemical environment of element
Electron microscopy	Chemical identity and structure of surface layers

Many of the surface science techniques listed in table 1.2 require UHV conditions [71]. Furthermore, in order to extract information concerning particular types of adsorption sites, single crystal surfaces are often employed. This leads to both a 'pressure' and 'materials' gap between the system being tested and the 'real' system (i.e. a supported catalyst operating at elevated pressure and temperature). This is not to detract from the overall contribution made by surface science studies over the last 50 years in understanding adsorption phenomenon. However, when extrapolating this data to high pressure and supported metal catalysts, care is required.

The surface science technique predominantly employed for the work presented in this thesis is cyclic voltammetry. One of the advantages of this technique is that it does not require the use of UHV conditions and therefore supported catalysts (on a conducting support) may be investigated. Hence the 'pressure' and 'materials' gaps are not so much of an issue. In addition, by comparison with the above systems, electrochemical techniques offer a relatively inexpensive route to catalyst characterisation.

1.2.3 Voltammetric techniques

1.2.3.1 Introduction

Voltammetry provides information on the electric current, through an electrode of interest, in relation to a varying voltage [72]. Linear sweep voltammetry (LSV) and cyclic voltammetry (CV) are just two of a wide range of potential-sweep techniques, where the electrode potential, E, is swept between two limits at a set rate and the resultant electrode current, i, is measured. A plot of current against voltage is known as a voltammogram and can be used to interpret the charge-transfer reaction that is occurring at the electrode-electrolyte interface [73].

1.2.3.2 Linear sweep voltammetry (LSV)

Linear sweep voltammetry [72-74] involves applying a linear potential sweep to the electrode and measuring the resultant current as described above (see figure 1.14). The sweep rate, ν, may be defined as :

$$\nu = dE/dt \qquad (1.3)$$

where:

dE is the change in potential between E_1 and E_2 and *dt* is the time taken to complete the sweep.

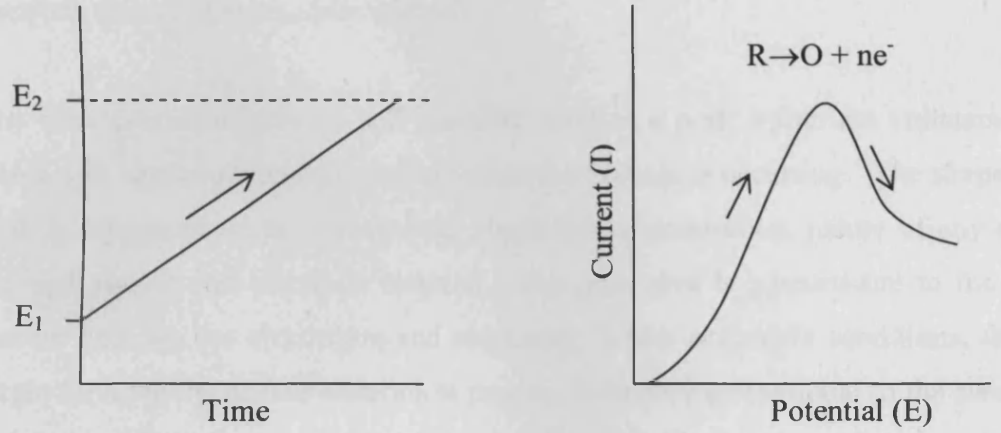

Figure 1.14: Waveform used in linear sweep voltammetry and the resultant voltammogram, where R is the reduced form and O is the oxidised form of the redox active species.

1.2.3.3 Cyclic voltammetry (CV)

Cyclic voltammetry [72-74] was first described in 1948 [75] and is based on the same principles as discussed in the previous section. However, here the potential sweep follows a 'saw-tooth' pattern (i.e. the potential is swept from E_1 to E_2 and then back to E_1) which results in a 'cyclic' voltammogram, as shown in figure 1.15.

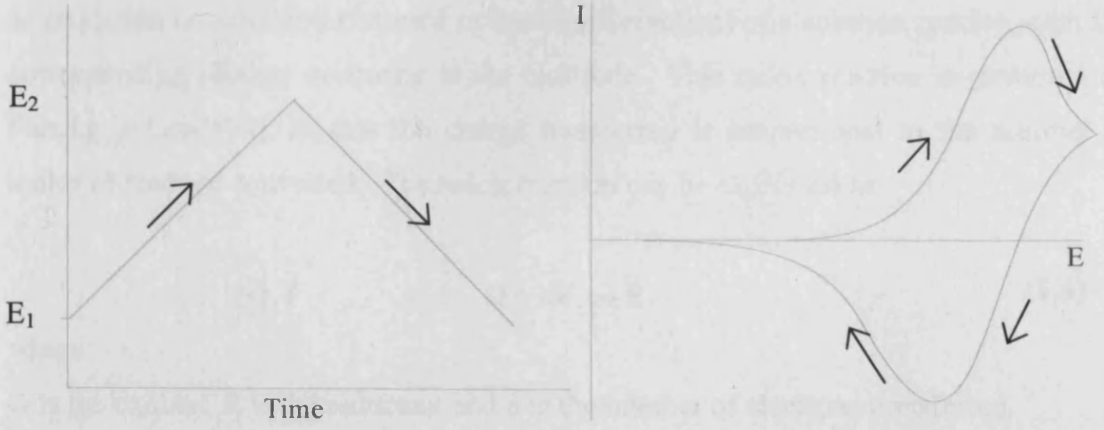

Figure 1.15: A "saw-tooth" potential sweep and the resultant cyclic voltammogram.

Both LSV and CV use three electrodes (working, counter and reference) immersed in an electrolytic solution. The electrodes are connected to a potentiostat which controls the potential applied to the working electrode, which is monitored relative to the reference electrode. On sweeping the potential (with respect to the reference) of the working electrode any current generated flows from the working electrode to the counter electrode (due to potentiostatic control).

Any electrochemical process will manifest itself as a peak within the voltammogram, which will appear at the potential at which the process is occurring. The shape of the peak is dependent on the sweep rate, electrolyte concentration, nature of any organic material present and electrode material. The peak area is proportional to the charge transfer between the electrolyte and electrode. Under reversible conditions, the peak height for a purely surface adsorption process is directly proportional to the sweep rate (see later). Since the magnitude of the electric current is also dependent on the surface area of the electrode, the current density, I_p, (equivalent to current/surface area) is used when comparing data on different electrodes.

1.2.3.4 Electrochemical processes

The current generated by any electrochemical reaction is the sum of two different processes, Faradaic and non-Faradaic charge transfer.

Faradaic Processes are associated with the transfer of charge between the electrolyte and electrode (known as charge transfer electrodes) without adsorption. This results in an oxidation or reduction (forward or backward reaction) of a solution species, with the corresponding process occurring at the electrode. This redox reaction is governed by Faraday's Law [76], in that the charge transferred is proportional to the number of moles of reactant converted. The redox reaction can be expressed as:

$$O + ne^- \leftrightarrow R \qquad \textbf{(1.4)}$$

where:

O is the oxidant, R is the reductant and n is the number of electrons transferred.

The electrochemical reaction is reversible when the transfer of electrons in both the forward and backward reaction is high. This is represented visually by the height of the oxidation and reduction peaks, which are of the same magnitude and are separated by a potential of $59/n$ mV at 298 K. This value arises from equation 1.5, shown below.

$$\left(E_p^{ox} - E_p^{red}\right) = 2.218\frac{RT}{nF} \qquad \textbf{(1.5)}$$

where:

E_p^{ox} is the oxidation potential, E_p^{red} is the reduction potential, R is the gas constant, T it the temperature, n is the number of electrons transferred and F is the Faraday constant.

Also, for a reversible reaction the peak current density is shown in equation 1.6. From this equation it is evident that peak height will increase with sweep rate, since the peak current is proportional to the square root of the sweep rate.

$$I_p = 2.75\times10^5 n^{3/2} v^{1/2} C^o D^{1/2} \qquad \textbf{(1.6)}$$

where:

I_p is the current density (A cm^{-2}), n is the number of electrons, v is the sweep rate, C^o is the concentration of electrolyte (mol l^{-1}) and D is the diffusion coefficient (cm^2 s^{-1})

Non-Faradaic Processes are associated with adsorption and desorption of ions from an electrode surface. If the adsorption process is reversible, then the anodic and cathodic peaks observed in the voltammogram will occur at the same potential. The adsorption process can be expressed as:

$$M^{n+}_{(aq)} + ne^- \rightarrow M_{(ads)} \qquad \textbf{(1.7)}$$

where:

M^{n+} is the metal ion, n is the number of electrons transferred and $M_{(ads)}$ is the adsorbed metal species.

For a first order reaction, the rate of the forward reaction can be expressed as:

$$V_F = k_F[M^{n+}](1-\theta) \quad \textbf{(1.8)}$$

where:

V_F is the rate of forward reaction, k_F is the rate constant of forward reaction, $[M^{n+}]$ is the concentration of the metal ion species and θ is the fraction of surface sites covered.

The reverse reaction rate can be expressed as:

$$V_R = k_R\theta \quad \textbf{(1.9)}$$

where:

V_R is the rate of reverse reaction and k_R is the rate constant for the reverse reaction.

At equilibrium, the forward and reverse reaction rates will be equal:

$$V_F = V_R \quad \textbf{(1.10)}$$

Therefore equations 1.8 and 1.9 can be combined and rearranged to give a Langmuir-type adsorption equation:

$$\frac{\theta}{1-\theta} = \frac{k_F}{k_R}\left[M^{n+}\right] \quad \textbf{(1.11)}$$

This equation differs from its gas phase equivalent in that the rate constants are dependent on the potential, since adsorption involves a charge transfer across the interface. When there is complete charge transfer (i.e. the ion is adsorbed as a neutral species on the electrode surface) the Gibbs energy of adsorption is given by equation 1.12. Here $\Delta G^{o}_{(ads)}$ represents the chemical potential of the metal and nFE represents the electrochemical part of the free energy of adsorption of the metal ion species.

$$\Delta G_{(ads)} = \Delta G^{o}_{(ads)} + nFE \qquad \textbf{(1.12)}$$

where:

$\Delta G_{(ads)}$ is the Gibbs free energy of adsorption, $\Delta G^{o}_{(ads)}$ is the Gibbs free energy of adsorption in the absence of an electric field, n is the number of moles of electrons transferred, F is the Faraday constant and E is the electrode potential.

The equilibrium constant can be expressed as:

$$K = \frac{k_F}{k_R} = \exp\left(\frac{-\Delta G_{(ads)}}{RT}\right) \qquad \textbf{(1.13)}$$

From equation 1.12:

$$K = \frac{k_F}{k_R} = \exp\left(\frac{-\Delta G^{o}_{(ads)} - nFE}{RT}\right) \qquad \textbf{(1.14)}$$

$$K = \exp\left(\frac{-\Delta G^{o}_{(ads)}}{RT}\right)\exp\left(\frac{-nFE}{RT}\right) \qquad \textbf{(1.15)}$$

At a constant temperature:

$$\exp\left(\frac{-\Delta G^{o}_{(ads)}}{RT}\right) = \text{constant} = K' \qquad \textbf{(1.16)}$$

By combining equations 1.15 and 1.16 and substituting into equation 1.11, the following is derived:

$$\frac{\theta}{(1-\theta)} = K'\exp\left(\frac{-nFE}{RT}\right)\left[M^{n+}\right] \qquad \textbf{(1.17)}$$

where:

K' is the adsorption equilibrium constant in the absence of an electric field.

When interactions occur between adsorbed species on the electrode surface, then the peak height and width will be modified. When these lateral interactions are taken into account, equation 1.18 results and is known as the Frumkin equation [77]:

$$\frac{\theta}{(1-\theta)}\exp\left(A\left(\theta-\frac{1}{2}\right)\right)=K'\exp\left(\frac{-nFE}{RT}\right)\left[M^{n+}\right] \qquad \textbf{(1.18)}$$

where:

$\left(A\left(\theta-\frac{1}{2}\right)\right)$ is the Van der Waals term for adlayer interactions and A is the magnitude of attractive, $-A$, or repulsive, $+A$, interactions.

From this isotherm it is possible to determine the surface coverage of any adsorbate, as long as the number of electrons transferred per adsorbate molecule involved is known.

1.2.4 The different adsorption regions of a voltammogram of a transition metal electrode

1.2.4.1 Introduction

Although this thesis is mainly concerned with supported gold catalysis, supported platinum and palladium are also investigated, as well as some single crystals. Traditionally, platinum has been the metal of choice for cyclic voltammetry studies of catalysis and hence the voltammogram regions will first be discussed in relation to platinum and qualifications added where gold exhibits different behaviour.

1.2.4.2 Mechanisms of hydrogen UPD and oxide formation

Underpotential deposition (UPD) occurs when a cation is deposited (as a neutral species) on to the surface of the electrode at more positive potentials than those predicted by the Nernst equation for bulk deposition [72, 78].

The adsorption of hydrogen onto a platinum electrode was first investigated in 1934 by Frumkin [77]. A polycrystalline platinum electrode gives rise to a number of different features when examined in aqueous acidic electrolytes against a hydrogen reference

electrode as can be seen from figure 1.16. This voltammogram has been run between 0.05 V and 1.55 V (more negative potentials result in hydrogen evolution and more positive potentials result in oxygen evolution) and displays three distinct regions. Regions A and E represent the hydrogen UPD region, C and D represent oxide formation and reduction and the shaded area B represents charging of the double layer. The UPD and oxide regions are discussed in detail below. The models proposed for region B are presented in appendix A.

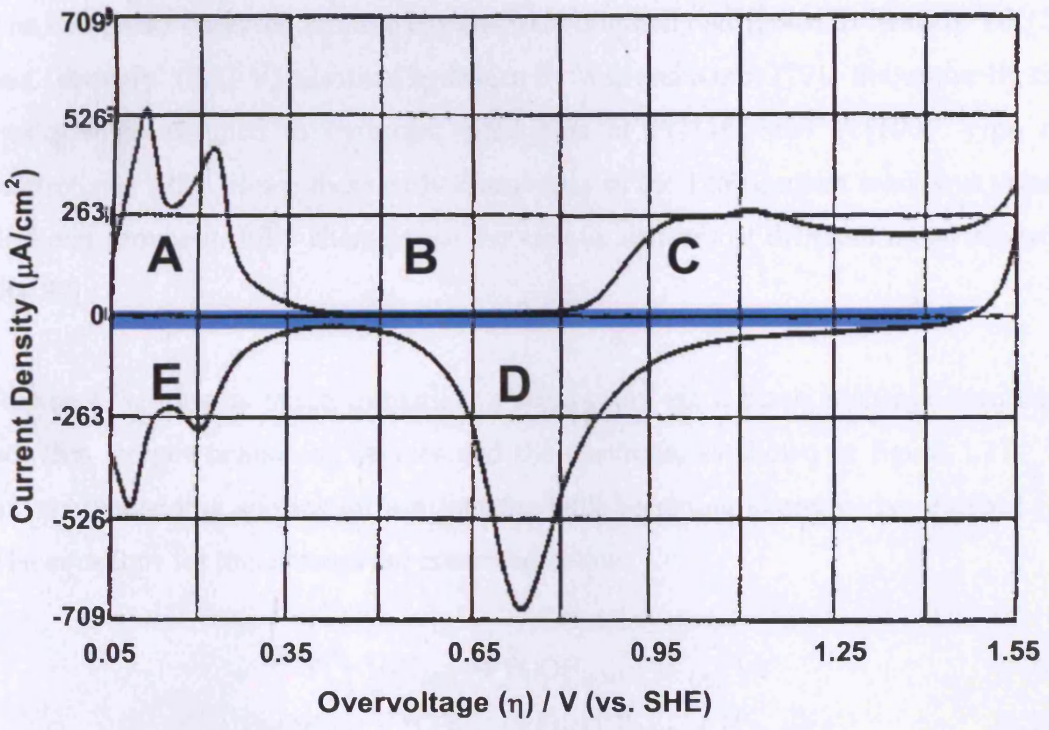

Figure 1.16: Cyclic voltammogram of a polycrystalline platinum electrode run in H_2SO_4 at a sweep rate of 100mVs^{-1}, reproduced from [79].

Region A represents desorption of the hydrogen atoms from the surface of the electrode. This results in the electrode being oxidised due to the loss of an electron from the metal, as such a current is generated that is directly proportional to the number of hydrogen atoms desorbed. Since one electron is transferred per surface atom, the total change in region A (as expressed by the area under the voltammetric peak) is proportional to the surface area of the electrode [80, 81]. Since the surface density of atoms in polycrystalline platinum is known, it can be seen that the change per unit area also translates as a surface coverage.

$$H_{(ads)} \rightarrow H^{+}_{(aq)} + e^{-} \quad \textbf{(1.19)}$$

Region E is the process of hydrogen ion electrosorption from the electrolyte, the reverse process of region A. When regions A and E are symmetrical about the potential axis this indicates that the processes are fully reversible.

$$H^{+}_{(aq)} + e^{-} \rightarrow H_{(ads)} \quad \textbf{(1.20)}$$

The two peaks observed in these regions were originally attributed to 'weakly' (0.12 V) and 'strongly' (0.27 V) adsorbed hydrogen by Will and Knorr [79]. Subsequently these peaks were assigned to hydrogen adsorption at Pt{110} and Pt{100} -type sites respectively [82]. Since these early discoveries in the 1960s, much work was done by different groups to fully characterise the various surfaces of different metal electrodes [83-87].

Region C represents oxide formation which occurs via a place exchange mechanism between oxygen-containing species and the electrode, as shown in figure 1.17. The oxygen containing species diffuse into the bulk becoming strongly chemisorbed [88]. The equations for this process are presented below.

$$Pt + H_2O_{(aq)} \rightarrow Pt\text{-}OH_{(ads)} + H^{+}_{(aq)} + e^{-} \quad \textbf{(1.21)}$$

$$Pt\text{-}OH_{(ads)} + H_2O_{(aq)} \rightarrow Pt\text{-}(OH)_{2(ads)} + H^{+}_{(aq)} + e^{-} \quad \textbf{(1.22)}$$

$$Pt\text{-}(OH)_{2(ads)} \rightarrow Pt\text{-}O_{(ads)} + H_2O_{(aq)} \quad \textbf{(1.23)}$$

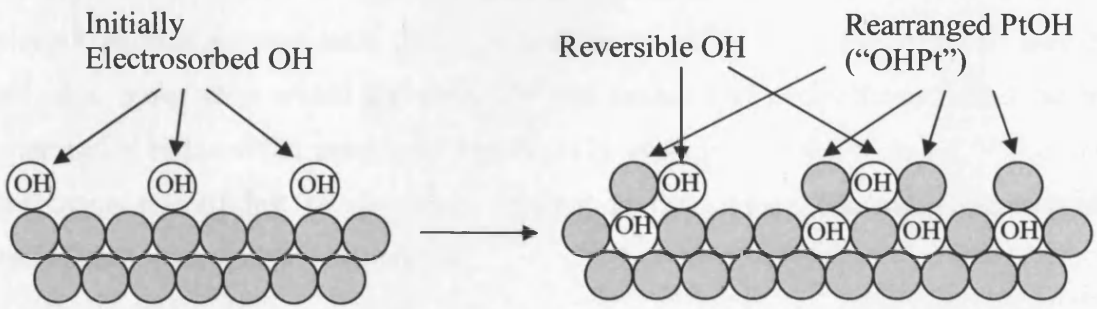

Figure 1.17: Schmatic diagram for the increasing extent of deposition of OH or O type species onto a Pt or Au electrode resulting in the place-exchange mechanism described above, reproduced from [89].

Region D represents the reduction of the oxide layer and has the same total area as region C. However, the potential at which it occurs and its shape are significantly different from region C. Unlike regions A and E which are due to purely surface related (and reversible) phenomena, regions C and D show significant hysteresis due to the kinetically slow nature of the place exchange mechanism. The overall equations for the process are shown below:

$$Pt\text{-}O_{(ads)} + 2H^{+}_{(aq)} + 2e^{-} \rightarrow Pt_{(s)} + H_2O_{(aq)} \qquad \textbf{(1.24)}$$

$$Pt\text{-}O_{(bulk)} + 2H^{+}_{(aq)} + 2e^{-} \rightarrow Pt_{(s)} + H_2O_{(aq)} \qquad \textbf{(1.25)}$$

1.2.4.3 Pt H_{UPD}

H_{UPD} has been extensively used to characterise platinum single crystals [90]. As stated earlier, the initial groundwork for the characterisation of peaks occurring in the voltammogram of polycrystalline and single crystal platinum was laid down by Will and Knorr [79, 82]. This discovery sparked great interest in this area of surface science and led to the assignment of each of the H_{UPD} to particular crystallographic planes [91-93] via combined electrochemical and UHV techniques.

However, doubt was cast on the validity of Will and Knorr's results when it was suggested that the repetitive cycling procedure used to prepare the platinum perturbed the surface and led to the creation of defect sites [94, 95]. The combined use of UHV and electrochemistry (ex situ studies) also led to problems due to the reactive nature of platinum which resulted in adsorption of contaminants on transfer from the UHV to electrochemical environments [96]. In addition, work by Kolb [97] showed that the potential range over which the electrode was cycled had a significant effect on the appearance of the voltammogram. For Pt{111} cycling from 0.0 V to 1.3 V (i.e. into the oxide region) just twenty times resulted in the surface becoming significantly reconstructed towards Pt{110} facets.

The method for the preparation of single crystals was changed forever in 1980, when Clavilier proposed a flame-annealing method [98]. In this method, the single crystal is

heated in a flame until hot (~1300 K) and then cooled in a stream of ultra-pure water. The surface of the crystal is then protected from the atmosphere by a droplet of ultra-pure water attached to the surface allowing it to be transferred to the electrochemical cell without contamination.

A comparison of the single crystal surfaces prepared by the Clavilier method and the more traditionally cycling method of Hubbard [91] showed that the crystals prepared by the Clavilier method produced sharp diffraction spots indicating a high degree of order and no contamination. In the case of the Hubbard method, the diffraction spots were diffuse indicating a loss of long range order [99]. By using the Clavilier preparation method it was no longer necessary to prepare the crystal by repeated cycling to remove contaminants and as such the associated surface reconstruction was not an issue. This led to a dramatic improvement in the reproducibility of cyclic voltammograms of platinum single crystals.

Examples of platinum cyclic voltammograms obtained by the Clavilier method are presented in figure 1.18. Three of the cyclic voltammograms are from the low Miller index planes and two are from stepped surfaces. In addition, the figure shows a representation of a platinum nanoparticle as a cubo-octahedron, which is representative of the particles as would be present in a supported catalyst. The cyclic voltammograms for the single crystals can be associated with the appropriate terraces and steps present with in the particle. Hence the cyclic voltammogram produced by a supported platinum catalyst can be thought of as the sum of the responses from the individual terraces and steps. Figure 1.19 shows a typical H_{UPD} cyclic voltammogram for graphite supported 5% Pt catalyst. The surfaces responsible for each peak are labelled accordingly.

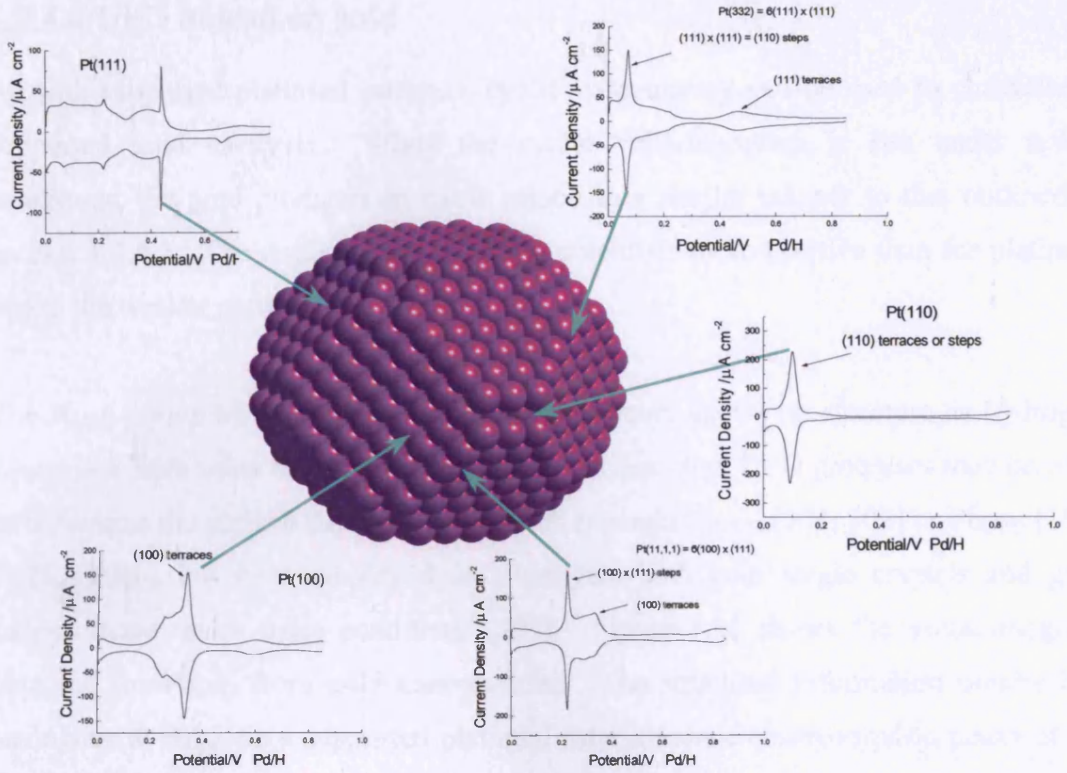

Figure 1.18: Representation of a Pt microcrystallite as a truncated cubo-octahehedron and five voltammograms for Pt single crystals (obtained in H_2SO_4) which relate to the various indicated surfaces (faces and edges) of the nanoparticle structure, reproduced from [100].

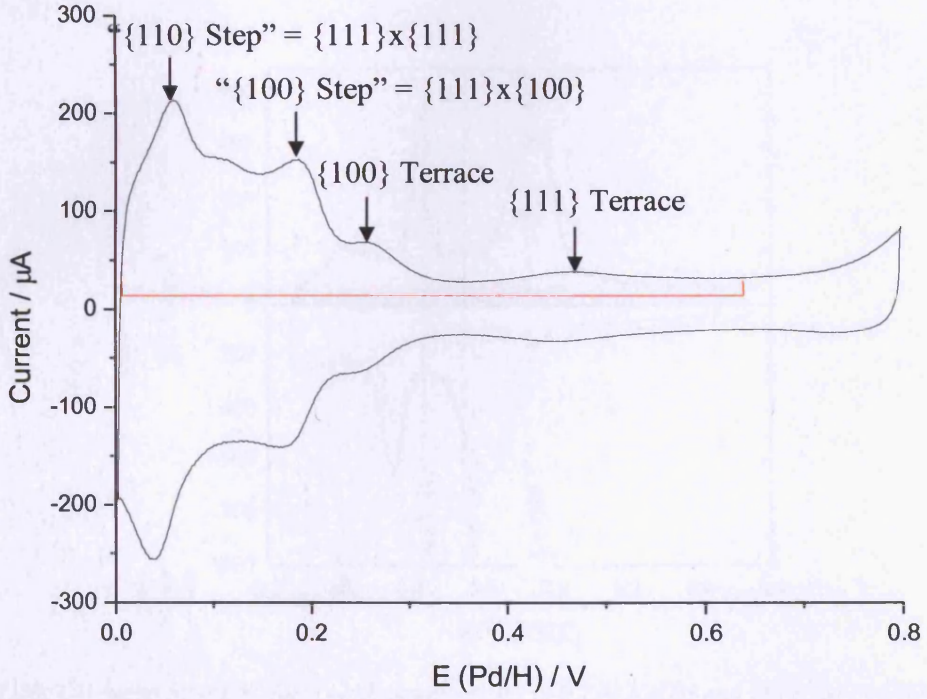

Figure 1.19: Voltammogram of 5% Pt/G run in 0.5 M H_2SO_4 at 10 mV s^{-1}.

1.2.4.4 UPD of lead on gold

As with supported platinum catalysts, cyclic voltammetry can be used to characterise supported gold catalysts. When the cyclic voltammogram is run under acidic conditions, the gold produces an oxide region in a similar manner to that outlined in section 1.2.4.2. The oxide region occurs at potentials more positive than for platinum due to the weaker gold-oxide bond.

The H_{UPD} region of the gold voltammogram however shows no structure as hydrogen does not adsorb on to the gold surfaces. Nonetheless other UPD processes may be used to determine the surface structure of gold, for example Cu_{UPD} [101, 102] or Pb_{UPD} [103-107]. Pb_{UPD} has been employed to investigate both gold single crystals and gold nanoparticles under basic conditions [107]. Figure 1.20 shows the voltammogram obtained for Pb_{UPD} from gold nanoparticles. The structural information obtained is analogous to H_{UPD} on a supported platinum catalyst, since electrosorption peaks of Pb on gold may be identified with particular single crystal sites. Furthermore, the relative intensities of the Pb_{UPD} peaks represent the relative distribution of adsorption sites within the nanoparticles. Hence Pb_{UPD} is well suited as a technique for characterisation of gold catalysts.

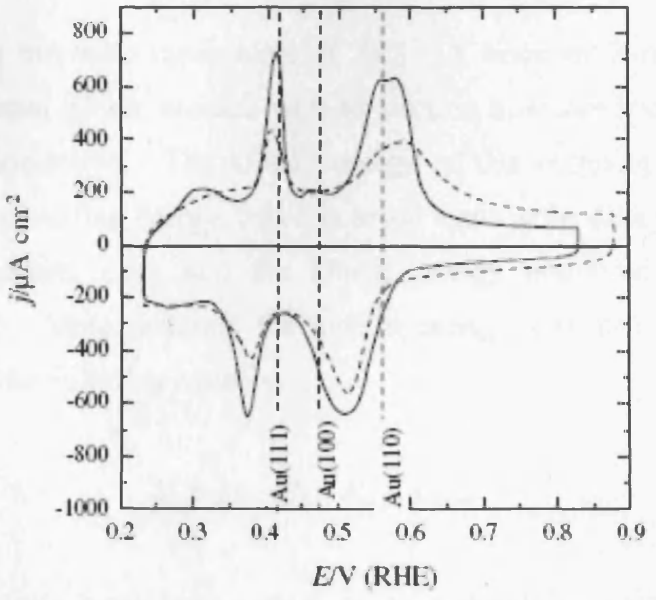

Figure 1.20: CV run at 50 mV s^{-1} for a gold nanoparticles in 0.1 M NaOH and 1x10^{-3} M $Pb(NO_3)_2$, after the initial deposition/dissolution of the PbO_2 film (—) and after one cycle between 0 and 1.7 V in 0.1 M NaOH (---), reproduced from [107].

1.2.5 Other methods of catalyst characterisation

1.2.5.1 Introduction

To support the electrochemical catalyst characterisation, two other surface science techniques were employed at various stages in this investigation. TEM data were provided by Johnson Matthey and will not be discussed. XPS data were collected at CCLRC laboratories in Daresbury and the theory associated with this technique will be discussed briefly.

1.2.5.2 X-ray Photoelectron Spectroscopy (XPS)

X-ray Photoelectron Spectroscopy (XPS) was developed by Siegbahn in 1967 [108] for which he was awarded the Noble Prize for Physics in 1981. It is a UHV technique which can be used to determine the surface composition (up to 10 nm depth) of a material. Since electrons in every type of atom have characteristic electron binding energies, E_b, (E_b = the total energy required for removing an electron from a particular orbital), it is possible to determine the surface composition of a material. Moreover, binding energy is dependent on chemical environment, for example, the carbon peaks for C in graphite and carbon monoxide will exhibit different binding energies. A handbook containing XPS standard spectra for all atoms is available [109].

Figure 1.21 shows the basic mechanism of XPS. A beam of X-rays irradiates the surface of the material which interacts with an electron in a core level and causes the ejection of a photoelectron. The kinetic energy of this outgoing photoelectron is representative of the binding energy, which in broad terms is the difference between the energy of the incident x-ray and the kinetic energy possessed by the emitted photoelectron [45]. More precisely the kinetic energy is related to the electronic binding energy by the following equation.

$$E_k = h\nu - E_b - E_r - \phi - \delta E \qquad \textbf{(1.26)}$$

where:

E_k is the kinetic energy of ejected photoelectron, $h\nu$ is the photon energy of X-ray, E_b is the electron binding energy, E_r is the recoil energy, Φ is the spectrometer work function and δE represents the electrostatic charging of the species.

E_r is a small quantity compared with the other terms and hence is generally ignored. Since the energy of the incident X-ray and the spectrometer work function are both set parameters and the kinetic energy of the photoelectron is determined experimentally, the binding energy for a given system can be determined. A typical spectrum for a supported 2% gold catalyst is shown in figure 1.22. The surface sensitivity of the method relies on the mean free path of electrons in the kinetic energy range 60 – 600 eV which is between 2-4 atomic layers. This means that only those electrons originating from the first few atomic layers of the solid surface will be detected.

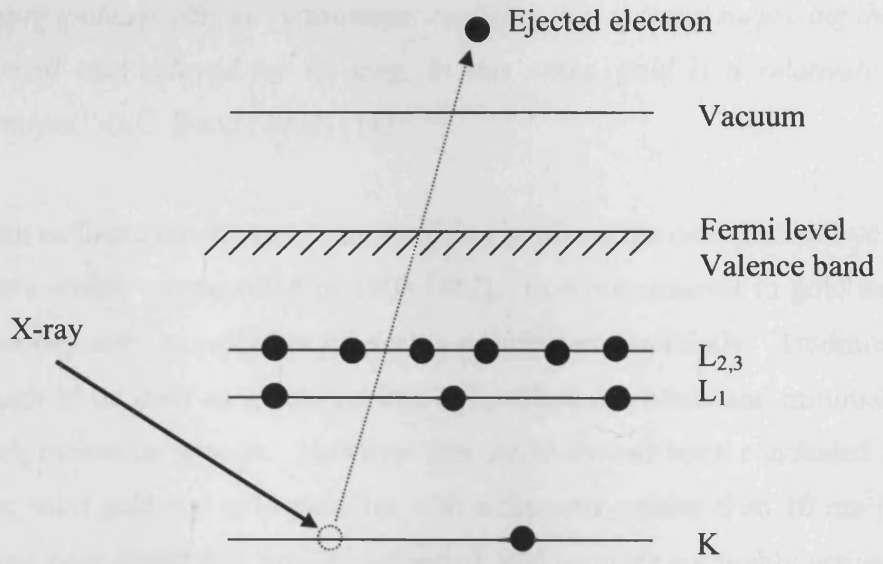

Figure 1.21: Diagram of the photoemission process, reproduced from [110].

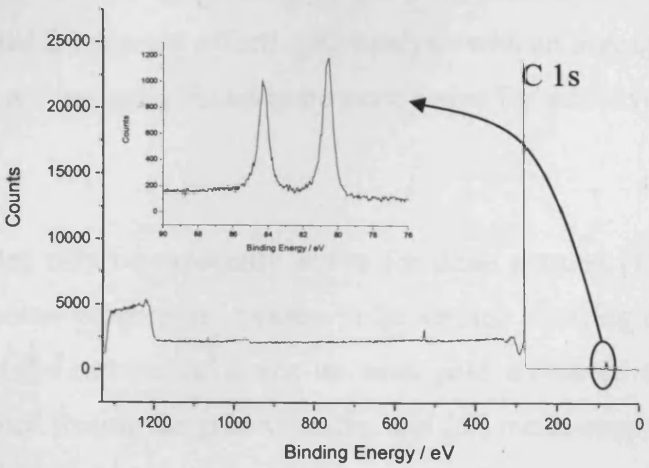

Figure 1.22: XPS spectrum for graphite supported 2% gold catalyst, with an insert of the peaks associated with Au 4f photo-electrons.

1.3 Gold Catalysts

1.3.1 Background

Over the centuries, the major uses for gold have been in the manufacture of coinage and jewellery. However the conductive and ductile properties of gold made it an excellent metal for use in the electronics industry and so, with the microchip revolution, gold has found new uses. More recently gold has found another potential application – in catalysis.

> *"Gold catalysis is a very special kind of animal, only manifesting itself under quite specific circumstances: realising this, it is not surprising that its arrival was delayed for so long. In this sense, gold is a relatively new catalyst."* G.C. Bond (2002) [111]

One of the earliest catalytic reactions involving gold was the oxidation of hydrogen over gold gauze which was reported in 1906 [112]. However interest in gold as a catalyst has developed only recently but interest is growing exponentially. Traditionally, gold was though to be inert as a catalyst due to its filled d-orbitals and minimal ability to chemisorb molecular species. However this inactivity had been concluded from work involving solid gold and gold particles with a diameter greater than 10 nm [113, 114]. It has since been found that smaller supported gold particles are highly active in a range of catalytic systems, such as water gas shift [115-117] together with carbon monoxide oxidation [118-120] and hydrogenation [121-123]. In particular supported (usually an oxide support is used for greatest effect) gold catalysts with an average particle diameter of around 1-2 nm are generally found to be most active for selective partial oxidations [113, 114].

Small gold particles may be especially active for three reasons [111]: (*i*) small gold particles have a greater proportion of atoms in the surface allowing more active sites to be present, (*ii*) as the number of atoms on each gold ensemble decreases the band structure is weakened freeing the gold valences, and (*iii*) metal-support interactions will become more important.

1.3.2 Gold as a catalyst

After the initial report that gold was an active oxidation catalyst in 1906 [112], gold was also found to be an active catalyst for CO oxidation in 1925 [124]. During the mid-1970s there was some interest in gold as a hydrogenation catalyst. Investigations into alkene hydrogenation at low temperature over supported gold were undertaken by Sermon and Bond *et al*, [125, 126]. In 1987 Haruta found that supported gold was a good catalyst for the low temperature oxidation of CO [127] and this discovery sparked much of the current interest in gold catalysis. More recently gold has been investigated for its activity in CO oxidation in relation to fuel cell technology (i.e. water gas shift reactions) [128]. Since Haruta's initial discovery gold has proved to be a useful catalyst for a range of different reactions. For example, the effectiveness of gold as a catalyst for the hydroclorination of ethyne to vinyl chloride was investigated by Hutchings *et al* [129] and more recently the hydrogenation of α,β unsaturated aldehydes over gold has been reported [129]. Investigations have also found that gold is active for the oxidation of propene to propene oxide [113]. Selectivity was high at 99% although conversion was low. However, similar platinum and palladium catalysts showed no activity for this reaction. Supported gold has also been employed to reduce nitric oxide to nitrogen at low temperature - another reaction for which platinum group metals require higher temperatures and are less selective.

The water gas shift reaction is used in industry to produce hydrogen gas from carbon dioxide and water. Interest in the reaction has revived due to the growing interest in fuel cells as efficient and non-polluting sources of energy. Gold catalysts have provided promising results but effectiveness is highly dependent on particle size, the method of preparation and the support used [130].

Gold catalysts are also extensively used in alloy systems; consider gold-palladium catalysts used to produce a vinyl acetate monomer [131, 132]. A full scale plant went into operation at the end of 2001 and represents one of the first large scale chemical process to use a gold catalyst [133].

1.4 Metal-catalysed selective oxidation of alcohols

1.4.1 Introduction

The traditional stoichiometric methods for alcohol oxidation are generally environmentally unfriendly producing toxic by-products and one of the main advantages of catalytic oxidation is that the reaction can be carried out under mild conditions sometimes in water with either air or oxygen as the oxidant. The catalytic oxidation of alcohols by metals has been studied for many years (predominantly on platinum group metals) and from these investigations many general principles have arisen. For platinum and palladium catalysts the rate of oxidation of a primary alcohol is faster than that of the corresponding secondary alcohol and oxidation only stops at the aldehyde stage when the primary alcohol function is adjacent to a double bond or an aromatic ring [134]. However as the pH is increased, the selectivity towards the aldehydes is decreased [135]. In all other cases primary alcohols are oxidised to carboxylic acids and secondary alcohols are oxidised to ketones. Since the oxidation of the primary alcohol occurs at a significantly faster rate, this allows selective oxidations when both primary and secondary alcohol functions are present together within a molecule. The mechanism for alcohol oxidation at metal surfaces follows an oxidative dehydrogenation route [134, 136, 137] which will be discussed later.

As well as platinum group metals, gold has also been shown to be an active catalyst for alcohol oxidation. Carbon-supported gold catalysts have shown a greater selectivity in both ethane-1,2-diol and propane-1,2-diol oxidation than carbon-supported Pt or Pd catalysts under basic conditions (where gold is most active) and exhibit a greater resistance to deactivation. Other diols have been investigated and have also shown a high selectivity over gold catalysts. This trend has been repeated with the oxidation of aminoalcohols [138, 139].

Carbon-supported gold catalysts have also been used for the oxidation of aldehydes where they have shown similar activity to platinum catalysts for the oxidation of propanal, butanal and 2-methyl-propanal. In addition the resistance of gold to deactivation by oxygen when reaction is carried out in an aqueous solvent is greater than that shown by platinum group metals [140].

1.4.2 Propanol oxidation

Propanol oxidation is important as a test reagent for total catalytic combustion of volatile organic compounds (VOCs) [141-143]. However in this investigation propanol oxidation was used solely as a test reaction to investigate any link between (*i*) the surface structure and activity of the catalysts and (*ii*) between catalytic and electrooxidation properties (see section 1.4.4). To that end the reaction was chosen for simplicity. 2-Propanol can only be oxidised to acetone (scheme 1.3) whereas 1-propanol can only be oxidised to two potential products (scheme 1.4), propanal and/or propionic acid (assuming overoxidation to CO_2 or aldol condensation does not occur [144]). From the discussion outlined above the reaction is unlikely to stop at the aldehyde stage over a supported metal catalyst, and hence this reaction acted as a basic test of the established literature.

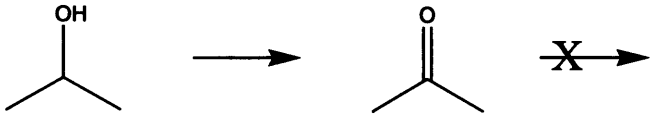

Scheme 1.3: 2-Propanol oxidation to acetone.

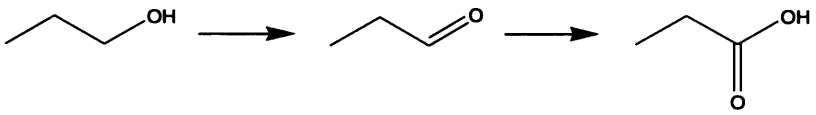

Scheme 1.4: 1-Propanol oxidation to propanaldehyde and propionic acid.

1.4.3 Glycerol oxidation

Glycerol oxidation was the main topic of interest in this work. It is a renewable feedstock which can be obtained from biosustainable sources; hence it is an ideal starting point for green chemistry. Glycerol is also a highly functionalised molecule which has the potential to provide a wide range of functionalised products (see scheme 1.5) which can be formed under mild conditions. Many of these products are useful intermediates for the production of fine chemicals.

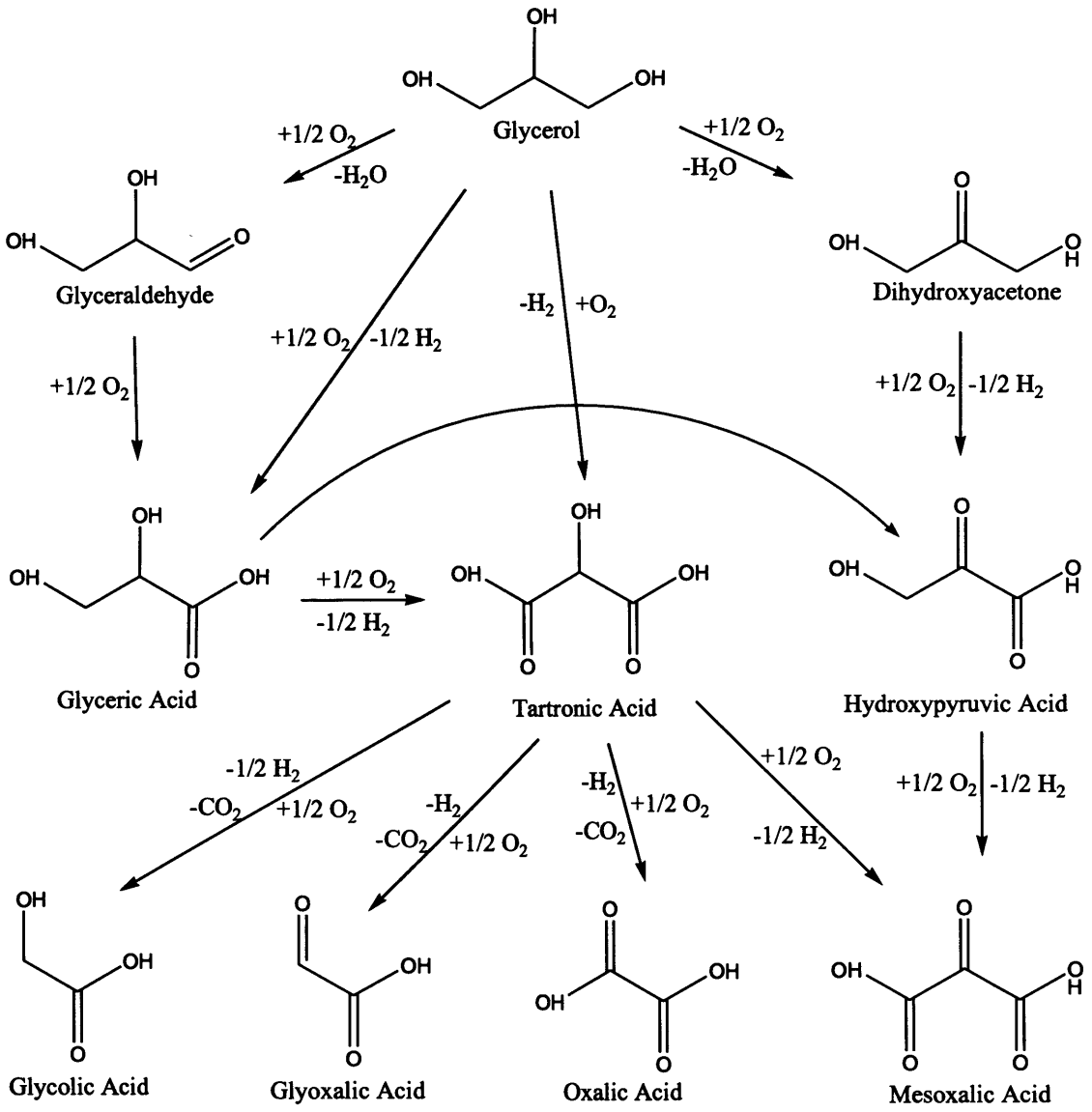

Scheme 1.5: The range of products available from the oxidation of glycerol, reproduced from [157].

The reaction has been extensively studied by Kimura [145, 146] and Gallezot [147-149] using supported platinum (sometimes with a bismuth promoter) and palladium catalysts. Kimura found that platinum gave the best selectivity towards dihydroxyacetone and the selectivity was increased by the addition of bismuth. It was suggested that bismuth was promoting the oxidation by selective-site blocking only, as its incorporation did not alter platinum's electronic structure. Platinum was found to be the only metal that showed any activity in acidic media. Gallezot found that bismuth promoted platinum catalysts, although having a high initial selectivity, were readily poisoned by the irreversible adsorption of the acid products.

Work carried out by Gallezot showed that a higher pH resulted in a higher reaction rate over palladium catalysts and a higher selectivity towards glyceric acid, the highest being a 95% selectivity at 100% conversion. Other products formed included dihydroxyacetone, tartronic and oxalic acid which all formed in less than 10% yield. If the reaction proceeded to completion, glyceric acid was subsequently converted to oxalic acid, which could then be converted to formic acid and finally to CO_2 [150]. Over platinum catalysts the maximum yield of glyceric acid was 55% at 90% conversion but a higher pH lowered the selectivity resulting in the formation of more minor products (slightly more than observed over palladium). Under basic conditions, Gallezot found that glyceric acid was predominantly oxidised to tartronic acid, whereas under acidic conditions the main product was hydroxypyruvic acid. At high conversions, over-oxidation to formic acid and glycolic acid was also noted.

More recently, supported gold catalysts have been investigated for glycerol oxidation by Hutchings [151-153], Prati [154-156] and Claus [157]. Hutchings *et al*, have investigated glycerol oxidation in a batch reactor under an ambient pressure of air over supported gold, platinum and palladium catalysts. Supported gold was found to be inactive under these conditions, whereas platinum and palladium catalysts gave a small selectivity to glyceric acid. However, when glycerol oxidation was carried out in a high pressure reactor under oxygen at a pressure of three bar, the reactivity was significantly improved. For 1% Au/activated carbon, conversion of glycerol was 56% with 100% selectivity to glyceric acid. These experiments were carried out in the presence of base and for both the platinum and gold catalysts the introduction of NaOH eliminated unwanted C1 by-products. In the case of gold, the absence of NaOH resulted in complete inactivity and it has been suggested that the role of base in the reaction was to aid the initial dehydrogenation of glycerol via H-abstraction of one of the primary OH groups. In other words, the mechanism of action is an oxidative dehydrogenation, as has been reported for platinum group metals [134, 136, 137], the difference being that the platinum group metals do not require the presence of NaOH, whereas gold does. Generally it was noted that selectivity to glyceric acid increased with increasing NaOH concentration and both conversion/selectivity increased with gold loading.

The Hutchings group has also used cyclic voltammetry to help characterise the active surface [153]. Cyclic voltammograms of three active gold catalysts (1%, 0.5%, and

0.25% Au/graphite) and one inactive supported gold catalyst (1% Au/carbon) were studied. For the active catalysts two reduction peaks were observed. One was attributed to desorption of oxide (as discussed in section 1.2.4.2) and the second was attributed to the formation of an oxide species in the presence of NaOH. This peak was noticeably broader for the 1% catalyst and it was suggested that this might be important in relation to the catalyst's selectivity. However no further explanation was offered as to the origin of this peak. It was also noted that the inactive 1% Au catalyst gave no structural features in its voltammogram.

Work carried out by Prati *et al* has focused on supported alloys of Au/Pt and Au/Pd. For the Au/Pd catalysts a higher activity than the corresponding monometallic catalyst was observed. In addition the Au/Pd catalysts showed a greater selectivity to glyceric acid than the Au/Pt catalysts. For the Au/Pt catalysts, over-oxidation to tartronic acid has been established, a feature not seen on the Au/Pd catalysts. In addition Prati confirmed and further investigated the dependency of glycerol oxidation on catalyst preparation method together with reaction conditions such as reaction temperature and reactant/hydroxide ratio. This was further confirmed by the work carried out by Claus, who investigated support effects, particle size, reaction time and reaction conditions.

When Prati tested catalysts prepared in the same way, on the same support and under similar reaction condition as Hutchings, a new by-product was detected - glycolate (from glycolic acid). It was noted that once complete conversion was obtained, the amount of glycolic acid present remained stable whereas the amount of tartronic acid increased at the expense of the glyceric acid. However, the total amount of glyceric acid plus tartronic acid remained constant. This led Prati to conclude that glycolic acid was not being formed from glyceric acid (via hydroxypyruvic acid or aldehyde). Scheme 1.6 shows the proposed mechanism based on these findings. Hence glycolic acid could be considered a probe of path (a) and likewise glyceric acid and tartronic acid were considered probes of path (b). However since it is possible for dihydroxyacetone and glyceric acid to interconvert, this finding unfortunately did not shed any light on whether the primary or secondary alcohol was being oxidised first.

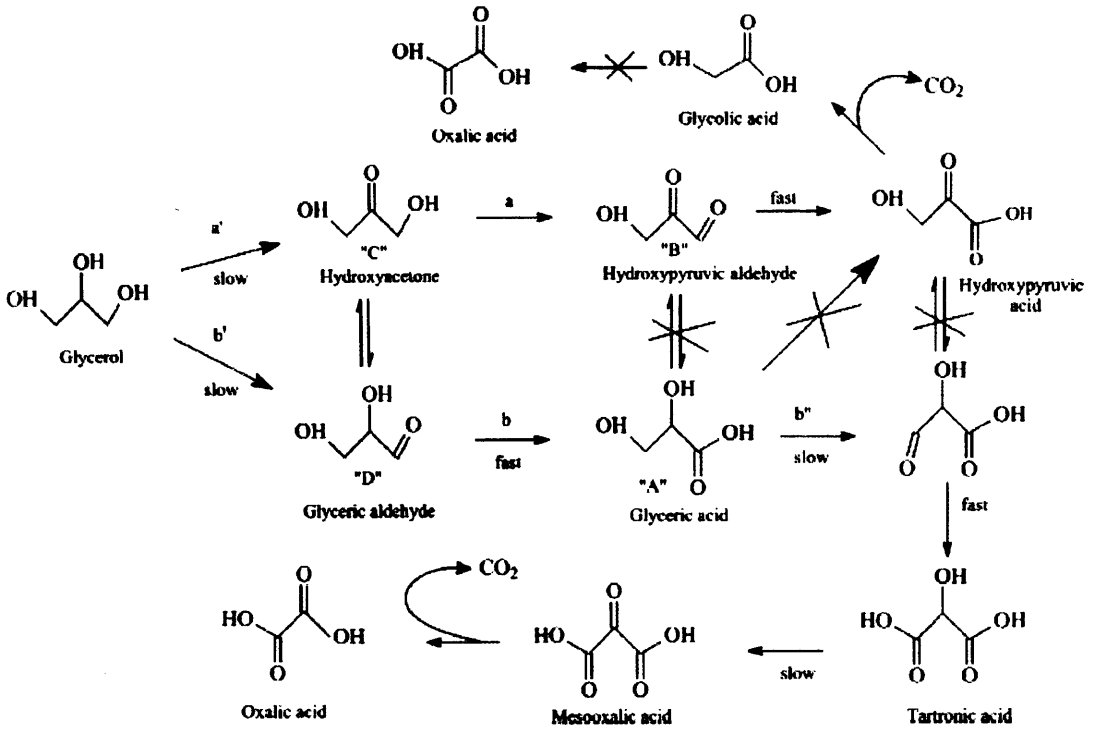

Scheme 1.6: The reaction mechanism proposed by Prati, reproduced from [154].

1.4.4 Electrooxidation

Electrooxidation occurs when a redox active species, for example an organic compound dissolved in an electrolyte is oxidised at an electrode surface by the applied potential. As discussed earlier, if a species is oxidised or reduced at an electrode surface as a function of potential, then this will result in a peak being observed in the voltammogram. Increased electrocatalytic ability results in a larger peak in the voltammogram, as has been seen on two platinum electrodes modified in different ways [158], since the current density is directly proportional to the rate of the electrooxidation.

Electrooxidation over gold has been carried out for a range of saturated oxygenated organic compounds (including glycerol) both in acidic and alkaline media [159]. It was reported that gold performed poorly as an electrocatalyst in acidic media, however under basic conditions, gold proved to be an excellent electrocatalyst. This reflects the catalytic situation discussed previously.

Electrooxidation of glycerol is complex and generally far from understood; however, it has been suggested that interactions occur between adsorbed glycerol and adsorbed OH^- species on the gold surface [160]. In addition it has been suggested that a complex forms between the glycerol and adsorbed hydroxide species [161]. This will be discussed in more detail later.

Glycerol electrooxidation on graphite supported platinum has been investigated at Cardiff [162, 163]. Inactive catalysts of course gave no response, but active catalysts gave well defined features in the voltammograms. From the results obtained it was suggested that a link might exist between the relative intensity/structure of the electrooxidation peak data and the catalytic data for the same catalyst. Thus cyclic voltammetry may be useful as an evaluation procedure for active catalysts.

1.5 Objectives of the investigation

The objectives of this investigation were as follows:

i. to prepare new types of gold catalyst by systematically altering a given "base" catalyst, either by addition of a promoter adatom or by altering the catalyst's morphology (i.e. by sintering) and subsequently using these catalysts in a simplified test reaction system;
ii. to fully characterise all catalysts, using CV (via H_{UPD} / oxide formation and Pb_{UPD}) and to broaden these findings using other surface science characterisation techniques (XPS and TEM) where necessary;
iii. to investigate the gold catalysts in propanol and glycerol oxidation and electrooxidation;
iv. to investigate any links between the surface structure of a catalyst, its voltammetric response, and its catalytic oxidation activity so that conclusions might be drawn as to new methods of characterising catalytic activity/selectivity based on voltammetric data alone.

1.6 References

1. M. Bowker, *The Basis and Application of Heterogeneous Catalysis*, Oxford Science Publications, 1998.
2. R.A. van Santen, J.W. Niemantsverdriet, *Chemical Kinetics and Catalysis*, Plenum Press, 1995.
3. E. Davey; *Philos. Trans. R. Soc.* London (1820).
4. J. Berzelius, *Edinburgh New Philosophical Journal*, 21 (1836) 223.
5. P.W. Atkins, *Physical Chemistry – Fifth Edition*, Oxford University Press, 1994.
6. J.M. Thomas, W.J. Thomas, *Principles and Practices of Heterogeneous Catalysis*, VCH Publications, 1997.
7. M. Haruta, T. Hobayashi, H. Samo, N. Yamada, *Chem. Lett.*, (1987) 405.
8. M. Haruta, N. Yamada, T.Kobayashi, S. Ijima, *J. Catal.* **115** (1989) 301.
9. M. Haruta, S. Tsubota, T. Kobayashi, H. Kageyama, M.J. Genet, B. Delmon, *J. Catal.*, **144** (1993) 175.
10. B. Nkosi, M.D. Adams, N.J. Coville and G.J. Hutchings, *J. Catal.*, **128** (1991) 378.
11. M. Bonarowska, B. Burda, W. Juszczyk, J. Pielaszek, Z. Kowalczyk, Z. Karpinski, *App. Catal. B*, **35** (2001) 13.
12. J. Luo, M.M. Maye, N.N. Kariuki, L. Wang, P. Njoki, Y. Lin, M. Schadt, H.R. Naslund, C.-J. Zhong, *Catal. Today,* **99** (2005) 291.
13. G.C. Bond, D.T. Thompson, *Catal. Rev.-Sci. Eng.*, **41** (1999) 319.
14. G.C. Bond, *Catal. Today,* **72** (2002) 5.
15. J.E. Lennard-Jones, *Trans. Faraday Soc.*, **28** (1932) 333.
16. G.C. Bond, *Catalysis by Metals*, Academic Press 1962.
17. G.C. Bond, *Heterogeneous Catalysis: Principles and Applications*, Clarendon Press, 1974.
18. M.V. Twigg, *Catalyst Handbook – Second Edition*, Wolf Publications, 1989.
19. G.A. Attard, C. Barnes, *Surfaces*, Oxford University Press, 1998.
20. G. Ertl, H. Knozinger, J. Weitkamp, *Handbook of Heterogeneous Catalysis Part B: Volumes 4-5 Catalytic Processes*, Wiley, 1997.
21. F. Haber, G. Van Oordt, *Z. Anorg. Chem.*, **43** (1904) 111.
22. F. Haber, R. L. Rossingnol, *Elektrochemie*, **14** (1908) 181.

23. M.J. Grunze, M. Golze, W. Hirschwald, H.-J. Freund, H. Pulm, U. Seip, M.C. Tsai, G. Ertl, J. Kuppers, *Phys. Res. Lett.*, **53** (1984) 850.
24. V.D. Sokolosvskii, G.M. Aliev, O.V. Buyesvskaya, A.A. Davydov, *Catal. Today*, **4** (1989) 293.
25. R. Burch, M.J. Hayes, *J. Molec. Catal. A*, **100** (1995) 13.
26. M. Calatayud, A. Markovits, M. Menetrey, B. Mguig, C. Minot, *Catal. Today*, **85** (2003) 125.
27. P. Marsand, D.W. van Krevelen, *Chem. Eng. Sci.*, **3** (1954) 41.
28. N. Gokon, Y. Oku, H. Kaneko, Y. Tamaura, *Solar Energy*, **72** (2002) 243.
29. C. Rhodes, B.P. Williams, F. King, G.J. Hutchings, *Catal. Comm.*, **3** (2002) 381.
30. E. Rombi, I. Ferino, R. Monaci, C. Picciau, V. Solinas, R. Buzzoni, *App. Catal. A*, **266** (2004) 73.
31. A. Shichi, A. Satsuma, T. Hattori, *App. Catal. B,* **30** (2001) 25.
32. A.E. Palomares, G. Eder-Mirth, M. Rep, J.A. Lercher, *J. Catal.*, **180** (1998) 56.
33. D. Barthomeuf, *Catal. Rev.*, **138** (1996) 521.
34. B.L. Su, D. Barthomeuf, *App. Catal. A*, **124** (1995) 73.
35. G. Delahay, S. Kieger, N. Tanchoux, P. Trens, B. Coq, *App. Catal. B*, **52** (2004) 251.
36. M. Lasperas, P. Graffin, P. Geneste, *J. Catal.*, **139** (1993) 362.
37. R.J. Davis, *J. Catal.*, **216** (2003) 396.
38. T.E. Fischer and S. R. Kelemen, *J. Catal.*, **53** (1978) 24.
39. R.B. Anderson, F.S. Karn, J.F. Shultz, *J. Catal.*, **4** (1965) 56.
40. J. Bayer, K. C. Stein, L.J.E. Hofer, R.B. Anderson, *J. Catal.*, **3** (1964) 145.
41. N. Escalona, J. Ojeda, P. Baeza, R. García, J.M. Palacios, J.L.G. Fierro, A. López Agudo, F.J. Gil–Llambías, *App. Catal. A*, **287** (2005) 47.
42. Z. Vít, J. Cinibulk, D. Gulková, *App. Catal. A*, **272** (2004) 99.
43. J. Cinibulk, D. Gulková, Y. Yoshimura, Z. Vít, *App. Catal. A*, **255** (2003) 321.
44. D. Wang, W. Qian, A. Ishihara and T. Kabe, *J. Catal.*, **203** (2001) 322.
45. I.M. Campbell, *Catalysis at Surfaces*, Chapman and Hall, 1988.
46. D. Douguet, J.-M. Bolla, H. Munier-Lehmann, G. Labesse, *Enzyme and Microbial Technology*, **30** (2002) 289.
47. R.P.H. Gasser, *An Introduction to Chemisorption and Catalysis by Metals*, Oxford Science Publications, 1987.

48. G.O. Alptekin, A.M. Herring, D.L. Williamson, T.R. Ohno, R.L. McCormick, *J. Catal.*, **181** (1999) 104.
49. B.Coq, J.M. Cognion, F. Figueras, D. Tournigant, *J. Catal.*, **141** (1993) 21.
50. P.P. Silva, F. A.Silva, H.P. Souza, A.G. Lobo, L.V. Mattos, F.B. Noronha, C.E. Hori, *Catal. Today*, **101** (2005) 31.
51. T. Mallat, Z. Bodnar, P. Hug, A. Baiker, *J. Catal.*, **153** (1995) 131.
52. A. Carlos, S. C. Teixeira, R. Giudici, *Chem. Eng. Sci.*, **54** (1999) 3609.
53. S. Scirè, C. Crisafulli, R. Maggiore, S. Minicò, S. Galvagno, *App. Sur. Sci.*, **93** (1996) 309.
54. P. Fordham, M. Besson, P. Gallezot, *Catal. Lett.*, **46** (1997) 195.
55. J. H. Sinfelt, J. L. Carter, D.J.C. Yates, *J. Catal.*, **24** (1972) 283.
56. P.F. Barbieri, A. de Siervo, M.F. Carazzolle, R. Landers, G.C. Kleiman, *J. Electron Spectrosc. Relat. Phenom.*, **135** (2004) 113.
57. R. Parsons, T. Van der Noot, *J. Electroanal. Chem.*, **257** (1988) 9.
58. W. Chen, H. Lu, C.-M. Pradier, J. Paul, A. Flodström, *J. Catal.*, **172** (1997) 3.
59. M. Lischka, C. Mosch, A. Groß, *Sur. Sci.*, **570** (2004) 227.
60. J.E. Bailie, G.J. Hutchings, *Catal. Comm.*, **2** (2001) 291.
61. C.H. Bartholomew, *App. Catal. A*, **212** (2001) 17.
62. P. Forzatti, L. Lietti, *Catal. Today*, **52** (1999) 165.
63. E.M. McCash, *Surface Chemistry*, Oxford University Press, 2001.
64. K.W. Kolasinski, *Surface Science – Foundations of Catalysis and Nanoscience*, Wiley, 2002.
65. M. Buerger, *Elementary Crystallography*, Wiley, 1963.
66. B. Lang, R.W. Joyner, G.A. Somorjai, *Sur. Sci.*, **30** (1972) 440.
67. M.A. Van Hove, R.T. Koestner, P.C. Stair, J.B. Biberian, L.L. Kesmodel, I. Bartos, G.A. Somorjai, *Surf. Sci.*, **30** (1972) 440.
68. R.J. Behm, D.K. Flynn, K.D. Jannison, G. Ertl, P.A. Thiel, *Phys. Rev. B*, **36** (1987) 9267.
69. W. Moritz, D. Wolf, *Surf. Sci.*, **88** (1979) L29.
70. W. Moritz, D. Wolf, *Surf. Sci.*, **163** (1985) L655.
71. Y. Margoninski, *Vacuum*, **28** (1978) 515.
72. A.C. Fisher, *Electrode Dynamics*, Oxford University Press, 1996.
73. A. Wiechowski, *Interfacial Electrochemistry – Theory, Experimental and Applications*, Marcel Dekker, 1999.

74. A.J. Bard, L.R. Faulkner, *Electrochemical Methods – Fundamentals and Applications (second edition)*, Wiley, 2001.
75. J. Randles, *Trans. Far. Soc.*, **44** (1948) 327.
76. M. Faraday, *Phil. Trans. Roy. Soc. A*, **124** (1834) 77.
77. A. Slygin, A. Frumkin, *Acta Physiochim. URSS*, 3 (1935) 791.
78. C.H. Hamann, A. Hamnett, W. Vielstich, *Electrochemistry*, Wiley-VCH, 1998.
79. F.G. Will, C.F. Knorr, *Z. Electrochem.*, **64** (1960) 258.
80. R. Durand, J. *Electroanal. Chem.*, **97** (1979) 293.
81. R. Parsons, G. Ritzzoulis, *J. Electroanal. Chem.*, **318** (1991) 1.
82. F.G. Will, *J. Electrochem. Soc.*, **112** (1965)451.
83. S.D. James, *J. Electrochem. Soc.*, **114** (1967) 1113.
84. R.M. Ishikawa, A.T. Hubbard, *J. Electroanal. Chem.*, **199** (1986) 187.
85. J. Clavilier, R. Faure, G. Guinet, R. Durand, *J. Electroanal. Chem.*, **107** (1980) 205.
86. K. Sashikata, Y. Matsui, K. Itaya, M.P. Songa, *J. Phys. Chem.*, **100** (1996) 20027.
87. N. Furuya, S. Koide, *Surf. Sci.*, **220** (1989) 18.
88. B.E. Conway, B. Barnet, H. Angerstein-Kozlowska, B. Tilka, *J. Phys. Chem.*, **93** (1990) 8361.
89. H. Angerstein-Kozlowska, B.E. Conway, A. Hamelin, *Electrochim. Acta*, **31** (1986) 1051.
90. M.P. Soriaga, *Progress in Surface Science*, **39** (1992) 325.
91. R.M. Ishiwaka, A.T. Hubbard, *J. Electroanal. Chem.*, **69** (1976) 317.
92. K. Yamamota, D.M. Kolb, R. Kotz, G. Lempfuhl, *J. Electroanal. Chem.*, **96** (1979) 233..
93. P.N. Ross, *J. Electroanal. Chem.*, **126** (1979) 67.
94. K. Itaya, S. Sugaware, K. Sashikata, N. Furuya, *J. Vac. Sci. Technol.*, A **8** (1990) 515.
95. D. Aberdam, R. Durand, R. Faure, F. El-Omar, *Surf. Sci.*, **171** (1986) 303.
96. F.T. Wagner, P.N. Ross, *J. Electroanal. Chem.*, **150** (1983) 141.
97. K. Yamamota, D.M. Kolb, R. Kotz, G. Lempfuhl, *J. Electroanal. Chem.*, **96** (1979) 233.
98. J. Clavilier, R. Faure, G. Guinet, R. Durand, *J. Electroanal. Chem.*, **107** (1980) 205.

99. F.H. Feddrix, E.B. Yeager, B.D. Cohen, *J. Electroanal. Chem.*, **330** (1992) 419.

100. G.A. Attard, A. Ahmadi, D.J. Jenkins, O.A. Hazzazi, P.B. Wells, K.G. Griffin, P. Johnston, J.E. Gillies, *Chem. Phys. Chem.*, **4** (2003) 123.

101. T. Hachiya, H. Honbo, K. Itaya, *J. Electroanal. Chem.*, **315** (1991) 275.

102. A. Martínez-Ruiz, J. Valenzuela-Benavides, L. Morales de la Garza, N. Batina, *Surf. Sci.*, **476** (2001) 139.

103. A. Hamelin, A. Katayama, G. Picq, P. Vennereau, *J. Electroanal. Chem.*, **113** (1980) 293.

104. A. Hamelin and A. Katayama, *J. Electroanal. Chem.*, **117** (1981) 221.

105. A. Hamelin and J. Lipkowski, *J. Electroanal. Chem.*, **171** (1984) 317.

106. E. Kirowa-Eisner, Y. Bonfil, D. Tzur, E. Gileadi, *J. Electroanal. Chem.*, **552** (2003) 171.

107. J. Hernández, J. Solla-Gullón, E. Herrero, *J. Electroanal. Chem.*, **574** (2004) 185.

108. K. Siegbahn, C. Nordling, A. Fahlman, R. Nordberg, K. Hamrin, J. Hedman, G. Johansson, T. Bergmark, S.E. Karlsson, I. Lindgren, B. Lindberg, *ESCA: Atomic, Molecular and Solid State Structure Studied by Means of Electron Spectroscopy*, Almquist and Wiksells, 1967.

109. J. Chastain, R.C. King Jr, H*andbook of x-ray photoelectron spectroscopy: a reference book of standard spectra for identification and interpretation of XPS data*, Eden Prairie, 1995.

110. J.M. Walls, R. Smith, *Surface Science Techniques*, Pergamon, 1994.

111. G.C. Bond, *Catal. Today*, **72** (2002) 5.

112. W.A. Bone, R.W. Wheeler, *Philos. Trans.*, **206a** (1906) 1.

113. M. Haruta, *Catal. Today*, **36** (1997) 153.

114. M. Haruta, N. Yamada, T. Kobayashi, S. Iijima, *J. Catal.*, **115** (1989) 301.

115. V. Idakiev, T. Tabakova, Z.Y. Yuan, B.L. Su, *App. Catal. A*, **270** (2004) 135.

116. H. Sakurai, T. Akita, S. Tsubota, M. Kiuchi, M. Haruta, *App. Catal. A*, in press (2005).

117. D. Andreeva, T. Tabakova, V. Idakiev, P. Christov, R. Giovanoli, *App. Catal. A*, **169** (1998) 9.

118. G.B. Hoflund, S.D. Gardner, D.R. Schryer, B.T. Upchurch, E.J. Kielin, *App. Catal. B*, **6** (1995) 117.

119. M.A. Bollinger, M. A. Vannice, *App. Catal. B*, **8** (1996) 417

120. K.-C. Wu, Y.-L. Tung, Y.-L. Chen, Y.-W. Chen, *App. Catal. B*, **53** (2004) 111.
121. P. Claus, *App. Catal. A,* In Press (2005).
122. G.J. Hutchings, *Catal. Today*, **72** (2002) 11.
123. S. Schimpf, M. Lucas, C. Mohr, U. Rodemerck, A. Brückner, J. Radnik, H. Hofmeister, P. Claus, *Catal. Today*, **72** (2002) 63.
124. W.A. Bone, G.W. Andrew, *Proc. Roy. Soc. A*, **109** (1925) 409.
125. G.C. Bond, P.A. Sermon, *Gold Bull* , **6** (1973) 102.
126. P.A. Sermon, G.C. Bond, P.B. Wells, *Faraday Trans.*, **75** (1979) 385.
127. M. Haruta, T. Kobayashi, H. Sano, N. Yamada, *Chem. Lett.*, **2** (1987) 405.
128. D. Cameron, R. Holliday, D. Thompson, *J. Power Sources*, **118** (2003) 298.
129. G.J. Hutchings, *Catal. Today*, **72** (2002) 11.
130. D. Andreeva, *Gold Bull.*, **35** (2002) 82.
131. M. Neurock, W.D. Provine, D.A. Dixon, G.W. Coulston, J.J. Lerou-Rutger, A. van Santen, *Chem. Eng. Sci.*, **51** (1996) 1691.
132. N. Macleod, J.M. Keel, R.M. Lambert, *App. Catal. A,* **261** (2004) 37.
133. *CatGold News*, 4 (2003).
134. T. Mallat, A. Baiker, *Catal. Today*, **19** (1994) 247.
135. K. Heyns, L. Blazejewicz, *Tet.*, **9** (1960) 67.
136. P. Gallezot, *Catal. Today*, **37** (1997) 405.
137. M. Besson, P. Gallezot, *Catal. Today*, **57** (2000) 127.
138. L. Prati, M. Rossi, *J. Catal.*, **176** (1998) 552.
139. S. Biella, G. L. Castiglioni, C. Fumagalli, L. Prati, M. Rossi, *Catal. Today,* **72** (2002) 43.
140. S. Baldi, L. Prati, M. Rossi, *J. Molec. Catal. A*, **197** (2003) 207.
141. M. Baldi, E. Finocchio, F. Milella, G. Busca, *App. Catal. B*, **16** (1998) 43.
142. S. Scirè, S. Minicòa, C. Crisafullia, C. Satrianoa, A. Pistone, *App. Catal. B,* **40** (2003) 43.
143. S.K. Samantaray, K. Parida, *App. Catal. B*, **57** (2005) 83.
144. N.D. Plint, N.J. Coville, D. Lack, G.L. Nattrass, T. Vallay, *J. Molec. Catal.* A, **165** (2001) 275.
145. H. Kimura, K. Tsuto, T. Wakisaka, Y. Kazumi, Y. Inaya, *App. Catal. A,* **96** (1993) 217.
146. H. Kimura, *App. Catal. A*, **105** (1993) 147.
147. R. Garcia, M. Besson, P. Gallezot, *App. Catal. A*, **127** (1995) 165.

148. P. Fordham, M. Besson, P. Gallezot, *App. Catal. A,* **133** (1995) L179.
149. P. Gallezot, *Catal. Today*, **37** (1997) 405.
150. B. Claudel, M. Nueilati, J. Andrieu, *App. Catal.*, **11** (1984) 217.
151. S. Carrettin, P. McMorn, P. Johnston, K.G. griffin, G.J. Hutchings, *Chem. Comm.*, (2002) 696.
152. S. Carrettin, P. McMorn, P. Johnston, K. Griffin, G.J. Hutchings, C.J. Kiely, *Phys. Chem. Chem. Phys*, **5** (2003) 1329.
153. S. Carrettin, P. McMorn, P. Johnston, K. Griffin, G.J. Hutchings, C.J. Kiely, G. Attard, *Top. Catal.*, **27** (2004) 131.
154. F. Porta, L. Prati, *J. Catal.*, **224** (2004) 397.
155. N. Dimitratos, F. Porta, L. Prati, *App. Catal. A*, In Press (2005).
156. C.L. Bianchi, P. Canton, N. Dimitratos, F. Porta, L. Prati, *Catal. Today*, **102-103** (2005) 203.
157. S. Demirel-Gülen, M. Lucas, P. Claus, *Catal. Today*, **102-103** (2005) 166 .
158. E.C. Venancio, W.T. Napporn and A.J. Motheo, *Electrochimica Acta*, **47** (2002) 1495.
159. B. Beden, I. Çetin, A. Kahyaoglu, D. Takky, C. Lamy, *J. Catal.* **104** (1987) 37.
160. A. Kahyaoglu, B. Beden, C. Lamy, *Electrochimica Acta*, **29** (1984) 1489.
161. M. L. Avramov-Ivic, J. M. Leger, C. Lamy, V. D. Jovic, S. D. Petrovic, *J. Electroanal. Chem.*, **308** (1991) 309.
162. M. Price, MPhil Thesis, Cardiff University, 2000.
163. S. Carrettin, PhD Thesis, Cardiff University, 2002.

Chapter Two

Experimental

2.1 Preparation of graphite-supported catalysts

2.1.1 Au/graphite

A slurry of Type 44 graphite (99 g) in deionised water (1 l) was stirred at room temperature for 15 min. The slurry was then heated to 333 K for a further 15 min, after which $NaHCO_3$ (5 g/g Au) was added. The slurry was then heated to 353 K for a further 30 min. An aqueous solution of $HAuCl_4$ (2.2 g/50 ml) was added dropwise to the slurry over a further 30 min. The slurry was then heated to boiling for 1 h. At this point the pH of the mixture was ~9. The slurry was then cooled to 353 K and HCHO (5 ml/g Au in 20 ml of deionised water) was added dropwise. The slurry was boiled for a final 30 min. The catalyst was cooled to room temperature and washed by the addition of 1 l deionised water. After the catalyst had settled, the water was decanted off. This cleaning procedure was repeated twice to remove traces of chloride. The catalyst was then filtered off under vacuum and dried in an oven overnight (383 K).

2, 1, 0.5, 0.25% Au/graphite catalysts have been prepared using this procedure.

2.1.2 Bi-Au/graphite

A sample of unmodified gold catalyst (~1 g) was placed in an evaporating basin together with a magnetic stirrer bar. A specific volume of $Bi(NO_3)_3$ (2.3×10^{-4} M) was added from a stock solution and the resultant slurry was stirred for 3 h. The catalyst was then filtered off under vacuum and washed with ultrapure water (250 ml). The catalyst was allowed to dry overnight at room temperature.

2.1.3 Pt/graphite

This catalyst was prepared at Johnson Matthey by Silvio Caritin; the preparation method is given elsewhere [1].

2.1.4 Au-Pt/graphite

A sample of the unmodified platinum catalyst (~1 g) was placed in a bubbler and NaOH (10 ml, 0.1 M) and ultrapure water (20 ml) were added. The bubbler was connected to a

hydrogen cylinder and hydrogen gas was passed through the slurry for 30 min prior to the addition of gold. This had two effects. Firstly, it maintained the catalyst in suspension and secondly, it subsequently aided the adsorption of the gold on to the surface of the platinum. The gold was then introduced as an aqueous solution of $HAuCl_4$ (various quantities) that was added drop-wise to the suspended slurry. The slurry was then transferred to a separating funnel that contained NaOH solution (50 ml, 0.1 M) and vigorously shaken to aid the adsorption of any last traces of gold in solution. The catalyst was then filtered under vacuum, washed with ultrapure water (500 ml) and dried at room temperature overnight.

2.1.5 Au Catalyst Sintering

A sample of the 2% Au/graphite catalyst was placed into a silica boat, which was placed into a Carbolite furnace. 5% H_2/Ar was passed through the furnace prior to experiment for 30 minutes to remove any air from the atmosphere inside the tube. The sample was then heated to the required temperature at a rate of 10 K min^{-1} under a constant flow of 5% H_2/Ar. On reaching the desired temperature, the sample was sintered for 3 h. On completion the furnace was switched off and allowed to cool under a constant flow of gas.

This procedure was carried out at 500 K, 600 K and 700 K resulting in a series of three catalysts. Another sample of the 2% Au/graphite was also treated in the same way and at the same temperatures but under air. This again resulted in a series of three catalysts.

2.2 Preparation of platinum single crystals

2.2.1 Pt{111}

A Pt{111} single crystal was prepared using the method developed by Clavilier in 1980 [2]. The tip of a Pt wire was melted in a methane-oxygen flame to create a single crystal bead about 3 mm in diameter. The crystal was mounted in a goniometer cradle and illuminated by a He-Ne laser (figures 2.1 and 2.2). From the defraction pattern obtained from the {111} and {100} facets on the crystal surface, it was possible to correctly position the crystal so that the appropriate face would be cut. The crystal was

then covered in two coatings of epoxy resin, which were allowed to set overnight; this treatment permitted the crystal to be held in place for grinding and polishing.

The initial crystal grinding (20 min) was carried out using a 600 grit paper wetted with distilled water, which removed the epoxy coating and began the grinding process. 1200 grit paper was then used for slightly finer grinding of the crystal (~1 h). Grinding was stopped just before the crystal reached halfway from the tip of the bead towards the stem (maximum surface area of hemispherical form).

The crystal was then polished using 2400 and 4000 grit papers to remove major scratches and imperfections from the surface, distilled water again being used as lubricant. The crystal was then polished with a Textmet polishing cloth coated in a 3 μm diamond spray, using blue diamond polishing lubricant for 1 h. This was then changed to a 1 μm diamond spray using red diamond polishing lubricant for 1 h. Finally, a 0.25 μm diamond spray was used again with the red diamond polishing lubricant. The quality of the crystal was checked at each stage using the laser.

Once a good surface had been obtained, the crystal was removed from the goniometer and heated gently using a cool Bunsen flame until it could be removed from the epoxy resin. It was then annealed in a hot Bunsen flame for 30 min to remove surface impurities.

The purity of the crystal was assessed from the diffraction pattern produced by the laser and by electrochemical characterisation. In previous cases the purity of a crystal had also been checked by LEED diffraction.

2.2.2 Other Pt crystals

Pt{755}, Pt{533}, Pt{110} and Pt{100} were also used in this study. These had been prepared at Cardiff previously by Robert Price [3].

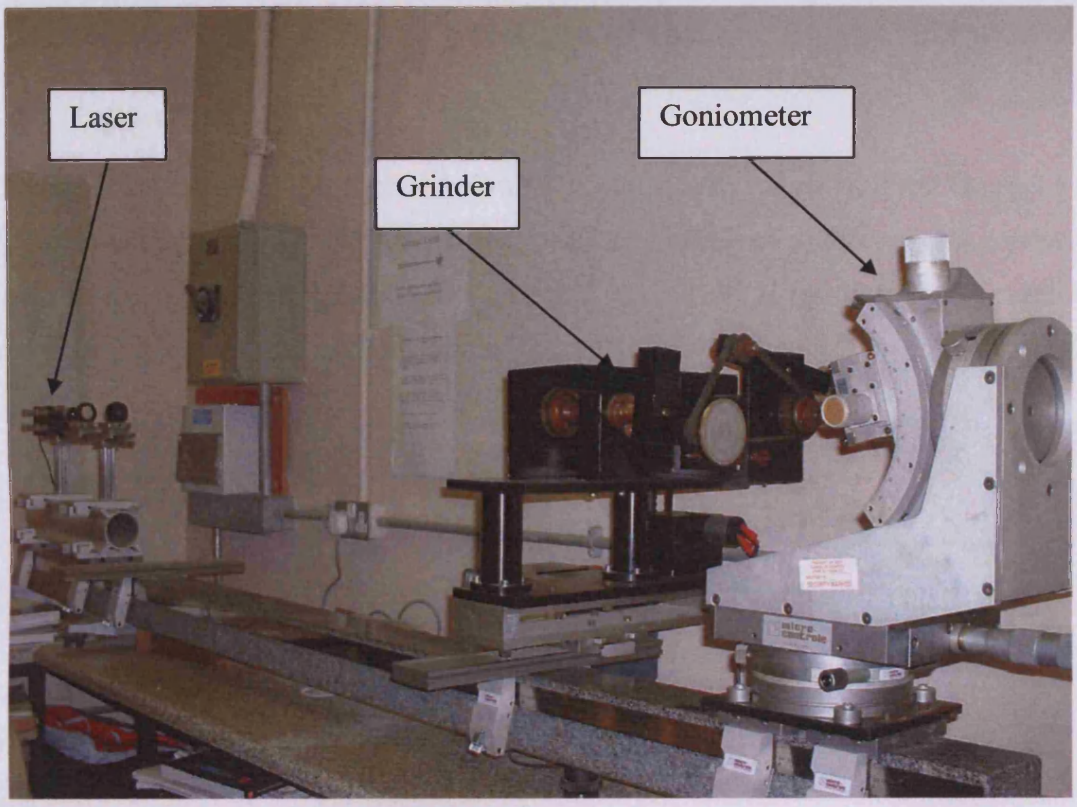

Figure 2.1: Single crystal preparation apparatus.

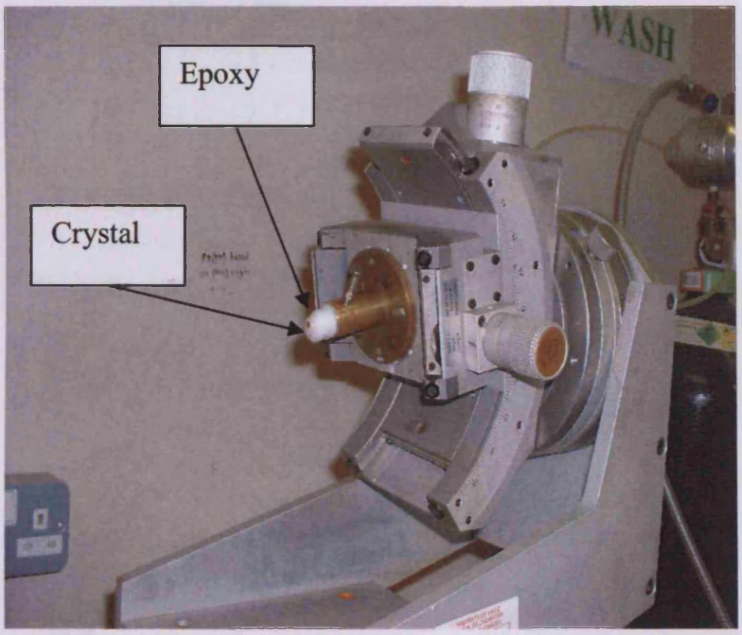

Figure 2.2: Goniometer and epoxy embedded crystal.

2.3 Electrochemical characterisation of metal catalyst surfaces

2.3.1 Apparatus

The electrochemical cell (described below) was connected to a potentiostat (Model 812 Electrochemical Analyser, CH Instruments) which in turn was connected to a computer running the control program CHI Version 2.06. This software allowed various techniques to be used and manipulation of the data obtained (figure 2.3).

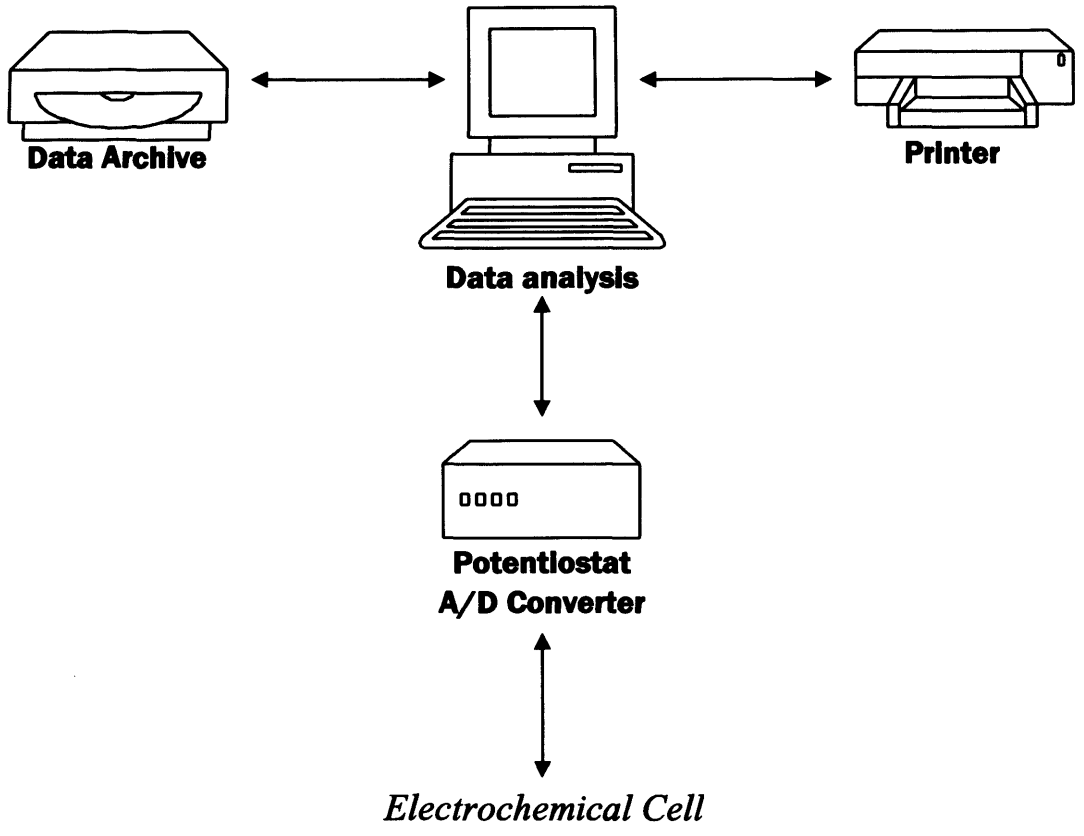

Figure 2.3: Schematic of the electrochemical set up.

A Milli-Q plus water system [4] (Millipore, Watford) provided ultrapure water for use in the preparation of electrolyte solutions and of solutions required for catalyst preparations. In addition this ultrapure water was used in the cleaning procedures employed when single crystals were being handled.

2.3.2 The electrochemical cell

The two-compartment electrochemical cell (figure 2.4) contained three electrodes, the working electrode, the reference electrode and the counter electrode. The working electrode was either a single crystal with a Pt wire contact attached or a piece of platinum mesh which supported the catalyst sample. Where the mesh was used typically 2 mg of catalyst was pressed into the mesh. The charged Pd/H reference electrode, housed in a second compartment, produced a stable potential for around 6 h. The counter electrode (a platinum mesh) was situated directly beneath the working electrode in a luggin capillary.

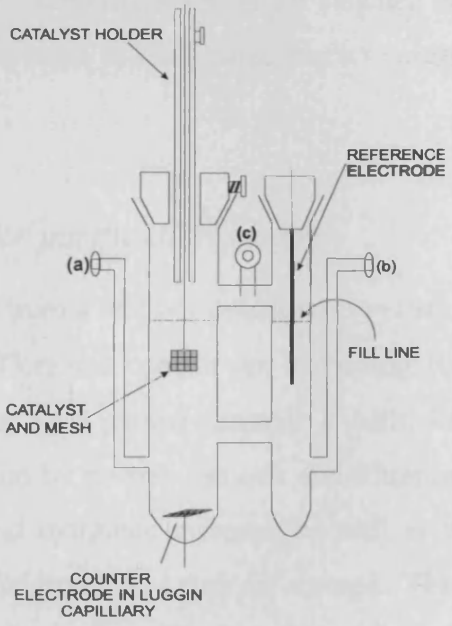

Figure 2.4: The electrochemical cell.

Two bridges connected the compartments. The lower bridge allowed a flow of electrolyte between the two halves of the cell. The upper bridge allowed N_2 gas to be established over the electrolyte solution which maintained anaerobic conditions in the electrolyte. One inlet was fitted to the bottom of each compartment; the one fitted to the reference half of the cell was used to introduce H_2 gas so as to charge the reference electrode, and the other was connected to the working electrode compartment so that N_2 could be bubbled through to de-gas the electrolyte.

2.3.3 Cleaning of the electrochemical cell

Due to the sensitivity of cyclic voltammetry of platinum to impurities, the cell and all ancillary glassware had to be thoroughly clean. To this end glassware was soaked overnight in "green acid" (concentrated H_2SO_4 acid into which a few grains of $KMnO_4$ had been dissolved). The colour of the $KMnO_4$ acted as a visual indicator to the cell's cleanliness, since a still dirty cell would cause the green acid to lose its colour, indicating that further cleaning was required. When fresh "green acid" gave no colour change the cell was emptied and then thoroughly washed with ultrapure water.

In the case of single crystal electrochemistry, a further step was used to ensure the glassware was ultra clean. Glassware was either steamed or boiled in ultra-pure water for 30 min. This was repeated at least twice more to ensure the glassware was ultra clean.

2.3.4 The Milli-Q water purification system

Ultrapure water obtained from a Milli-Q purification system, showed a resistivity of 18 $M\Omega\ cm^{-1}$ and had a total organic content not exceeding 10 ppb. In the first stage of purification, mains water was passed through a Milli-RO 10 plus system, which provided initial purification by reverse osmosis and filtration through activated carbon. This removed organic and inorganic material, as well as bacteria and chloride. The purified water was then fed into a 60 l tank for storage. This tank was connected to the second purification apparatus, the Milli-Q system, which consisted of a mixed resin purification pack through which the water was continually cycled until the resistivity of 18 $M\Omega\ cm^{-1}$ was reached.

2.3.5 Preparation of the electrochemical cell

The palladium-hydrogen reference electrode was charged before each electrochemical experiment. First the electrode was heated red-hot in a Bunsen flame to remove surface contaminants [2]. It was then placed in the cell, which had been filled to the mark with ultrapure water. H_2 gas was then bubbled over the reference electrode, which maintained a constant potential of 50 mV vs. SHE for up to 6 hours. The cell was then emptied of water and filled with the appropriate electrolyte.

Finally the contents of cell were 'de-gassed' by passing N_2 through the electrolyte for 20 min. This removed any dissolved oxygen. The N_2 was then passed over the surface of the electrolyte to maintain it in an oxygen-free state.

2.3.6 Procedure used to obtain a cyclic voltammogram: supported catalysts

The platinum mesh working electrode and its attached wire were held in a Bunsen flame until yellow-hot, to remove any surface contaminants. After the mesh had cooled, a sample of the catalyst to be tested was pressed into the mesh. The wire was then fed into a glass capillary that was, in turn, held in a Teflon holder (see figure 2.4). The electrode was then placed in the electrochemical cell, just above the electrolyte. The potentiostat leads where then connected to the cell electrodes in the following order: reference electrode, counter electrode and finally the working electrode. The mesh was then lowered into the electrolyte by loosening the screw on the side of the Teflon holder; this allowed the glass capillary to be lowered so that contact could be made. The screw was then retightened. Before the commencement of the electrochemical sweep, it was necessary to hold the potential at 0 V for 2 min. This was done to remove the oxide layer that was present on the surface of the catalyst and relieve the associated surface reconstruction [5]. The effect this had on the voltammogram obtained can be seen below (figure 2.5). The electrochemical experiment could then be undertaken. Typically catalyst voltammograms were run at 10 mV s^{-1} in order to minimise Ohmic drop.

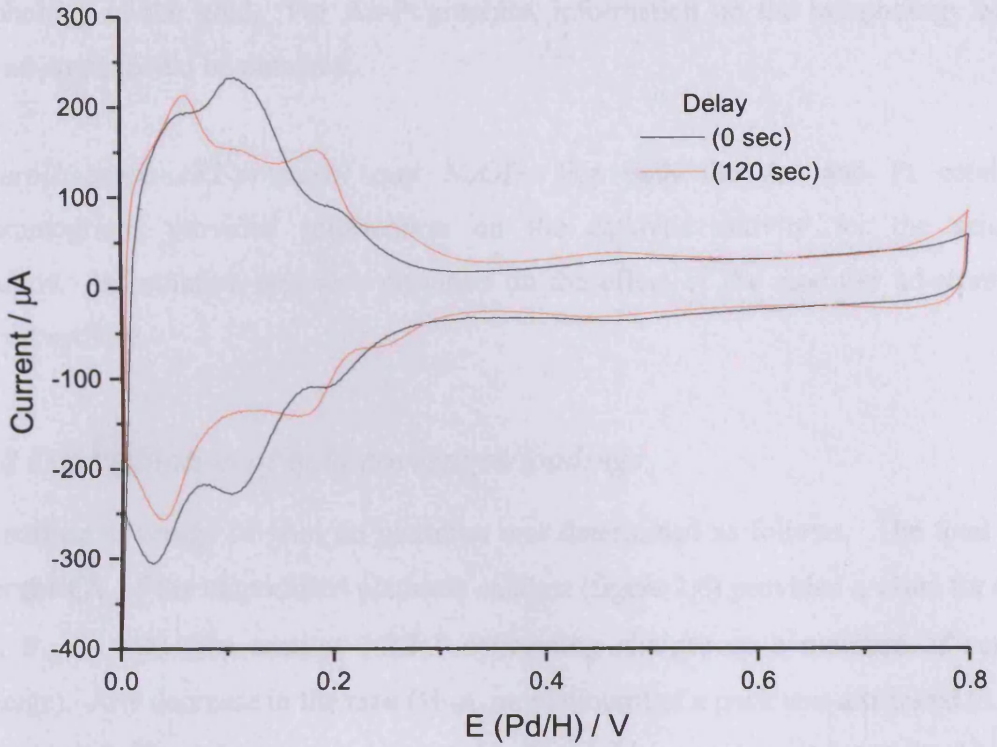

Figure 2.5: Voltammograms produced by a platinum working electrode wire held in glass capillary and Teflon holder. The stripping of the platinum oxide surface layer results in a reconstructed, clean platinum surface.

2.3.7 Electrochemical characterisation methods

Depending on the electrolyte used, various types of morphological and catalytic information could be obtained by cyclic voltammetry. Unless stated otherwise the concentration of the electrolyte was 0.5 M.

H_2SO_4 electrolyte: For Bi-Au/graphite, voltammograms provided information on the amount of bismuth adsorbed and its state (i.e. monolayer or multilayer). For Au-Pt/graphite voltammograms provided information on the extent of gold coverage and the location of Au atoms on the surface of the platinum.

NaOH electrolyte: For Bi-Au/graphite, voltammograms showed the presence or absence of a reduction peak that was linked to catalytic activity and its modification by the introduction of the bismuth.

Pb electrolyte: For Bi-Au/graphite, voltammograms provided information on the morphology of the gold. For Au-Pt/graphite, information on the morphology of the gold ad-atoms could be obtained.

Glycerol/1-propanol/2-propanol and NaOH: For both the Au and Pt catalysts, voltammograms provided information on the catalytic activity for the selected oxidation. Information was also provided on the effect of the modifier ad-atoms on catalyst activity.

2.3.8 Determination of gold coverages/loadings

The surface coverage of gold on platinum was determined as follows. The total area under the CV of the unmodified platinum catalyst (figure 2.6) provided a value for θ_{Pt} = 1.00, θ_{Au} = 0.00 (see section 1.2.3.3 concerning charges as a measure of surface coverage). Any decrease in the area (H_{UPD} on platinum) of a peak was attributed to gold coverage since H_{UPD} does not occur on gold. The gold coverage was determined by use of the following equation:

$$\theta_{Au} = \theta_{Pt=1} - \theta_{Pt} \qquad \textbf{(2.1)}$$

where:

θ_{Au} is the calculated gold coverage, $\theta_{Pt=1}$ is the platinum coverage before gold is introduced and θ_{Pt} is the platinum coverage after gold has been introduced.

In all cases θ is defined from the relative charges under the H_{UPD} peaks with the clean platinum surface defined as $\theta_{Pt=1}$. The area used for this calculation is indicated below and takes into account the {110} step, the {100} step, the {100} terrace and the {111} terrace.

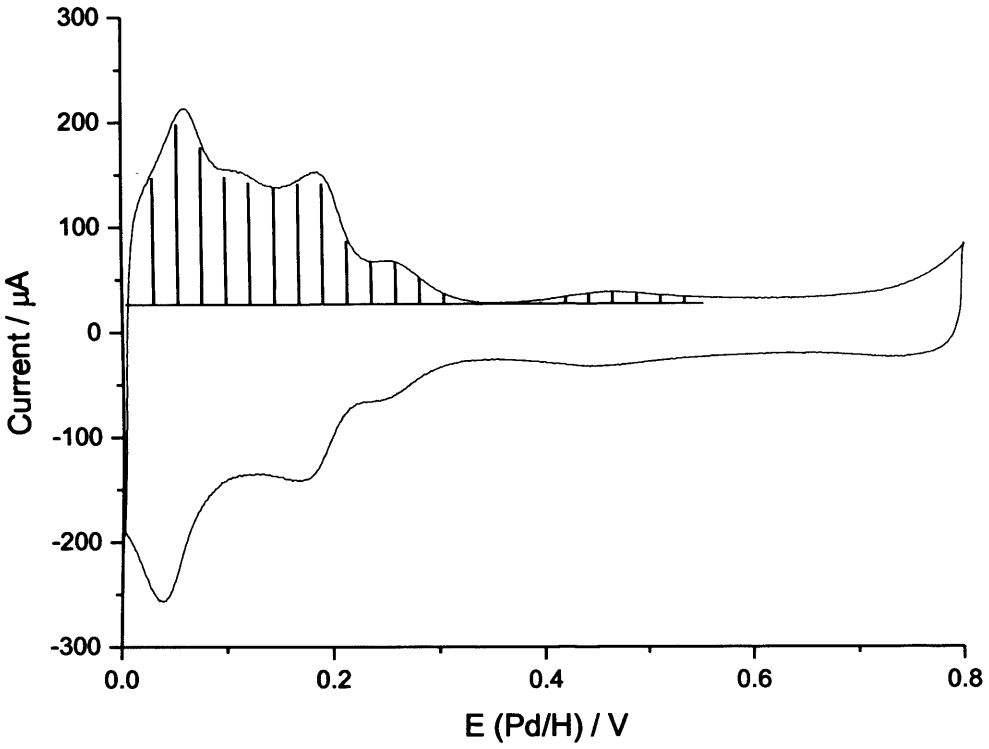

Figure 2.6: Voltammogram in 0.5 M H_2SO_4 at 10 mV s^{-1} showing the H_{UPD} region for the 5% Pt/graphite catalyst and the area used to calculate the relative coverage is shaded.

In principle, the relative surface area of the gold catalysts could be calculated in a similar manner, but using Pb_{UPD} as the probe.

2.3.9 Procedure used to obtain cyclic voltammograms: single crystal catalysts

Each platinum single crystal was attached to a platinum wire. The wire was fed into a vertical glass capillary, and the crystal manoeuvred with tweezers until the flat surface was exactly parallel with the electrolyte surface and horizontal. The crystal was then etched in concentrated nitric acid for 10 sec to remove any adsorbed metal atoms and rinsed with ultrapure water. The crystal was then flame annealed in a Bunsen flame until yellow-hot to remove any surface contaminants and to ensure that the surface was well ordered [2]. The crystal was then removed from the flame and as soon as the colour had faded, the crystal was placed in a hydrogen bubbler (Fig 2.7), just above the level of the water. The crystal was then allowed to cool for a further 30 sec in a flow of

hydrogen before being lowered into the ultra-pure water. This procedure prevented stressing the crystal by rapid quenching and thermal shock and hence prolonged its lifetime. The crystal was then lowered into the ultrapure water for one second and withdrawn; this caused a droplet of water to adhere to the surface of the crystal and this prevented contamination by air as it was transferred to the electrochemical cell.

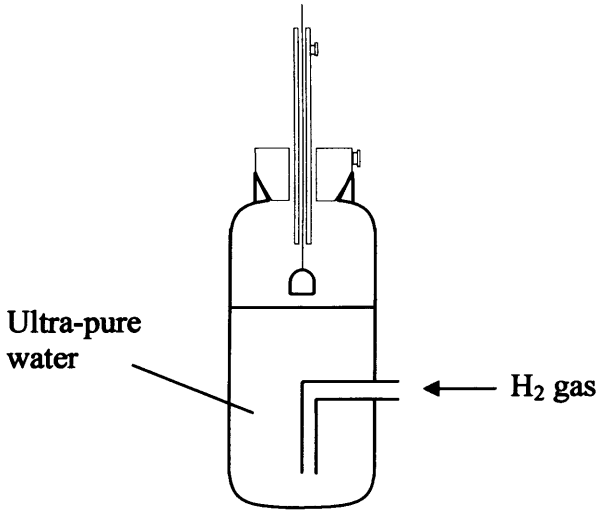

Figure 2.7: Hydrogen bubbler.

After connecting the electrodes as previously described, the crystal was lowered until it just touched the surface of the electrolyte, and then slightly withdrawn so as to establish a good meniscus contact (figure 2.8). Typically, single crystal voltammograms were run at 50 mVs^{-1}.

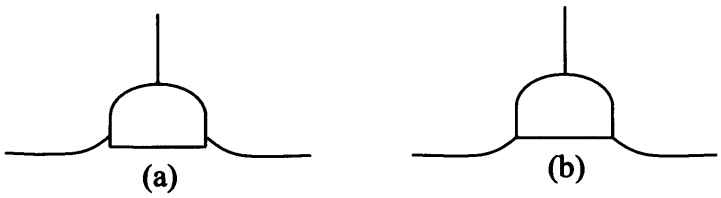

Figure 2.8: (a) A bad meniscus contact (sides of crystal wetted) and (b) a good meniscus contact (only flat, polished surface is in contact with the electrolyte).

2.3.10 Gold deposition onto platinum single crystals

2.3.10.1 The immersion method

A flame-annealed Pt crystal, protected by a droplet of ultrapure water, was dipped into an aqueous solution of chloroauric acid for ten seconds. The crystal was then rinsed with ultrapure water and transferred to the cell. If a higher coverage of Au was required the dipping procedure was repeated.

2.3.10.2 The forced deposition method

The forced deposition method [6] was used to obtain a high coverage of gold. The technique follows the immersion method up to the point where the crystal is dipped in chloroauric acid solution. The crystal was dipped for just a second, to obtain a droplet of the solution on the end of the crystal, and then transferred to the hydrogen bubbler. Hydrogen adsorbed onto the Pt surface and dissociated producing electrons and protons which caused reduction of the $Au^{3+}_{(aq)}$ to ions $Au_{(ads)}$. After 30 sec in the bubbler, the crystal was removed, washed with ultrapure water and transferred to the electrochemical cell.

2.3.11 Electrooxidation of organic molecules using single crystals

The electrooxidation of organic molecules on single crystals required the use of two cells. The first, filled with 0.1 M H_2SO_4, was used to check the structure and composition of the Pt and Au-modified Pt single crystals. The second was filled with NaOH (0.1 M) and the organic compound to be oxidised (0.1 M). The prepared Pt or Au-Pt crystal was placed into the first cell; a CV was obtained, and then transferred to the second cell where electrooxidation was carried out.

2.4 Oxidations in the high pressure reactor

2.4.1 Parr reactor

Oxidations were carried out in a Parr high-pressure reactor (fig 2.9). The 50 ml reaction vessel was made from 316-grade stainless steel and was fitted with a Teflon liner. Reactions were typically run using 3 bar pressure of pure O_2. A mechanical impeller

stirred the reactor and was driven by an integrated motor controlled by a separate unit. This unit also controlled the vessel temperature via a thermocouple and heating ring. Reactions were typically conducted at 333 K.

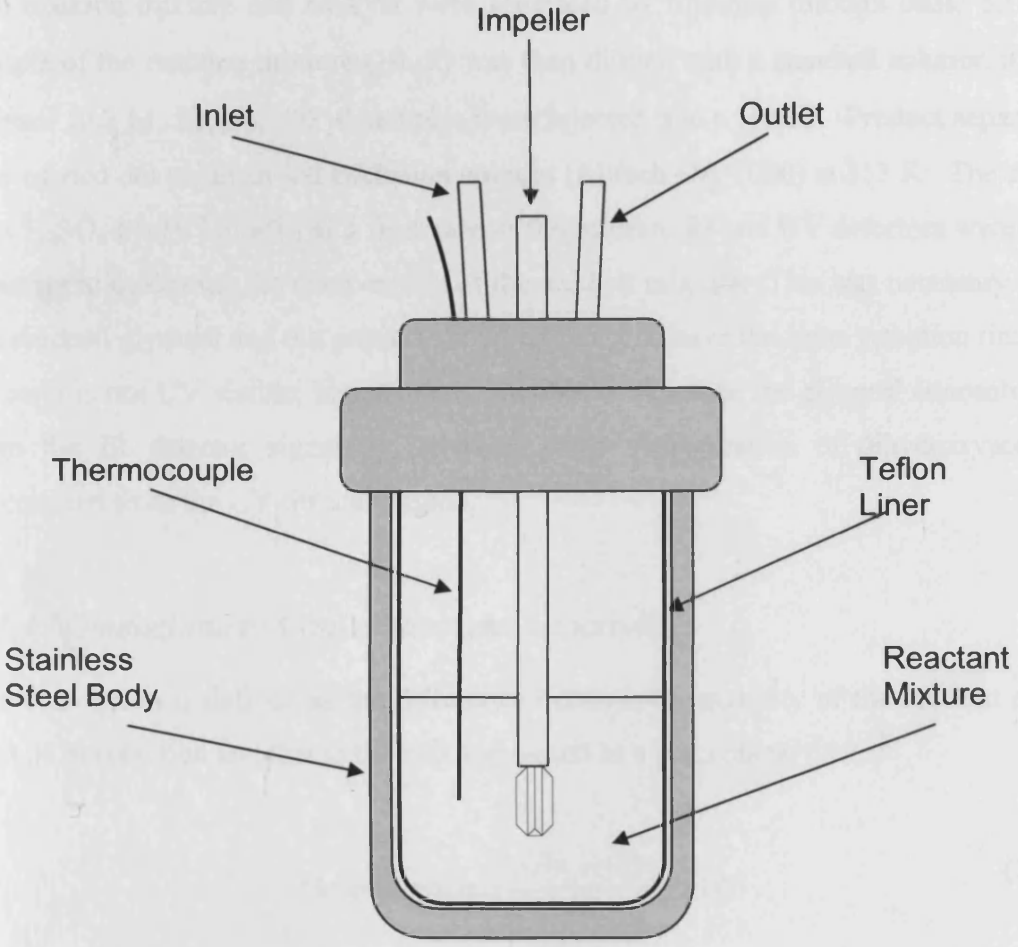

Figure 2.9: Schematic of Parr reactor.

2.4.2 Typical procedure

Reactant (equimolar with NaOH) was dissolved in 20 ml of distilled water and placed in the Teflon liner. NaOH (0.5 g, 12.5 mmol) was then added, followed by the appropriate amount of catalyst. The liner was then placed in the vessel and the reactor was sealed. After connecting all instruments, the headspace within the reactor was purged with O_2 three times to remove air. The vessel was then pressurised to 3 bar O_2 and heated to 333 K. Once this temperature had been reached, the stirrer was engaged and set to 1500

rpm, and reaction started. Reactions were run for 3 h. Variations in method are indicated were applicable.

2.4.3 Product recovery

The reaction mixture and catalyst were separated by filtration through celite 521. A sample of the reaction mixture (10 μl) was then diluted with a standard solution of iso-butanol (0.2 M, 100μl). 20 μl samples were injected into a HPLC. Product separation was carried out using an ion exclusion column (Alltech OA-1000) at 353 K. The eluent was H_2SO_4 ($4x10^{-4}$ mol/L) at a flow rate of 0.8 ml/min. RI and UV detectors were used in series to determine the composition of the product mixture. This was necessary since the reactant glycerol and the product dihydroxyacetone have the same retention time but glycerol is not UV visible; hence it was possible to calculate the glycerol concentration from the IR detector signal by subtracting the concentration of dihydroxyacetone determined from the UV detector signal.

2.4.4 Nomenclature: Conversion and selectivity

The conversion is defined as the difference between the quantity of the reactant at the start of the reaction and that at the end, expressed as a percentage:

$$\%Conversion = \frac{(Gly_i - Gly_f)}{Gly_i} \times 100 \qquad \textbf{(2.2)}$$

where:

Gly_i is the initial concentration of glycerol in the reaction vessel and Gly_f is the final concentration of glycerol in the reaction vessel.

The selectivity is defined as the number of moles of an individual product formed over the total number of moles of reactant consumed (i.e. conversion) [7].

$$\%Selectivity = \frac{product_M}{conversion_M} \times 100 \qquad \textbf{(2.3)}$$

where:

$product_M$ is the amount of individual product formed expressed in mol l^{-1} and $Conversion_M$ is the total extent of conversion obtained expressed in mol l^{-1}.

2.5 XPS

The XPS data presented in this thesis was obtained at the CCLRC laboratories in Daresbury using a Scienta ESCA300 Spectrometer (figure 2.10).

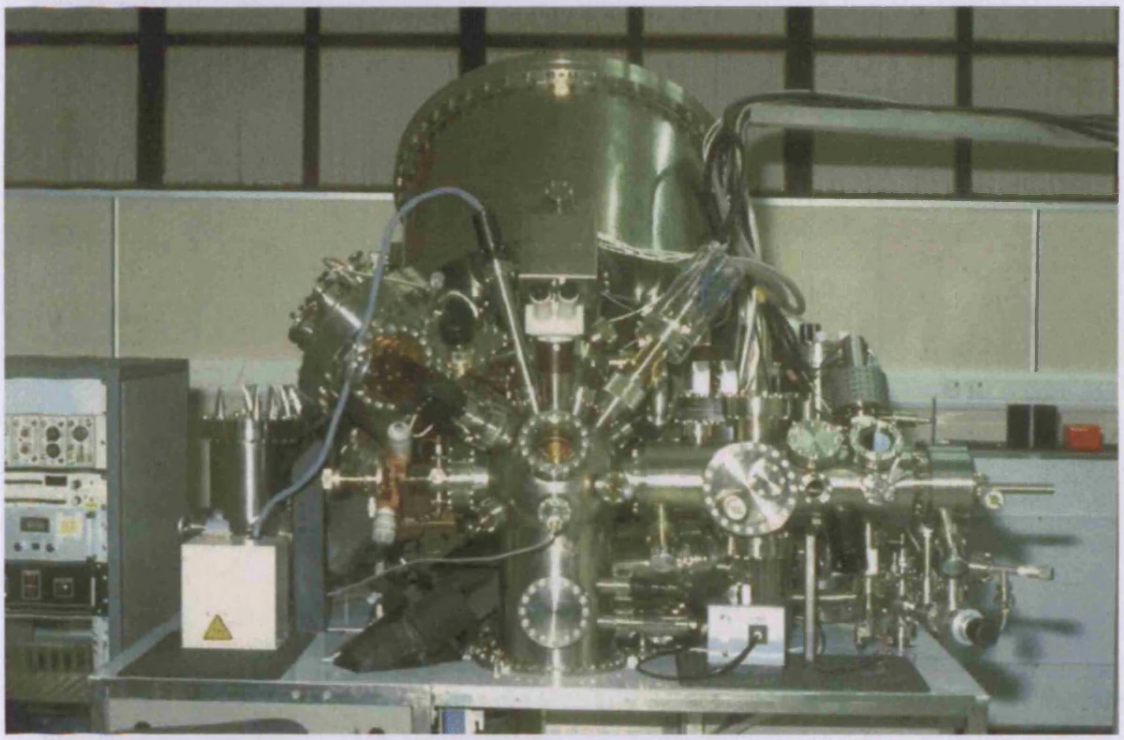

Figure 2.10: Scienta ESCA300 Spectrometer.

A thin layer of the catalyst to be tested was attached to a silver holder by double sided sticky tape. This was placed onto a rack-and-pinion transfer arm in the fast-entry chamber, which was then sealed and pumped down to $5x10^{-5}$ mbar by opening valve (a), which was connected to the turbo pump. On reaching the appropriate pressure valve (a) was closed and valve (c) was opened. The sample was then wound across into the preparation chamber where it was transferred to a second rack-and-pinion transfer arm via a wobble stick. The first arm was then wound back to the fast-entry chamber and valve (c) closed. Once the pressure in the preparation chamber had reached $2x10^{-8}$ mbar, valve (d) was opened and the rack-and-pinion transfer arm wound into the sample

chamber. The sample was then transferred to the Manipulator cradle via a wobble stick and the transfer arm wound back to the preparation chamber. Valve (d) was then closed and the sample positioned in front of the x-ray source by external *x*, *y*, *z* and θ manipulators. The experiment was then carried out and controlled by computer. To remove the sample from the chamber the reverse of the above procedure was employed and when the sample was back in the fast-entry chamber, dry nitrogen was pumped in by opening valve (b), bring the chamber up to ambient pressure.

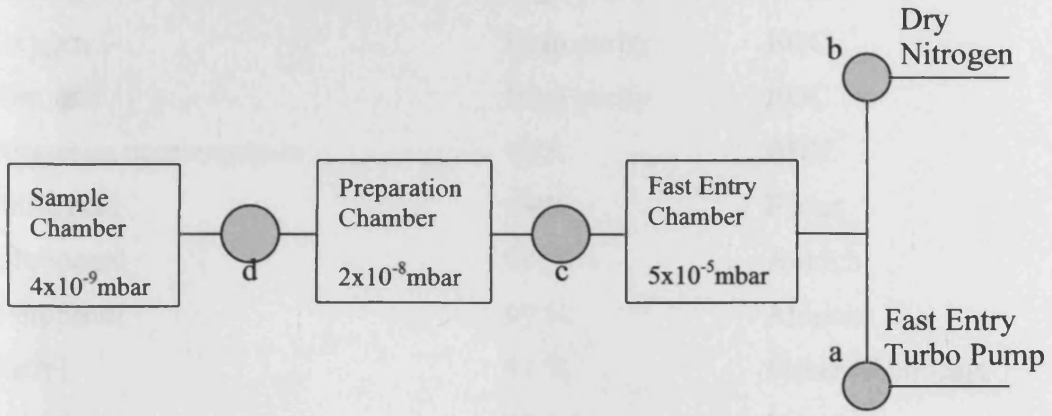

Figure 3.11: Schematic of the separate chambers within the Scienta ESCA300 Spectrometer.

2.6 TEM

TEM images of the Au and Bi-Au/graphite catalysts were obtained by Gregory Goodlet of JM at Sonning.

2.7 Chemical Reagents Used

Table 2.1: Table of chemical reagents used during experimentation.

Reagent	Quality	Supplier
Chloroauric acid	99.99 %	Johnson Matthey
Bismuth nitrate	98 %	BDH
Sulphuric acid	GPR	Fisher Chemicals
Sulphuric acid	Aristar	BDH
Hydrogen	High purity	BOC
Oxygen	High purity	BOC
Nitrogen	High purity	BOC
Potassium permanganate	GPR	BDH
Nitric acid	GPR	Fisher
1-Propanol	99 %	Aldrich
2-propanol	99 %	Aldrich
NaOH	97 %	Fisher Chemicals
Lead nitrate	99.5 %	Fisons
Platinum wire	99.999 %	Goodfellows
Glycerol	99 %	Fisher Chemicals
Gold wire	99.999 %	Goodfellows

2.8 References

1. S. Carrettin, PhD Thesis, Cardiff University, 2002.
2. J. Clavilier, R. Faure, G. Guinet, R. Durand, *J. Electroanal. Chem.*, **107** (1980) 205.
3. R. Price, PhD Thesis, Cardiff University, 1995.
4. Millipore General Catalogue, Millipore Ltd, Watford.
5. G.A. Attard, J.E. Gillies, C.A. Harris, D.J. Jenkins, P. Johnston, M.A. Price, D.J. Watson, P.B. Wells, *Appl. Catal. A.*, **222** (2001) 393.
6. J. Clavilier, M.J. Llorca, J.M. Feliu, A. Aldaz, *J.Electroanal. Chem.*, **351** (1993) 299.
7. I.M. Campbell, *Catalysis at Surfaces*, University Press, 1988.

Chapter Three

Results

3.1 Graphite-supported and single crystal Au-Pt catalysts: characterisation and activity towards propanol oxidation

3.1.1 Introduction

All experiments carried out in this section involved the use of the 5% Pt/graphite catalyst described in section 2.1.3. Cyclic voltammetry was used to determine the location of gold ad-atoms on the surface of the Pt/graphite catalyst and to determine the morphology of the gold (i.e. which facets were present). This characterisation data was complimented by an XPS analysis. Voltammograms were acquired under basic conditions to investigate the second oxide peak observed by Hutchings on supported gold catalysts [1]. Electrooxidation was carried out to determine the effect gold had on the activity of platinum for propanol electrooxidation. Oxidation was then performed in a high-pressure reactor to determine catalytic conversion and selectivity under reaction conditions. A single crystal study was undertaken to illuminate the results obtained.

Gold modified platinum catalysts were chosen for this section of work as gold-platinum alloys have already been investigated for glycerol oxidation by Prati and found to be active [2-3]. Hence an understanding of the relationship between the surface structure of gold modified platinum catalysts and activity was desirable. In addition since platinum undergoes H_{UPD}, the relative gold loading on the platinum could be determined and so the relationship between surface structure and activity could be more thoroughly investigated than with pure gold catalysts. Hence gold modified supported platinum catalysts appeared to offer an ideal starting point for this investigation.

As stated in the introduction propanol oxidation was chosen as the introductory test reaction due to the limited number of liquid phase products which could be obtained from it [4]. It was again hoped that this simplicity would allow a better understanding of the relationship between surface structure and activity.

3.1.2 Characterisation of gold-modified platinum catalysts: CVs collected under acidic conditions

Figure 3.1.1 shows that the unmodified Pt/graphite catalyst consisted of well defined steps ({110} and {100}) and terraces ({100} and {111}). Even though {111} steps are not directly identifiable, it is likely that they contribute to the overall signal obtained in the 0 – 0.2 V region of the voltammogram. The peak at 0.1 V is associated with {110}-type defects [5] and this can indicate a rough surface. A series of six gold-modified platinum catalysts were prepared by dosing 5% Pt/graphite with increasing quantities of gold (see section 2.1.4). The increasing gold loading was observed in the CVs as a decrease in the size of the platinum H-UPD peaks due to gold blocking the platinum surface (figure 3.1.1), as has been observed with gold deposited onto platinum electrodes [6]. The initial introduction of gold removed a significant portion of the platinum {110} steps and {100} terraces. At medium to high doses of gold all of the platinum peaks were reduced at the same rate. This indicated that gold showed an initial preference for the {110} step and {100} terrace sites before becoming non-site specific in its adsorption. This is in contrast to other metals adsorbed on platinum, which have shown high site specificity (e.g. bismuth and sulphur) [7].

Also of note is a slight positive shift in the potential of all the peaks corresponding to catalysts dosed with gold. This may indicate a change in the electronic properties of the platinum due to the introduction of gold and may be important in relation to the catalytic properties of these catalysts, which will be discussed later.

Table 3.1.1 shows the volumes of the gold solution used to dose the catalyst and the corresponding platinum blocking obtained (based on the CVs presented in figure 3.1.1). Obtaining very low gold coverages ($\theta_{Au} < 0.1$) or high gold coverages ($\theta_{Au} > 0.7$) proved to be difficult. When attempting to create $\theta_{Au} < 0.1$ either no gold would be deposited or too much was adsorbed. This was also the case when high gold loadings were attempted. As such getting a steady progression of gold adsorbed on to the platinum was not possible and instead the gold went on in stages, as seen in figure 3.1.1. This is exemplified by table 3.1.1 where the platinum coverage more than doubled on progression from the 5 ml to the 10 ml gold dosed catalysts, but a six fold increase in gold dosing (between 10 ml and 60 ml) did not even come close to doubling the

platinum surface coverage. This may indicate that the gold was either adsorbing onto the support or that the gold was growing as islands on the platinum surface. Hence gold loading would not be proportional to the extent of platinum site blocking.

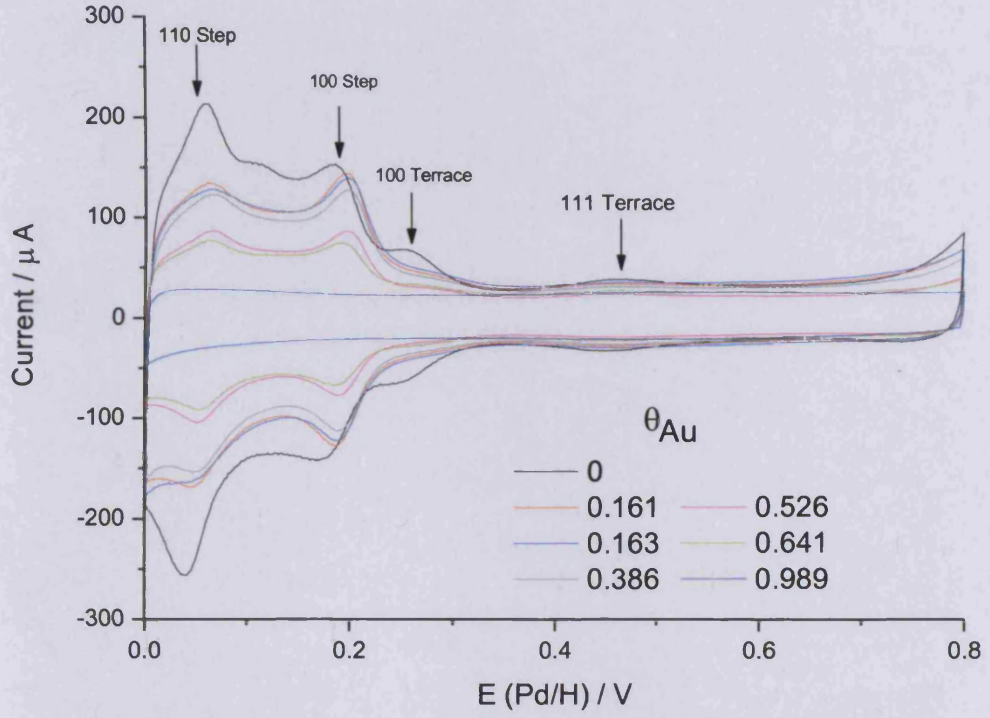

Figure 3.1.1: CVs in 0.5 M H_2SO_4 at 10 mV s^{-1} showing the hydrogen-UPD region for the 5% Pt/graphite catalyst and its subsequent change in structure on adsorption of gold.

Table 3.1.1: Dosing volumes used in the modification of 5% Pt/graphite and the corresponding Au coverage as determined from CVs.

Gold Dosing / ml	Surface coverage / θ_{Au}
0	0
1	0.161
5	0.163
10	0.386
15	0.526
60	0.641
100	0.989

By sweeping the applied potential to values beyond 0.8 V the oxide region of the CVs was obtained (figure 3.1.2). At these more positive potentials, further peaks were observed in the voltammogram which were attributed to the formation and loss of oxide layers on the platinum and gold surfaces. At low loadings, gold suppressed platinum oxide formation by site-blocking, as represented by a peak that extended from 0.7 V to 1.6 V in the forward cycle. A peak which only became visible at medium to high loadings of gold (present at 1.4 V in the forward cycle) was attributed to gold oxide formation. It was not observed at low gold loadings due to the platinum oxide masking the signal. In the reverse sweep the platinum oxide-reduction peak was visible at 0.5 V on the unmodified platinum catalyst. Deposition of small quantities of gold modified this peak, which grew in intensity and moved to more positive potential. Higher gold additions caused the peak to shift positive again but this time with a decrease in intensity. This suggested that the introduction of gold modified the electronic properties of the platinum by weakening the Pt-oxide bond and at higher gold loadings the extent of exposure of the platinum surface to the electrolyte was reduced by site-blocking, hence the quantity of Pt-oxide was reduced as well.

The gold oxide reduction peak was observed at 1.1 V in the reverse sweep and grew with gold loading. However the growth of the gold peak was not systematic and did not precisely correspond with the amount of gold coverage determined by the extent of platinum blocking observed in table 3.1.1. This again suggests that some of the gold might have been deposited onto the graphite support and not on the platinum. If this was the case then the extent of platinum blocking would not be a true indication of the extent of gold loading. Alternatively the gold might have been adsorbing as islands on the surface of the platinum and not layers, such as in the case of the Volmer-Weber model which suggests 3-D crystallite growth [8] or in the case of the simultaneous multilayers [9] growth model.

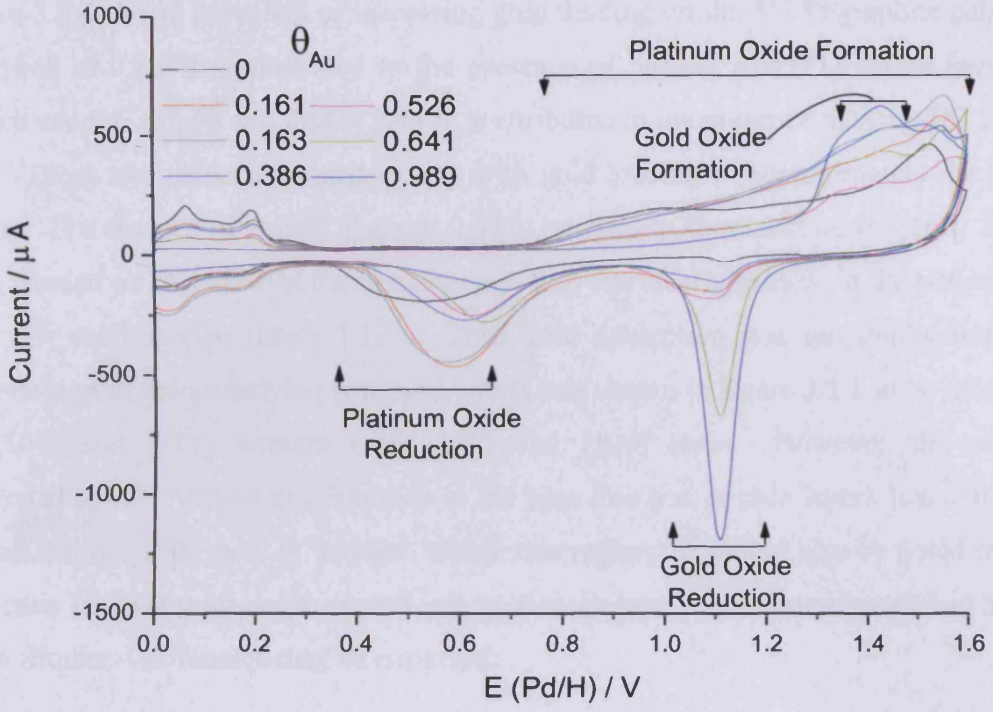

Figure 3.1.2: CVs in 0.5 M H_2SO_4 at 10 mV s^{-1} showing the hydrogen-UPD region and the oxide region of the 5% Pt/graphite catalyst and its subsequent modification on adsorption of gold.

3.1.3 Characterisation of gold-modified platinum catalysts: CVs involving Pb_{UPD}

Since both platinum and gold were potentially active catalysts for the reaction under investigation, it was necessary to more thoroughly investigate the extent of gold loading by means other than H_{UPD}. To this end Pb_{UPD} was carried out on the catalysts. In addition to determining the relative gold loading on each catalyst, this technique was also used to determine the surface structure of the gold deposited on the platinum, as shown by figure 3.1.3. Care needed to be taken with the interpretation as far as Au{110} facets were concerned. Clearly Pb_{UPD} on Pt sites overlaps with the process of Pb UPD on Au{110}. In spite of this, it is evident that at $\theta_{Au} = 0.99$, all voltammeteric features are representative of a gold surface as judged by interpretation of similar data [10]. However due to the close proximity of the Pt and Au{110} features, it was not possible to determine the true gold loading quantitatively; rather it was evaluated qualitatively.

Figure 3.1.4 shows the effect of increasing gold loading on the 5% Pt/graphite catalyst. The peak at 0.28 V is attributed to the presence of narrow Au{111} facets (average terrace under 6 atoms) and that at 0.45 V is attributed to the presence of Au{110} facets [10]. These two peaks increased in size with gold loading to approximately the same extent. The absence of a peak at about 0.37 V appears to show that no Au{100} facets were formed on this catalyst surface although they are clearly present in the underlying platinum catalyst (see figure 3.1.1). Thus gold adsorption was not duplicating the morphology of the underlying platinum which was shown in figure 3.1.1 to be made up of {100} and {111} terraces with {110} and {100} steps. However, the current generated at 0.37 V does not diminish to the base line (i.e. double layer), hence it may be that the Au{100} peak is 'hidden' within this region. It should also be noted that in reference 10, *bulk* gold single crystal, not gold monolayers were investigated and hence some structural difference may be expected.

Increasing gold loading resulted in the Au{111} peak increasing in size indicating a greater amount of gold had been adsorbed. This is in agreement with the general trends established by the voltammograms showing H_{UPD} and oxide formation. However the H_{UPD} showed the gold blocking of platinum as occurring in groups, here (apart from the 0.161 and 0.163 catalysts) the peak sizes increased consistently with gold loading. This increased gold response for some catalysts without the appropriate increase in H_{UPD} blocking of the Pt indicated that excess gold was adsorbing either on to the graphite or that the gold was building in islands on the surface of the platinum, as was predicted from the earlier results. On progressing to 0.989 coverage, the size of the Au{111} peak had not increased significantly, however the Au{110} peak had. This indicated that the significant increased platinum blocking seen in H_{UPD} was a result of the formation of the Au{110} sites over the platinum. These would correspond to sites associated with the junction between two {111} planes.

The peak at 0.45 V (Au{110}) generally increased with gold loading. However, it is of interest that the peak for the 0.526 catalyst appears to be out of sequence compared with this trend. The fact that the 0.526 catalyst is out of order indicates that the catalyst is behaving somewhat differently from the others and this may result in an unusual electrocatalytic or catalytic activity trend being observed later.

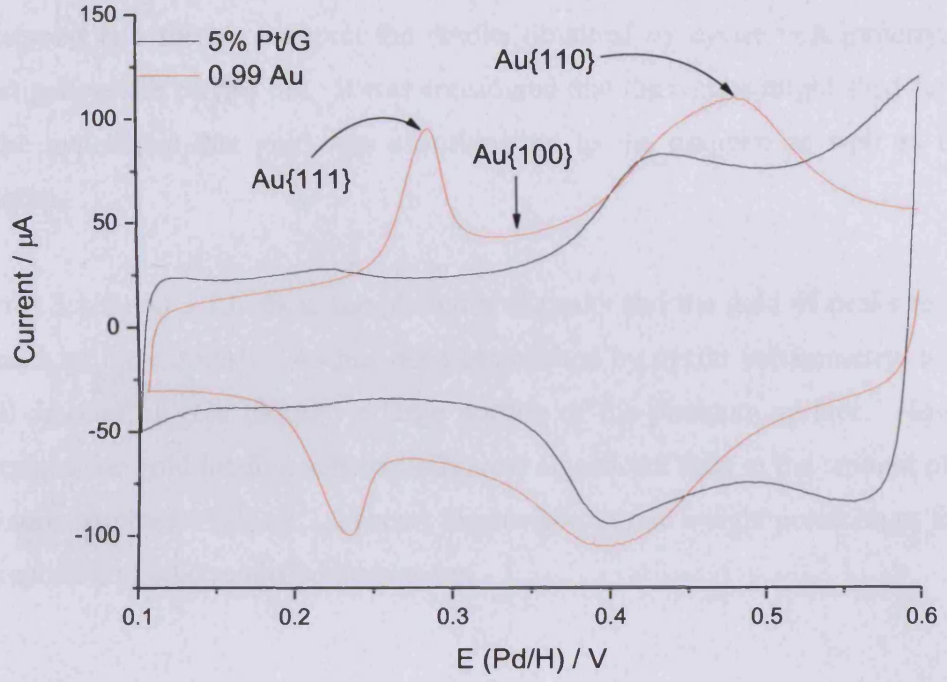

Figure 3.1.3: CVs of 5% Pt/graphite and 0.989 catalysts in 1.0 mM lead nitrate and 0.1 M NaOH showing lead UPD which is indicative of the various facets of gold formed.

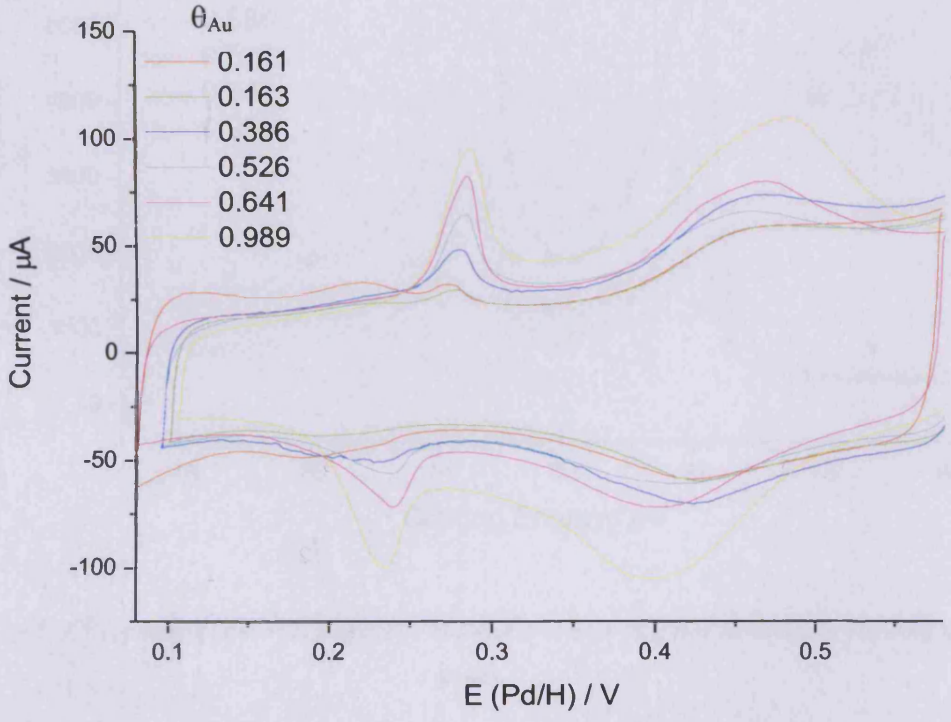

Figure 3.1.4: CVs in 1.0 mM lead nitrate and 0.1 M NaOH showing lead-UPD which is indicative of the various facets of gold formed on the 5% platinum catalyst.

3.1.4 Characterisation of gold-modified platinum catalysts: XPS analysis

To support and further interpret the results obtained by cyclic voltammetry, an XPS investigation was carried out. It was considered that the results might shed further light on the hypothesis that gold was adsorbing on to the graphite as well as on to the platinum.

Figures 3.1.5 and 3.1.6 show the platinum 4f peaks and the gold 4f peaks respectively for each of the catalysts. As has been established by cyclic voltammetry, a relatively small amount of gold blocked a large portion of the platinum surface. However, on increasing the gold loading substantially, less significant falls in the amount of exposed platinum occurred. Table 3.1.2 shows the surface atomic weight percentages for the 5% Pt/graphite and gold modified derivatives.

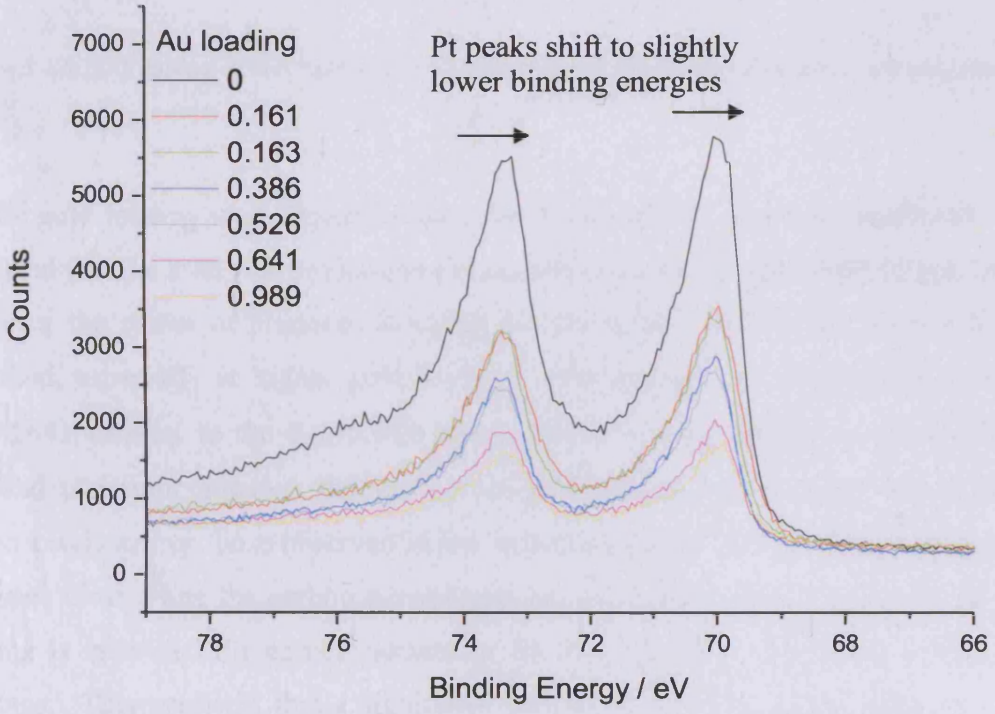

Figure 3.1.5: XPS spectra of the 5% Pt/graphite catalyst and gold modified derivatives, showing the Pt 4f peaks.

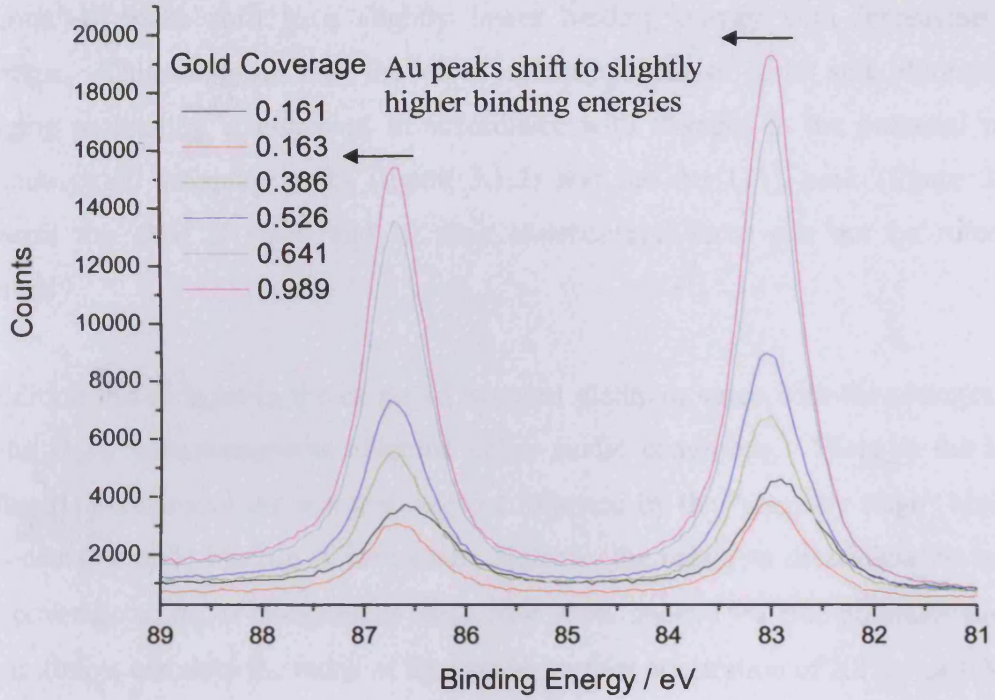

Figure 3.1.6: XPS spectra of the 5%Pt/graphite catalyst and gold modified derivatives, showing the Au 4f peaks.

As the gold loading was increased, the amount of exposed platinum decreased. This indicated that the gold was predominantly adsorbing on to the platinum and blocking it. However the extent of platinum blocking did not exactly mirror the amount of gold adsorbed, especially at higher gold loadings. For example on progressing from the θ_{Au}=0.641 catalyst to the θ_{Au}=0.989 catalyst there is little change in the amount of exposed platinum; however the amount of gold present has increased considerably. These trends mirror those observed in the voltammograms. This apparent discrepancy becomes clear when the carbon percentages are examined (table 3.1.2). As the gold loading is increased the carbon percentage falls significantly, especially at high gold loadings. This confirms that a significant portion of the gold is adsorbing on to the graphite. Also of interest is that the gold surface percentages and the associated curves presented above are in close agreement with the information obtained about the gold from the voltammograms run under Pb_{UPD}.

It is noteworthy that the gold 4f peaks shift to slightly higher binding energies and the platinum 4f peaks shift to a slightly lower binding energy with increasing gold coverage. This suggests that the electronic properties of gold and platinum are changing as loading is increased in accordance with changes in the potential of the platinum oxide stripping peaks (figure 3.1.2) and the Au{111} peak (figure 3.1.4). However the shift is small and as such experimental error can not be ruled out absolutely.

In addition the changes in the extent of exposed platinum agree with the changes seen for the H_{UPD} voltammograms obtained under acidic conditions. There is the initial substantial blocking of the platinum surface followed by the "stage by stage" blocking that occurs as gold loading is increased. Notably, the catalysts determined to have a gold coverage of $\theta_{Au} = 0.989$ under H_{UPD} here show about 19% free platinum surface. This is almost certainly the result of the greater surface penetration of XPS over CV.

Table 3.1.2: Surface atomic weight percentages for the 5% Pt/graphite and gold modified derivatives.

Catalyst	C %	Pt %	Au %
0	97.4	2.6	0
0.161	97.6	1.4	0.8
0.163	97.7	1.4	0.7
0.386	97.6	1.1	1.3
0.526	97.3	1.0	1.7
0.641	96.0	0.6	3.4
0.989	95.3	0.5	4.1

3.1.5 Characterisation of gold-modified platinum catalysts: CVs collected under basic conditions

From the work carried out by Hutchings *et al* [1], it has been suggested that supported gold catalysts tested under basic conditions can exhibit a second reduction peak which was linked to an increased catalytic selectivity. To investigate this proposed link, the 5% Pt/graphite catalyst and more importantly the gold modified derivatives were investigated in basic media.

As with the voltammograms obtained under acidic solution, unmodified platinum showed peaks between 0.1 and 0.4 V corresponding to hydrogen adsorption/desorption at the surface sites present in the catalyst surface (figure 3.1.7). Of note is that the grouping of the catalysts H_{UPD} signals is significantly different from that observed for the same catalysts tested in acidic conditions and more closely mimics the distribution observed from the XPS results. Platinum oxide formation began at 0.7 V and the oxide reduction peak in the reverse sweep was present at 0.6 V. On deposition of small amounts of gold, the intensity of the platinum sites dropped significantly, but on the introduction of further gold, the decline was slower. The platinum oxide reduction peak narrowed and shifted to slightly higher potential, suggesting that the gold was modifying the electronic properties of the platinum, both features following the trends established so far.

The gold itself provided an oxide peak at 1.2 V which grew with gold loading. The gold oxide reduction peak, (a), appeared at 1.0 V in the reverse sweep. This peak has been observed for polycrystalline gold and as such is regarded as the "standard" gold oxide reduction peak. This peak also grew with gold loading, yet the extent of the growth of both the gold oxide formation and oxide reduction peak did not correspond directly to the gold loading as determined from the loss of H_{UPD} area. This again suggests that the gold was adsorbed on the graphite as well as the Pt.

The second oxide reduction peak, (b), which was observed by Hutchings and linked to the catalytic properties of the catalyst, is present at ~0.8 V for all gold modified catalysts. Although small, it remains present for all gold modified catalysts and hence it will be interesting to see if the gold doped catalysts show significantly improved activity compared with the platinum.

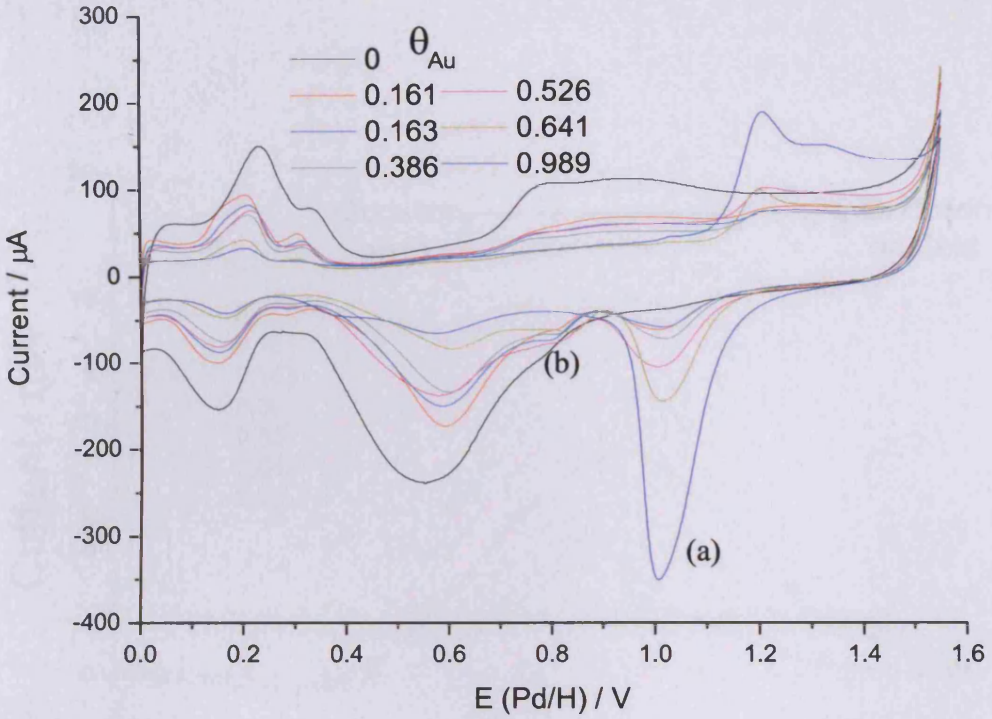

Figure 3.1.7: CVs in 0.5 M NaOH at 10 mV s^{-1} showing the hydrogen-UPD region and oxide region of the 5% Pt/graphite catalyst response in basic media and its subsequent modification upon adsorption of gold.

3.1.6 1-Propanol oxidation in the electrochemical cell

Activity for 1-propanol electrooxidation was investigated by use of cyclic voltammetry (figure 3.1.8). The broad peak at 0.9 V was established as being oxidation occurring on the platinum due to it being present when the 5% Pt/graphite catalyst was tested. The deposition of gold onto the platinum surface had a considerable effect on this platinum electrooxidation peak. With the exception of the curve for θ_{Au}= 0.53 (this catalyst showed an unusually small electrochemical response), there was a steady enhancement in the size of the platinum electrooxidation peak with increasing θ_{Au}. In addition a new peak appeared at 1.2 V for the gold-modified catalysts; this peak was small in comparison with the enhanced platinum peak and overlapped with it to a significant extent. This suggests that the deposited gold was catalysing 1-propanol electrooxidation as well as enhancing the activity of the platinum component of the catalyst. If this was the case, a visual comparison of the area of the two peaks indicates that the extent of oxidation on the gold surface was less than that occurring on the

modified platinum surface. Overall, activity was significantly enhanced by the presence of gold.

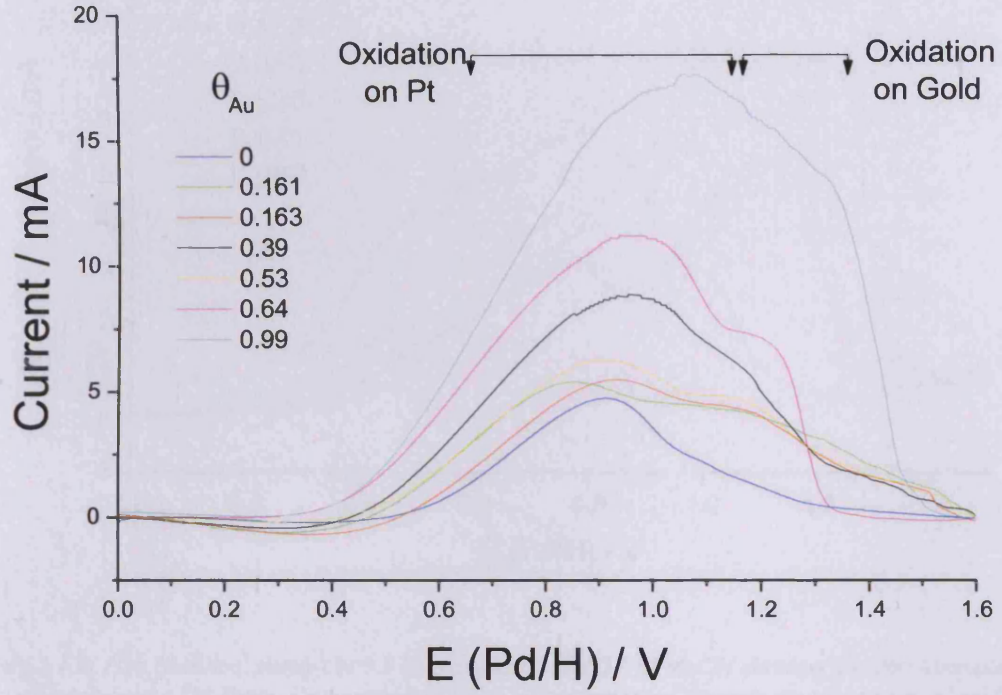

Figure 3.1.8: CVs (forward sweep) in 0.5 M 1-propanol and 0.5 M NaOH showing electrooxidation occurring on the 5% Pt/graphite catalyst and its subsequent modification on adsorption of gold.

3.1.7 2-Propanol oxidation in the electrochemical cell

The cyclic voltammograms obtained for the electrooxidation of 2-propanol on the 5% Pt/graphite and gold-modified variants are shown in figure 3.1.9. The Pt/graphite catalyst provided a response at 0.5 V, which decreased on the introduction of gold to the surface. Gold generated a peak at 1.0 V, which grew with increasing gold loading (especially at high loading) and became the dominant surface feature for electrooxidation of 2-propanol. This suggested that gold was deactivating the platinum for the electrooxidation of 2-propanol, the opposite of the result obtained for the same catalysts tested on 1-propanol oxidation. The extent of electrooxidation occurring on gold sites broadly followed the order of increasing gold loading.

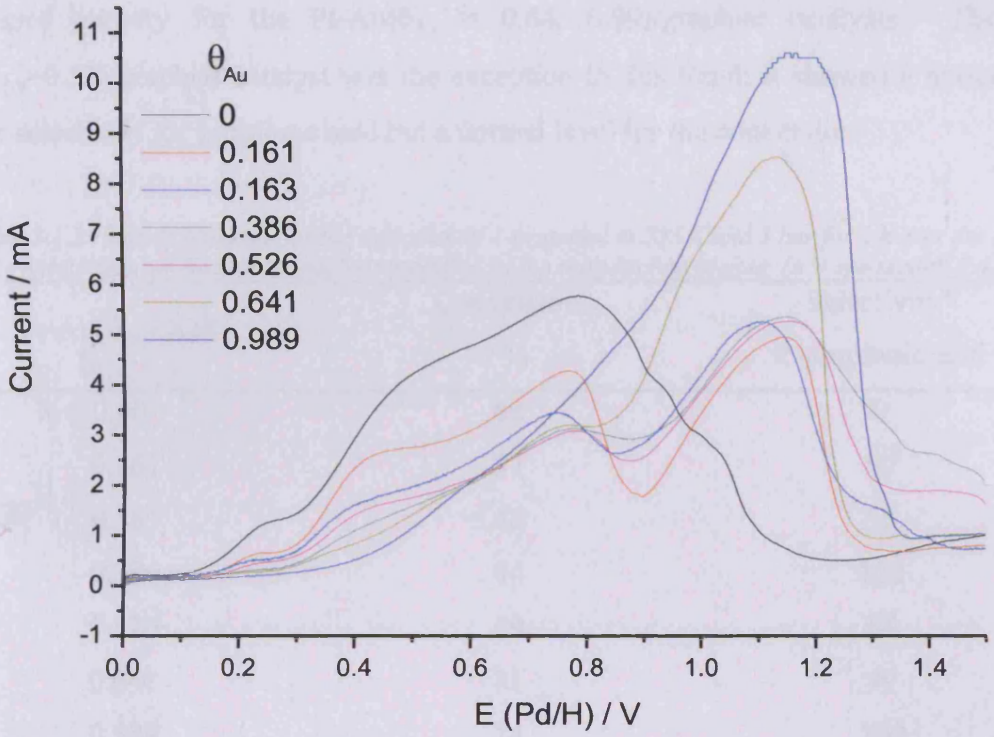

Figure 3.1.9: CVs (forward sweep) in 0.5 M 2-propanol and 0.5 M NaOH showing the electrooxidation occurring on the 5% Pt/graphite catalyst and its subsequent modification on adsorption of gold.

3.1.8 1-Propanol oxidation in the high-pressure reactor

5% Pt/graphite and all of the gold-dosed variants were tested in a high-pressure reactor to determine their catalytic activity and selectivity. Reactions were carried out as described in section 2.4.2. The results obtained (table 3.1.3) show that only one liquid product was produced (propionic acid). However over-oxidation (probably to CO_2) was evident by a lack of mass balance.

The 5% Pt/graphite catalyst showed a moderate activity, but zero selectivity to liquid products. It is inferred that the catalyst produced only over-oxidation products such as CO_2 that were not detected by HPLC. On the introduction of small quantities of gold there was a decrease in the overall conversion of 1-propanol but a significant selectivity for propionic acid was observed. A relatively constant level of activity (40-50%) was maintained for the various low to medium coverages of gold. By contrast the selectivity increased steadily up to Pt-Au(θ_{Au} = 0.39)/graphite where the catalyst became completely selective for propionic acid production. This high level of selectivity was

maintained for all of the higher gold coverage catalysts and was accompanied by an increased activity for the Pt-Au(θ_{Au} = 0.64, 0.99)/graphite catalysts. The Pt-Au(θ_{Au}=0.53)/graphite catalyst was the exception to this trend; it showed a noticeably lower selectivity for propionic acid but a normal level for the conversion.

Table 3.1.3: Results obtained for the oxidation of 1-propanol at 333 K and 3 bar for 3 h over the 5% Pt/graphite catalyst and those catalysts modified by the introduction of gold. (a = see section 2.4.4).

Pt-Au(θ_{Au}=X)/G	Conversion / %	Selectivity[a] to propionic acid
X = 0.00	62	0
0.161	37	59
0.163	48	56
0.386	44	100
0.526	49	64
0.641	81	99
0.989	74	100

3.1.9 2-Propanol oxidation in the high pressure reactor

The 5% Pt/graphite and the gold-doped variants were tested in the high-pressure reactor under the conditions previously described. The analytical results are presented in table 3.1.4. Acetone was the only liquid product detected. 5% Pt/graphite provided a very low conversion and no detectable liquid phase products; such products as were formed were probably the result of over-oxidation. Catalysts with a low to medium loading of gold Pt-Au(θ_{Au} = 0.16 - 0.53)/graphite showed increasing conversions which rose steadily to 60%. This increasing conversion was accompanied by an increasing selectivity to acetone over the same range except in the case of the Pt-Au(θ_{Au} = 0.53)/graphite catalyst, which showed the expected increase in conversion, but nevertheless showed a reduced selectivity. The θ_{Au} = 0.64 catalyst continued the conversion trend previously established and also showed the highest selectivity. The catalyst with the highest loading of gold showed a lower conversion and selectivity than was expected based on these trends.

A brief comparison of the electrochemical and reactor results (for both 1- and 2-propanol) shows that, very broadly, the extent of electrooxidation as represented by the size of features in the voltammograms provide a reasonable measure of the catalytic activity/selectivity as observed in the reactor studies. However there were some significant discrepancies which will be discussed later.

Table 3.1.4: Results obtained for the oxidation of 2-propanol at 333 K and 3 bar for 3 h over the 5% Pt/graphite catalyst and those catalysts modified by the introduction of gold.

Pt-Au(θ_{Au}=X)/G	Conversion %	Selectivity to acetone
X=0.00	4	0
0.161	35	62
0.163	51	64
0.386	53	74
0.526	60	58
0.641	71	97
0.989	60	87

3.1.10 1-Propanol oxidation on platinum single crystals in the presence of gold

To improve the understanding of the processes involved in the electrooxidation occurring on supported catalysts, a single crystal study was undertaken. Since no support was involved the systems were simplified considerably. The electrooxidation of 1-propanol and 2-propanol was investigated on the three low Miller indices of platinum single crystal surfaces ({111}, {100} and {110}) and on two stepped surfaces ({533} and {755}). Each was investigated at various levels of gold deposition (and hence gold coverage) on the platinum surface. The {111}, {100} and {110} surfaces represent the facets that were predominant in the supported platinum microcrystals in the catalyst sample (as seen from the CVs presented in section 3.1.2). Pt{533} and Pt{755} are stepped surfaces which exhibit 4-atom and 6-atom wide {111} terraces respectively which are separated by {100} steps. It was hoped that the study would provide information as to which sites where most active for electrooxidation; as well as

indicating if the gold interacted differently with individual facets as opposed to when these facets where combined (i.e. terraces vs. steps).

Electrooxidation of 1-propanol was carried out in an electrochemical cell as described in section 2.3.7. Cyclic voltammograms were obtained for the Pt single crystals and gold-doped variants in acidic conditions and are shown at the top of each figure. The voltammograms at the bottom of each figure show the corresponding 1-propanol electrooxidation: the peak between 0.7 V - 0.8 V represents oxidation on the platinum, whereas that between 1.0 V - 1.2 V represents oxidation on the gold. These assignments were made on the same principle as used for the supported catalysts, i.e. if the introduction of a new material produced a new peak in the voltammogram then the two must be linked. Unfortunately, due to time constraints and equipment problems, an imperfect Pt{111} had to be used in this investigation.

For the low miller indices (figures 3.1.10 - 3.1.12) the introduction of gold was far more controllable than had been seen with the supported catalyst. Generally the electrooxidation voltammograms show that 1-propanol oxidation took place on the platinum surface and only a small proportion occurred on the adsorbed gold. This is with the exception of the Pt{100} surface, where the extent of electrooxidation on the platinum and gold surfaces showed a similar magnitude but significantly lower activity (when compared with the other surfaces) for 1-propanol oxidation.

The extent of oxidation occurring on Pt{100} initially increased on the introduction of gold, before falling to lower levels. Oxidation occurring on the gold also showed a maximum with increasing coverage. This suggests that the gold was promoting oxidation on the platinum surface at low coverages before deactivating it at medium to high coverages. This indicates that gold initially acted as a site-blocker, before the coverage became so high that the gold blocked the active platinum sites as well and prevented electrooxidation from occurring.

The Pt{110} and Pt{111} surfaces exhibited similar trends on exposure to gold. The difference being that the majority of electrooxidation occurred on platinum sites and gold was responsible for only a small amount of electrooxidation. However, on introduction of gold the extent of Pt-catalysed electrooxidation increased dramatically.

The total extent of electrooxidation passed through a maximum at θ_{Au} = 0.47 on Pt{110} and at θ_{Au} = 0.66 on Pt {111}, after which the extent of oxidation decreased dramatically. On reaching nearly complete gold coverage the crystal surfaces became practically inactive. This again suggests that the gold was promoting reaction by means of site-blocking.

Stepped Pt{533} and Pt{755} surfaces (figures 3.1.13 and 3.1.14 respectively) also catalysed oxidation predominantly on the platinum surface. Again oxidation passed through a maximum at θ_{Au} = 0.7 on Pt{533} and at θ_{Au} = 0.82 on Pt{755}. In each case this maximum was preceded by a slight dip in activity at medium gold coverages. The CVs in acidic solution show that the maximum activity corresponded to the complete blocking of the step sites by the gold. This indicated that the Pt step sites were active for poisoning and hence their removal increased the overall activity of the catalyst. The sudden drop-off in catalytic activity at high potential is due to the onset of oxide formation which poisons the catalyst surface. The trends seen here suggest that Pt{111} and Pt{110} surfaces provide the largest contribution to the observed activity of the supported catalysts. In addition from the stepped crystals it would appear that Pt{100} is readily poisoned and this may account for its low activity when comparing the low Miller indices. Also the effect of gold seems to be predominantly as a site-blocker. These results may be more clearly interpreted from figures 3.1.15 and 3.1.16 which present the total electrooxidation areas as bar graphs.

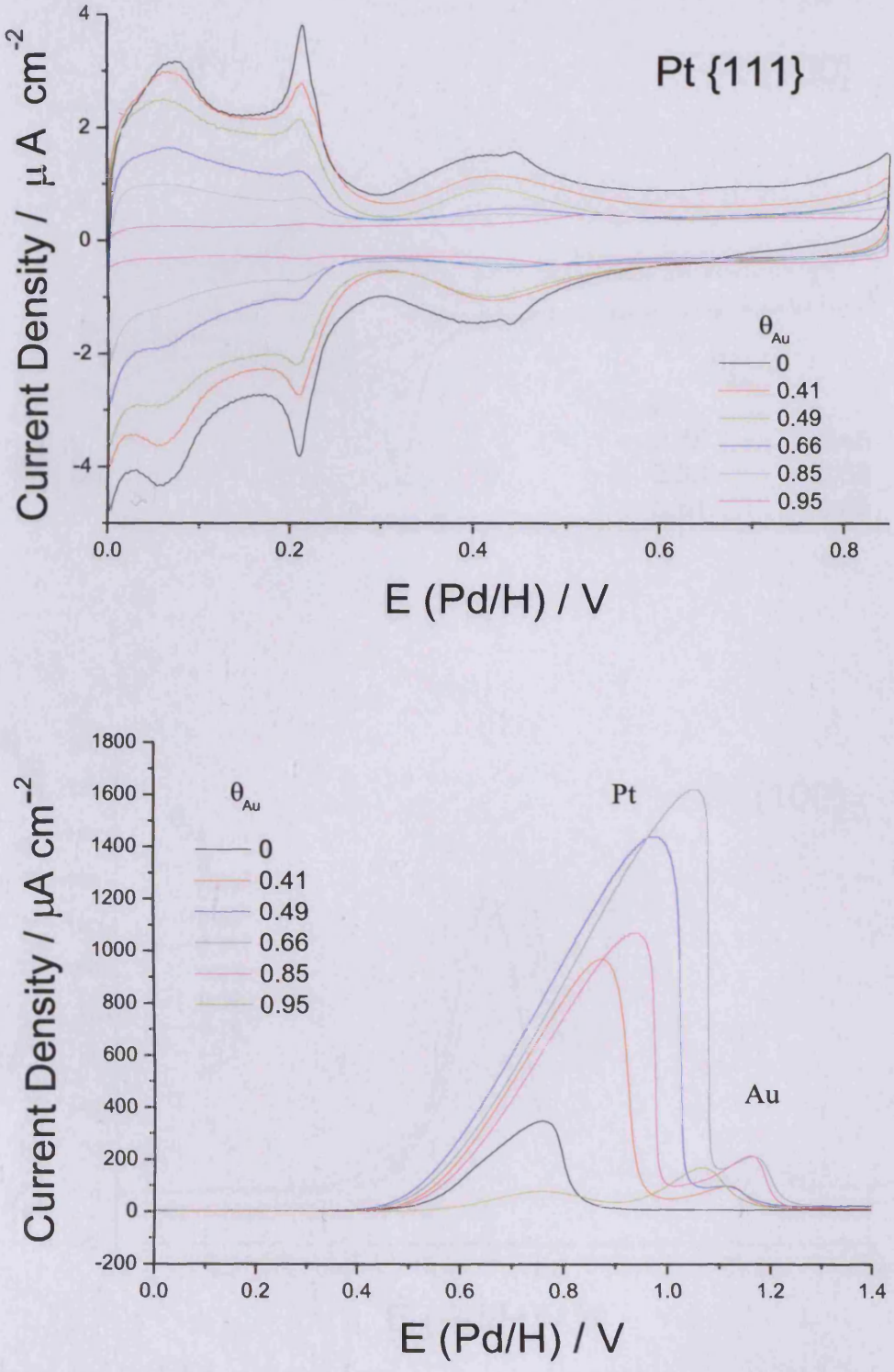

Figure 3.1.10: CVs in 0.1 M H_2SO_4 (top) and 0.1 M NaOH, 1 mM 1-propanol (bottom) showing the gold coverage obtained and the corresponding electro-oxidation respectively for Pt{111} and its gold modified derivatives.

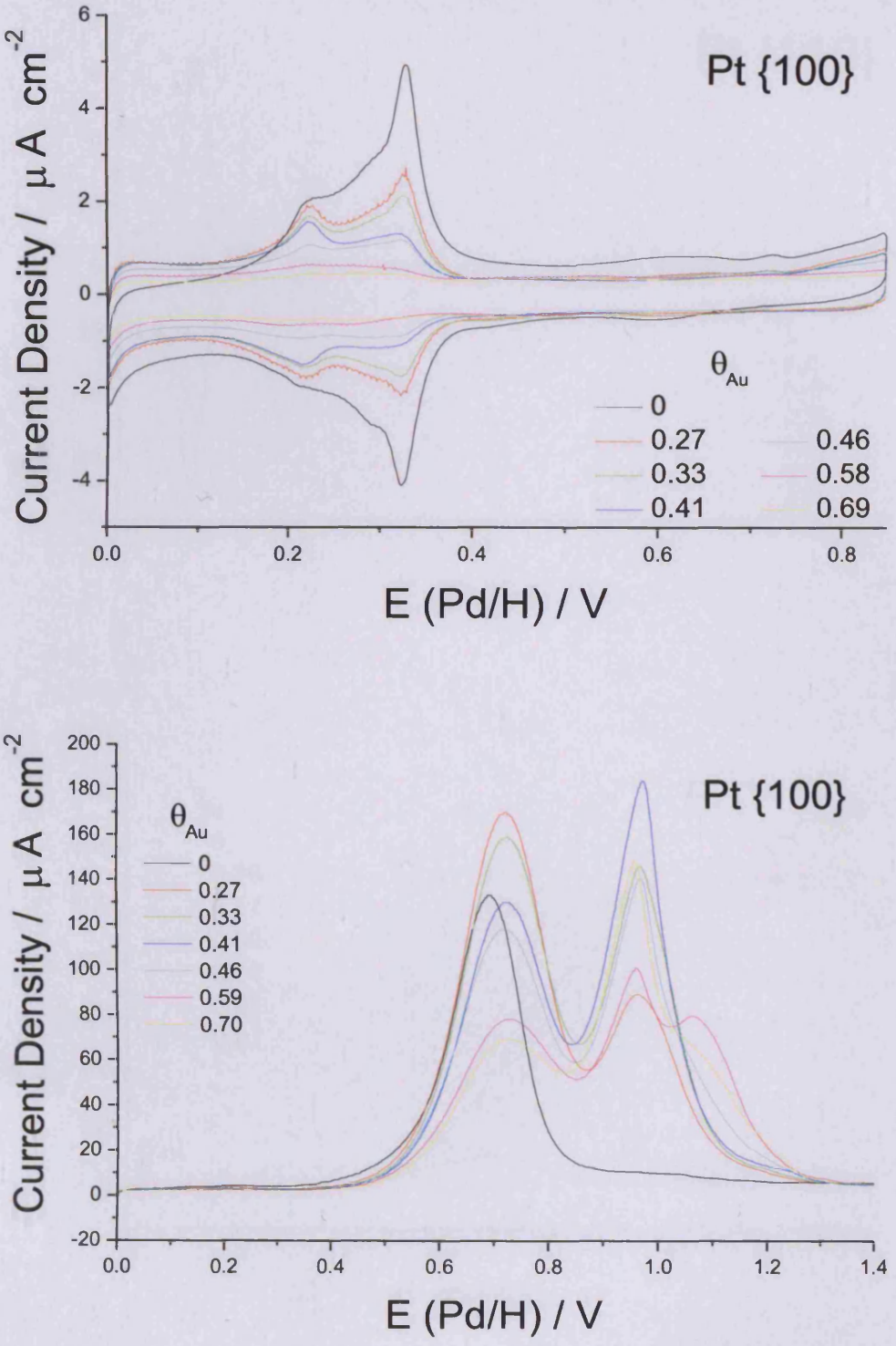

Figure 3.1.11: CVs in 0.1 M H_2SO_4 (top) and 0.1 M NaOH, 1 mM 1-propanol (bottom) showing the gold coverage obtained and the corresponding electro-oxidation respectively for Pt{100} and its gold modified derivatives.

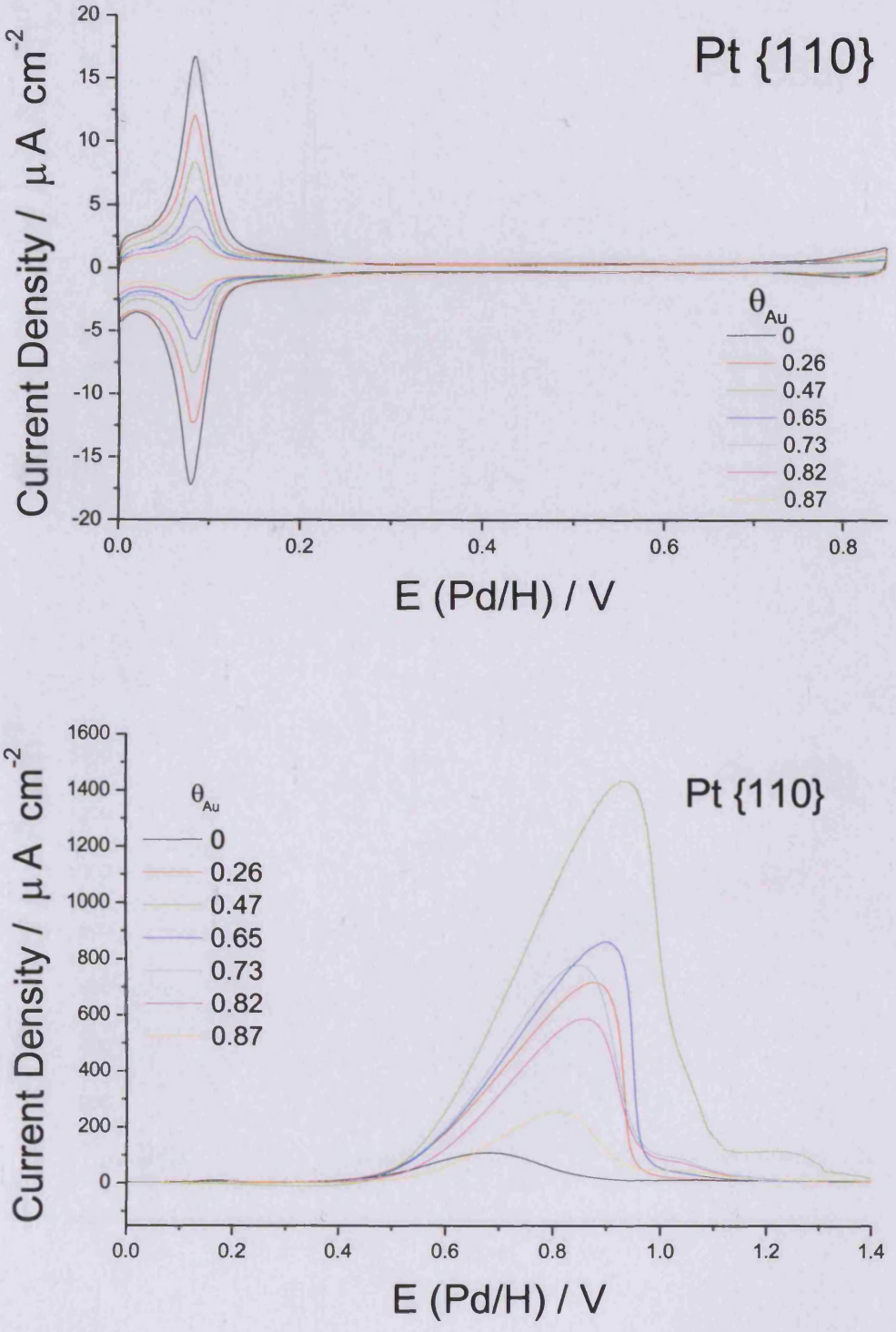

Figure 3.1.12: CVs in 0.1 M H_2SO_4 (top) and 0.1 M NaOH, 1 mM 1-propanol (bottom) showing the gold coverage obtained and the corresponding electro-oxidation respectively for Pt{110} and its gold modified derivatives.

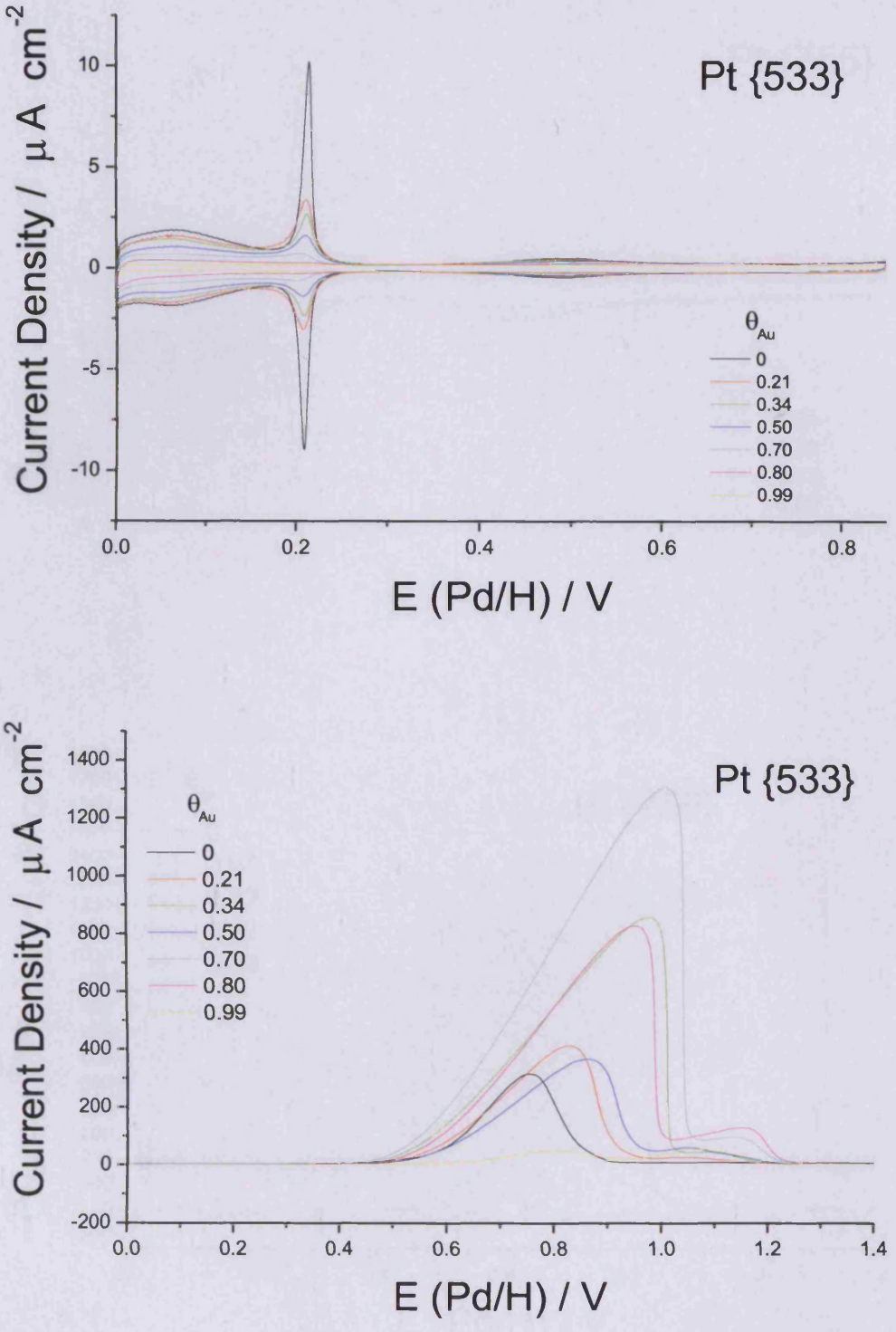

Figure 3.1.13: CVs in 0.1 M H_2SO_4 (top) and 0.1 M NaOH, 1 mM 1-propanol (bottom) showing the gold coverage obtained and the corresponding electro-oxidation respectively for Pt{533} and its gold modified derivatives.

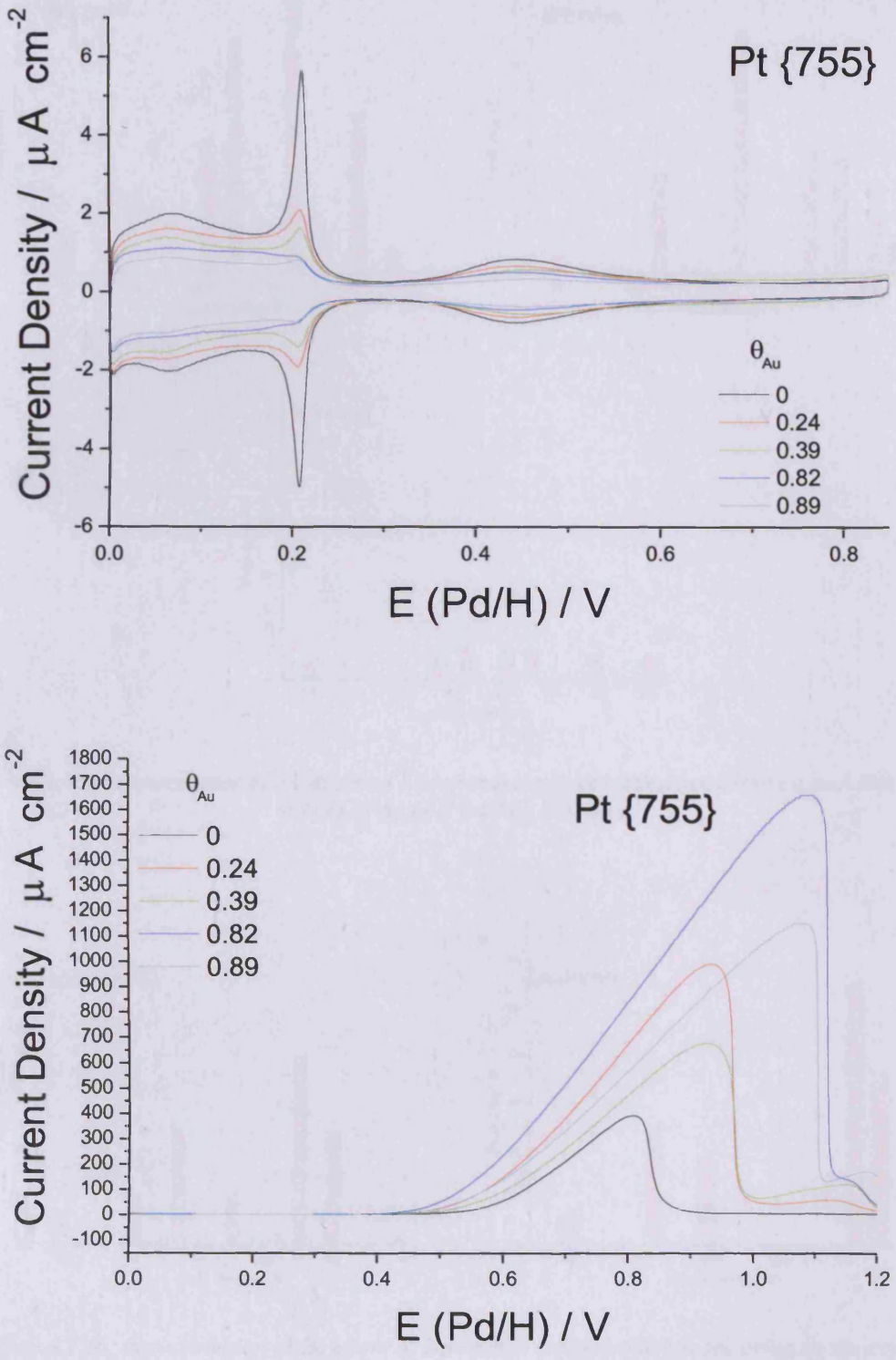

Figure 3.1.14: CVs in 0.1 M H_2SO_4 (top) and 0.1 M NaOH, 1 mM 1-propanol (bottom) showing the gold coverage obtained and the corresponding electro-oxidation respectively for Pt{755} and its gold modified derivatives.

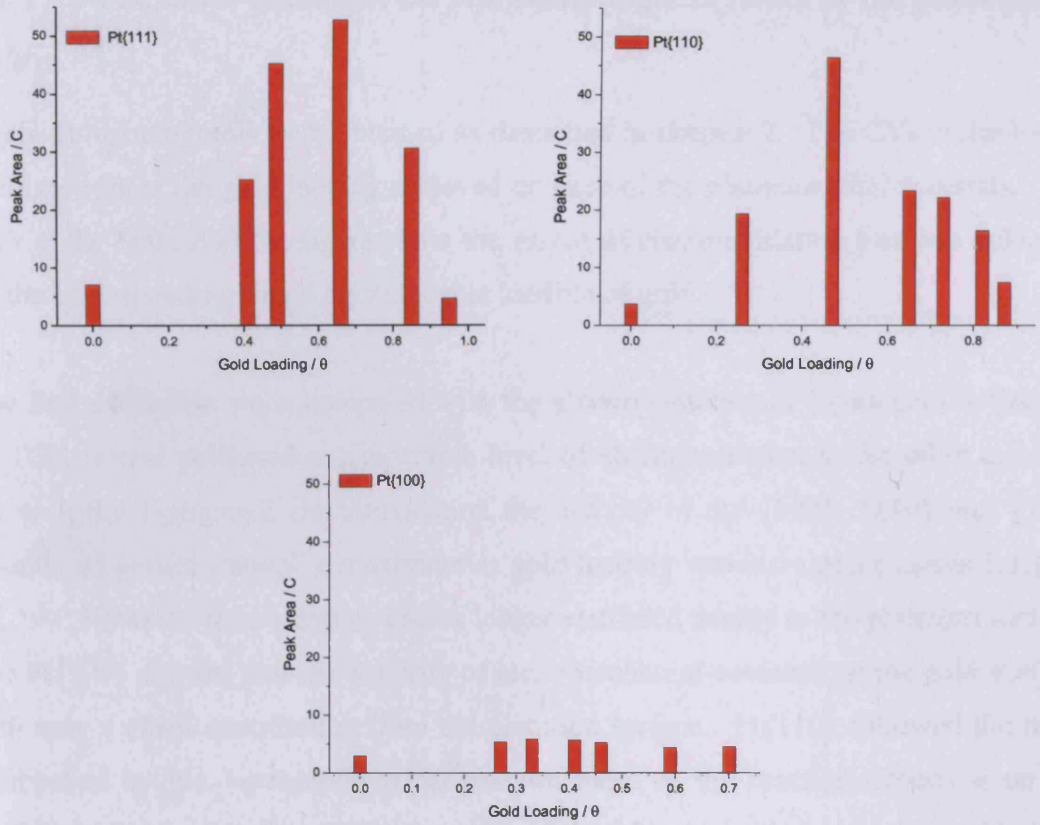

Figure 3.1.15: Representation of the extent of 1-propanol electrooxidation occurring on each low Miller indices at the gold loading indicated.

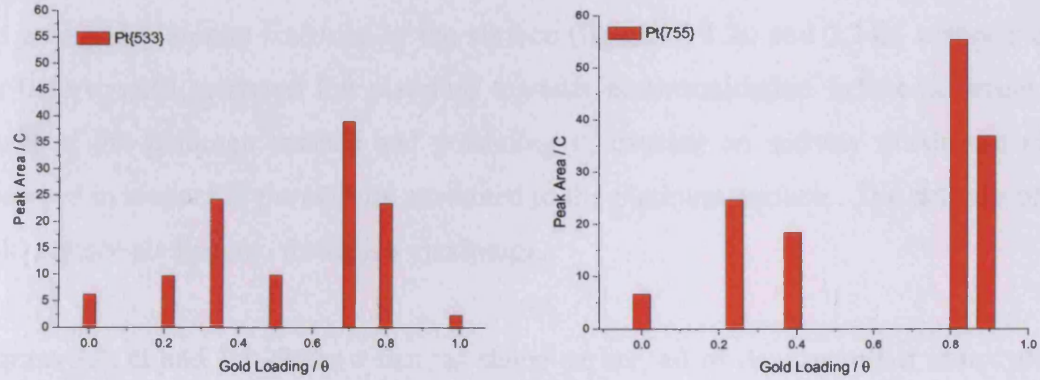

Figure 3.1.16: Representation of the extent of 1-propanol electrooxidation occurring on the stepped crystal surface at the gold loading indicated.

3.1.11 2-Propanol oxidation on platinum single crystals in the presence of gold

Again voltammograms were obtained as described in chapter 2. The CVs at the top of the figure show the gold loading achieved on each of the platinum single crystals. The CVs at the bottom of the figure show the extent of electrooxidation that was achieved by the corresponding single crystal at that loading of gold.

The first difference when compared with the electrooxidation of 1-propanol is that the Pt{100} crystal produced a comparable level of electrooxidation to the other crystals. As with the 1-propanol electrooxidation the activity of the {100}, {110} and {111} crystals all passed through a maximum as gold loading was increased (figures 3.1.17 – 3.1.19). However the oxidation was no longer restricted mostly to the platinum surface. The Pt{100} showed that the majority of electrooxidation occurred on the gold surface, with only a small contribution from the platinum surface. Pt{110} followed the trend established by the 1-propanol oxidation with most of the reaction occurring on the modified platinum surface and only a little being due to oxidation on the gold. The Pt{111} crystal produced comparable levels of oxidation on both the platinum and gold sites.

The Pt{533} and Pt{755} crystals provided the same extent of electrooxidation on both the gold and platinum fractions of the surface (figures 3.1.20 and 3.1.21 respectively). As before, gold activated the platinum towards electrooxidation before covering too much of the platinum surface and poisoning it, causing an activity maximum to be observed in respect of the activity attributed to the platinum surface. The activity of the gold surface also passed through a maximum.

Figures 3.1.22 and 3.1.23 show that, as stated earlier, all of the low miller index planes provide a maximum in activity with increasing gold loading. When compared to the graphs obtained for the electro-oxidation of 1-propanol, it is evident that the extent of oxidation due to 2-propanol is significantly less. Also the extent of oxidation occurring on the stepped crystals did not pass through a maximum as gold coverage was increased but rather it increased to a maximum.

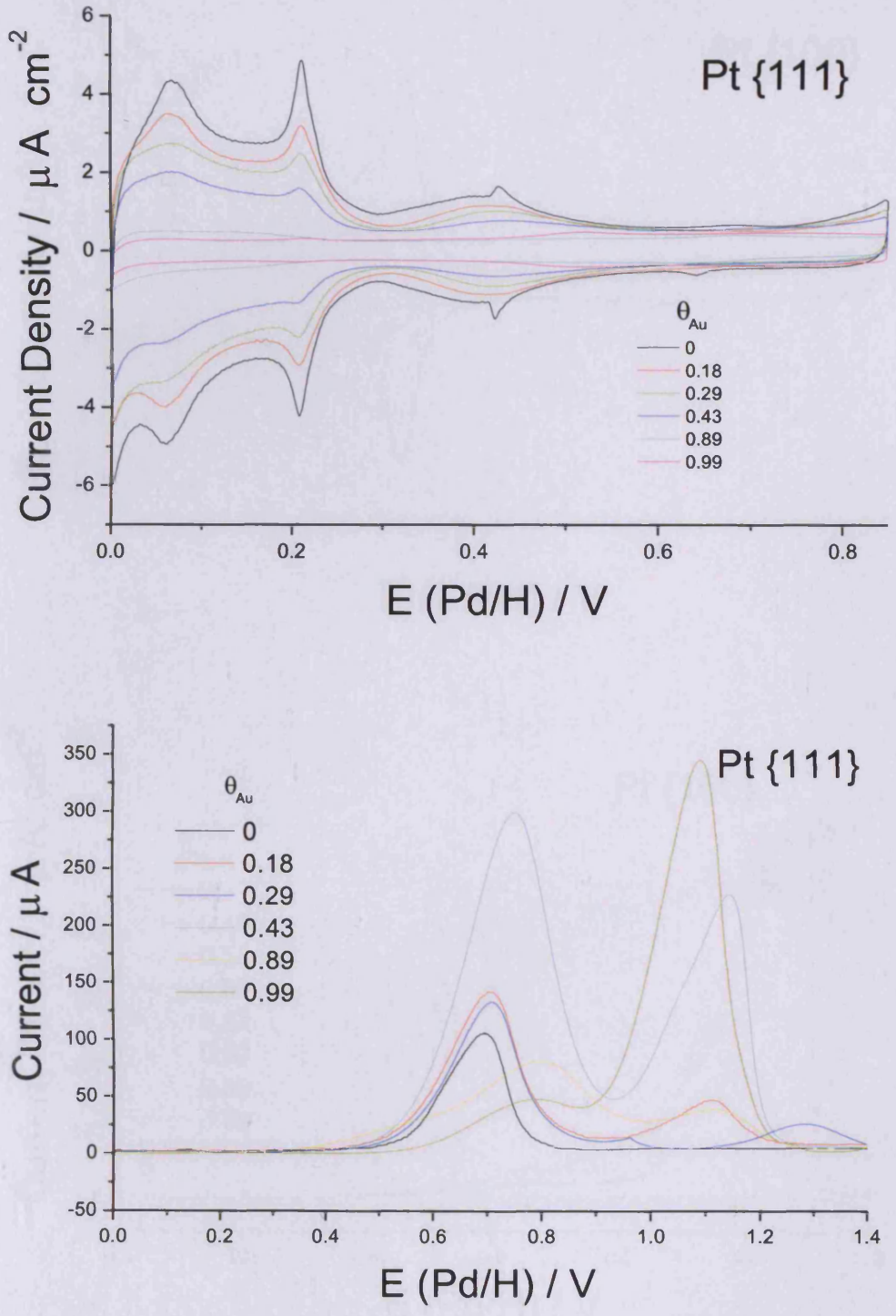

Figure 3.1.17: CVs in 0.1 M H_2SO_4 (top) and 0.1 M NaOH, 1 mM 2-propanol (bottom) showing the gold coverage obtained and the corresponding electro-oxidation respectively for Pt{111} and its gold modified derivatives.

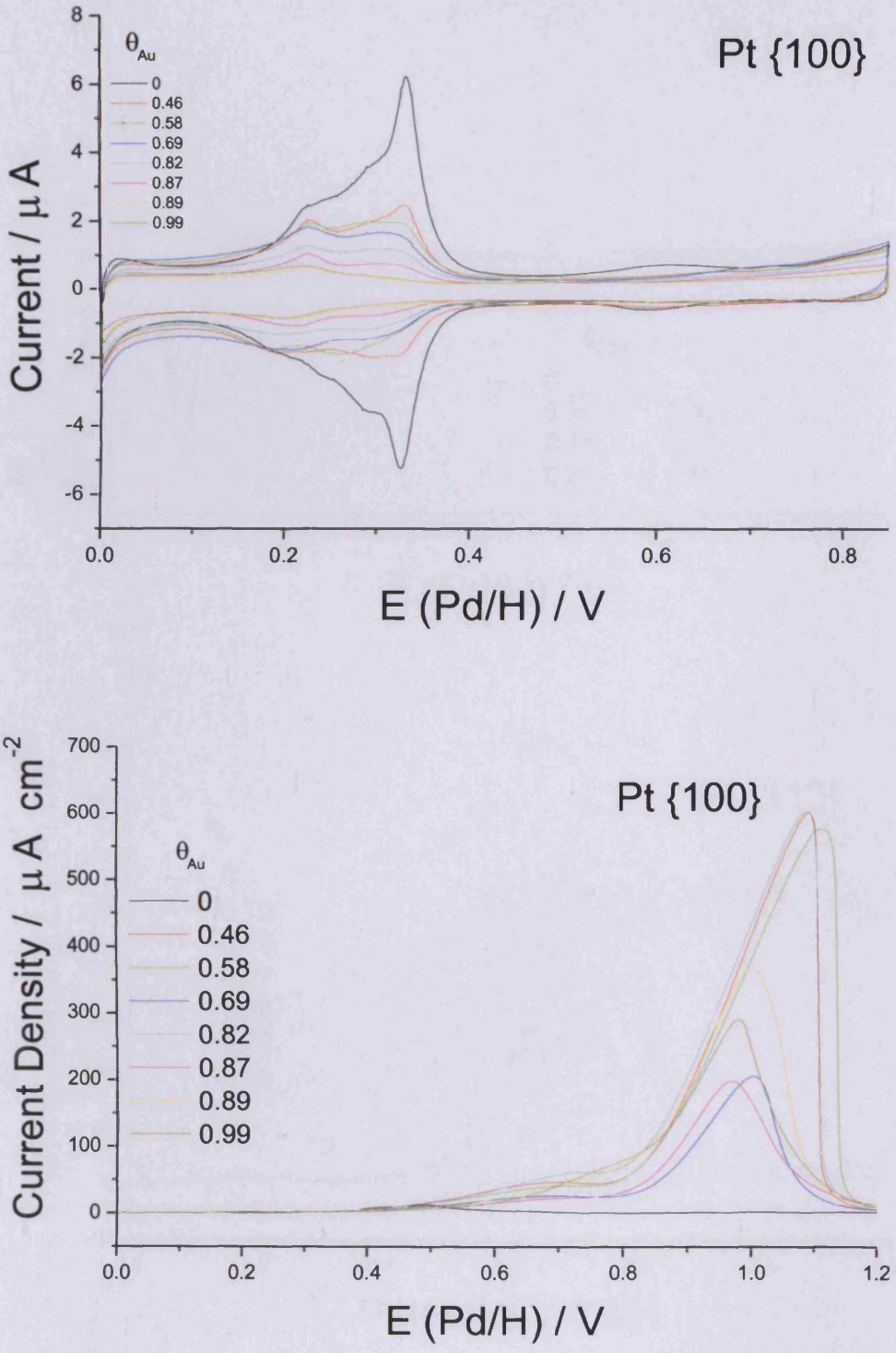

Figure 3.1.18: CVs in 0.1 M H_2SO_4 (top) and 0.1 M NaOH, 1 mM 2-propanol (bottom) showing the gold coverage obtained and the corresponding electro-oxidation respectively for Pt{100} and its gold modified derivatives.

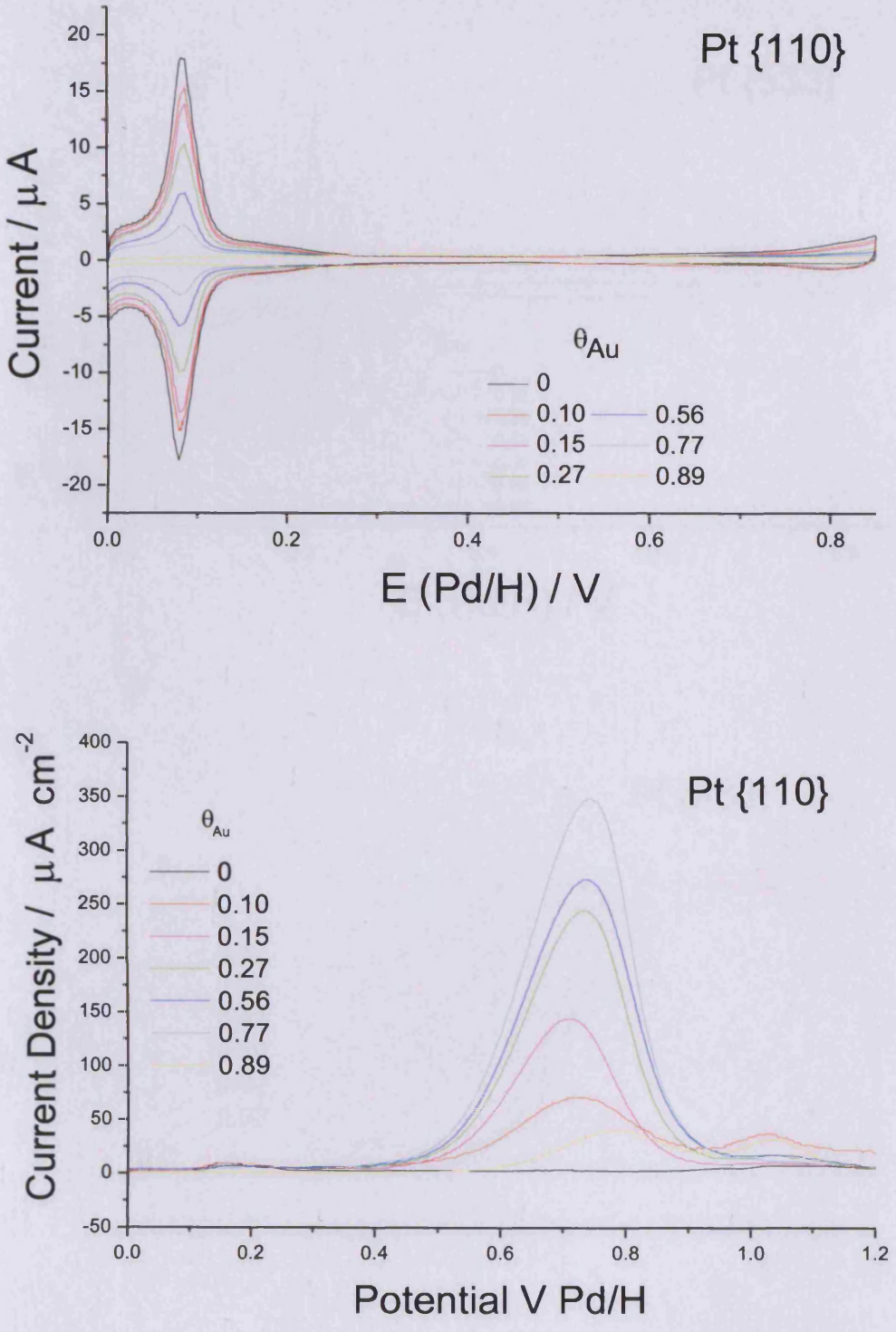

Figure 3.1.19: CVs in 0.1 M H_2SO_4 (top) and 0.1 M NaOH, 1 mM 2-propanol (bottom) showing the gold coverage obtained and the corresponding electro-oxidation respectively for Pt{110} and its gold modified derivatives.

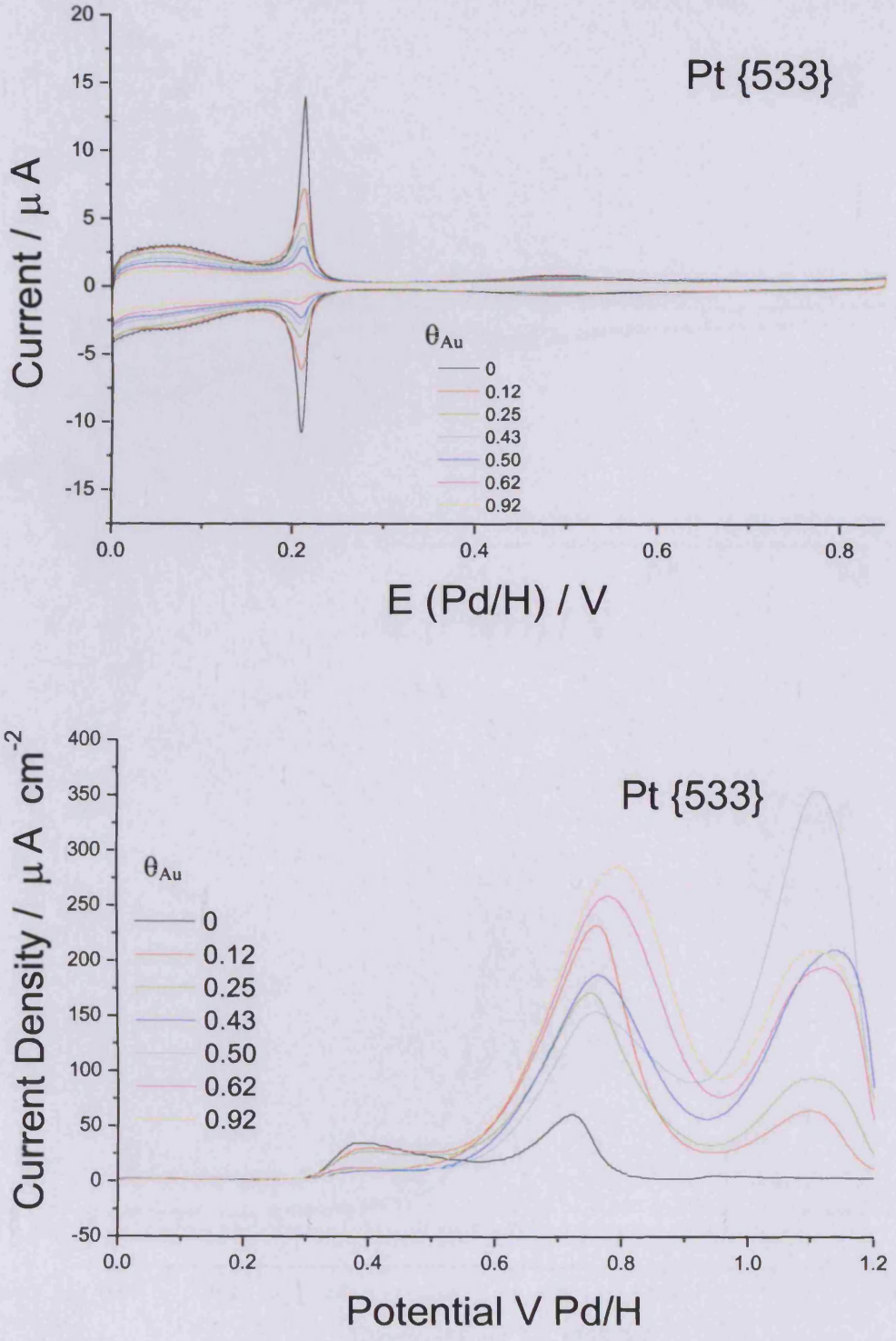

Figure 3.1.20: CVs in 0.1 M H_2SO_4 (top) and 0.1 M NaOH, 1 mM 2-propanol (bottom) showing the gold coverage obtained and the corresponding electro-oxidation respectively for Pt{533} and its gold modified derivatives.

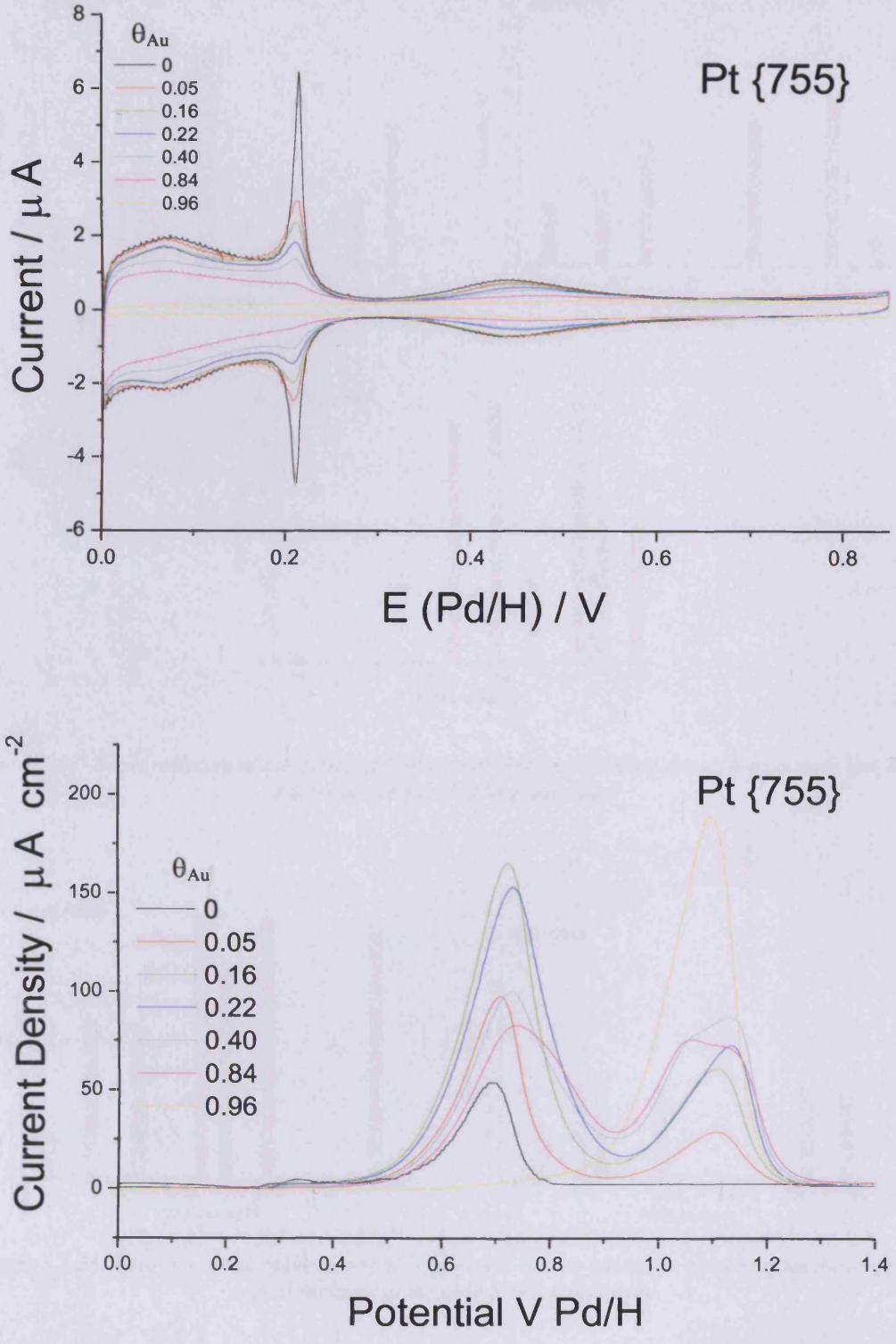

Figure 3.1.21: CVs in 0.1 M H_2SO_4 (top) and 0.1 M NaOH, 1 mM 2-propanol (bottom) showing the gold coverage obtained and the corresponding electro-oxidation respectively for Pt{755} and its gold modified derivatives.

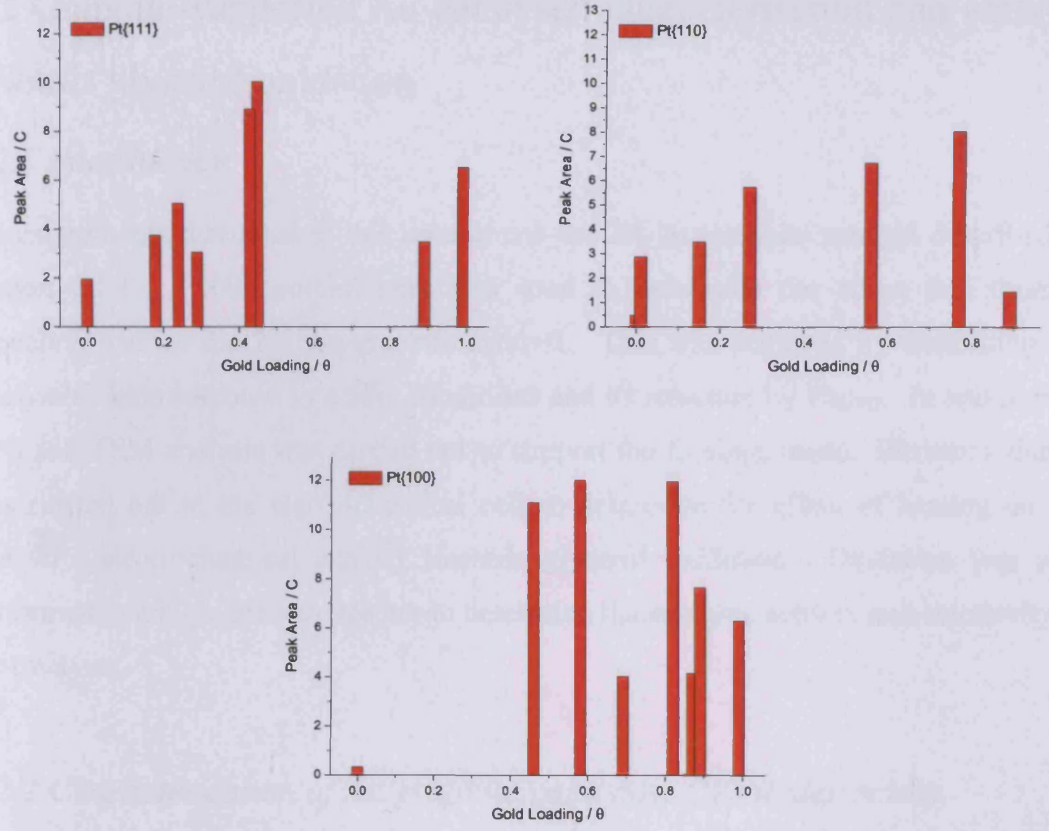

Figure 3.1.22: Representation of the extent of 2-propanol electro-oxidation occurring on each low Miller indices at the gold loading indicated.

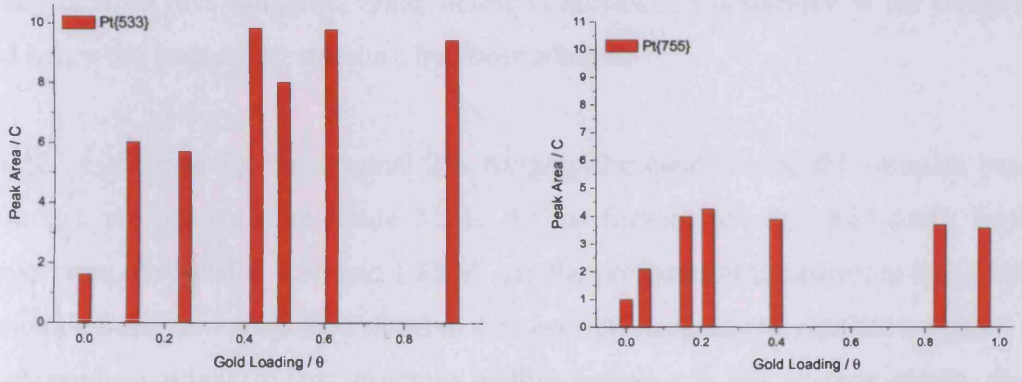

Figure 3.1.23: Representation of the extent of 2-propanol electro-oxidation occurring on the stepped crystal surfaces at the gold loading indicated.

3.2 Graphite-supported Au catalysts: characterisation and activity towards glycerol oxidation

3.2.1 Introduction

All experiments discussed in this section use the 2% Au/graphite catalyst described in section 2.1.1. Cyclic voltammetry was used to determine the effect that thermal annealing had on the 2% Au/graphite catalyst. This was achieved by examining the catalyst's oxide response in acidic conditions and its structure by Pb_{UPD}. In addition an XPS and TEM analysis was carried out to support the findings made. Electrooxidation was carried out in the electrochemical cell to determine the effect of heating on the catalyst's electrochemical activity towards glycerol oxidation. Oxidation was also performed in a high-pressure reactor to determine the catalytic activity and selectivity of the catalysts.

3.2.2 Characterisation of Au/graphite catalysts: CVs under acidic conditions

Two series of thermally annealed catalysts were prepared by heating the 2% Au/graphite catalyst to 500, 600 and 700 K in either air or 5% H_2/Ar. The resultant catalysts were first examined under acidic conditions to determine if the oxide region and hence the underlying structure had been altered.

The CVs obtained for the original 2% Au/graphite catalyst and the samples heated in hydrogen are presented in figure 3.2.1. In the forward sweep, gold oxide formation peaks were observed at 1.35 and 1.55 V. As the preparation temperature was increased, the oxide formation peaks decreased in size and the Au/graphite catalyst prepared at 700 K showed significantly less structure in this region. In the reverse sweep, the gold oxide-reduction peak was observed at 1.1 V. As the preparation temperature was increased the intensity of the oxide-reduction peak decreased. However this reduction was not systematic, the catalysts prepared at 500 K and 600 K was reduced to roughly the same extent, but the catalyst prepared at 700 K had a significantly smaller oxide-reduction peak. This suggested that the surface area of the gold particles had decreased, albeit not systematically, indicating that the gold particles were sintering.

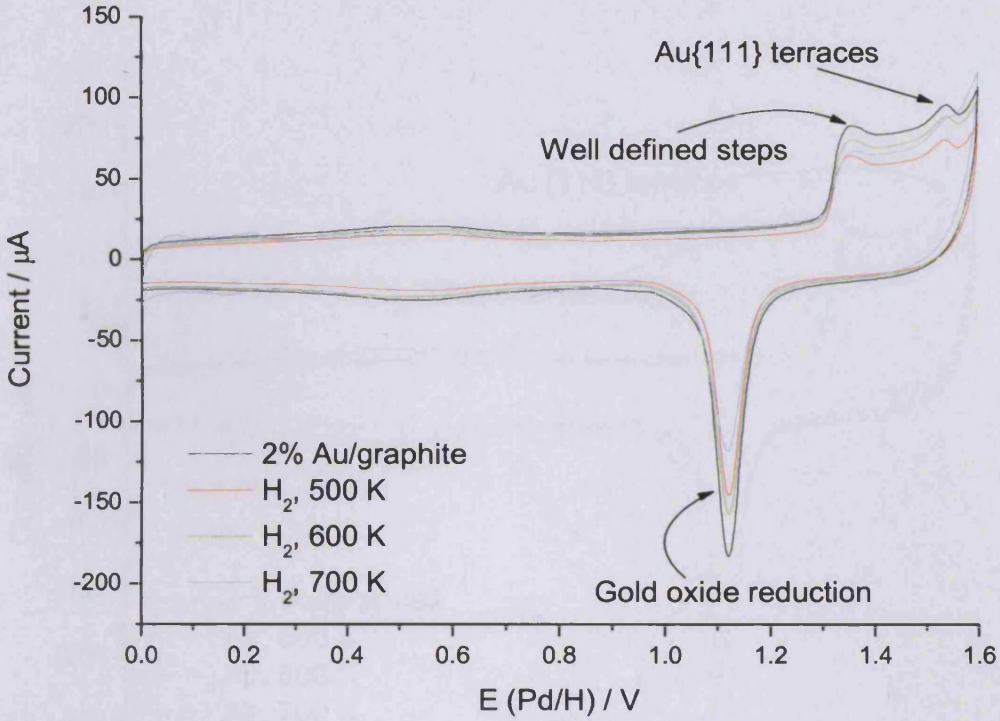

Figure 3.2.1: CVs of 2% Au/graphite in 0.5 M H_2SO_4 at 10 mV s^{-1} showing features associated with gold oxide formation and reduction and the modifications brought about by heating in hydrogen.

CVs for the 2% Au/graphite catalyst and the catalysts prepared by thermal annealing in air are shown in figure 3.2.2. In the forward sweep the gold oxide-formation peaks were again observed at 1.35 and 1.55 V. When compared with the untreated 2% Au/graphite catalyst the catalyst prepared at 500 K showed no observable change in the structure of these peaks, however there was a decrease in the overall area. The Au/graphite catalysts prepared at 600 and 700 K showed a marked increase in the size of the oxide-formation peaks. This indicated that the gold was becoming more "structured" i.e. average step and terrace sizes were increasing. In the reverse sweep the gold oxide-reduction peak at 1.1 V decreased in area as preparation temperature was increased, indicating that the gold particles were sintering. In addition, this peak became sharper, better defined and shifted slightly to a more positive potential with increasing preparation temperature. These changes were most obvious for the 2% Au/graphite catalyst prepared at 700 K. The shift in potential indicated a change in the electronic properties of the gold surface, due to the weaker Au-O bond. This in turn

might indicate a change in the catalytic properties of the 2% Au/graphite catalyst prepared at 700K in air.

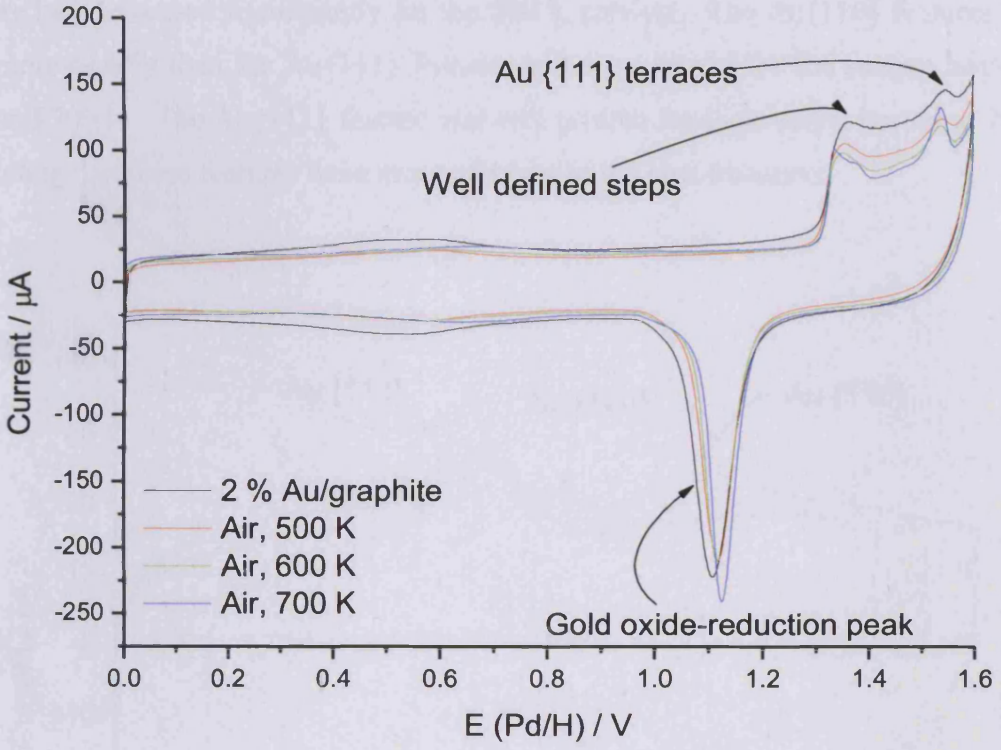

Figure 3.2.2: CVs of 2% Au/graphite in 0.5 M H_2SO_4 at 10 mV s^{-1} showing features associated with gold oxide formation and reduction and subsequent modification resulting from heating in air.

3.2.3 Characterisation of Au/graphite catalysts: CVs involving Pb_{UPD}

The 2% Au/graphite and heated variants were further characterised by Pb_{UPD} to determine whether any changes in the structure of the gold occurred due to the effects of heating. On examining the 2% Au/graphite catalyst and the catalysts heated under hydrogen (figure 3.2.3), it became evident that only Au{111} and Au{110} facets were present (see features at 0.30 V and 0.44 V respectively). There was no direct indication of the presence of Au{100} features. This was also the case using Au-modified platinum catalysts (see section 3.1).

Heating the 2% Au/graphite catalyst resulted in a loss of peak area and peak definition for both the Au{111} and Au{110} features, indicating that long range order was being

reduced, with the exception of the sample heated to 500 K. On heating the 2% Au/graphite catalyst to only 500 K, the definition of the Au{111} feature improved indicating that the catalyst now contained better defined Au{111} facets. This suggests that the Au{111} facets were expanding at the expense of the Au{110} facets, since this feature had decreased significantly for the 500 K catalyst. The Au{110} features were lost more rapidly than the Au{111} features and were absent for the sample heated to 600 and 700 K. The Au{111} feature was still present for the catalyst heated at 700 K indicating that these features were more resistant to the heat treatment.

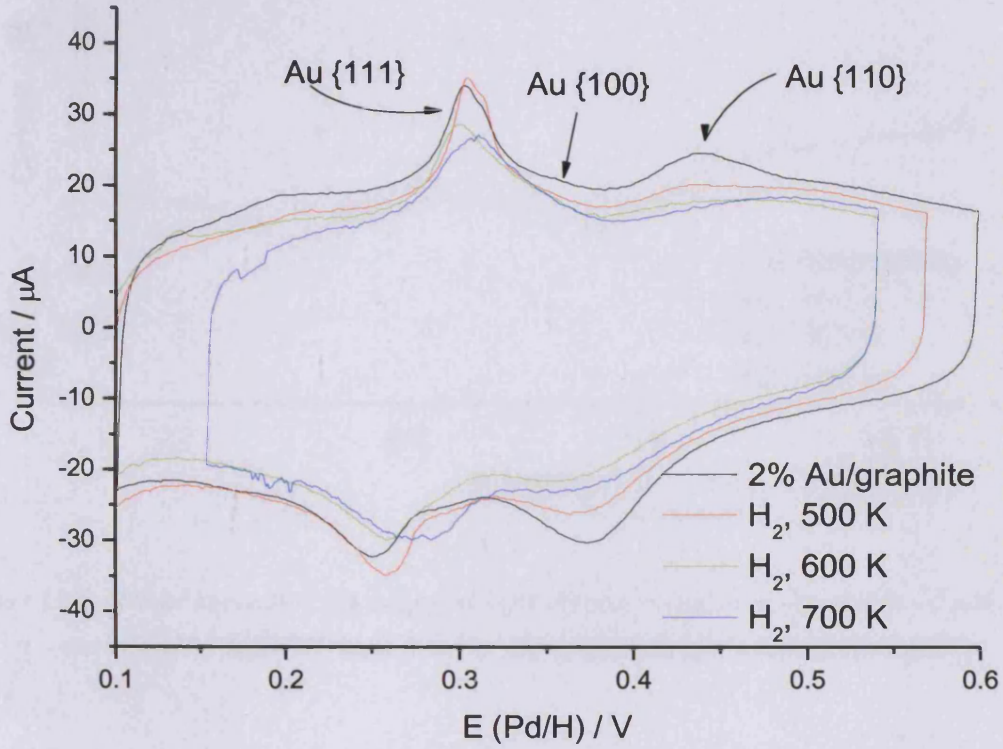

Figure 3.2.3: CVs for as-received 2% Au/graphite and variants heated in hydrogen obtained in 1.0 mM lead nitrate and 0.1 M NaOH run at 10 mV s^{-1} showing details of the gold morphology.

Figure 3.2.4 shows the CVs obtained when the 2% Au/graphite catalyst and the variants prepared under air were examined by the technique of Pb_{UPD}. As before, Au{111} and Au{110} features are shown by the catalysts at 0.30 V and 0.44 V respectively and the Au{100} peak is again absent. Heating the 2% Au/graphite catalyst in air resulted in a steady growth and sharpening of both the {111} and {110} features. This is especially true of the catalyst heated to 700 K where, in addition to sharpening, the peaks also

split. This indicates a significant increase in the extent of the Au{111} facets on these gold surfaces. The possibility of an increased particle size is unlikely and can be ruled out by the XPS analysis (see later).

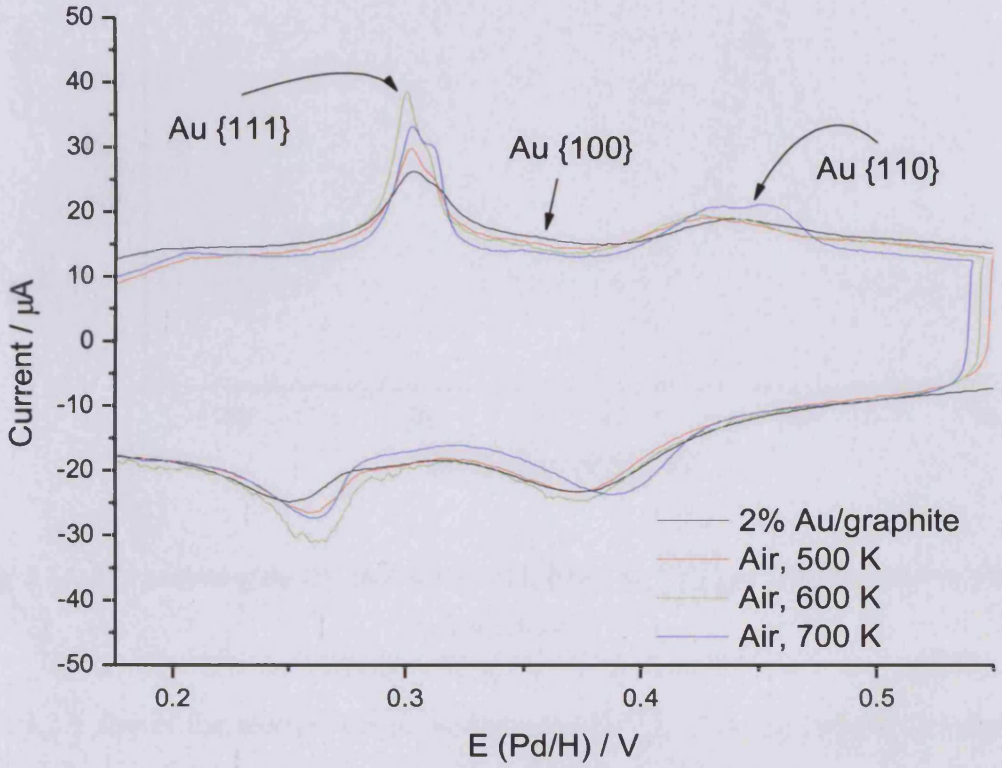

Figure 3.2.4: CVs for as-received 2% Au/graphite and variants heated in air obtained in 1.0 mM lead nitrate and 0.1 M NaOH run at 10 mV s^{-1} showing details of the gold morphology.

3.2.4 Characterisation of Au/graphite catalysts: XPS analysis

Figure 3.2.5 shows the gold 4f peaks for the 2% Au/graphite and samples heated under hydrogen. The peaks representing the 500 K and 600 K catalysts are almost identical in size, but the 700 K catalyst's response is slightly smaller. This indicates that the surface area of the gold has decreased, although not systematically, with increasing preparation temperature. This is the same trend as was established by the relative oxide-reduction peaks observed in the CVs of section 3.2.2.

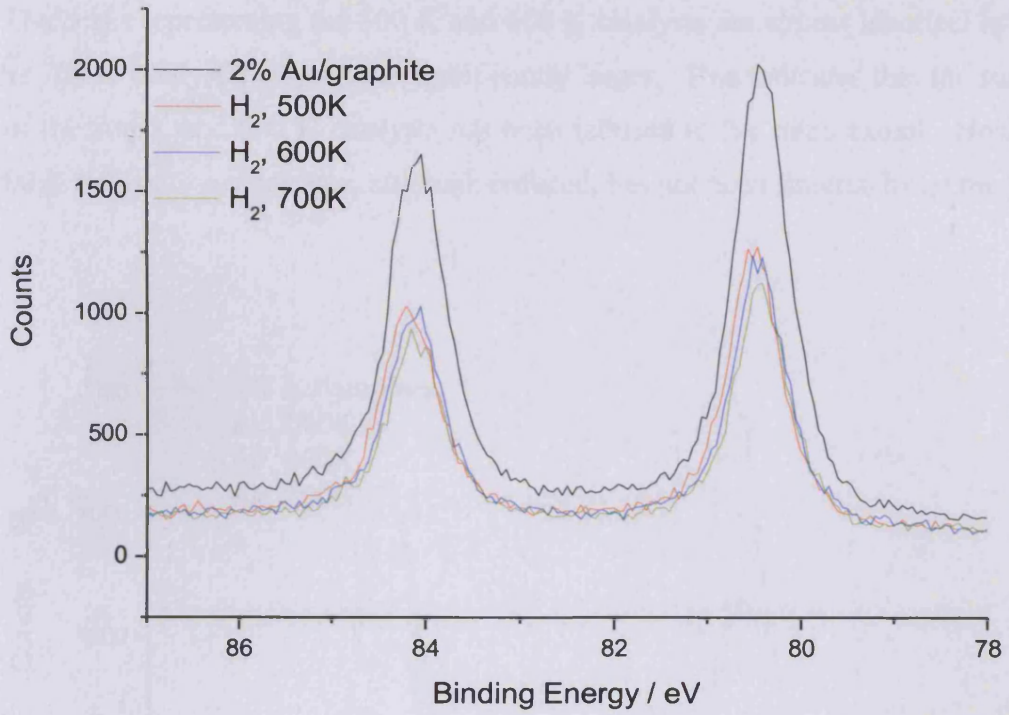

Figure 3.2.5: XPS analysis of the 2% Au/graphite catalyst and the hydrogen treated derivatives, showing the gold 4f peaks.

Table 3.2.1 shows the atomic weight percentages for the 2% Au/graphite catalyst and the hydrogen treated derivatives. This table confirms that there is a loss of gold loading (i.e. sintering has occurred) and also indicates that the amount of carbon present has not altered. It is assumed therefore that there has been little effect on the carbon caused by thermal annealing of the sample.

Table 3.2.1: Surface atomic weight percentages for the 2% Au/graphite catalyst and the hydrogen treated derivatives.

Catalyst	% C	% Au
2% Au/graphite	99.7	0.3
H_2, 500	99.8	0.2
H_2, 600	99.8	0.2
H_2, 700	99.8	0.2

Figure 3.2.6 shows the gold 4f peaks for the 2% Au/graphite and the samples heated in air. The peaks representing the 500 K and 600 K catalysts are almost identical in size, but the 700 K catalyst's response is significantly larger. This indicates that the surface area of the 500 K and 600 K catalysts has been reduced to the same extent. However the 700 K catalyst's surface area, although reduced, has not been sintered by as much.

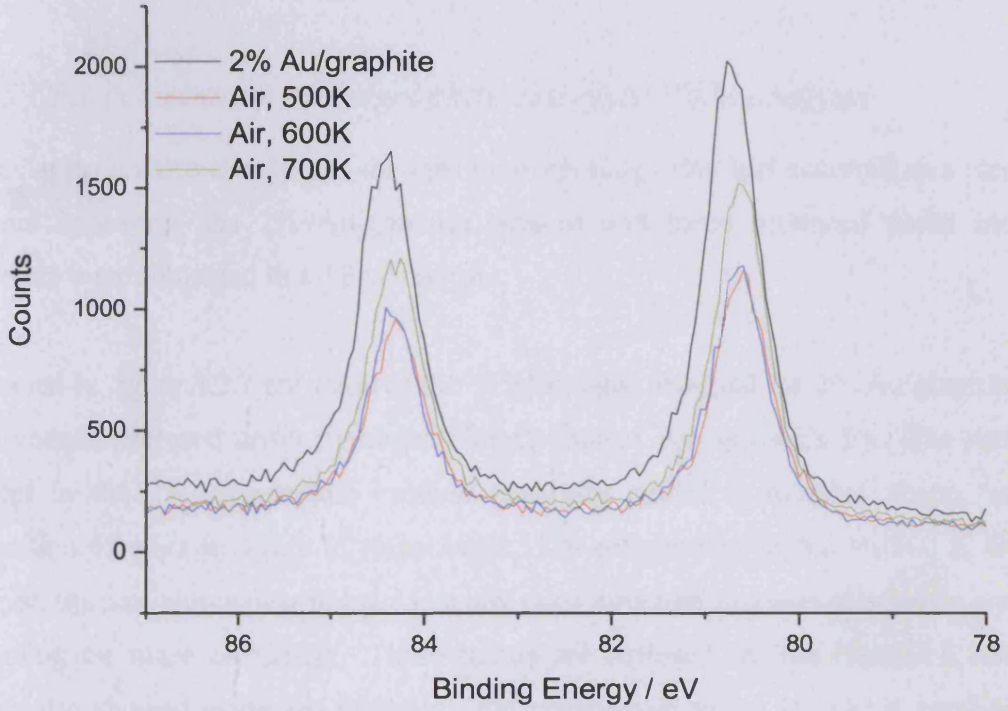

Figure 3.2.6: XPS analysis of the 2% Au/graphite catalyst and the air treated derivatives, showing the gold 4f peaks.

Table 3.2.2 shows the atomic weight percentages for the 2% Au/graphite catalyst and the air treated derivatives. Notably, the percentage of carbon again does not change notably between the catalysts confirming that the graphite support in not being lost during sintering. In addition the percentage gold observed for the 700 K catalyst is larger than that seen for the other sintered catalysts, again confirming that this gold catalyst has not been affecting in the same way as the others by the thermal annealing process.

Table 3.2.2: Surface atomic weight percentages for the 2% Au/graphite catalyst and the hydrogen treated derivatives.

Catalyst	% C	% Au
2% Au/graphite	99.7	0.3
Air 500	99.8	0.2
Air 600	99.8	0.2
Air 700	99.7	0.3

3.2.5 Characterisation of Au/graphite catalysts: TEM analysis

To understand more clearly any changes in morphology that had occurred as a result of thermal annealing, the 2% Au/graphite catalyst and those produced under air and hydrogen were subjected to a TEM analysis.

Presented in figure 3.2.7 are some of the TEM images obtained for 2% Au/graphite and the catalysts prepared under hydrogen (for all images see appendix B). The particles present in the 2% Au/graphite catalyst generally exhibit a rounded shape, with a suggestion of edge structure in some cases. On progressing to the H_2/500 K treated catalyst, the particles appear to have lost any edge structure that was previously present, becoming far more elongated. These trends are repeated for the H_2/600 K catalyst which also showed elongated particles. On progression to the H_2/700 K catalyst, the particles are on average noticeably more rounded than the previous images.

The CVs presented in section 3.2.2 showed a decrease in surface area with increasing temperature. In addition the voltammogram showed a significant decrease in structure for the H_2/700 K catalyst. These trends appear to be confirmed by the current data. The CVs presented in section 3.2.3 generally showed a loss of structure with increasing temperature and this trend is again confirmed here. Notably, in the voltammogram results the H_2/500 K catalyst showed a slight increase for Au{111} and in the TEMs presented below the catalyst exhibits some faceting that may account for the increased structure observed in the CVs. Visually there appear to be fewer particles at increased temperatures and comparison with the XPS data confirms that there are significantly fewer particles present on the thermally annealed catalysts compared with the 2% Au/graphite. This indicates that the catalysts are sintering.

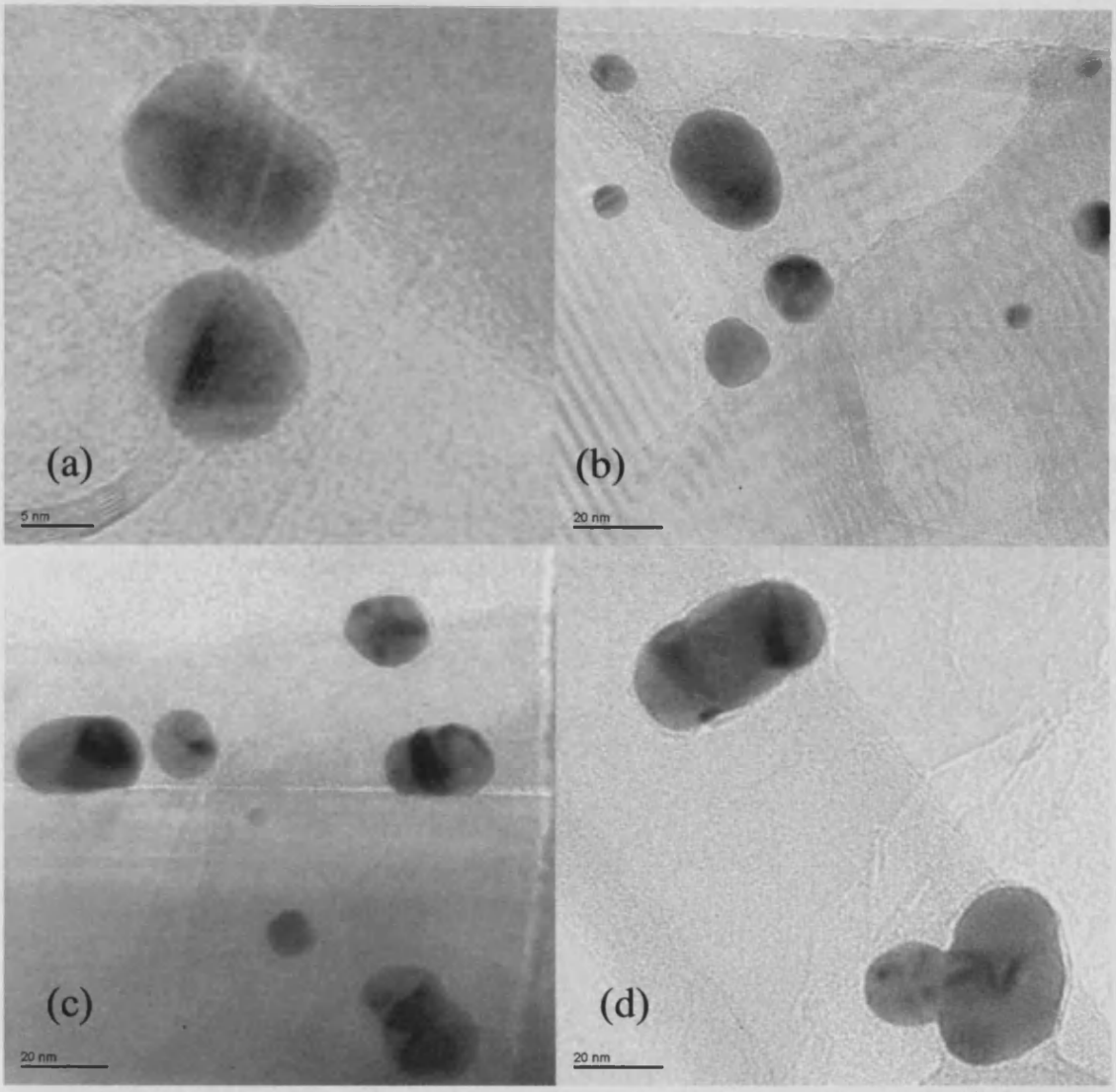

Figure 3.2.7: TEM of (a) 2% Au/graphite catalyst and (b) H_2, 500 K, (c) H_2, 600 K, (d) H_2, 700 K sintered catalysts.

Presented in figure 3.2.8 are TEM images obtained for 2% Au/graphite and the catalysts annealed under air. The particles present for the 2% Au/graphite catalyst generally exhibit a rounded shape, with a suggestion of edge structure in some cases. Electron microscopy is complicated by diffraction and other optical effects with particular "overlayers" on different graphite planes. However it was noticeable that a greater number of "dark" patches, with sharp boundaries and particular shapes (triangles and straight lines) were obtained with the air treated gold particles. If these artefacts are associated with well ordered crystal planes, it would correspond to findings revealed via CV. This is purely speculation at the present time and requires further study. However, throughout the thesis, such phenomena will be referred to as *"structured" catalysts particles*.

On moving to the air/500 K treated catalyst, the particles exhibit an increase in structure in some cases. This is visually represented as a criss-cross network running over the surface of the particles. These trends are repeated and exaggerated for the air/600 K catalyst. On progression to the air/700 K catalyst, the particles appear to contain far more structure.

The voltammograms presented in section 3.2.2 showed a decrease in surface area and an increase in {111} structure (especially for the air/700 K catalyst) with increasing temperature. These trends are in agreement with the current data. The voltammograms presented in section 3.2.3 generally showed an increased structure with increasing temperature and this trend is again confirmed here.

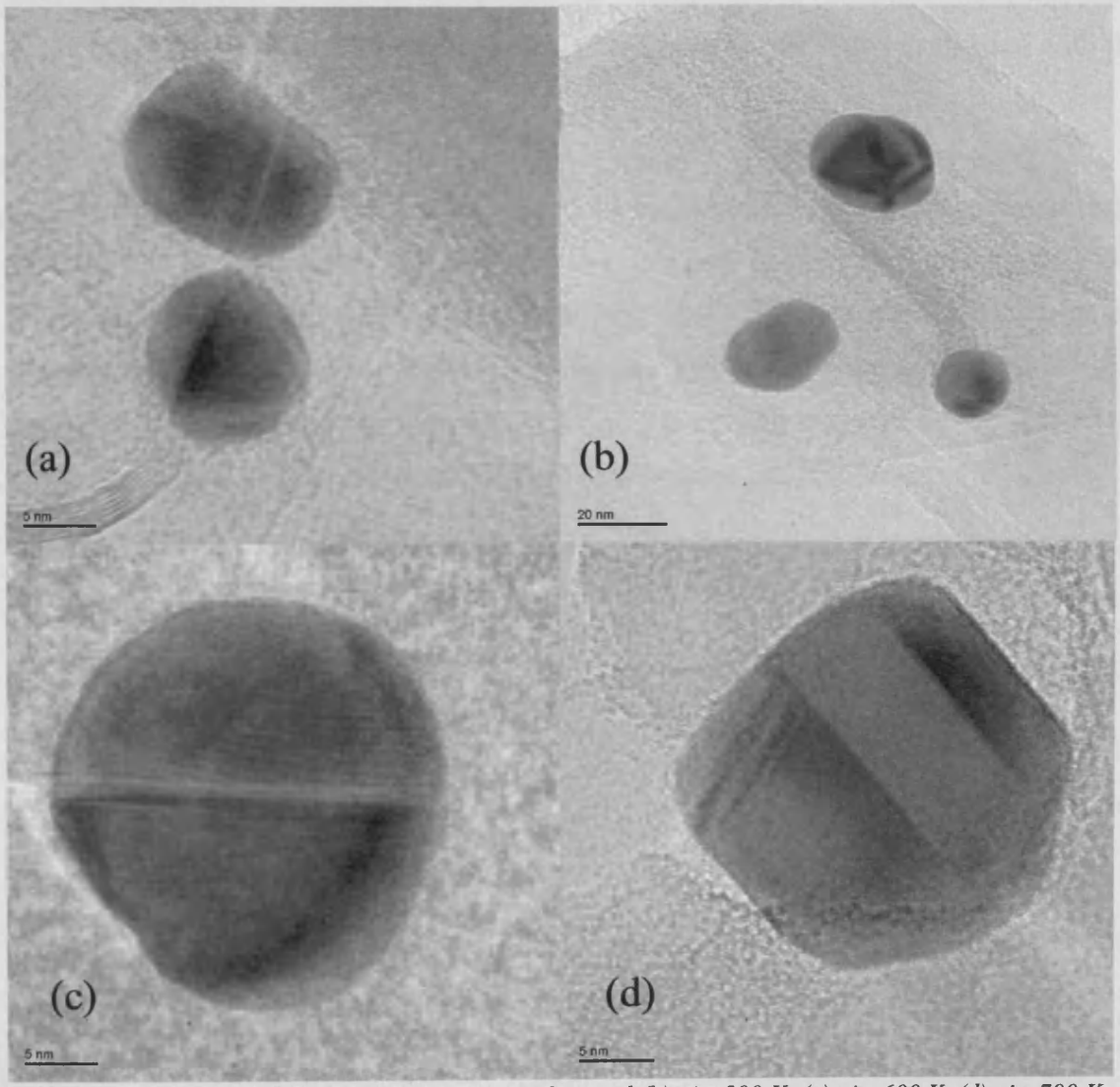

Figure 3.2.8: TEM of (a) 2% Au/graphite catalyst and (b) air, 500 K, (c) air, 600 K, (d) air, 700 K sintered catalysts.

3.2.6 Characterisation of Au/graphite catalysts: CVs in basic conditions

Figure 3.2.9 shows voltammograms recorded in basic electrolyte for the 2% Au/graphite catalyst and the variants prepared at elevated temperatures under hydrogen. In the forward sweep the gold oxide formation peak occurred at 1.2 V. In the reverse sweep the "normal" gold oxide-reduction peak, (a), occurred between 1.0 and 1.1 V. The shape and structure of this peak remained constant for all of the catalysts with the exception of the 2% Au/graphite catalyst prepared at 700 K, which appeared at a slightly greater potential. The second oxide-reduction peak, (b), first observed by Hutchings *et al* occurring at 0.8 V initially increased in size for the catalyst heated at 500K, before dropping in intensity for the sample heated to 600 K. The peak is almost absent for the sample heated to 700 K. Based on this finding and the link between this peak and catalytic selectivity proposed by Hutchings, it would be a reasonable prediction that the selectivity of these catalysts should go through a maximum with the 500 K catalyst.

The extent of oxygen evolution appears to be independent of annealing temperature. The H_2/700 K treated catalyst produces the smallest oxygen evolution peak. The unmodified 2% Au/graphite catalyst and the H_2/600 K variant produce a similar extent of oxygen evolution and the H_2/500 K produces by far the largest oxygen evolution peak. Yet it is interesting to note that this order is exactly mirrored by the size of the reduction peak, (b). This apparent link will be discussed in detail later.

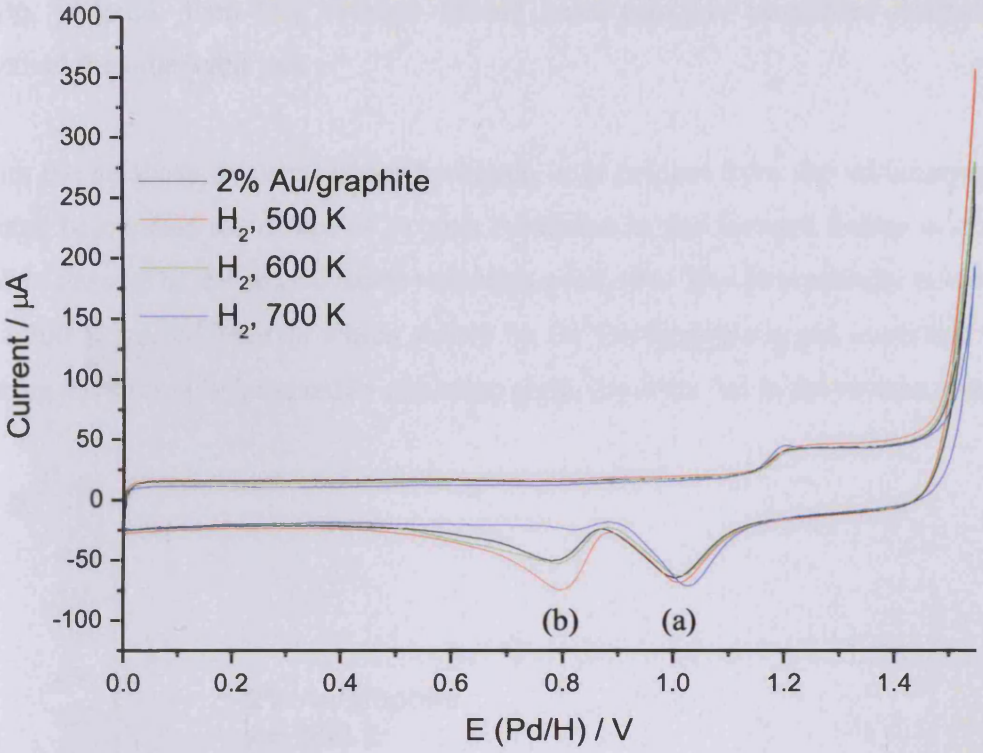

Figure 3.2.9: CVs for as-received 2% Au/graphite and the variants heated under hydrogen in 0.5 M NaOH at 10 mV s^{-1} showing the features associated with gold oxide formation and oxygen evolution in the forward sweep and reduction in the reverse sweep.

Figure 3.2.10 shows the voltammograms obtained for the 2% Au/graphite catalyst and the variants prepared under air when run in a basic solution. The features present in these CVs are the same as those seen for the catalysts treated under hydrogen. In the reverse sweep the gold oxide-reduction peak at 1.0 V, decreased slightly in size for the heat treated catalysts, but otherwise remained unaffected. This may again indicate that the surface area of the gold particles was slightly reduced as a result of sintering. The second peak at 0.8 V in the reverse sweep (linked to catalyst selectivity) initially shrank in size relative to the untreated 2% Au/graphite catalyst before returning to its former intensity (500 K and 600 K catalyst). On heating to 700 K a marked increase and shift in the size of this peak was evident. This suggested, based on Hutchings model, that the effect of heating would be to initially decrease the selectivity of the gold catalyst and then increase for the catalysts heated to higher temperatures. The effect of heating to 700 K appears to have been to increase the intensity of the gold catalyst's oxide

stripping peak at 0.7 V significantly and if the proposed link between activity and peak intensity is valid, then this catalyst should have catalytic properties dramatically different to the other catalysts.

As with the catalysts prepared under hydrogen, it is evident from the voltammograms presented below that the extent of oxygen formation in the forward sweep is directly related to the size of the second oxide reduction peak, (b). This is especially evident for the air/700 K treated catalyst which shows by far the largest oxygen evolution peak, mirroring the unusually large oxide-reduction peak, (b) observed in the reverse sweep.

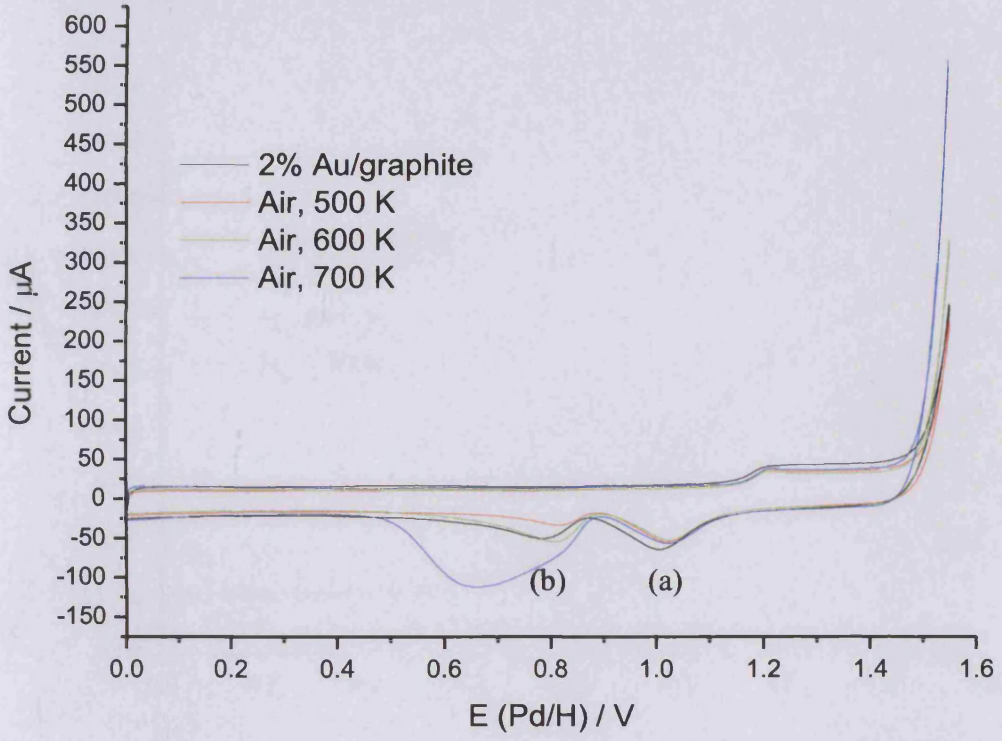

Figure 3.2.10: CVs for as-recieved 2% Au/graphite and variants heated under air in 0.5 M NaOH at 10 mV s^{-1} showing the features associated with gold oxide formation and oxygen evolution.

3.2.7 Glycerol oxidation in the electrochemical cell

Figure 3.2.11 shows voltammograms obtained for 2% Au/graphite and the catalysts formed by heating under hydrogen when they were used for the electrooxidation of

glycerol. All of the catalysts gave a response in this electrolyte indicating that they were all active for glycerol electrooxidation. The catalysts that had been treated at 500 K and 600 K show a significantly larger response than the untreated 2% Au/graphite, indicating that the extent of electrooxidation occurring over these catalysts was significantly greater than over the untreated catalyst. The extent of electrooxidation occurring on the catalyst heated to 700 K corresponded approximately to the level given by the untreated catalyst. In addition the shoulder present at 1.1 V for all other catalysts is now absent and the onset of oxide formation occurred at the lower potential of 1.4 V. This may indicate that the catalyst heated to 700 K was not producing such a wide range of products and that it was generally less effective as a catalyst.

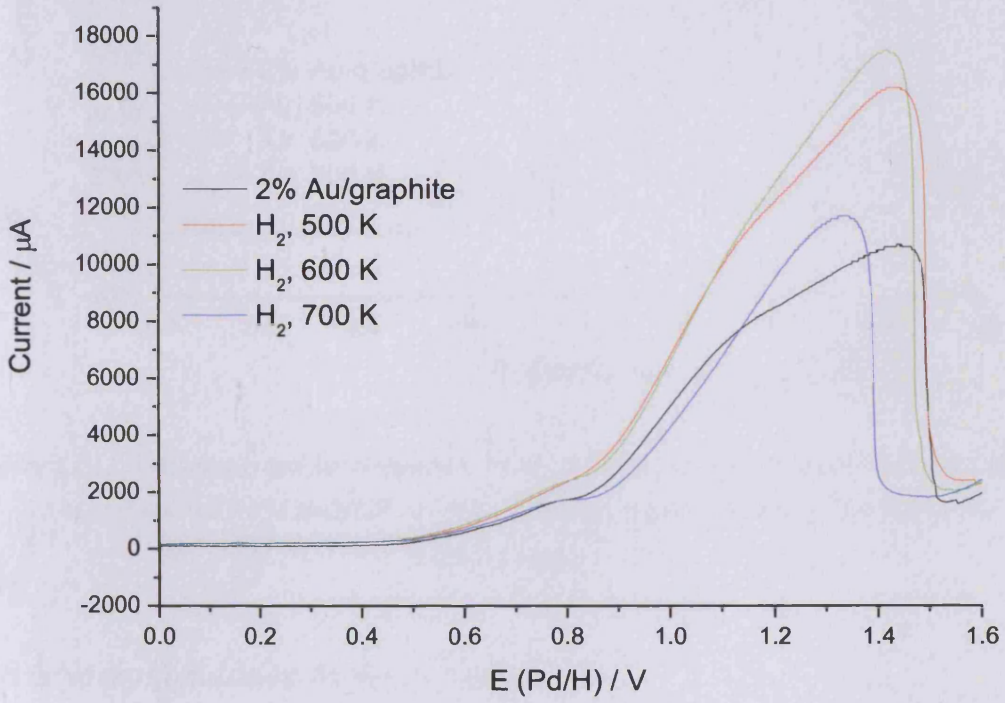

Figure 3.2.11: Voltammograms for as-received 2% Au/graphite catalyst and variants heated under hydrogen in 0.5 M glycerol and 0.5 M NaOH at 10 mV s^{-1} showing the features associated with glycerol electrooxidation.

Figure 3.2.12 shows the CV obtained when the air treated catalysts were used for glycerol electrooxidation. These catalysts followed the same pattern of behaviour as was established by the catalysts treated under hydrogen and the same conclusions are drawn. However, there is one significant difference with respect to the catalyst heated

to 700 K. The slight shoulder present for all of the catalysts at 1.0 – 1.1 V becomes a distinct peak. This indicates that this catalyst can perform electrooxidation of glycerol at a significantly lower potential and as such this catalyst may be found to be more active or selective than the others when tested in a high-pressure reactor.

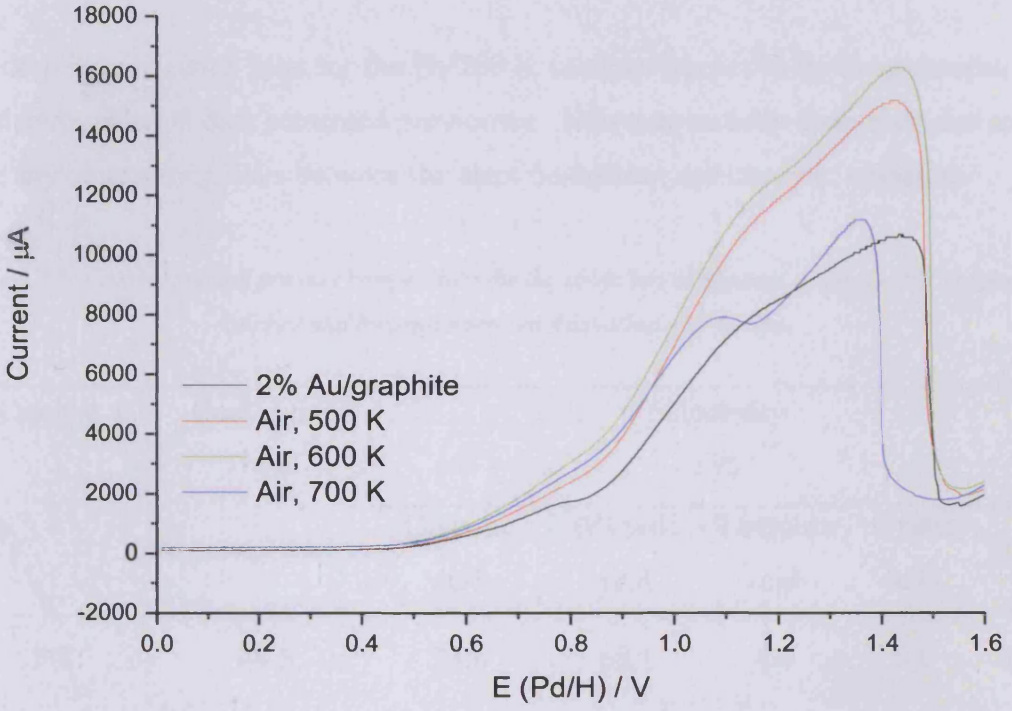

Figure 3.2.12: Voltammograms for as-received 2% Au/graphite and the variants heated under air in 0.5 M glycerol and 0.5 M NaOH at 10 mV s^{-1} showing the features associated with glycerol electrooxidation.

3.2.8 Glycerol oxidation in the reactor

The results obtained for the catalytic oxidation of glycerol over the 2% Au/graphite and the hydrogen treated derivatives are presented in table 3.2.1. There appears to be no trend within the extent of conversion on progression to higher annealing temperatures. However it is of interest that the conversion recorded for the H_2/700 K catalyst is significantly lower than the other values obtained.

From the selectivity data, it is evident that the main products formed were glycolic acid and glyceric acid. As with the conversion, the product distribution did not change

consistently between the different catalysts. However, the H_2/500 K catalyst did show a tendency to produce a larger amount of glycolic acid than the surrounding catalysts and from the Pb_{UPD} voltammograms it was found that this catalyst had better defined Au{111} regions, which may be responsible for this change. Also of note was that the H_2/700 catalyst produced greater quantities of minor products and significantly less of the glyceric acid.

The drop in conversion seen for the H_2/700 K catalyst appears to be in agreement with the electrooxidation data presented previously. However initially there does not appear to be any other strong links between the electrooxidation and catalytic oxidation.

Table 3.2.1: Conversion and product composition for the oxidation of glycerol using the 2% Au/graphite catalyst and hydrogen treated derivatives (50°C, 2h).

Catalyst	Conversion / %	Selectivity / %				
		Glycolic acid	Glyceric acid	Tartronic acid	Oxalic acid	HPA
2%	48.5	23.6	68.1	4.0	0.9	3.4
500K	35.6	30.7	62.2	3.0	0	4.1
600K	58.5	20.0	74.0	3.1	0.6	2.4
700K	5.3	35.5	46.4	6.1	7.2	4.9

Table 3.2.2 shows the results obtained for the catalytic oxidation of glycerol over the 2% Au/graphite and the air treated derivatives. As with the data presented above, there appears to be no overall trend in the extent of conversion. However it is noteworthy that the air/500 K catalyst shows a significantly lower conversion than the other catalysts. The selectivity towards glycolic acid exhibited by the catalysts appears to increase at the expense of the glyceric acid and some of the minor products.

The air/700 K catalyst, that previously had a significantly low conversion, was now more comparable with the other data. However the air/700 K also shows an unremarkable product distribution. There appears to have been no significant changes in catalytic selectivity as a result of the structure changes within this catalyst observed by the characterisation techniques (CV and TEM).

In addition there appears to be no significant links between either the electrooxidation results nor the basic voltammograms and the catalytic data presented below.

Table 3.2.2: Conversion and product composition for the oxidation of glycerol using the 2% Au/graphite catalyst and air treated derivatives (50°C, 2h).

Catalyst	Conversion / %	Selectivity / %				
		Glycolic acid	Glyceric acid	Tartronic acid	Oxalic acid	HPA
2%	48.5	23.6	68.1	4.0	0.9	3.4
500 K	13	36.9	56.4	0	0	6.7
600 K	78.4	27.5	65.2	2.6	0.8	3.9
700 K	39.3	23.8	69.2	2.6	1.2	3.1

3.3 Graphite-supported Bi-Au catalysts: characterisation and activity in glycerol oxidation

3.3.1 Introduction

From previous work carried out on glycerol oxidation, bismuth was found to be an excellent promoter for supported platinum catalysts [11, 12]. Hence the use of bismuth promoted gold catalysts was considered. All experiments described in this section involved the use of the Au/graphite catalysts described in chapter 2. Cyclic voltammetry was used to determine (i) where bismuth was adsorbed on the gold surface and the nature of the adsorbed bismuth, and (ii) whether the introduction of the bismuth influenced the activity or selectivity of the gold catalysts for glycerol electrooxidation. XPS and TEM examinations were also carried out to support the electrochemical characterisation results obtained. Finally glycerol oxidation was carried out in a high-pressure reactor to determine the activity and selectivity of the catalysts.

3.3.2 Characterisation of gold and bismuth-modified gold catalysts: CVs in acidic conditions

Four Au/graphite catalysts were prepared as described in section 2.1.1. Each of these catalysts was then used in the preparation of a subsequent series of bismuth-modified catalysts, as described in section 2.1.2. Voltammograms of the Bi-Au/graphite catalysts were obtained with the samples mounted on a platinum mesh (the mesh gave characteristic H_{UPD} peaks between 0.0 V and 0.3 V in the forward sweep and the platinum oxide-reduction peak at 0.7 V in the reverse sweep). Platinum was used as a support since the signals produced are well documented [13] and hence did not interfere with those attributed to gold.

The CVs obtained for the four Au/graphite catalysts are presented in figure 3.3.1. 2% Au/graphite gave peaks at 1.35 and 1.55 V in the forward sweep; they are attributed to oxide formation at well defined Au steps and Au{111} terraces respectively. On progressing to lower gold loadings these peaks first diminished in intensity and then disappeared indicating that either smaller, less well defined Au particles had been formed during the preparation of these catalysts or fewer particles were present. In the

reverse sweep all of the gold catalysts produced an oxide-reduction peak at 1.12 V. The area of this peak increased steadily with gold loading (table 3.3.1). The invariance of the potential at which this peak appeared suggested that the gold particle size distribution was the same for all of the catalysts and that it was the numbers of particles present that changed with gold loading.

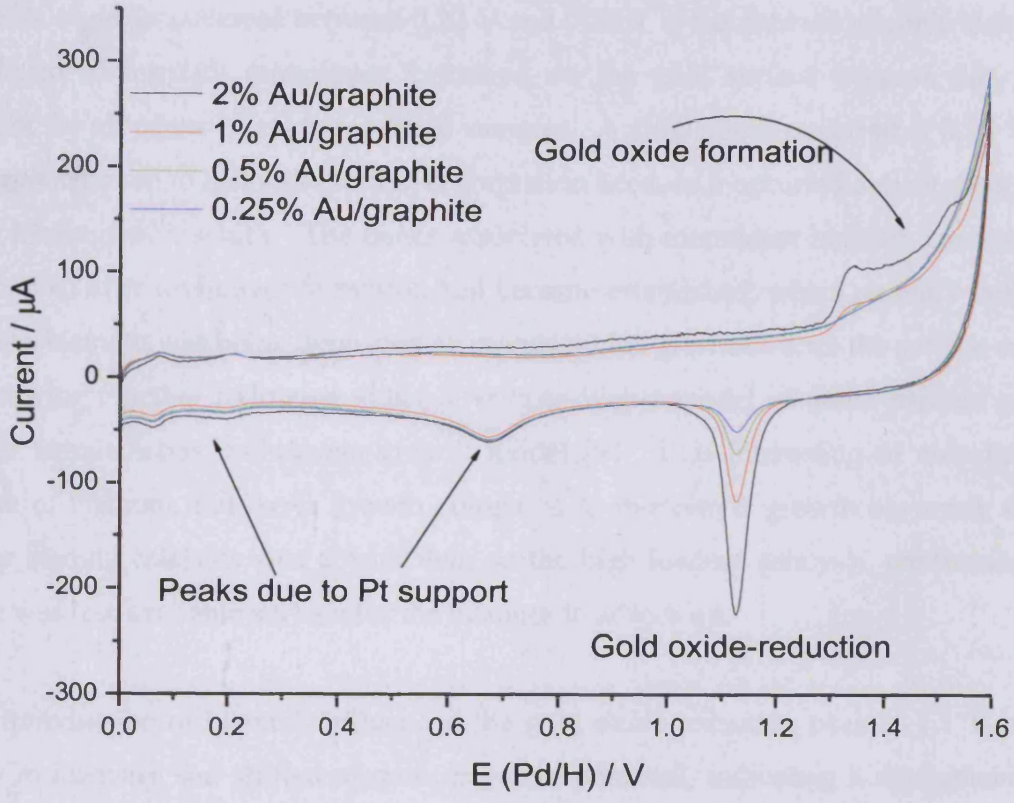

Figure 3.3.1: CVs in 0.5 M H_2SO_4 at 10 mV s^{-1} showing gold oxide formation and reduction peaks for the four Au/graphite catalysts.

Table 3.3.1: Variation of the gold oxide-reduction peak area with gold loading.

Catalyst loading	Area of peak at 1.12 V / mC
2% Au	0.64
1%	0.29
0.5%	0.17
0.25%	0.08

Presented in figures 3.3.2 - 3.3.5 are the voltammograms obtained for the 2% Au/graphite, 1% Au/graphite, 0.5% Au/graphite, and 0.25% Au/graphite catalysts along with their bismuth modified variants. Bismuth adsorbed in two distinct forms – undergoing both monolayer and multilayer growth. These voltammograms all exhibit similar features and as such will be discussed together. Any deviations from these trends will of course be noted.

A series of peaks occurred between 0.22 V and 0.50 V in the forward sweep which were attributed to bismuth monolayer formation on the gold surface because they were present for all of the bismuth modified samples. A single peak occurred at 0.18 V and this was ascribed to bismuth multilayer formation because it occurred only at medium to high loadings of bismuth. The peaks associated with monolayer bismuth continued to grow even after multilayer formation had become established, which strongly indicated that the bismuth was being deposited as islands which grew out from the surface as well as growing together following either a Volmer-Weber model of metal particle growth [8] or simultaneous multilayers growth model [9]. It is interesting to note that the extent of bismuth multilayer growth compared to monolayer growth occurring on the lower loading catalysts was greater than on the high loading catalysts, confirming that there was less available surface for the bismuth to adsorb on.

The introduction of bismuth influenced the gold oxide-reduction peak at 1.1 V, which grew in intensity and shifted to more negative potential, indicating a strengthening of the Au-O bond. This signifies that bismuth ad-atoms were altering the electronic properties of the gold and hence possibly its catalytic properties. So the effect of bismuth promotion on gold might be both as a site-blocker and electronic promoter.

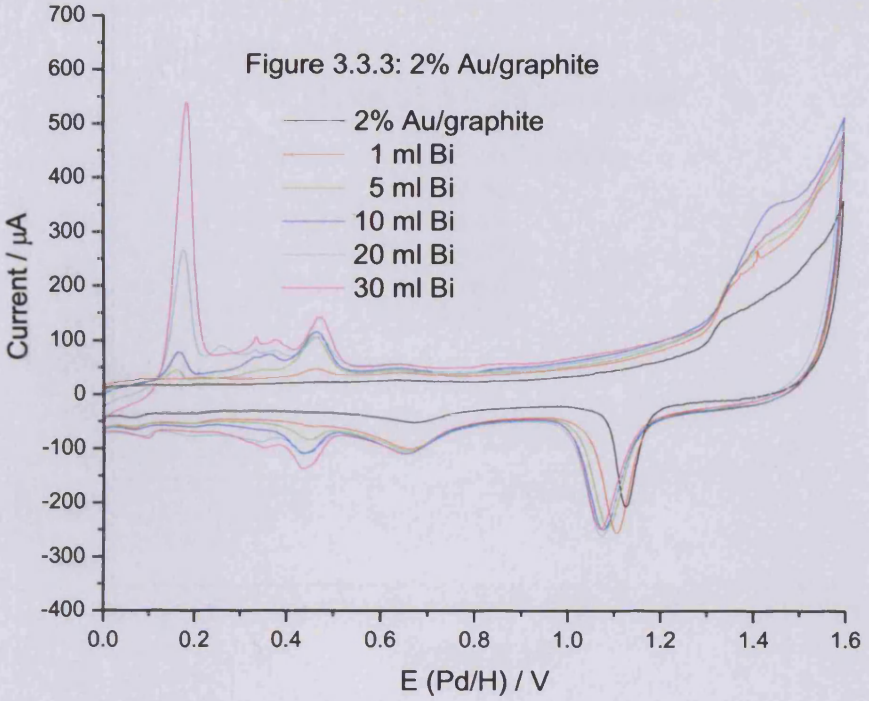

Figure 3.3.2: CVs for the 2% Au/graphite catalyst and bismuth modified variants in 0.5 M H_2SO_4 at 10 mV s^{-1} showing gold oxide formation / reduction and Bi growth.

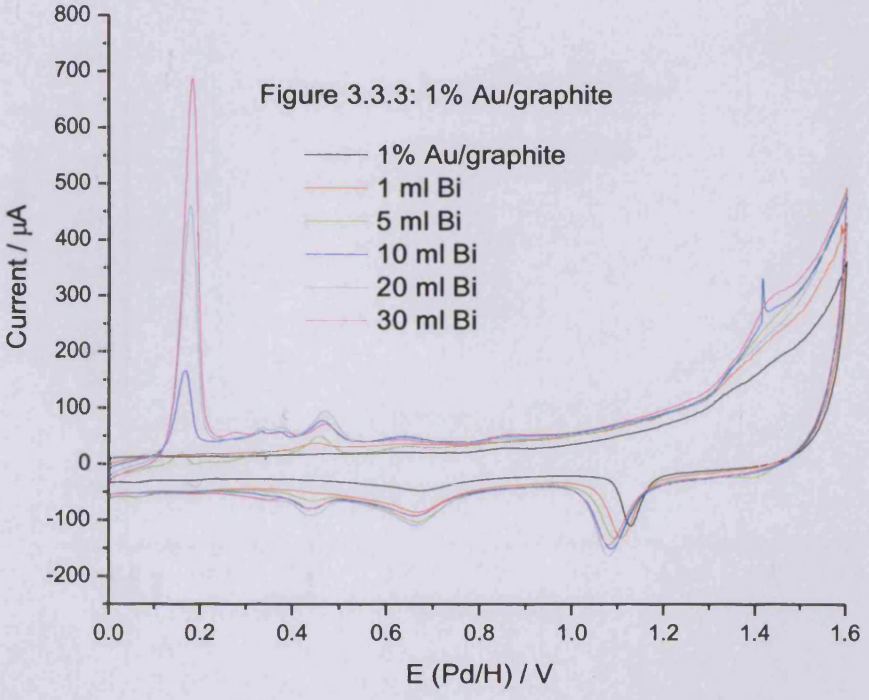

Figure 3.3.3: CVs for the 1% Au/graphite catalyst and bismuth modified variants in 0.5 M H_2SO_4 at 10 mV s^{-1} showing gold oxide formation / reduction and Bi growth.

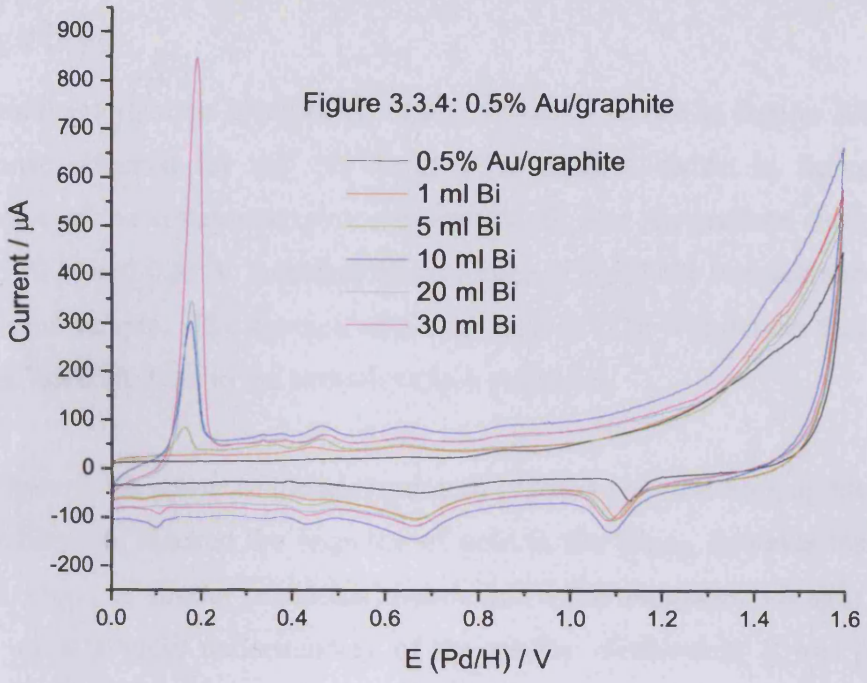

Figure 3.3.4: CVs for the 0.5% Au/graphite catalyst and bismuth modified variants in 0.5 M H_2SO_4 at 10 mV s^{-1} showing gold oxide formation / reduction and Bi growth.

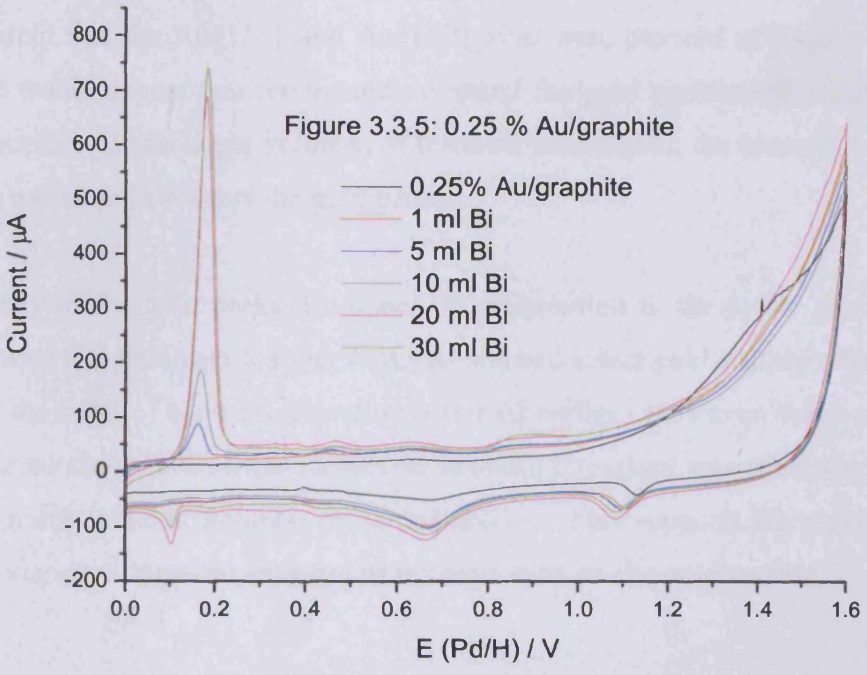

Figure 3.3.5: CVs for the 2% Au/graphite catalyst and bismuth modified variants in 0.5 M H_2SO_4 at 10 mV s^{-1} showing gold oxide formation / reduction and Bi growth.

3.3.3 Characterisation of gold and bismuth-modified gold catalysts: CVs involving Pb_{UPD}

The structural information obtained by use of Pb_{UPD} is shown in figures 3.3.6 -3.3.9. The response obtained for the 2% Au/graphite catalyst shown in figure 3.3.6 is representative of the voltammograms obtained for all four Au/graphite catalysts. The peaks at 0.19 V and 0.33 V indicated the presence of Au{111} terraces and Au{110} surfaces in the sample. The absence of a clear peak at 0.26 V indicates that Au{100} terraces did not contribute to the overall surface structure.

The figures show the effects of the adsorption of bismuth onto the Au/graphite catalysts. Bismuth adsorption blocked the response of gold to the Pb_{UPD}, however bismuth also underwent Pb_{UPD} at similar potentials, hence the voltammograms are spilt over two graphs to allow a better understanding of the results. Fortunately it was possible to determine which gold sites where being blocked by the bismuth and the extent to which the gold surface was blocked overall.

From the voltammograms of catalysts containing both high and low loadings of bismuth it was evident that the Au{111} and Au{110} sites were blocked at roughly the same rate, i.e. it would appear that the bismuth covered the gold surface uniformly and was not site-specific. When larger volumes of bismuth were added, the bismuth peaks grew to such an extent as to obscure the gold peaks.

The intensity of the gold peaks decreased on progression to the lower gold loadings. This indicated that the lower loading catalysts showed lower gold surface areas with the result that the onset of bismuth saturation occurred earlier. However, some of the gold sites remained visible even when multilayer bismuth formation was underway (compare voltammograms in acidic solution presented above). This supports the conclusion that bismuth underwent three-dimensional island formation on the gold surface.

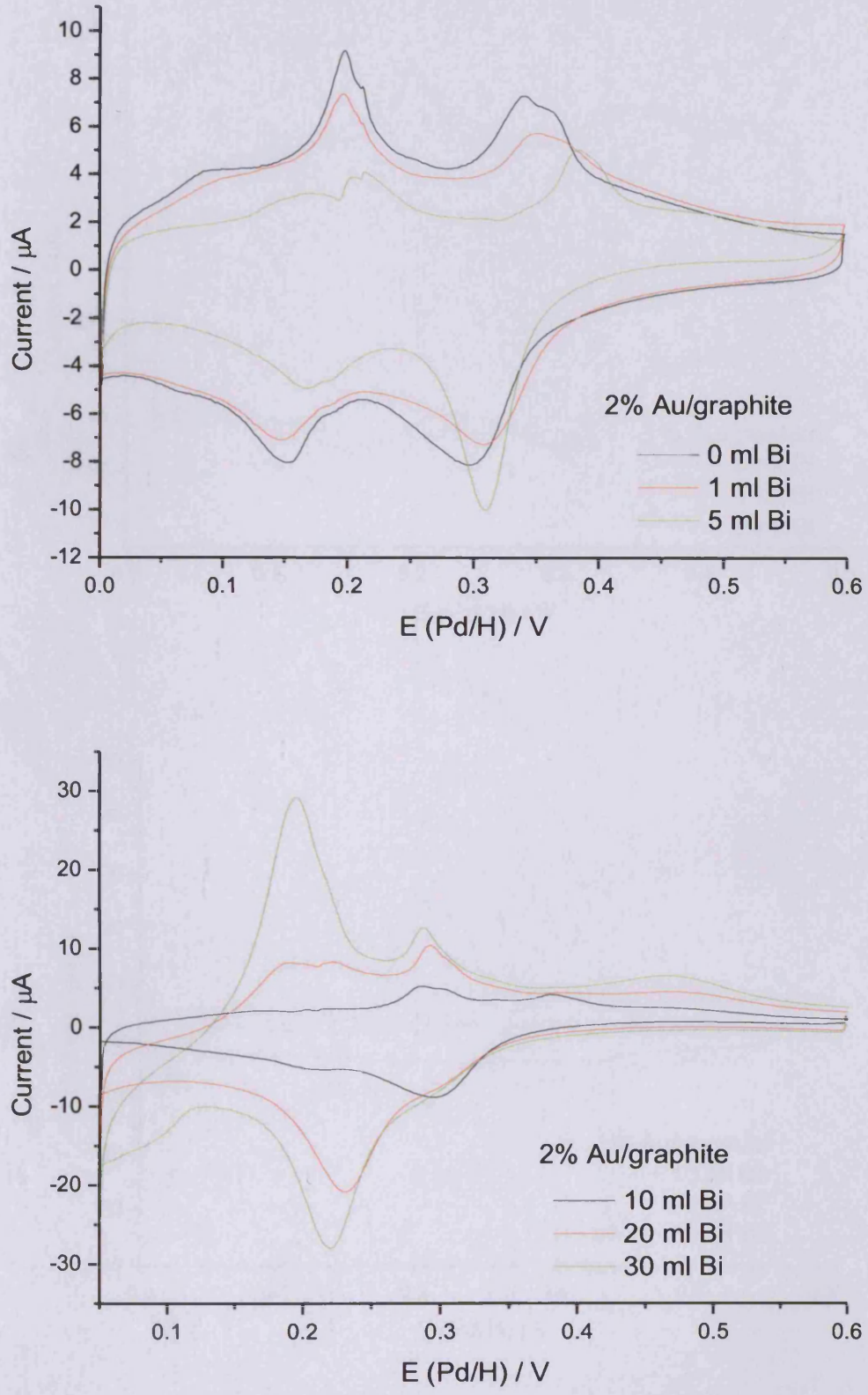

Figure 3.3.6: CVs for 2% Au/graphite in 1.0 mM lead nitrate and 0.1 M NaOH run at 10 mV s^{-1}: effects of bismuth adsorption.

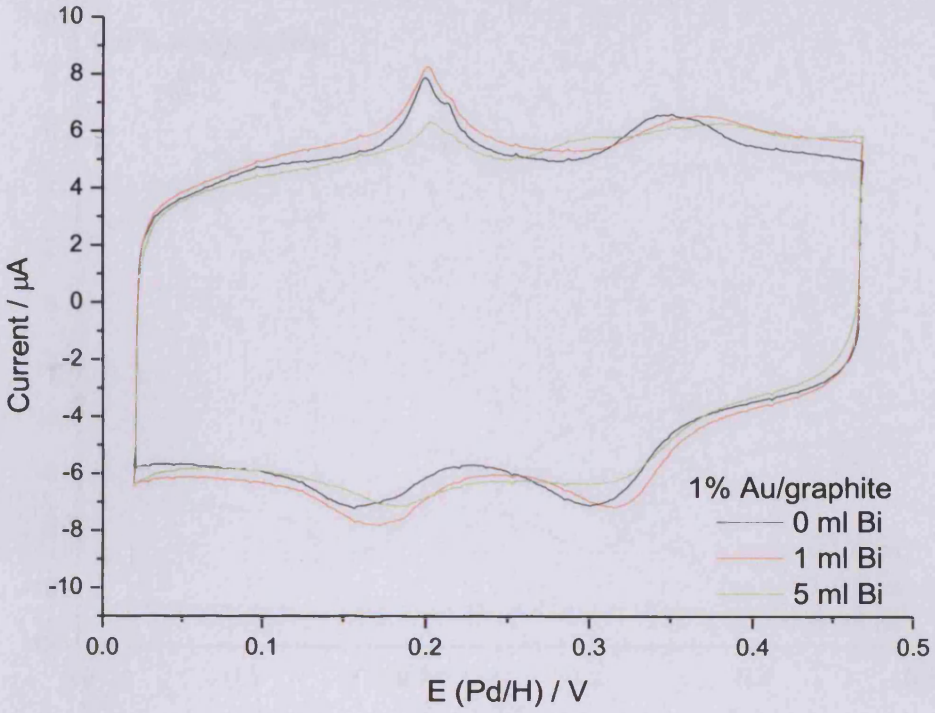

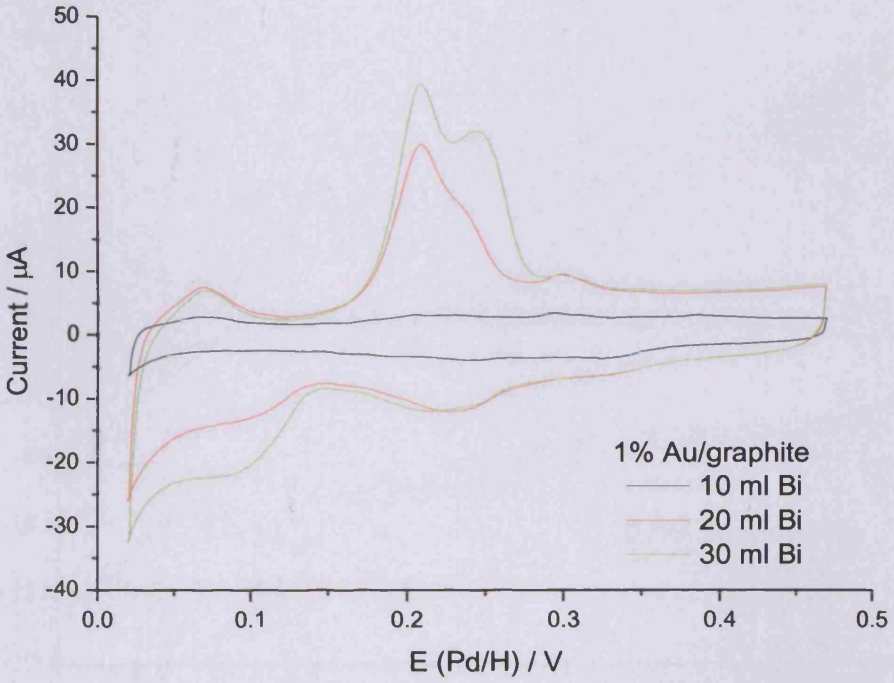

Figure 3.3.7: CVs for 1% Au/graphite in 1.0 mM lead nitrate and 0.1 M NaOH run at 10 mV s^{-1}: effects of bismuth adsorption.

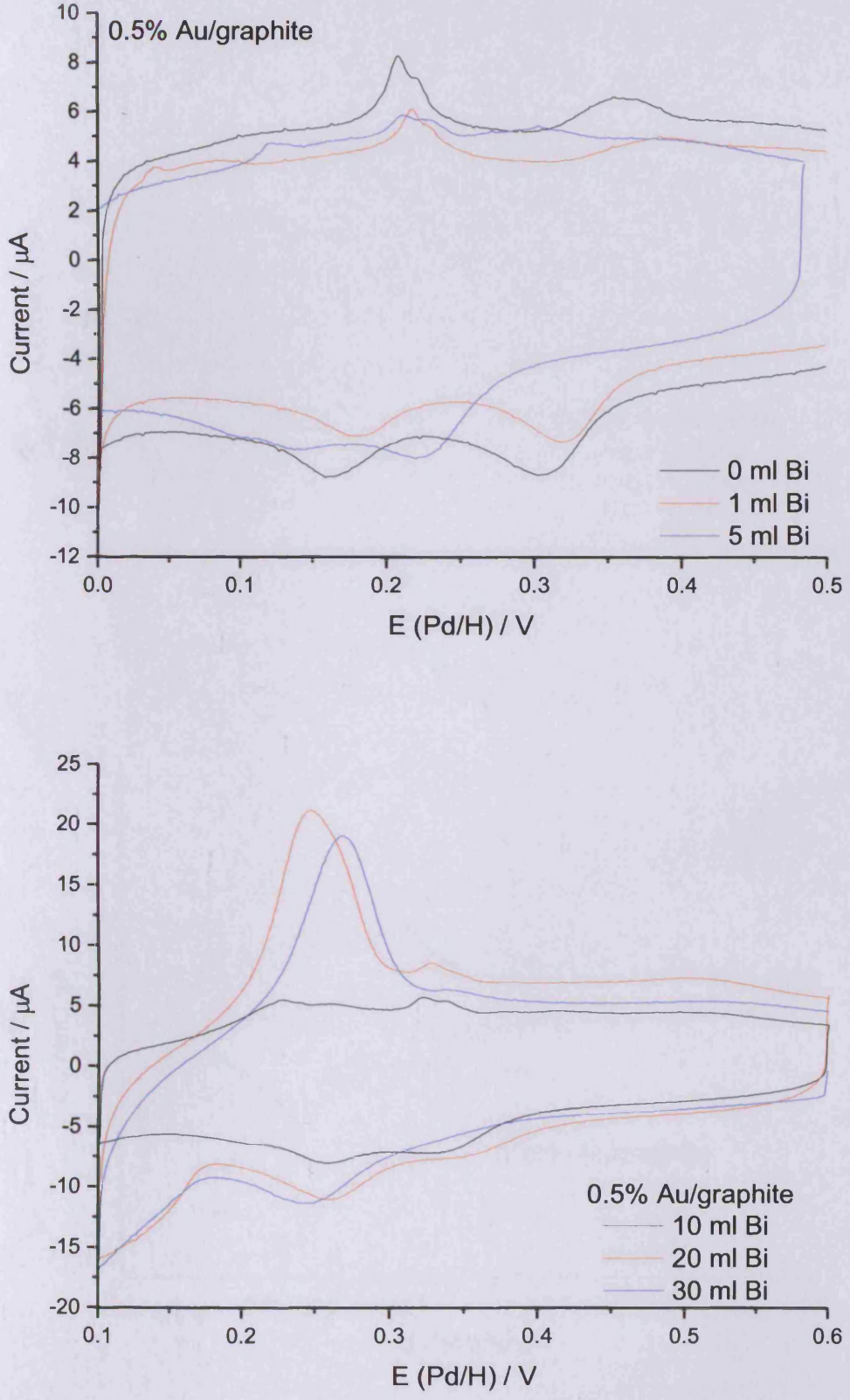

Figure 3.3.8: CVs for 0.5% Au/graphite in 1.0 mM lead nitrate and 0.1 M NaOH run at 10 mV s^{-1}: effects of bismuth adsorption.

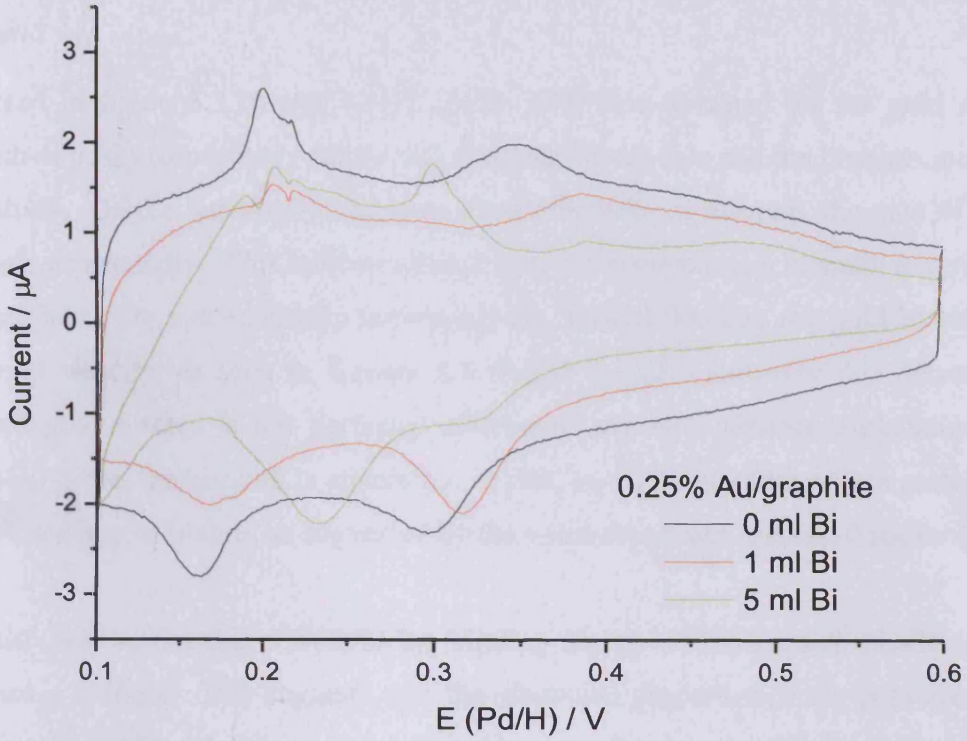

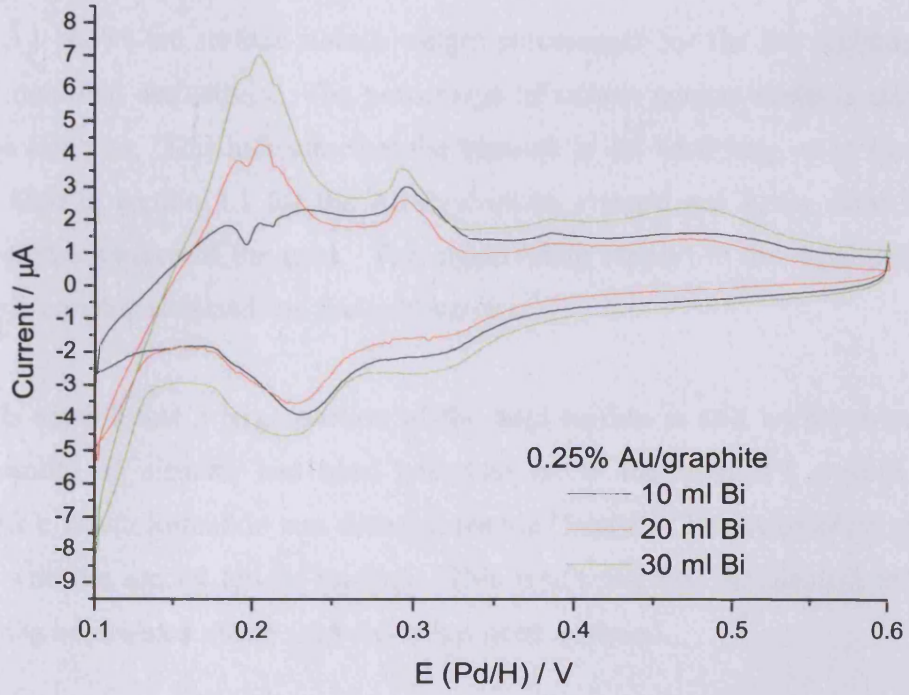

Figure 3.3.9: CVs for 0.25% Au/graphite in 1.0 mM lead nitrate and 0.1 M NaOH run at 10 mV s^{-1}: effects of bismuth adsorption.

3.3.4 Characterisation of gold and bismuth-modified gold catalysts: XPS analysis

Presented in figure 3.3.10 and 3.3.11 is the XPS data obtained for the gold 4f and bismuth 4f peaks respectively for the 2% Au/graphite catalyst and the bismuth modified derivatives. On the introduction of even small quantities of bismuth, the gold 4f peaks decrease substantially. This indicates that it does not require much bismuth to cover the gold surface. On systematically increasing the bismuth loading the gold blocking is increased steadily, as seen in figures 3.3.10 and 3.3.11. However this decrease in exposed gold surface is not perfectly systematic and two possible explanations are possible. Either the bismuth is adsorbing, in part, on to the graphite or it is growing on the gold surface as islands, as suggested by the voltammograms discussed earlier.

It is also noteworthy that a shift in the binding energy of the bismuth modified gold catalysts is evident. This suggests that the electronic properties of the gold are being modified by the introduction of bismuth. However there is no change in the binding energy of bismuth, even on moving from monolayer to multilayer forms.

Table 3.3.1 shows the surface atomic weight percentages for the 2% Au/graphite and bismuth modified derivatives. The percentage of carbon present remains constant for all of the catalysts. This indicates that the bismuth is not adsorbing on to the graphite (as was seen in section 3.1 for the Au-Pt/graphite system) and hence must solely be located on the surface of the gold. This again lends support to the argument that the bismuth is growing as islands on the gold surface.

Also it is notable that a large portion of the gold surface is still visible even when a large quantity of bismuth had been adsorbed on to the catalyst's surface and yet multilayer bismuth formation was detected for the (5 ml)Bi-(2%)Au/graphite catalyst; a catalyst with the second lowest loading. This confirmed that the bismuth multilayers are forming before a complete monolayer has been achieved.

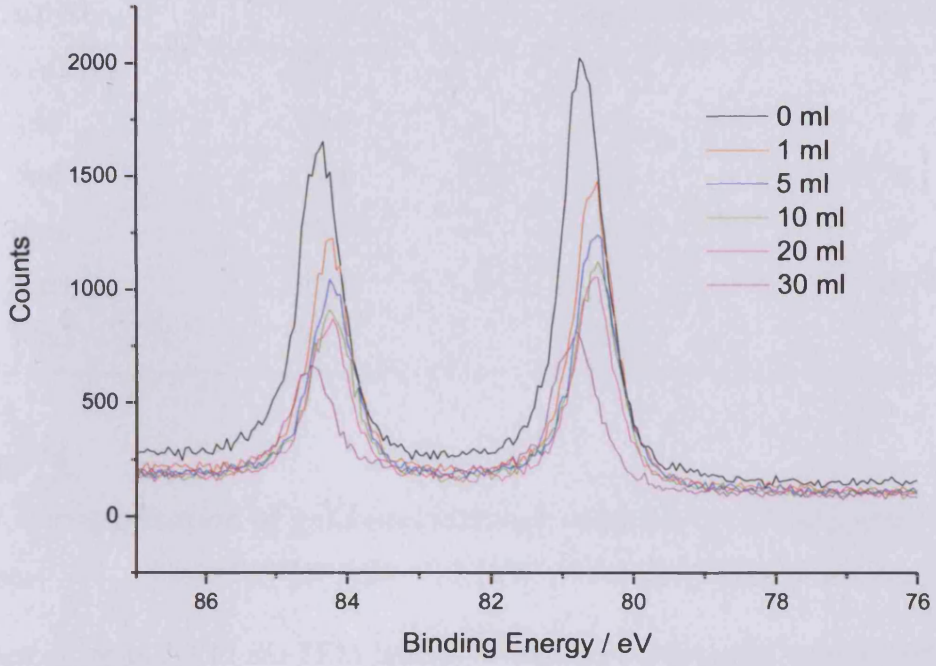

Figure 3.3.10: XPS spectra of the 2% Au/graphite catalyst and bismuth modified derivatives, showing the Au 4f peaks.

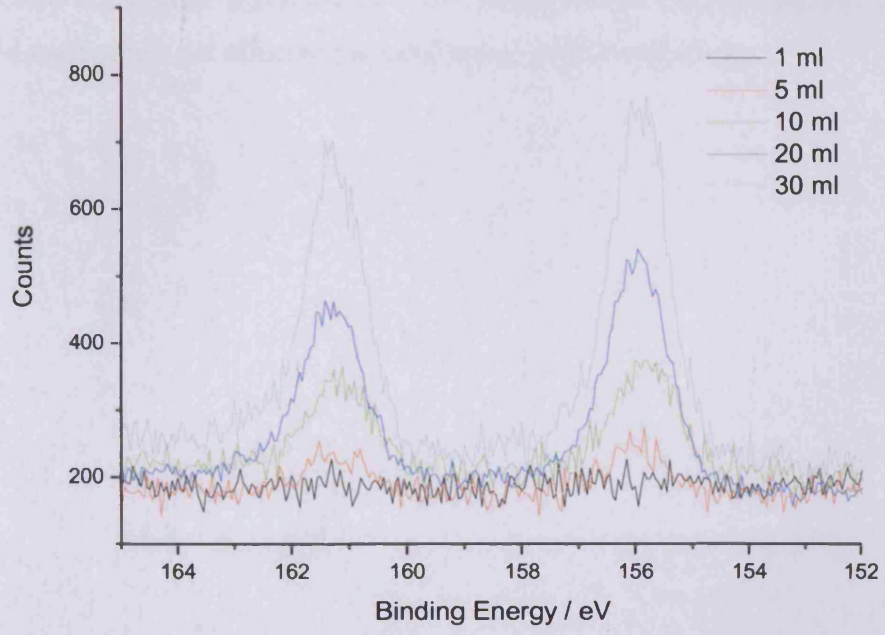

Figure 3.3.11: XPS spectra of the 2% Au/graphite catalyst and bismuth modified derivatives, showing the Bi 4f peaks.

Table 3.3.2: Surface atomic weight percentages for the 2% Au/graphite and bismuth modified derivatives.

Catalyst	C %	Au %	Bi %
2% Au/G	99.7	0.3	0
1ml	99.7	0.2	0
5ml	99.8	0.2	0
10ml	99.7	0.2	0
20ml	99.7	0.2	0.1
30ml	99.7	0.2	0.1

3.3.5 Characterisation of gold and bismuth-modified gold catalysts: TEM analysis

Presented in figure 3.3.12 are TEM images for the 2% Au/graphite catalyst and the Bi-Au/graphite catalysts that have been prepared with 1 ml Bi, 10 ml Bi and 30 ml Bi solution. The particles present for the 2% Au/graphite catalyst generally exhibited a rounded or in some cases slightly elongated shape. There is a suggestion of edge structure in some cases. On moving to the bismuth modified catalysts, the particle size and shapes do not change significantly. This suggests that the introduction of bismuth to the gold surface has not affected the underlying gold morphology.

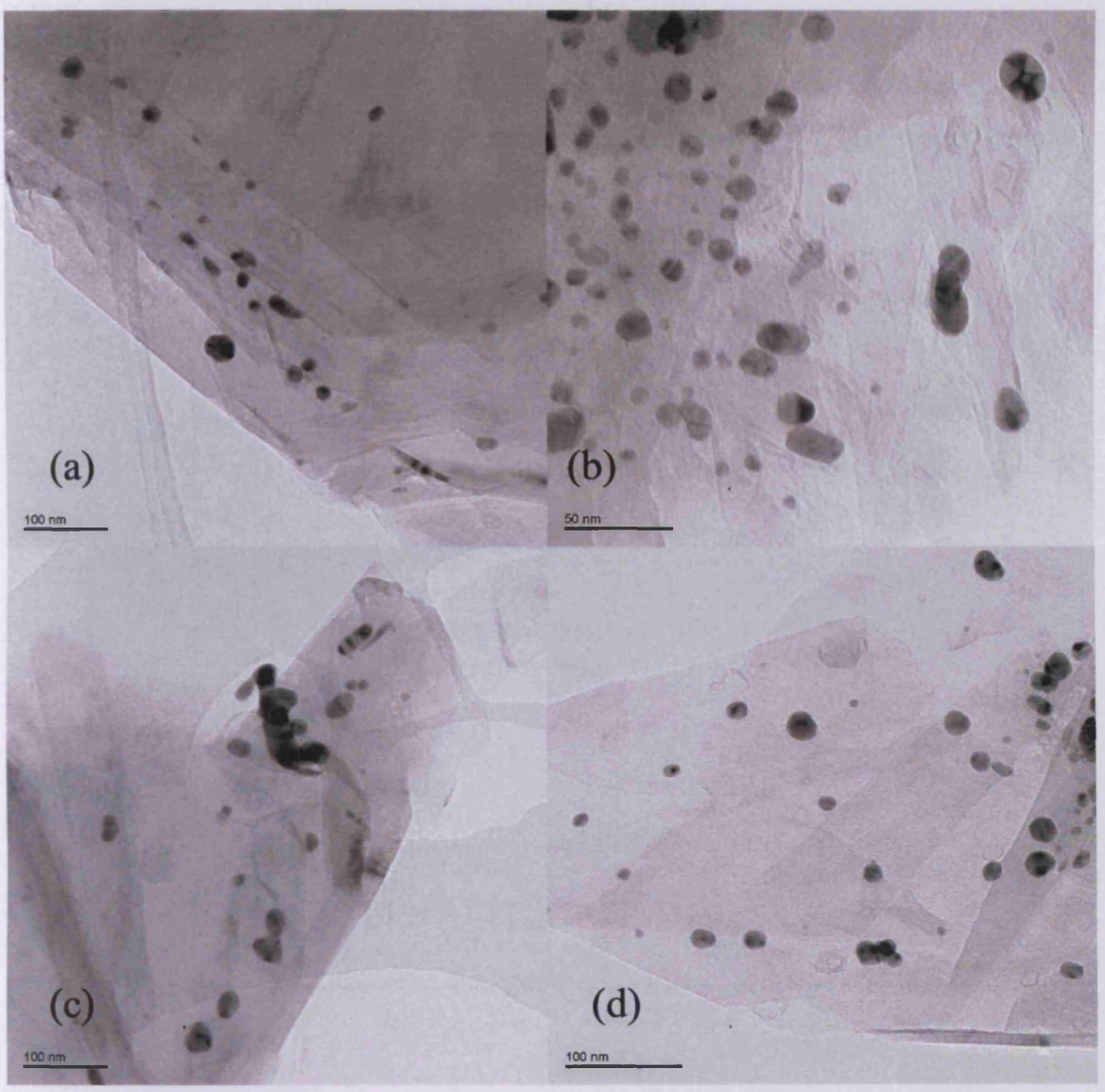

Figure 3.3.12: TEM of (a) 2% Au/graphite, (b) 1 ml Bi, (c) 10 ml Bi and (d) 30 ml Bi.

3.3.6 Characterisation of gold and bismuth-modified gold catalysts: CVs in basic conditions

Figure 3.3.13 shows the voltammograms obtained for the 2%, 1%, 0.5% and 0.25% Au/graphite catalysts run under basic conditions. In the forward sweep gold oxide was formed between 1.2 and 1.5 V. On sweeping the potential to 1.6 V the oxide formation is superseded by the onset of oxygen evolution characterised by the large, currents at 1.55 V. In the reverse sweep "normal" gold oxide-reduction, (a), occurred at 1.0 V and a second reduction peak (b), occurred between 0.6 - 0.7 V – the peak observed by Hutchings *et al.*

As would be expected, the gold oxide-reduction peak steadily increases in size with increasing gold loading. This is also true of the second oxide-reduction peak and as previously suggested, based on the findings of Hutchings *et al*, this might indicate an increased catalytic selectivity.

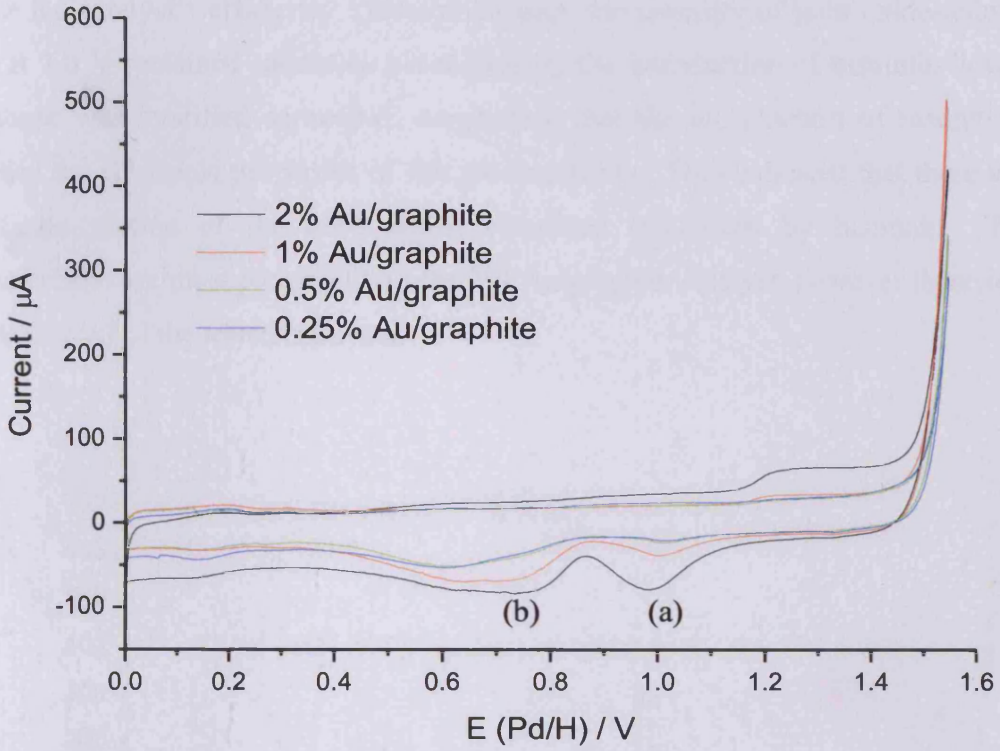

Figure 3.3.13: CVs of Au/graphite catalysts in 0.5 NaOH run at 10 mV s^{-1} showing gold oxide formation /reduction and oxygen evolution.

The Bi-Au/graphite catalysts were also studied under basic conditions. Figures 3.3.14 – 3.3.17 show the CVs obtained for the 2%, 1%, 0.5% and 0.25% bismuth modified samples respectively. Monolayer bismuth was evident from the series of peaks between 0.45 and 0.60 V and multilayer bismuth from the single peak growing at 0.39 V. This peak assignment was made because the peaks which were present between 0.45 and 0.60 V were present on all of the catalysts and the peak at 0.39 V was only present on the catalysts with the higher doses of bismuth. The formation of multilayer bismuth began earlier on the catalysts having lower gold loadings, as seen previously. This is consistent with there being less gold surface area in the lower loading catalysts and

hence less surface for the bismuth to cover in monolayer form. Also mirroring the acid voltammograms is the fact that the monolayer and multilayers were seen to form at the same time.

On the introduction of bismuth the second gold oxide-reduction peak at 0.7 V in the reverse sweep was removed. This might suggest that the effect of bismuth was to reduce the catalyst's efficiency. By comparison, the intensity of gold oxide-reduction peak at 1.0 V remained relatively untouched by the introduction of bismuth, however the shape was modified somewhat, suggesting that the introduction of bismuth had changed the electronic properties of the gold catalysts. This indicated that there was a significant portion of the gold which remained unblocked by bismuth. These characteristics are most prominent on the 2% Au/graphite catalyst; however these trends do apply to all of the tested catalysts.

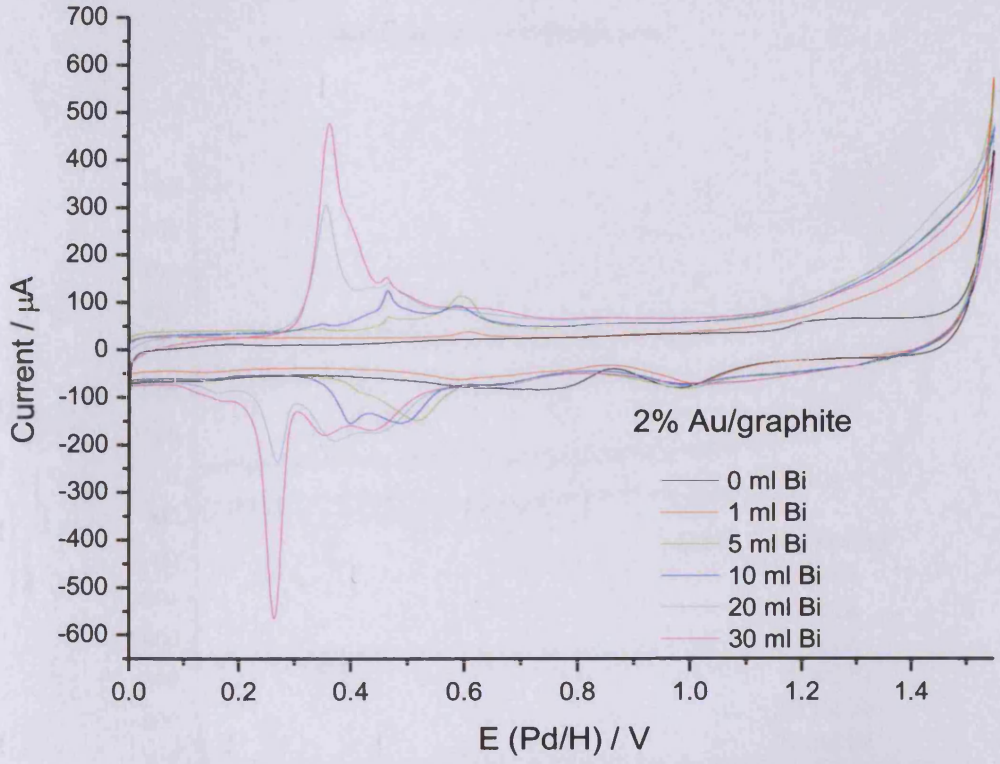

Figure 3.3.14: CVs of Bi-Au/graphite catalysts in 0.5 NaOH run at 10 mV s^{-1} showing oxygen evolution and oxide formation/reduction.

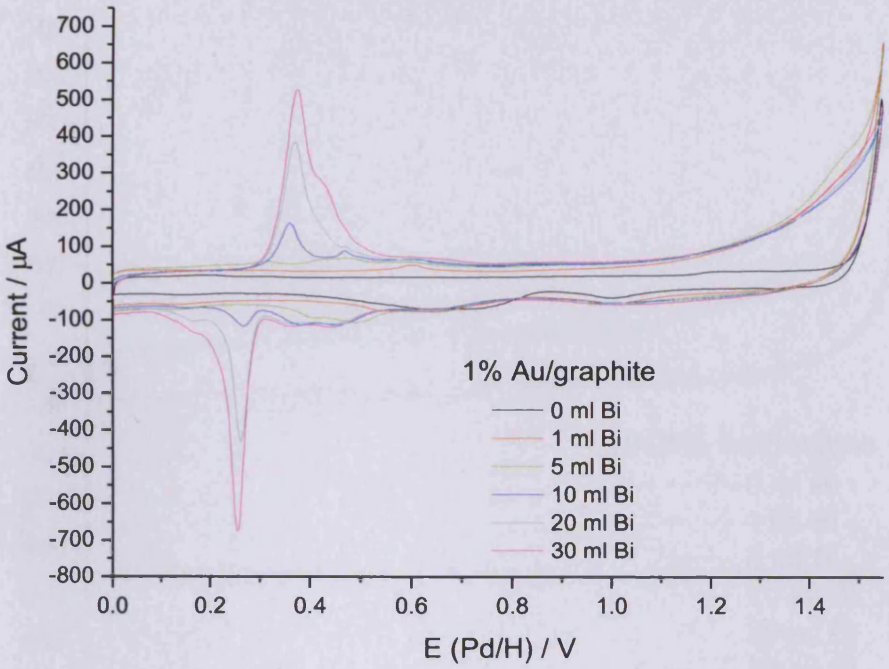

Figure 3.3.15: CVs of Bi-Au/graphite catalysts in 0.5 NaOH run at 10 mV s^{-1} showing oxygen evolution and oxide formation/reduction.

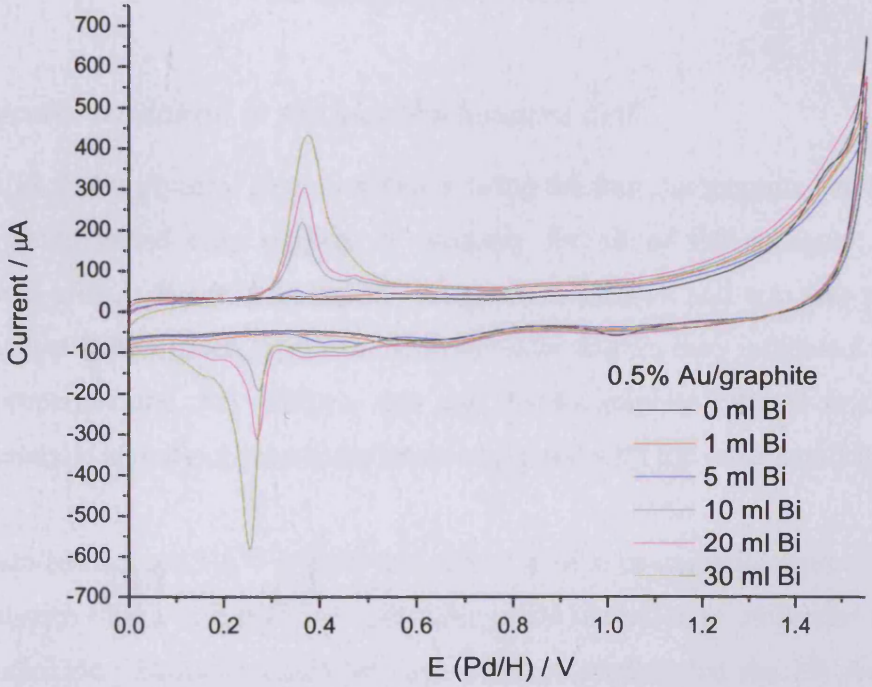

Figure 3.3.16: CVs of Bi-Au/graphite catalysts in 0.5 NaOH run at 10 mV s^{-1} showing oxygen evolution and oxide formation/reduction.

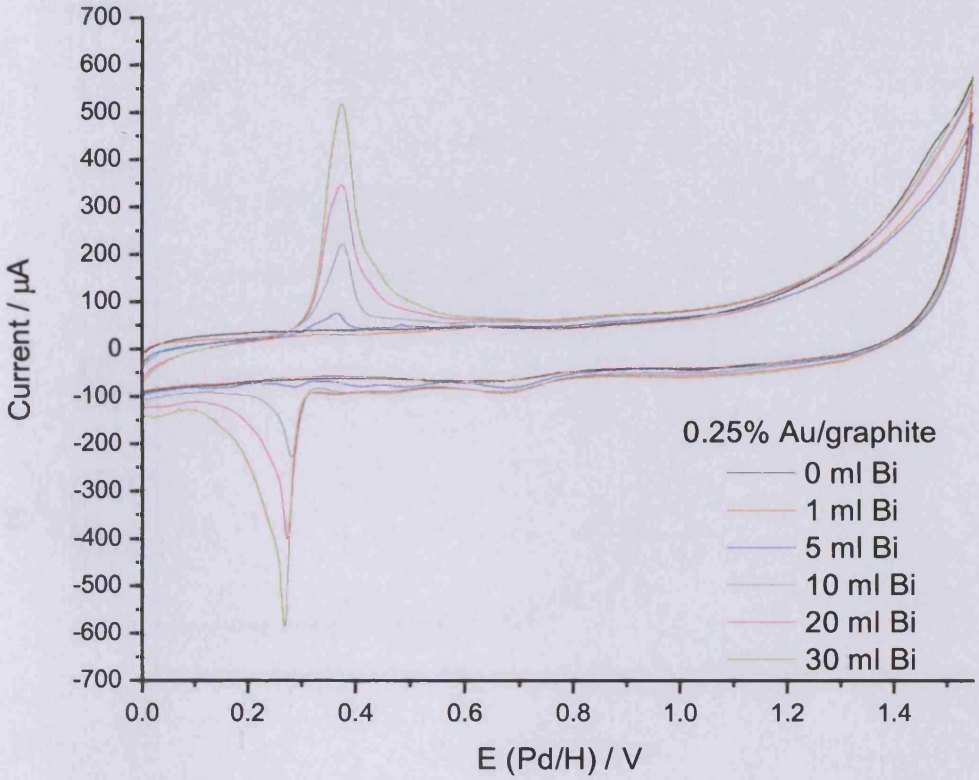

Figure 3.3.17: CVs of Bi-Au/graphite catalysts in 0.5 NaOH run at 10 mV s^{-1} showing oxygen evolution and oxide formation/reduction.

3.3.7 Glycerol oxidation in the electrochemical cell

Figure 3.3.18 shows glycerol electrooxidation using the four Au/graphite catalysts. The voltammograms varied only slightly in intensity for all of the catalysts. A large shoulder was present at 1.0 V on the 2% Au/graphite catalyst and was also present on the 1% catalyst (albeit much smaller). This shoulder feature may indicate a change in catalytic properties and may indicate that the 2% Au/graphite catalyst would give a different catalytic activity or selectivity when compared with the other catalysts.

The rise between 1.5 and 1.6 V may be an indication of over-oxidation, since the feature occurred at such a high potential and may indicate the oxidation of molecular fragments to carbon dioxide. Hence it might be reasonable to predict that the 1% Au/graphite catalyst will show less over-oxidation than the other catalysts.

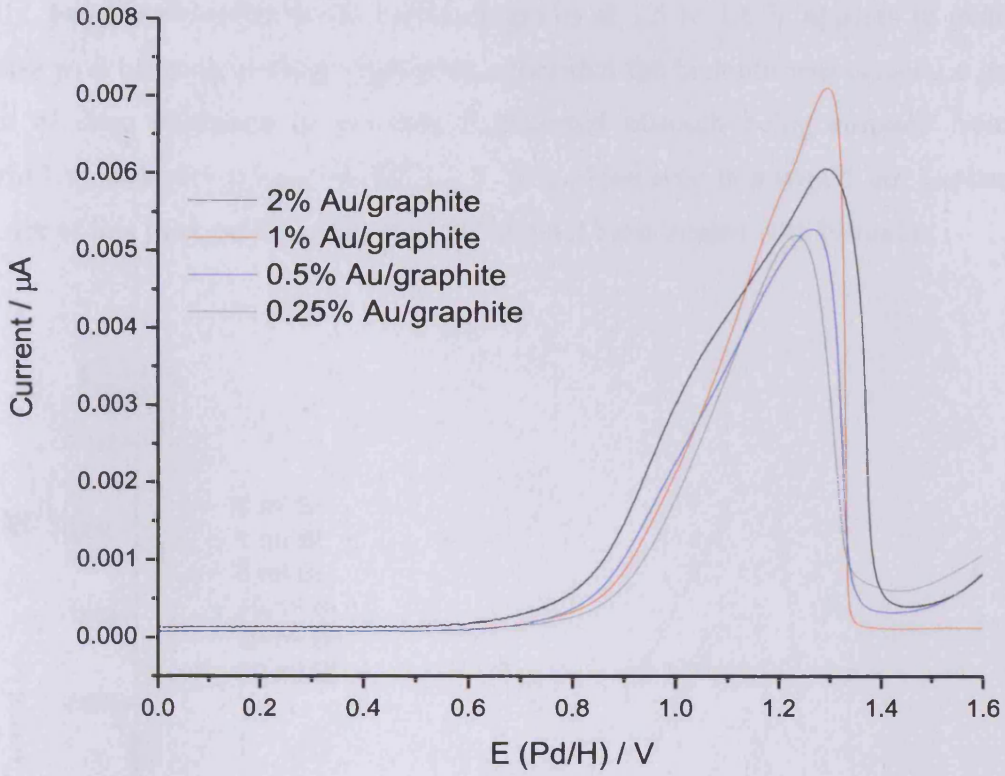

Figure 3.3.18: CVs for Au/graphite catalysts in 0.5 M glycerol and 0.5 M NaOH run at 10 mV s^{-1} showing the electro-oxidation of glycerol.

Figures 3.2.19 to 3.3.22 show the voltammograms obtained for the bismuth modified gold catalysts. The introduction of bismuth resulted in a decrease of the electrooxidation peak. This trend generally followed the increasing bismuth loading. However in the case of the 5ml Bi - 1% Au/graphite catalyst, the electrooxidation voltammogram is notable out of sequence with the other catalysts and hence it will be interesting to note the catalytic behaviour of this catalyst.

It is also of interest that the shoulder that was present on the 2% and 1% Au/graphite catalysts is removed instantly on the introduction of bismuth, which may indicate a change in catalytic activity/selectivity for these catalysts. It is noteworthy that the voltammogram for the 5 ml Bi – 2% Au/graphite and 1 ml Bi - 0.5% Au/graphite catalyst both show a new shoulder at higher potential than the main peak. Again the relationship between this peak and the catalytic properties will be studied closely.

Finally, the rise observed in the voltammograms at 1.5 to 1.6 V appears to generally increase with bismuth loading suggesting either that the bismuth was causing a greater extent of deep oxidation or possibly it reflected bismuth being stripped from the adsorbed monolayers ($Bi_{(ads)} \rightarrow Bi^{3+}_{(aq)} + 3e^-$). However this would not explain the presence of this peak on the catalysts that have not been treated with bismuth.

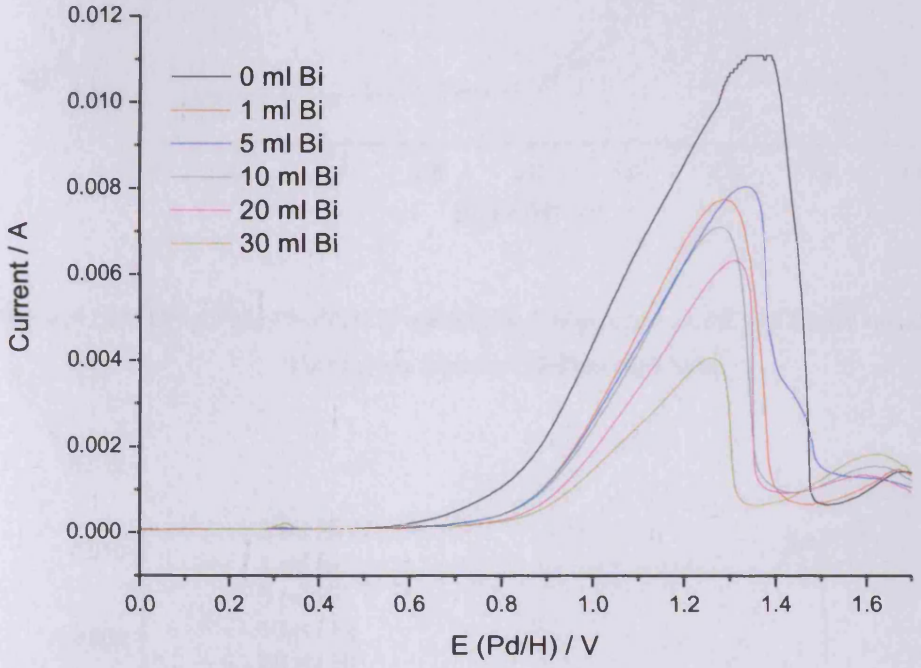

Figure 3.3.19: CVs for the 2% Bi-Au/graphite in 0.5 M glycerol and 0.5 M NaOH run at 10 mV s^{-1} showing the electrooxidation of glycerol.

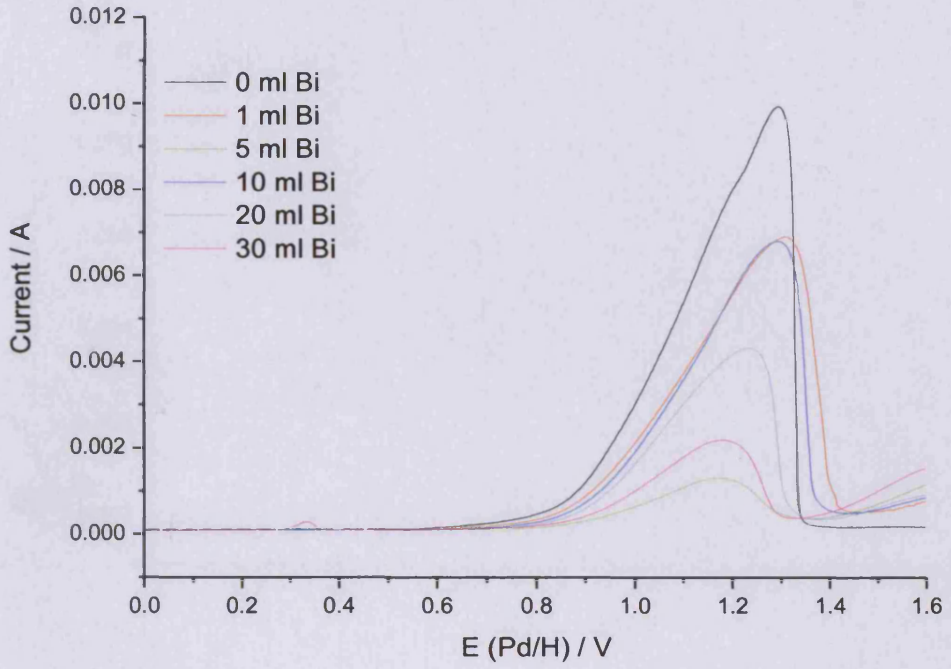

Figure 3.3.20: CVs for the 1% Bi-Au/graphite in 0.5 M glycerol and 0.5 M NaOH run at 10 mV s^{-1} showing the electrooxidation of glycerol.

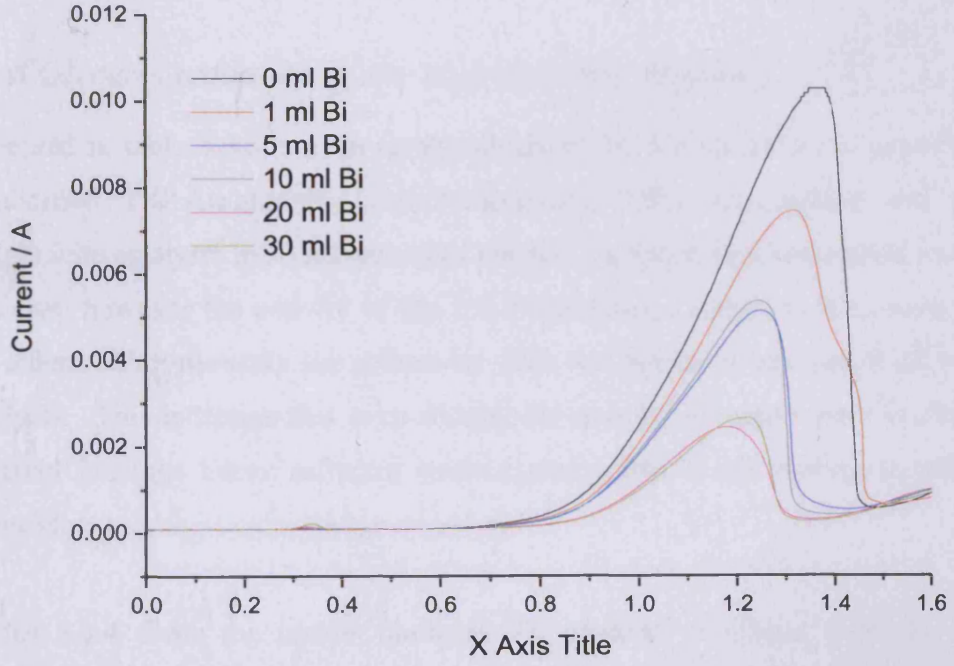

Figure 3.3.21: CVs for the 0.5% Bi-Au/graphite in 0.5 M glycerol and 0.5 M NaOH run at 10 mV s^{-1} showing the electrooxidation of glycerol.

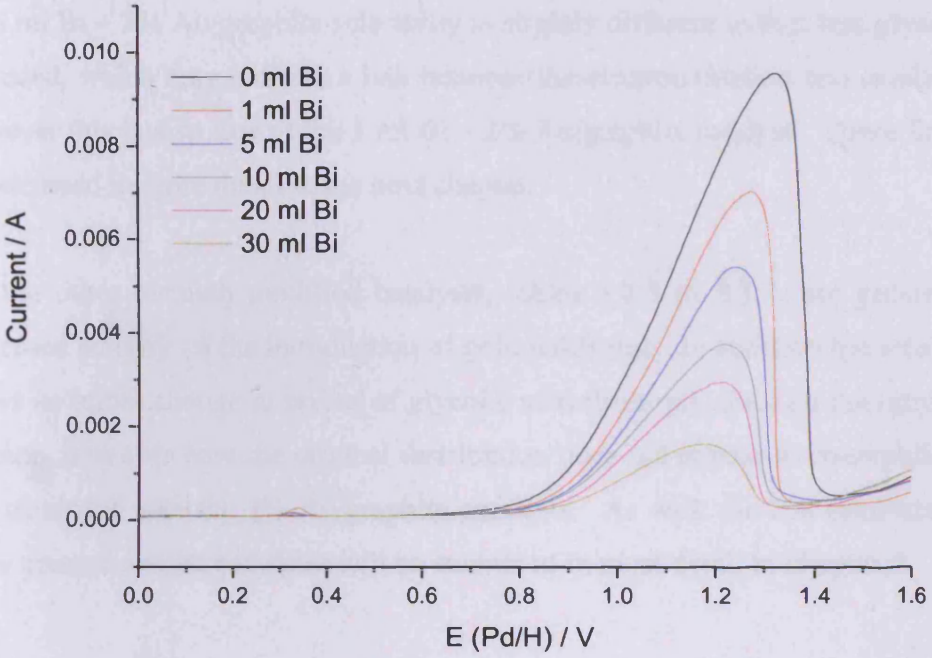

Figure 3.3.22: CVs for the 0.25% Bi-Au/graphite in 0.5 M glycerol and 0.5 M NaOH run at 10 mV s^{-1} showing the electrooxidation of glycerol.

3.3.8 Glycerol oxidation in the high-pressure reactor

Presented in table 3.3.3 are the results obtained for the oxidation of glycerol over the unmodified 2% Au/graphite, 1% Au/graphite, 0.5% Au/graphite and the 0.25% Au/graphite catalysts in a high-pressure reactor. A reasonable conversion is obtained in all cases; however the activity of the 1% Au/graphite catalyst is somewhat lower than the others. Unfortunately the selectivity does not appear to change at all between the catalysts. This indicates that even though the number of active sites is changing (i.e. different loadings hence different surface areas) this is not having an effect on the selectivity.

Tables 3.3.4 show the results obtained for glycerol oxidation over the parent 2% Au/graphite catalyst and the bismuth modified derivatives. Generally the effect of bismuth is to reduce the extent of conversion; however this is not a systematic decrease. The change in product distribution observed on the introduction of bismuth is that glycolic acid is formed at the expense of glyceric acid. Yet as the bismuth loading is

increased, the glyceric acid re-establishes itself at the expense of the glycolic acid. For the 5 ml Bi – 2% Au/graphite selectivity is slightly different in that less glyceric acid is produced, which may indicate a link between the electrooxidation and catalytic results. However this is also true of the 1 ml Bi – 2% Au/graphite catalyst. These findings will be discussed in more detail in the next chapter.

For the other bismuth modified catalysts, tables 3.3.5 to 3.3.7, the general trend of decreased activity on the introduction of gold holds true. In addition the selectivity also shows an initial change in favour of glycolic acid (from glyceric) on the introduction of bismuth, however here the original distribution does not appear to re-establish itself as was observed with the 2% Au/graphite catalysts. As with the 2% catalysts, there are some unusual results and these will be examined in more detail in chapter 4.

Table 3.3.3: Conversion and product composition for the oxidation of glycerol using the Au/graphite catalysts (50°C, 2h).

Catalyst	Conversion / %	Product Yield / %				
		Glycolic acid	Glyceric acid	Tartronic acid	Oxalic acid	HPA
2%	43.2	29.7	63.1	2.8	0.7	3.8
1%	23.6	29.7	63.1	2.8	0.7	3.8
0.5%	44.9	28.4	61.8	5.4	0.9	3.5
0.25%	44.8	26.9	63.6	5.8	0.8	2.9

Table 3.3.4: Conversion and product composition for the oxidation of glycerol using the 2% Au/graphite catalyst and bismuth modified derivatives (50°C, 2h).

Catalyst	Conversion / %	Product Yield / %				
		Glycolic acid	Glyceric acid	Tartronic acid	Oxalic acid	HPA
2%	43.2	29.7	63.1	2.8	0.7	3.8
1ml	17.1	38.0	54.2	1.8	1.4	4.7
5 ml	13.9	39.5	50.7	2.3	2.0	5.5
10 ml	30.9	33.4	59.3	2.0	0.9	4.4
20 ml	24.9	32.3	60.9	2.0	1.0	3.9
30 ml	33.6	31.3	61.9	2.1	0.8	3.9

Table 3.3.5: Conversion and product composition for the oxidation of glycerol using the 1% Au/graphite catalyst and bismuth modified derivatives (50°C, 2h).

Catalyst	Conversion / %	Product Yield / %				
		Glycolic acid	Glyceric acid	Tartronic acid	Oxalic acid	HPA
1%	23.6	29.7	63.1	2.8	0.7	3.8
1ml	1.75	69.8	22.0	0	0	8.3
5 ml	18.6	30.8	63.9	1.5	0	3.9
10 ml	6.2	62.5	28.8	0	0	8.7
20 ml	2.27	65.1	20.7	0	0	14.3
30 ml	6.5	50.2	39.1	0	0	10.7

Table 3.3.6: Conversion and product composition for the oxidation of glycerol using the 0.5% Au/graphite catalyst and bismuth modified derivatives (50°C, 2h).

Catalyst	Conversion / %	Product Yield / %				
		Glycolic acid	Glyceric acid	Tartronic acid	Oxalic acid	HPA
0.5	44.9	28.4	61.8	5.4	0.9	3.5
1ml	10.0	43.2	50.7	0	0	6.1
5 ml	11.4	35.9	58.9	1	0	4.2
10 ml	5.1	45.2	48.0	0	0	6.9
20 ml	11.2	38.2	55.5	0	0	6.3
30 ml	12.2	45.8	42.9	4.1	0	7.2

Table 3.3.7: Conversion and product composition for the oxidation of glycerol using the 0.25% Au/graphite catalyst and bismuth modified derivatives (50°C, 2h)

Catalyst	Conversion / %	Product Yield / %				
		Glycolic acid	Glyceric acid	Tartronic acid	Oxalic acid	HPA
0.25%	44.8	26.9	63.6	5.8	0.8	2.9
1ml	-	-	-	-	-	-
5 ml	-	-	-	-	-	-
10 ml	6.7	47.9	40.5	0	0	11.6
20 ml	14.6	31.2	49.3	8.6	6.1	4.8
30 ml	20.3	33.6	50.9	6.4	4	5.0

3.3.9 Electrochemical investigation into catalyst stability

Irrespective of how effective a catalyst is for a given reaction, its stability under reaction conditions is of paramount importance and much emphasis is placed on finding catalysts that do not exhibit leaching of the active phase [14-16]. To investigate this

possibility, the Au/graphite and Bi-Au/graphite catalysts (used in both section 3.2 and 3.3) were investigated for their electrochemical stability by continually cycling a sample of each catalyst both in basic and in acidic media. This procedure was used to determine whether gold was irreversibly adsorbed onto the graphite surface, and whether bismuth was irreversibly adsorbed onto the gold surface.

Figures 3.3.16 / 3.3.17 show the voltammograms obtained when the gold catalysts were cycled in acidic and basic media respectively. After the first (cleaning) cycle the voltammograms did not change, indicating that the gold was stable on the surface of the graphite under both pH conditions.

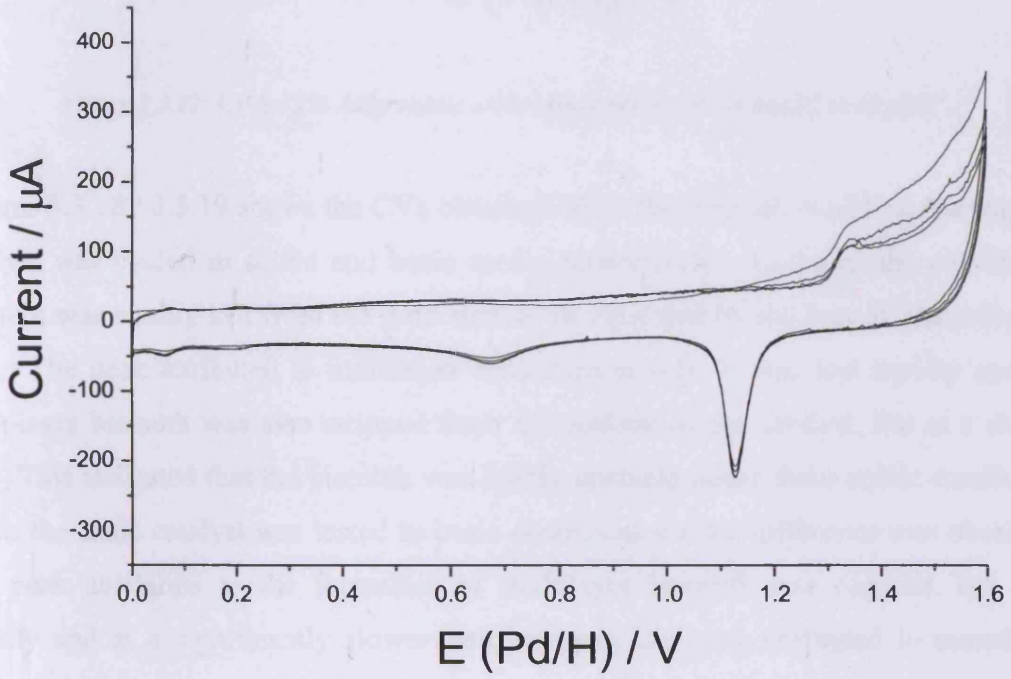

Figure 3.3.16: CV for 2% Au/graphite cycled four times in 0.5 M H_2SO_4. at 10 mVs^{-1}.

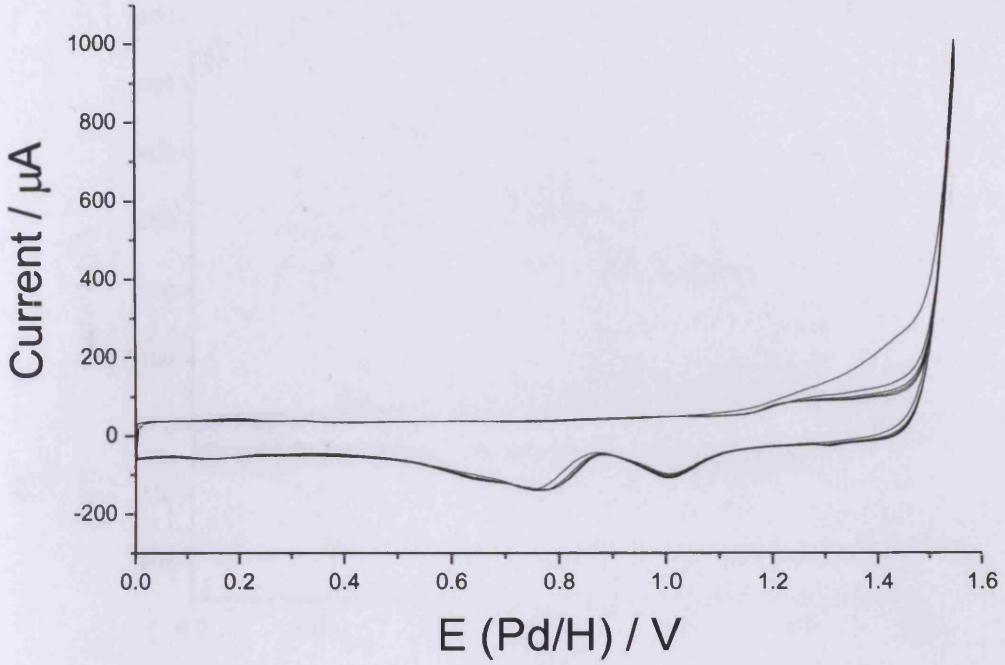

Figure 3.3.17: CV for 2% Au/graphite cycled five times in 0.5 M NaOH at 10 mVs^{-1}.

Figures 3.3.18 / 3.3.19 shows the CVs obtained when the bismuth modified Au/graphite catalyst was cycled in acidic and basic media respectively. Under acidic conditions, bismuth was readily lost from the gold surface as indicated by the loss of bismuth peak area. The peak attributed to multilayer formation at 0.18 V was lost rapidly and the monolayer bismuth was also stripped from the surface of the catalyst, but at a slower rate. This indicated that the bismuth was highly unstable under these acidic conditions. When the same catalyst was tested in basic conditions a clear difference was observed. The peak attributed to the formation of multilayer bismuth was reduced, but only slightly and at a significantly slower rate, whereas the peak attributed to monolayer bismuth remained unchanged. This indicates that bismuth is far more stable under basic conditions and hence is less likely to be removed during reaction in the high pressure reactor.

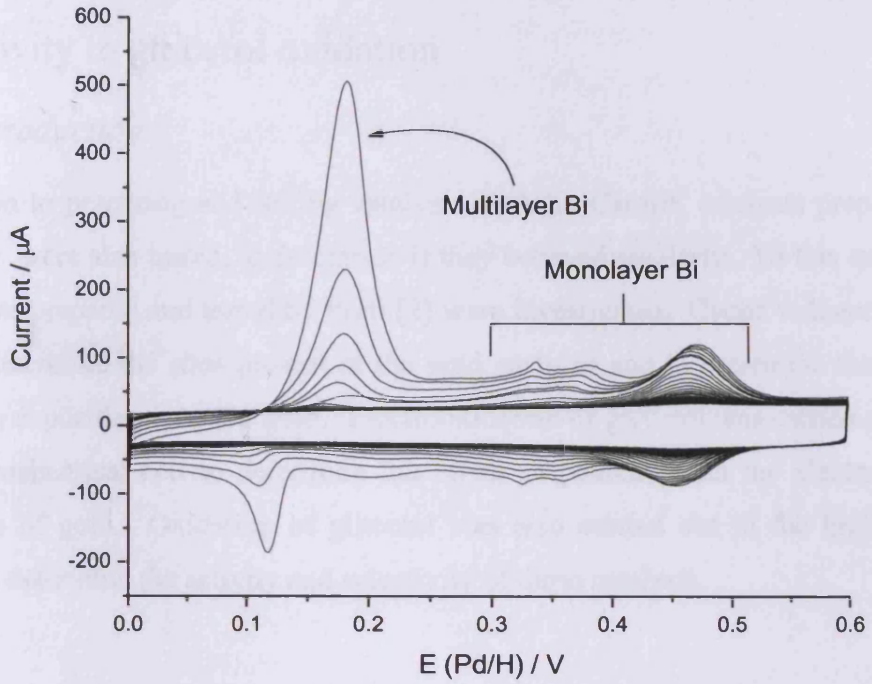

Figure 3.3.18: CVs for 2% Au/graphite modified by 30 ml Bi solution; repetitive cycles in 0.5 M H_2SO_4. at 10 mVs^{-1}.

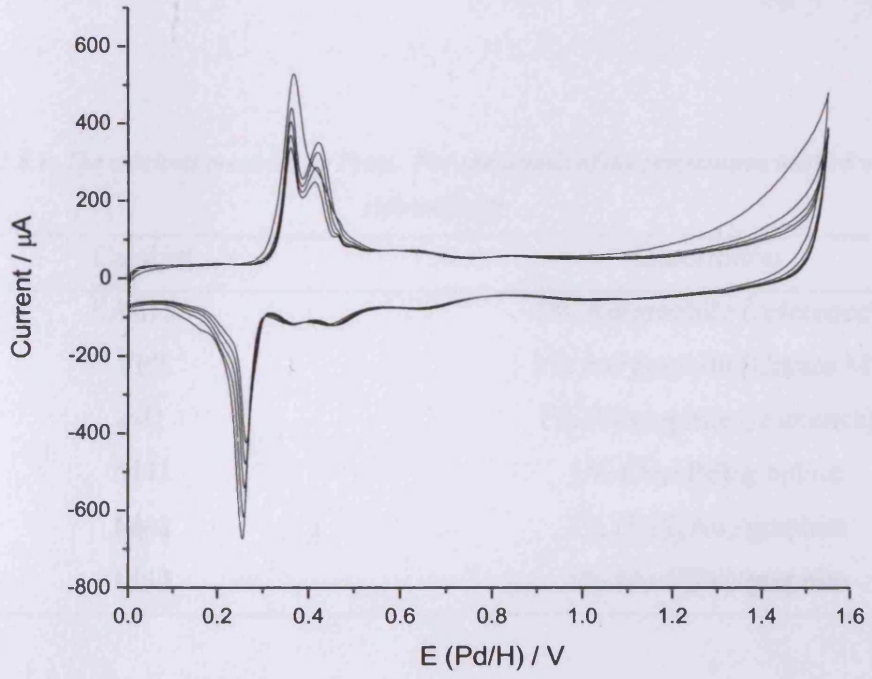

Figure 3.3.19: CV for 2% Au/graphite modified by 30 ml Bi solution; repetitive cycles in 0.5 M NaOH at 10mVs^{-1}.

3.4 Graphite-supported Au and Pd-Au catalysts: Characterisation and activity in glycerol oxidation

3.4.1 Introduction

In addition to preparing and testing catalysts made in Cardiff, catalysts prepared by a third party were also tested, to determine if they behaved similarly. To this end a range of catalysts prepared and tested by Prati [2] were investigated. Cyclic voltammetry was used to determine the sites present at the gold surfaces and to determine the effect of palladium deposition onto the gold. Electrooxidation of glycerol was carried out within the electrochemical cell to determine the effect of palladium on the electro-catalytic properties of gold. Oxidation of glycerol was also carried out in the high pressure reactor to determine the activity and selectivity of these catalysts.

3.4.2 Characterisation of gold and palladium-modified gold catalysts: CVs in acidic conditions

Table 3.4.1 shows the named catalysts obtained from Prati and a description of the relative loadings of gold and palladium.

Table 3.4.1: The catalysts provided by Prati. For the details of the preparation method used see reference [2].

Catalyst	Description
Au15	1% Au/graphite (reference)
FP7	1% Au/graphite (Citrate M)
Pd1	1% Pd/graphite (reference)
M41	1% (Au+Pd)/graphite
M42	1% (Pd@Au)/graphite
M43	1% (Au@Pd)/graphite

Figure 3.4.1 shows the voltammograms obtained for the Au/graphite, Pd/graphite and Pd-Au/graphite catalysts when tested under acidic conditions in the electrochemical cell. The two catalysts Au15 and FP7 gave significantly different responses. In the forward sweep Au15 gave a large, broad oxide-formation peak at 1.4 V and a broad oxide-reduction peak at 1.1 V in the reverse sweep. By contrast FP7 gave two small oxide peaks at 1.3 and 1.5 V in the forward sweep and a much sharper oxide-reduction peak in the reverse sweep. The presence of the two oxide-formation peaks in the forward sweep indicated the presence of Au {111} terraces and the sharpness of the oxide-reduction peak indicated that this catalyst was less heterogeneous in structure.

The pure Pd catalyst, Pd1, showed an oxide-reduction peak at 0.55 V but few other features. The peak present at 1.13 V in the reverse sweep is due to oxide-reduction of the gold mesh on which the catalyst was placed. However on comparing the potential at which the gold and palladium oxide-reduction peaks appear, it is evident that the bi-metallic catalysts (M41-M43) are alloyed due to the shifted potentials at which their oxide-reduction peaks appear. M42 is the least alloyed of the catalysts, since the oxide-reduction peaks have only slightly shifted in potential from those values observed for the pure metals. On this basis M41 and M43 appear to be alloyed to the same extent. However M43 shows a gold oxide formation peak at 1.4 V in the forward sweep indicating that the gold may be dominating the surface of the alloy.

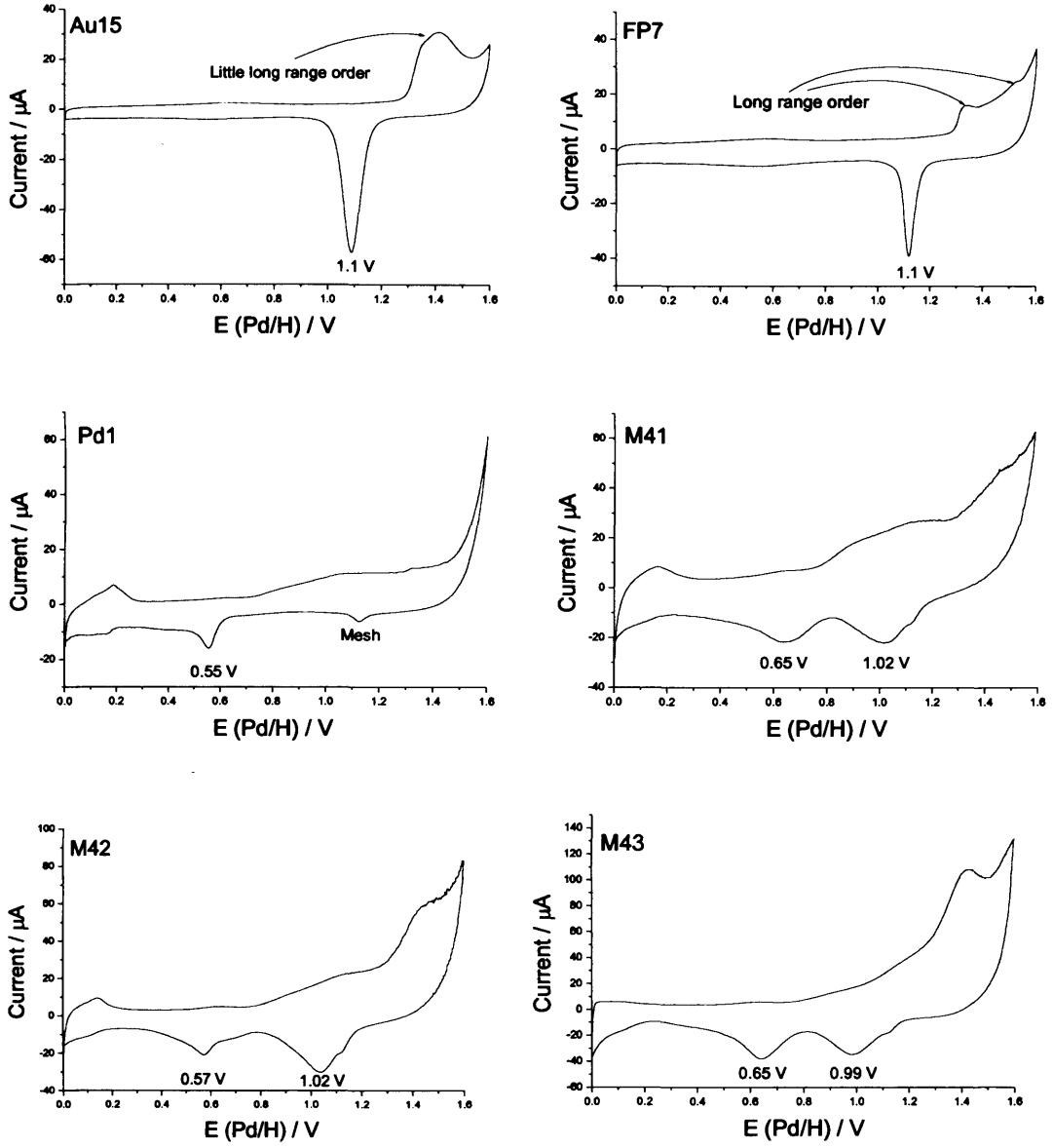

Figure 3.4.1: CVs in 0.5 M H_2SO_4 at 10 mVs^{-1} showing the oxide formation and oxide-reduction peaks for graphite-supported gold (Au15, Fp7), palladium (Pd1) and palladium-gold (M41-M43).

3.4.3 Characterisation of gold and palladium-modified gold catalysts: CVs involving Pb_{UPD}

Figure 3.4.3 shows the CVs obtained when the catalysts underwent lead-UPD. Au15 showed broad features at 0.35 and 0.5 V indicative of poorly defined Au{110} and Au{100} surface regions. There was no evidence for the presence of Au{111} surface regions. In contrast, FP7 provided sharp features at 0.3 and 0.5 V indicating the presence of well ordered Au{111} and Au{110} surfaces. Evidence for Au{100} sites was limited. The Pd catalyst (Pd1) showed no significant peaks for lead UPD and

unfortunately the presence of the palladium in the alloyed catalysts masked any signal from the gold (see M41-M43).

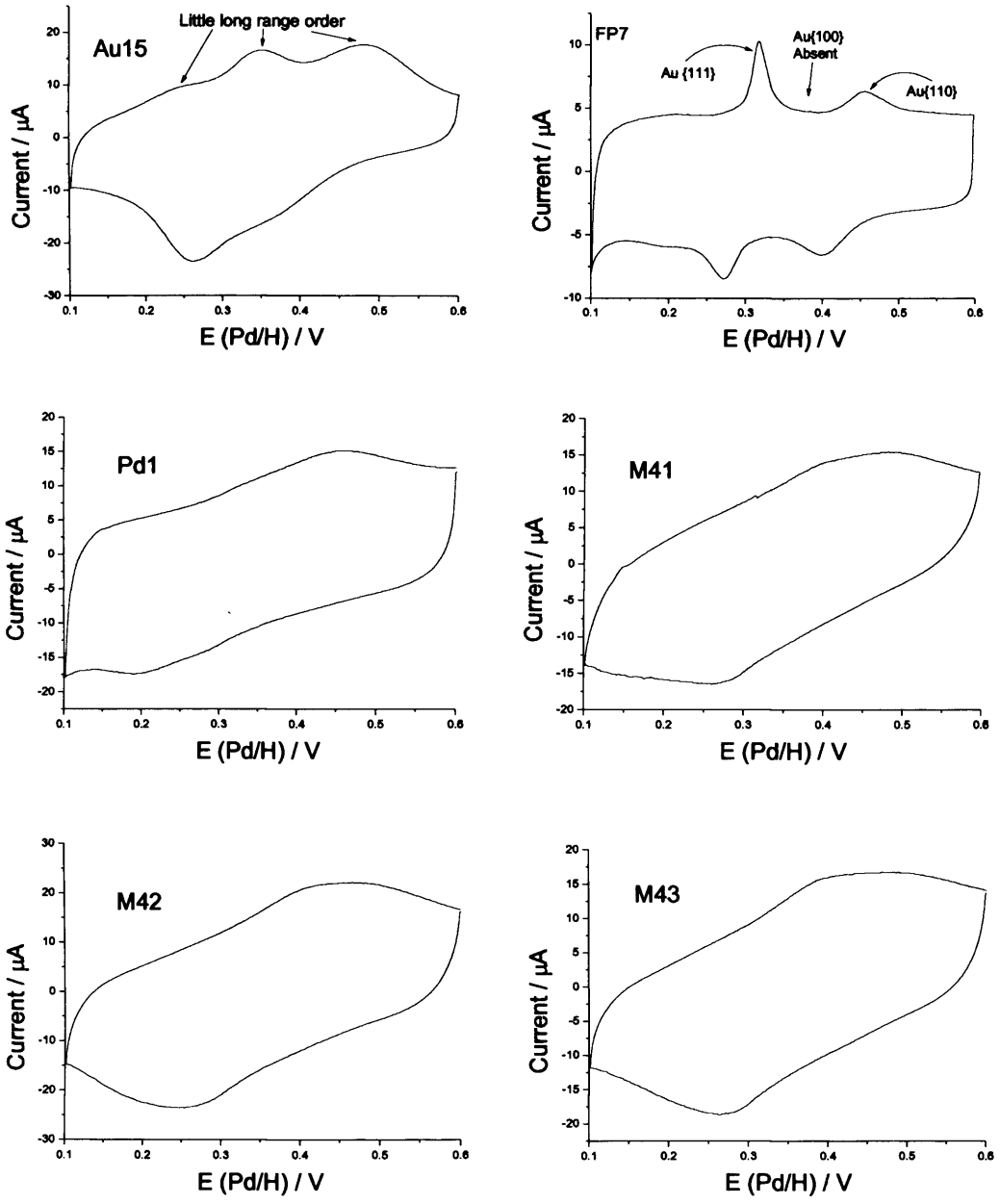

Figure 3.4.2: CVs in 1.0 mM lead nitrate and 0.1 M NaOH at 10 mVs^{-1} showing lead-UPD on gold (Au15, FP7), palladium (Pd1) and palladium-gold (M41-M43).

3.4.4 Characterisation of gold and palladium-modified gold catalysts: CVs in basic conditions

Figure 3.4.2 shows the voltammograms obtained when the Au/graphite, Pd/graphite and Pd-Au/graphite catalysts were tested under basic condition. Au15 showed the gold oxide formation peak in the forward sweep at 1.3 V and the oxide-reduction peak in the reverse sweep at 1.0 V, both of which were much broader than normal. Notably, this catalyst did not evolve oxygen in the forward sweep and this can be related to the lack of the "second" gold oxide-reduction peak observed in the reverse sweep, as has been discussed previously. In the forward sweep FP7 showed the gold oxide-formation peak at 1.2 V and an oxygen evolution peak at 1.6 V. In the reverse sweep the gold oxide-reduction peak and the second oxide-reduction peak observed by Hutchings *et al* were present at 1.0 and 0.8 V respectively. The palladium catalyst (Pd1) showed its oxide-reduction peak at 0.4 V which shifted to higher potentials on the alloyed catalysts. The Pd modified catalysts showed no "second" oxide-reduction peak which suggested that these catalysts might be less active than the pure gold catalyst, FP7. In addition the "normal" gold oxide-reduction peak for the alloys was small by comparison with that for the pure gold catalysts, indicating that there was less gold on the surface of the catalyst.

It is noteworthy that the relative extent of alloying for M41-M43 (as determined by the shift in potential of the oxide-reduction peaks) reflects that observed for the peaks observed in acidic media.

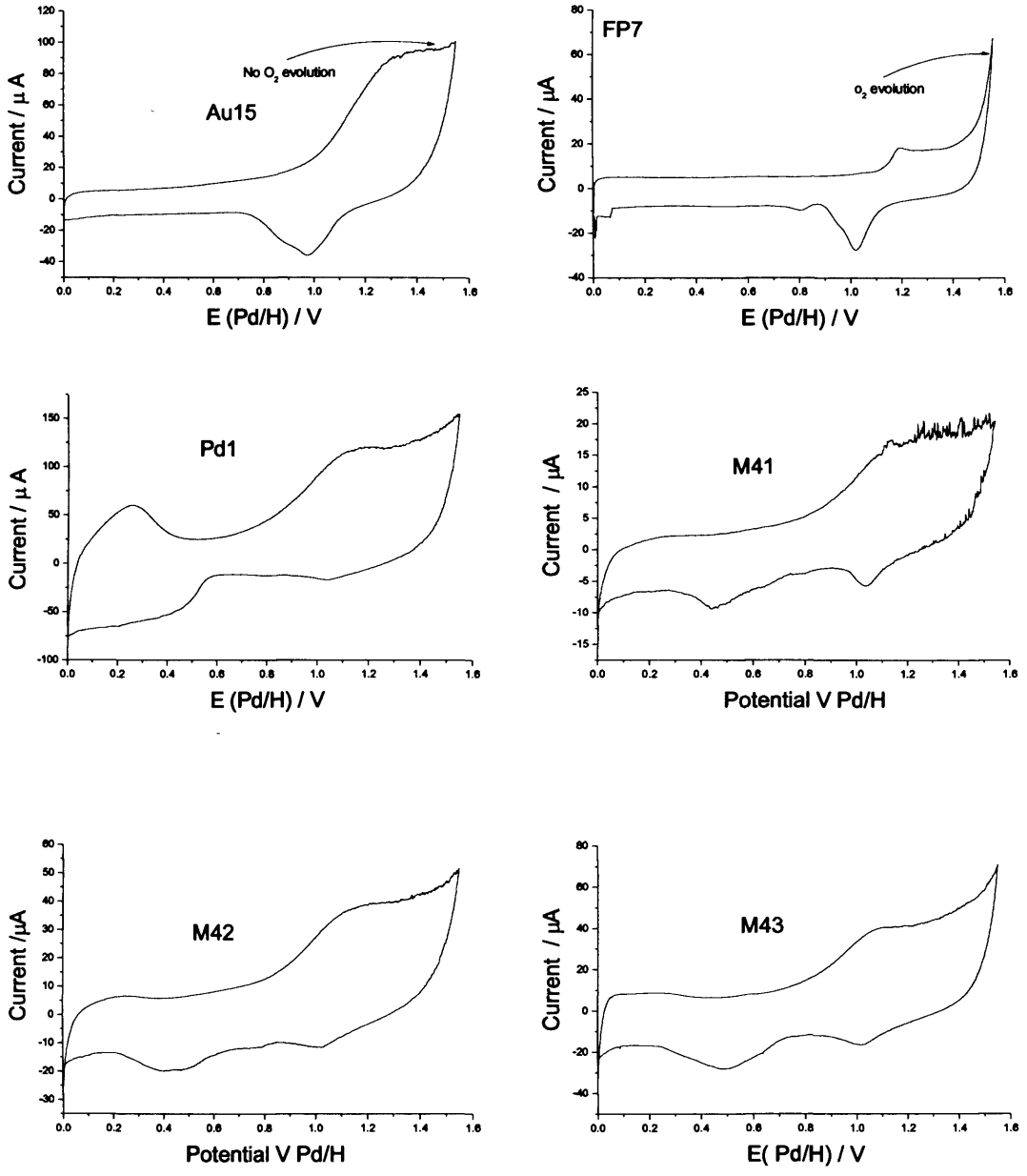

Figure 3.4.3: CVs in 0.5 M NaOH at 10 mVs^{-1} showing the oxide formation and oxide-reduction peaks for gold (Au15, Pp7), palladium (Pd1) and palladium-gold (M41-M43) and the extent of oxygen evolution.

3.4.5 Glycerol oxidation in the electrochemical cell

Figure 3.4.4 shows the voltammograms obtained when the catalysts were tested for the electro-oxidation of glycerol. All of the catalysts were active for glycerol oxidation; FP7 showing significantly higher activity than the other catalysts. This catalyst was also the most active for O_2 evolution as discussed previously. Furthermore, for FP7, a number of shoulders were present on the main peak indicating that several products were being formed. The remainder of the catalysts provided very similar electro-

oxidation curves, suggesting that there were few differences between them in terms of conversion and selectivity.

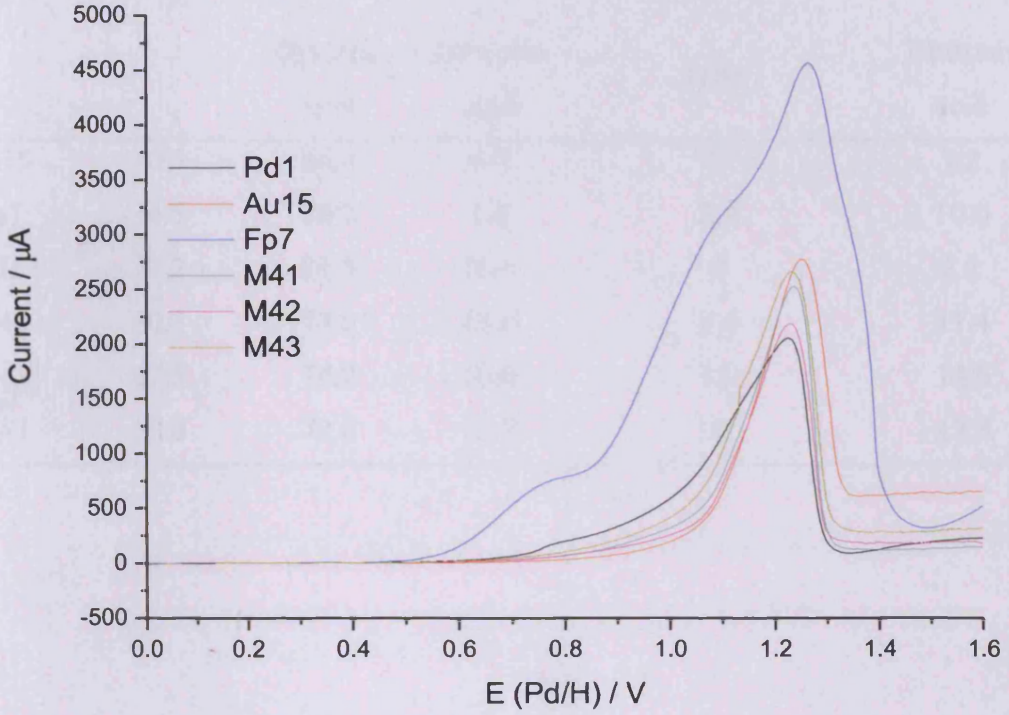

Figure 3.4.4: CVs in 0.5 M glycerol and 0.5 M NaOH run at 10 mVs-1 showing the electrooxidation of glycerol over the Au/graphite, Pd/graphite and Pd-Au/graphite catalysts.

3.4.6 Glycerol oxidation in a high pressure reactor

Table 3.4.1 shows product compositions obtained from reactions over Au/graphite and Pd-Au/graphite catalysts at 323 K and 3 bar. Reactions were run for 0.5 h. The least active catalyst was Au15. By contrast the other gold catalyst, FP7, which contains well defined Au {111} sites, shows activity and selectivity approaching that of the Pd and Pd/Au catalysts. It is interesting that the catalyst FP7 which stood out in terms of its electrooxidation behaviour provided a more typical behaviour in the high pressure reactor. The catalysts M41, M42 and M43 although alloyed to different extents show very similar catalytic activity and selectivity. None of the catalysts produced over-oxidation of glycerol.

Table 3.4.1: Reactivity data for the Au/graphite, Pd/graphite and Pd-Au/graphite catalysts (Oxalic Acid = 0%).

Catalyst	Conversion / %	Selectivity / %			
		Glyceric acid	Glycolic acid	HPA	Tartronic acid
Au15	10.3	86.4	6.4	0	7.2
Fp7	34.5	79.2	8.4	2.4	10.0
Pd1	27.2	81.5	10.4	0	8.1
M42	50.5	73.0	13.0	2.6	11.4
M41	67.5	74.2	10.0	1.2	14.6
M43	52.8	73.5	13.7	0	12.8

3.5 References

1. S. Carrettin, P. McMorn, P. Johnston, K.G Griffin, G.J. Hutchings, C.J. Kiely, G.A. Attard, *Top. Catal.*, **27** (2004) 131.
2. N. Dimitratos, F. Porta, L. Prati, *App. Catal. A*, **291** (2005) 210.
3. C.L. Bianchi, P. Canton, N. Dimitratos, F. Porta, L. Prati, *Catal. Today*, **102-103** (2005) 203.
4. N.D. Plint, N.J. Coville, D. Lack, G.L. Nattrass, T. Vallay, *J. Molec. Catal.* A, **165** (2001) 275.
5. J. Clavilier, K. El-Achi, A. Rhodes, *J. Electroanal. Chem.*, **272** (1989) 253.
6. N. Furuya and S. Motoo, *J. Electroanal. Chem.*, **88** (1978) 151.
7. D.J. Jenkins, PhD Thesis, Cardiff University, 2004.
8. M. Volmer, A. Weber, *Z. Phys. Chem.*, **119** (1926) 277.
9. D. Kaschiev, *J. Crystal Growth*, **40** (1977) 29.
10. J. Hernández, J. Solla-Gullón, E. Herrero, *J. Electroanal. Chem.*, **574** (2004) 185.
11. H. Kimura, *App. Catal. A*, **105** (1993) 147.
12. P. Gallezot, *Catal. Today*, **37** (1997) 405.
13. F.G. Will, C.F. Knorr, *Z. Electrochem.*, **64** (1960) 258.
14. M. E. Halttunen, M. K. Niemelä, A. O. I. Krause, A. I. Vuori, *J. Molec. Catal. A*, **144** (1999) 307.
15. D. Mandelli, M.C.A. van Vliet, U. Arnold, R.A. Sheldon, U. Schuchardt, *J. Molec. Catal. A*, **168** (2001) 165.
16. Adrián M.T. Silva, Ana C.M. Oliveira, Rosa M. Quinta-Ferreira, *Chem. Eng. Sci.*, **59** (2004) 5291.

Chapter Four

Discussion

4.1 Introduction

In this chapter the results presented in chapter three will be discussed in detail. Models will be proposed for the trends and unusual features observed. In addition, a critical appraisal will be given of whether or not cyclic voltammetry can be used to predict catalyst activity/selectivity for graphite supported gold catalysts.

4.2 Discussion of results presented in section 3.1

The main objective of this section of the work was a preliminary survey for glycerol oxidation. Au-Pt/graphite catalysts were used because supported platinum is well established as a good oxidation catalyst [1-3] and the introduction of gold was hoped to produce changes in the catalytic response, as has been observed previously in a number of different systems [4, 5]. Propanol oxidation was the reaction of choice since it contained only one alcohol functional group, as opposed to three in glycerol. Thus it was hoped that the relationships between electrochemical responses and catalytic activity for propanol oxidation would be more straightforward to interpret. A foundation for the understanding of the more complicated glycerol system could then have been established.

The characterisation techniques used (H_{UPD}, oxide formation, Pb_{UPD} and XPS) gave information that was generally in good agreement. The voltammograms in figure 3.1.1 show that gold was blocking the platinum H_{UPD} region slowly and in distinct stages, even though the gold loading was being increased steadily (as seen in table 3.1.1 and in the oxide and Pb_{UPD} voltammograms presented in figures 3.1.2 and 3.1.4 respectively). This led to the hypothesis that the gold was either following an island growth model [6, 7] or that a portion of the gold was adsorbing onto the graphite. XPS showed a significant drop in the percentage carbon present at higher gold loadings confirming that gold was adsorbing onto the graphite support.

Based on the work carried out by Hutchings *et al* [9], a second oxide-reduction peak, (b), present in the reverse sweep of a supported gold catalyst tested in basic conditions can be an indicator of increased activity/selectivity. On running the Au-Pt/graphite catalysts under basic conditions (see figure 3.1.7), only a small reduction peak, (b), was

observed for all of the catalysts. Unfortunately this meant that any association of peak b with enhanced activity could not be investigated with gold modified platinum catalysts.

Electrooxidation of 1- and 2-propanol showed that gold was having a markedly different effect in each reaction. For 1-propanol oxidation, the introduction of gold substantially increased the extent of electrooxidation occurring on the platinum, which was by far the greater contributor to the overall electrocatalytic activity. By contrast for 2-propanol electrooxidation, the gold was by far the more active surface.

When the catalysts were tested in the high-pressure reactor for 1- and 2-propanol oxidation, there was a general increase in conversion and selectivity as gold loading was increased. This broadly agreed with the results obtained for the electrooxidation of 1- and 2-propanol suggesting that electrooxidation of 1- and 2-propanol might be used as a predictive tool for catalytic activity/selectivity. It was of particular interest that 0.53 Au-Pt/graphite showed lower activity than expected for both the electrooxidation and catalytic oxidation of 1- and 2-propanol. This further supports the use of cyclic voltammetry as a predictor of catalytic activity. However there was not an exact correlation between the conversion / selectivity and the electrooxidation results, which might indicate different processes were occurring in the two systems.

Maximum catalytic activity was achieved at a coverage of between 0.6-0.7 gold in both 1- and 2-propanol oxidation. Progressing to higher loadings of gold resulted in a loss of conversion (and in the case of 2-propanol selectivity as well). Referring back to the oxide voltammograms, it can be seen that maximum catalytic oxidation activity was obtained when there was a significant shift in the Pt-O reduction peak. The peak is shifted even more on progressing to the θ_{Au}=0.99 catalyst; however, it is also significantly smaller in intensity. This suggests that the gold is increasing the activity of the platinum either by site-blocking effects or by altering its electronic structure and at high gold loadings the surface is too heavily blocked by gold to allow a significant amount of reaction to occur.

A disadvantage with the system presented above is that gold adsorbed onto the graphite as well as onto the platinum. Hence, it is not certain if the enhanced electrooxidation is

solely due to the gold adsorbed on the platinum. The influence of the graphite support was removed by using platinum single crystals as catalysts; the situation was thereby simplified as gold could only adsorb on to the platinum surface. Systems involving gold deposited onto reconstructed Pt{100} have been studied by Borg [10], who found that gold formed islands of monolayer height and nucleation occurred at both steps and terraces. Interestingly second monolayer formation started well before completion of the first monolayer and the monolayer and multilayer growth occurred together.

From the single crystal study (see sections 3.1.10 and 3.1.11) it became evident that the electrooxidation of 1-propanol occurred mainly on the platinum surface as had been observed for the supported catalyst and thus the gold acted predominantly as a "promoter" since electroactivity on gold was of much lower magnitude than on platinum. The Pt{100} surface was different in that gold and platinum were observed to catalyse the reaction to a similar extent. However electrooxidation occurring on the Pt{100} surface gave by far the smallest peaks (see figures 3.1.11 and 3.1.15). Note that little Au{100} was present based on Pb_{UPD} results (see figure 3.1.4). Hence it is reasonable to assume that this surface would not have contributed significantly to the overall activity of the supported catalyst. On examining the stepped surfaces (see figures 3.1.13, 3.1.14 and 3.1.16) it was discovered that the highest activity was achieved when the step sites were blocked ({110} and {100}), hence it was deduced that steps site were active for forming catalytic poisons. Poison formation on extended Pt{100} planes may account for the low activity of Pt{100} compared with the other surfaces studied. Also electrooxidation went through a maximum with increasing gold loading which would again suggest that the catalyst was acting as a site-blocker to the formation of surface poisons. This was also observed in the electrooxidation voltammograms and was reflected in the trend present for the catalytic oxidation studies.

For 2-propanol the single crystal study (see section 3.1.11) revealed that both platinum and gold catalysed the reaction to the same extent, however the currents were significantly lower than those observed for 1-propanol electrooxidation. This is in reasonable agreement with the 2-propanol electrooxidation data collected on the supported catalysts in that 2-propanol currents were slightly smaller than those for 1-propanol. Again the extent of electrooxidation went through a maximum (see figures

3.1.15 and 3.1.16) suggesting high gold loadings would poison the catalyst, as seen in the catalytic results (see table 3.1.4). From these results it is evident that the adsorption of gold partly onto the graphite did not significantly influence the electrooxidation properties of the supported catalysts.

Thus, it was concluded that cyclic voltammetry can be used as a good characterisation tool for platinum and gold modified platinum catalysts so far as 1- and 2-propanol are concerned, there being broad agreement between the electrooxidation and catalytic results. However a closer analysis is required to confirm more detailed links between the two. This could be achieved by repeating the measurements with more systematic changes in gold coverage and perhaps exceeding one monolayer of gold coverage. It is interesting that when compared with the presence of peak (b) on "massive" gold (sections 3.2 and 3.3) these monoatomic thin gold films on platinum do not give rise to a similar peak.

4.3 Discussion of results presented in section 3.2

In respect of glycerol oxidation, this investigation was mostly concerned with trends within supported gold catalysts because platinum had been extensively investigated for this reaction by others [11-15] and gold-platinum catalysts had been investigated by Prati [16]. In addition, work by Hutchings *et al* [9, 17-18] had shown gold catalysts to be very active for glycerol oxidation. To this end a 2% Au/graphite catalyst was prepared for glycerol oxidation to determine if thermally annealing under various conditions would lead to changes in morphology that could be detected by cyclic voltammetry and have an effect on activity or selectivity.

From the CVs presented in figures 3.2.1 and 3.2.2 it was evident that catalysts thermally annealed under hydrogen lost significant surface area through sintering and lost much of the long range {111} order that was initially evident in the 2% Au/graphite catalyst. In contrast, the catalysts sintered under air showed a loss of surface area, but a significant increase in long range {111} terrace structure. These results were confirmed by the Pb_{UPD} voltammograms which showed a general decrease in {111} terraces for the

hydrogen sintered catalysts, but showed an increase in {111} terraces for the catalysts treated under air.

XPS spectra showed a distinct loss of gold surface area for both the hydrogen and air treated catalysts, in agreement with the electrochemical results just discussed. TEM results showed a general loss of structure within the particles for the hydrogen treated catalysts; an opposite effect was seen for the air treated catalysts, which showed a significant increase in TEM internal structure with increasing treatment temperature. These results are again in agreement with what was observed for the voltammograms it being suggested that the "dark" patches are associated with {111} terraces (triangles) and {110} steps (linear bar-like dark patches).

On testing the catalysts under basic conditions (see section 3.2.6), the second reduction peak, (b), was observed for all catalysts. For the hydrogen treated catalysts, the peak was largest on the 500K catalyst. However it remained larger than for the untreated catalyst. This correlates again with the extent of {111} terraces. The catalysts treated under air showed a slight increase in the size of the peak (b) for the catalyst treated at 500 and 600 K, but a significantly larger peak was present for the catalyst treated at 700 K. Based on the Hutchings interpretation, this would suggest that all of the air treated catalysts should give a better selectivity than the unmodified 2% Au/graphite and also the H_2/500 K treated catalyst. In fact catalytic oxidation using the air/700 K catalyst should be significantly greater than that observed on any other gold catalysts since peak (b) is so large.

When testing the catalysts for the electrooxidation of glycerol, H_2 and air treated catalysts proved to be very similar in their response. The 500 and 600 K catalysts in both systems gave a significantly larger electrochemical peak than both the unmodified catalyst and the H_2/700 K catalyst, which were of the same intensity. However the catalyst treated in air at 700 K (which gave the abnormally large second peak (b)) displayed a distinct shoulder at 1.0 V. This may well indicate a change in the oxidation mechanism, as the oxidation is occurring at lower potentials. Apart from this, there appeared to be little agreement between the magnitude of peak (b) and the magnitude of the glycerol electrooxidation curve. Neither does there appear to be any link between changes in the catalyst morphology and the electrooxidation data obtained.

The reactor data for the hydrogen treated catalysts shows no real trend in either conversion or selectivity with increasing thermal annealing. However, the 700 K catalyst shows a significantly lower conversion, as well as a markedly different product distribution. Referring back to the electrooxidation voltammogram, it is evident that as well as having a notably different shape (less broad), the drop-off of oxidation occurs at a much lower potential. These changes in shape may be linked to the change in activity of this catalyst. However the 500 K catalyst also shows a lower conversion and product distribution and yet its electrooxidation voltammogram is almost identical to the produced for the 600 K catalyst. On examining the catalytic data obtained for the catalysts prepared under air, it is again noted that there are no consistent trends in activity with annealing temperature. The only apparent link between the electrooxidation data and the catalytic results is the for the 700K catalyst, the conversion is greater than what would have been expected based on the results obtained for the hydrogen treated catalysts and this might be ascribed to the presence of the shoulder in the electrooxidation voltammogram. However as with the hydrogen treated catalysts, there appear to be few other links between the electrooxidation and catalytic results. For example the electrooxidation voltammograms suggest that the 500 K and 600 K catalysts should show similar catalytic properties, however the conversion and product distribution obtained for these catalysts is the most discrepant of the series. This would suggest that any links drawn between electrooxidation and catalytic results are at best tenuous for glycerol oxidation, in contrast to the assertions made by Hutchings [9].

From the voltammograms run under basic conditions, it was expected that the air/700 K catalyst would show a significantly different catalytic response when compared to the other catalysts. However the only difference appears to be that it provides a slightly higher conversion than that obtained for the equivalent hydrogen catalyst. In addition the voltammograms of the gold modified catalysts all gave larger responses for this peak than the 2% Au/graphite and hence it was predicted that the catalytic response of these catalysts would all be greater than that of the 2% Au/graphite. However the catalytic results show that, relative to the 2% Au/graphite catalyst, there is no such trend in either the activity or selectivity of the catalyst. Again this would suggest that any

conclusions drawn between the presence of this peak in basic media voltammograms and catalytic results are very weak.

A successful outcome from this section of work was the good agreement found between the different characterisation methods (CV, TEM and XPS) in terms of characterising the morphology and growth mode changes of the different catalysts.

4.4 Discussion of results presented in section 3.3

Bismuth was chosen as a promoter for gold catalysts, as previous work had shown its effectiveness as a promoter on platinum [11-15]. The objective of this section of work was to determine if the introduction of bismuth at various loadings would influence the activity of the parent catalyst towards the oxidation of glycerol.

From the oxide voltammograms, bismuth was observed to adsorb onto the gold as both monolayers and multilayers. The peaks associated with bismuth monolayer formation continued to grow even when multilayer formation was established. This led to the suggestion that the bismuth was forming islands on the surface of the platinum, possible following either the Volmer-Weber or simultaneous multilayer growth models [6, 7]. In addition the gold oxide-reduction peak was observed to move to lower potentials on the introduction of bismuth, suggesting that bismuth was altering the electronic properties of the parent catalyst. The extent of perturbation of the peak correlated with increasing bismuth loading.

From the Pb_{UPD} voltammograms, it was apparent that the bismuth is non-site specific in its adsorption. Hence it is not be possible to link catalytic activity to a particular surface site, as has been the case in some investigations of enantioselective hydrogenation over Pt/Bt-catalysts in this laboratory.

From the XPS spectra it was clear that substantially increasing the amount of bismuth did not result in a correspondingly large decrease in gold surface area. This indicated that bismuth was adsorbing as islands. In addition the carbon percentages remained constant indicating that the bismuth was not adsorbing onto the graphite.

The TEM images showed no significant changes on the introduction of bismuth, indicating that the structure of the gold was not being modified by the introduction of bismuth.

When the catalysts were tested under basic conditions (see section 3.3.6), the second-reduction peak (b) was observed to grow with gold loading, suggesting that the catalytic properties of the 2% Au/graphite catalyst would be significantly higher than that of the other catalysts. On the introduction of bismuth, peak (b) was lost rapidly in all cases.

Electrooxidation of the unmodified catalysts showed that the 2% Au/graphite catalyst had a noticeable shoulder on the main glycerol electrooxidation peak, possibly indicating a different product distribution. The 1% Au/graphite catalyst gave a sharper peak and no up-turn in the voltammogram sweep at 1.6 V. This could be interpreted as indicating no deep-oxidation products are formed on this catalyst. The introduction of bismuth resulted in the reduction of the glycerol electrooxidation peak in all cases.

On investigating the catalysts in the high-pressure reactor, it was found that the conversion obtained for the 1% Au/graphite catalyst was significantly lower than that obtained on the other unmodified catalysts. In addition the introduction of bismuth resulted in a decrease in the observed conversion. Therefore there appears to be a link between the catalytic results and the electrooxidation voltammograms. However, it should be recalled that the 2% catalyst, which showed the shoulder, was unremarkable in its catalytic properties compared to the other gold catalysts.

Comparing the catalytic results with the voltammograms obtained in basic electrolyte, it is apparent that there is no link between the data sets. The second oxide-reduction peak was largest on the 2% Au/graphite catalyst; however this catalyst does not show any substantial changes in either its activity or selectivity. In addition the introduction of bismuth dramatically reduced the size of the oxide-reduction peak, but there is no consistent change in the product distribution. Hence it would appear that the second oxide-reduction peak is not an indicator of catalytic selectivity.

4.5 Discussion of results presented in section 3.4

To determine if the procedures used so far could be applied to another system to investigate their surface structure and activity, a range of Au, Pd and Au-Pd catalysts supplied by Prati [16, 19] were investigated.

On examining the catalysts in acidic electrolyte, the palladium and gold oxide peaks became visible in the voltammograms. The gold catalysts gave very different responses; this indicated that the preparation methods used had produced two very different catalysts. Comparing the gold and palladium catalysts with the bi-metallic catalysts showed that they were alloyed to a different extent, with M42 being the least alloyed catalyst. The extent of alloying could be gauged by the relative shift of the oxide stripping peaks from those of the pure metals. The relative Au/Pd surface composition could be attained by using the ratio of Au/Pd charge under the oxide peaks.

Pb_{UPD} showed that the FP7 catalyst was highly structured and contained Au {111} and Au{110} sites. By comparison, the Au15 catalyst showed little structure; the catalytic activities are noted below. Unfortunately the palladium catalyst gave no structural information and the bi-metallics were dominated by the palladium and as such gave no structural information.

The electrooxidation (figure 3.4.4) results showed that the FP7 catalyst gave by far the largest peak area, when compared with the other catalysts. The other catalysts produced approximately the same extent of electrooxidation and this might be indicative of the catalytic results.

On testing the catalysts in a high pressure reactor, the FP7 catalyst showed a significantly higher activity than the other gold catalyst. This might be related to the larger electrooxidation peak observed in the voltammograms. However, the activity of both of the gold catalysts was significantly lower than that observed for the alloy catalysts. Hence the size of the electrooxidation peak does not appear to correspond to catalytic activity under high pressure conditions.

However it is notable that the FP7 catalyst which showed the higher catalytic activity had the greater long range order, as determined from figure 3.4.1 and 3.4.2. In addition the most alloyed catalyst, M41, showed the highest activity.

4.6 Discussion of the second reduction peak observed for catalyst voltammograms tested under basic conditions

According to Hutchings et al [9], the shape of this oxide-reduction peak "*may be of importance with respect to the nature of the selective oxidant*". This statement linked this second peak to an increased catalytic activity and had been attributed to "*some surface oxide or peroxide formed in presence of NaOH*". However the true nature and origin of this feature had not been discovered. From the data presented in chapter three it is evident that the proposed link between this peak and the catalytic properties does not apply to the catalysts tested in this investigation. Hence it became important to identify the origin of this peak.

Presented in figure 4.1 are the voltammograms that were discussed in section 3.2. From these voltammograms it is evident that the size of the peak in the reverse sweep is closely linked to the size of the oxygen evolution peak observed in the forward sweep at 1.5 V. This indicated that the second peak in the reverse sweep was in some way the result of oxygen being evolved in the cell in the forward sweep. Hence the second oxide-reduction peak visible in the reverse sweep is most probably due to the reduction of oxygen.

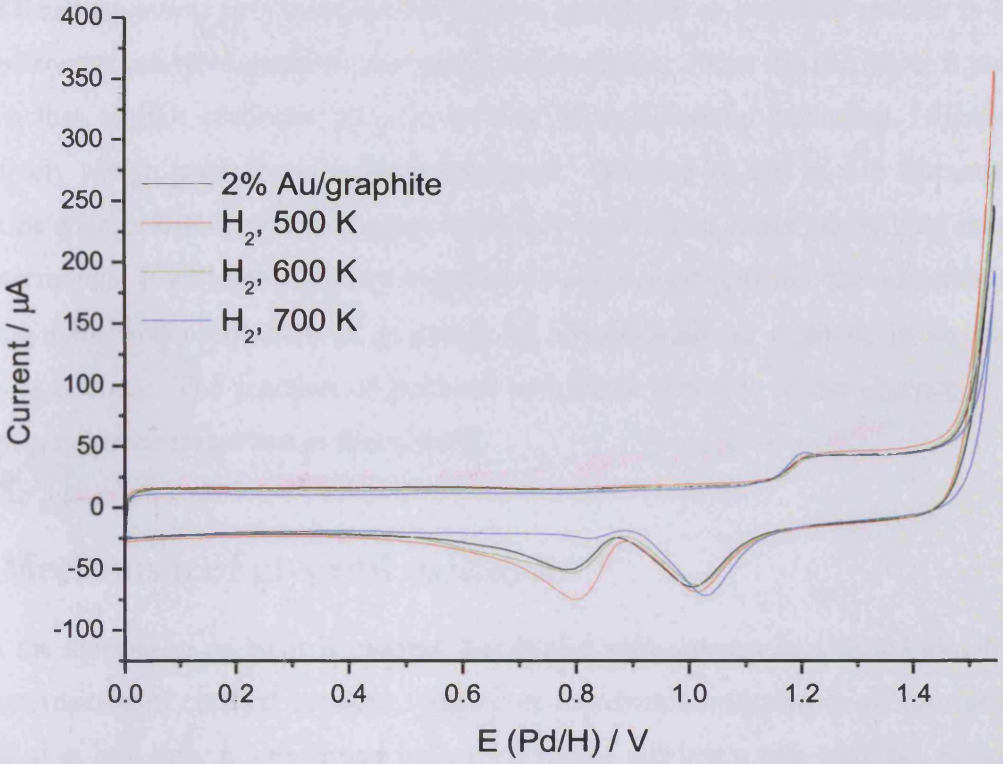

Figure 4.1: CVs for as-received 2% Au/graphite and the variants heated under hydrogen in 0.5 M NaOH at 10 mV s^{-1} showing the features associated with gold oxide formation and oxygen evolution in the forward sweep and reduction in the reverse sweep.

From a literature survey of papers focussing on oxygen reduction over gold single crystals [20-22] and supported catalysts [23-24] in both basic and acidic conditions, it is highly likely that the peak observed in figure 4.1 is a result of oxygen reduction, since the peak is so closely linked with the oxygen evolution peak seen in the forward sweep. The reaction follows either a 2 or 4 electron process [25], as outlined below, depending on experimental conditions and the catalyst being used.

Two-electron process

$$O_2 + H_2O + 2e^- \rightarrow HO_2^- + OH^- \quad \textbf{(4.1)}$$

$$HO_2^- + H_2O + 2e^- \rightarrow 3OH^- \quad \textbf{(4.2)}$$

Four-electron process

$$O_2 + 2H_2O + 4e^- \rightarrow 4OH^- \quad \textbf{(4.3)}$$

From these equations it is evident that either a hydroxide or peroxide species is being formed by the catalysts prepared and tested in this thesis. From the literature, it is well-known that, unlike platinum, gold gives rise to a 2-electron reduction. Hence we tentatively assign peak (b) to a peroxo-species. Whether or not in situ formation of peroxide species from gaseous oxygen is the key to catalytic oxidation by gold needs to be determined. It will be of interest in future work to investigate this phenomenon more thoroughly as the production of peroxide by electrochemical methods is an area of growing interest. The reaction of glycerol with basic peroxide in the absence of gold catalysts might be important in this regard.

4.7 Mechanism of glycerol oxidation

From the discussion so far it is evident that cyclic voltammetry is a useful tool for the characterisation of catalyst surfaces. However the electrooxidation in all four sections provided at best only a very broad indication of the catalyst's true ultimate activity as tested in a reactor. One explanation for this discrepancy is that the electrooxidation and the catalytic oxidation were carried out under very different conditions. In the cell experiments were conducted at room temperature and pressure over a short period of time. In the reactor the experiment was run at elevated temperature and pressure, over a much greater time. Yet the explanation for the discrepancy between the electrochemical and catalytic results might be far more fundamental than just a difference in reaction conditions.

As discussed in the introduction the proposed mechanism for the oxidation of the liquid phase alcohols over a metal surface follows an oxidative dehydrogenation mechanism [15, 26]. This was elucidated, in part, from isotopic labelling of oxygen for 2-propanol oxidation [27]

$$RCH_2OH \rightarrow RCH_2O_{(ads)} + H_{(ads)} \quad \textbf{(4.4)}$$

$$RCH_2O_{(ads)} + O_{(ads)} \rightarrow RCHO + OH_{(ads)} \quad \textbf{(4.5)}$$

$$H_{(ads)} + OH_{(ads)} \rightarrow H_2O \quad \textbf{(4.6)}$$

Although the majority of the investigations of mechanism were carried out on platinum and other platinum group metals, an oxidative dehydrogenation mechanism holds true for supported gold catalysts. It is important to note that base is essential for alcohol oxidation over gold catalysts to occur. This has been explained by the inability of gold to extract the hydride species – the first step in the oxidative dehydrogenation mechanism [17, 28-29]. Even though there have been a number of different variations proposed, the overall mechanism for catalytic oxidative dehydrogenation of an alcohol is reasonably well understood.

It has been established that if glyceraldehyde results from the catalytic oxidation of glycerol it is rapidly converted to glyceric acid and hence is generally only observed as a transient species during reaction. However, from electrolysis of glycerol in basic media over platinum, glyceraldehyde was found to be the major product formed, with glyceric acid and glycolic acid being only secondary products [30]. Two mechanisms have been proposed for this transformation and are presented in figure 4.2. It is perhaps unsurprising that there was considerable discrepancy between the catalytic results and the electrooxidation results given that the primary product was different in each case.

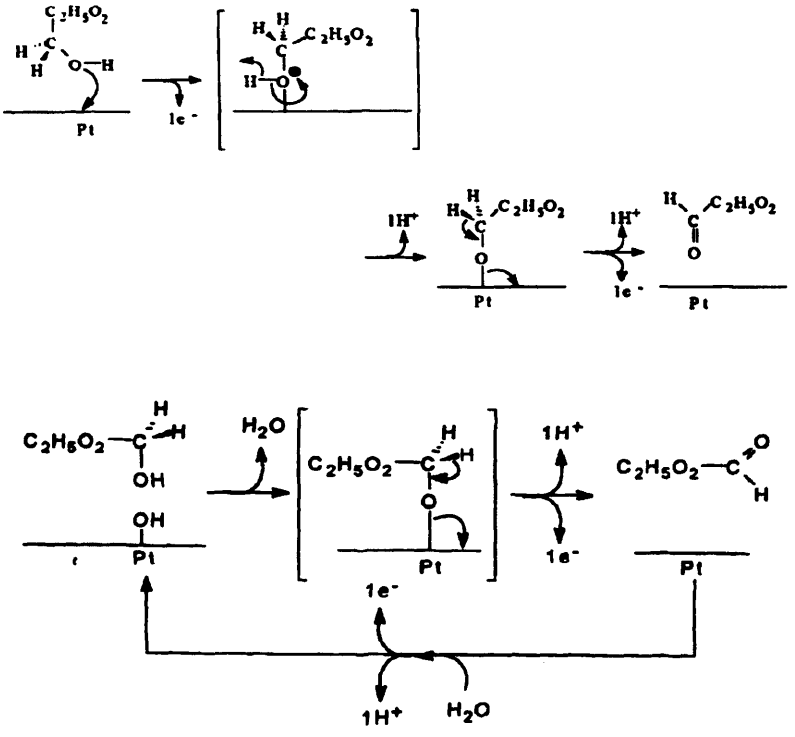

Figure 4.2: The two proposed mechanisms for glycerol oxidation on platinum surfaces. Reproduced from [30].

4.8 Conclusions

Three series of catalysts (Au-Pt/graphite, sintered Au/graphite and Bi-Au/graphite) were prepared and used for the oxidation of propanol and glycerol. In addition a set of Pd-Au/graphite catalysts were provided by Prati. All of these catalysts were characterised by a range of techniques, mainly cyclic voltammetry, but also XPS and TEM. Generally good agreement was obtained between the results of these characterisation techniques.

Broad links have been established between the electrooxidation and catalytic oxidation of 1- and 2-propanol.

There appeared to be no link between the voltammetric responses obtained and the catalytic activity in the case of the more complex oxidation of glycerol. Furthermore no link between the second oxide-reduction peak, (b), and catalytic activity could be established.

Further experiments might include testing the catalysts for an oxidation of less complexity than that of glycerol. Since propanol gave some indication of links between the electrochemical and catalytic results, it would be logical to investigate simple alcohols of various carbon chain length to determine if this has an effect on the relationship. Further investigation of peak (b) is also required to determine beyond doubt its true nature and whether it is fundamentally linked to the catalytic activity of the gold catalysts.

Further catalytic investigation into the stability of bismuth on gold would also be appropriate. Under electrochemical reaction conditions, bismuth was found to be stable in basic electrolyte; however, at elevated temperature and pressure (i.e. true reaction conditions) this might not hold true.

It would be beneficial to prepare gold modified platinum catalysts with more sequential gold loadings to confirm the results obtained so far.

Finally, further single crystal studies utilising bismuth modified gold surfaces would be valuable since they would allow the surfaces of variable geometry to be investigated for their activity.

4.9 References

1. A. Schwartz, L.L. Holbrook, H. Wise, *J. Catal.*, **21** (1971) 199.
2. H.E. Van Dam, A.P.G. Kieboom, H. Van Bekkum, *App. Catal.*, **33** (1987) 361.
3. H. E. Van Dam, P. Duijverman, A. P. G. Kieboom, H. van Bekkum, *App. Catal.*, **33** (1987) 373.
4. A. van der Burg, J. Doornbos, N.J. Kos, W.J. Ultee, V. Ponec, *J. Catal.*, **54** (1978) 243.
5. T. Mallát, J. Petró, *App. Catal.*, **4** (1982) 257.
6. M. Volmer, A. Weber, *Z. Phys. Chem.*, **119** (1926) 277.
7. D. Kaschiev, *J. Crystal Growth*, **40** (1977) 29.
8. R.M. Ishikawa, A.T. Hubbard, *J. Electroanal. Chem.*, **69** (1976) 317.
9. S. Carrettin, P. McMorn, P. Johnston, K.G. Griffin, G.J. Hutchings, C.J. Kiely, G.A. Attard, *Top. Catal.*, **27** (2004) 131.
10. C. Berg, H.J. Venvik, F. Strisland, A. Ramstad, A. Borg, *Surf. Sci.*, **409** (1998) 1.
11. H. Kimura, K. Tsuto, T. Wakisaka, Y. Kazumi, Y. Inaya, *App. Catal. A,* **96** (1993) 217.
12. H. Kimura, *App. Catal. A*, **105** (1993) 147.
13. R. Garcia, M. Besson, P. Gallezot, *App. Catal. A*, **127** (1995) 165.
14. P. Fordham, M. Besson, P. Gallezot, *App. Catal. A,* **133** (1995) L179.
15. P. Gallezot, *Catal. Today*, **37** (1997) 405.
16. C.L. Bianchi, P. Canton, N. Dimitratos, F. Porta, L. Prati, *Catal. Today*, **102-103** (2005) 203.
17. S. Carrettin, P. McMorn, P. Johnston, K.G. Griffin, G.J. Hutchings, *Chem. Comm.*, (2002) 696.
18. S. Carrettin, P. McMorn, P. Johnston, K.G. Griffin, G.J. Hutchings, C.J. Kiely, *Phys. Chem. Chem. Phys*, **5** (2003) 1329.
19. N. Dimitratos, F. Porta, L. Prati, *App. Catal. A*, In Press 2005.

20. S. Strbac, R.R. Adzic, *Electrochim. Acta,* **41** (1996) 2903.
21. C. Paliteiro, N. Martins, *Electrochim. Acta*, **44** (1998) 1359.
22. H. Naohara, S. Ye, K. Uosaki, *Electrochim. Acta*, **45** (2000) 3305.
23. M.S. El-Deab, T. Ohsaka, *Electrochem. Commun.* **4** (2002) 288.
24. M.S. El-Deab, T. Ohsaka, *J. Electroanal Chem.*, **553** (2003)107.
25. V.B. Baez, D. Pletcher, *J. Electroanal. Chem.*, **377** (1994) 231
26. M. Besson, P. Gallezot, *Catal. Today*, **57** (2000)127.
27. M. Rottenberg, P. Baertschi, *Helv. Chim. Acta*, **39** (1956) 1973
28. L. Prati, F. Porta, *App. Catal. A*, In Press 2005.
29. S. Demirel-Gulen, M. Lucas, P. Claus, *Catal. Today*, **102-103** (2005) 166.
30. L. Roquet, E.M. Belgsir, J.-M. Leger, C. Lamy, *Electrochem. Acta*, **39** (1994) 2387.

Appendix A

The development of models for the electrical double layer

A.1 Models of the electrical double layer

A.1.1 Introduction

The double layer observed in cyclic voltammograms is a result of the electrode/electrolyte interface and the applied potential. As stated in section 1.2.4.2, several models have been proposed to explain the phenomenon and these models are discussed in this section.

A.1.2 The Helmholtz model

This, the earliest model, was proposed by Helmholtz in the mid-nineteenth century [1-3]. It was based on the concept that the interface between the electrode and electrolyte was analogous with a capacitor in that charge could be stored. It was proposed that the electrode possessed a charge as a result of either electron excess or deficiency and that this charge was balanced by the solution at the interface which held an opposite charge equal to the electrodes. Figure A.1 shows this proposed model of electrode-electrolyte interface as two rigid rows of ions of balanced opposing charge (hence the name "double layer"). This model is the earliest and hence the most simplistic of the models presented in this section, however it also represents a major intellectual feat, since it is the first true microscopic description of the structure of an electrode/electrolyte interface.

The arrangement of positive ions next to the surface of the negatively charged electrode results in a potential difference occurring across the interface. From this a potential curve results which is characteristic of the model (also shown in figure A.1). In this case it is a linear decay of the potential profile with increasing distance from the electrode surface. Helmholtz defined the double layer capacitance per unit area as shown in equation A.1 and this is of importance since it shows that a macroscopic measurement could be related to the microscopic model.

$$C_H = \frac{\varepsilon}{4\pi d} \qquad \textbf{(A.1)}$$

Where:

C_H is the double layer capacitance, ε is the dielectric constant and d is the thickness of the double layer.

This is a reasonable model for polarisable electrodes that use electrolytes at a high concentration, however at lower concentrations new features became evident that are not explained by this model. This is explained by the fact that from equation A.1 it would appear that capacitance should remain constant with changing potential. However, experimental studies have proven that the capacitance is dependent on the potential and electrolyte concentration. In addition the model does not take into account any interactions that are occurring away from the electrode surface.

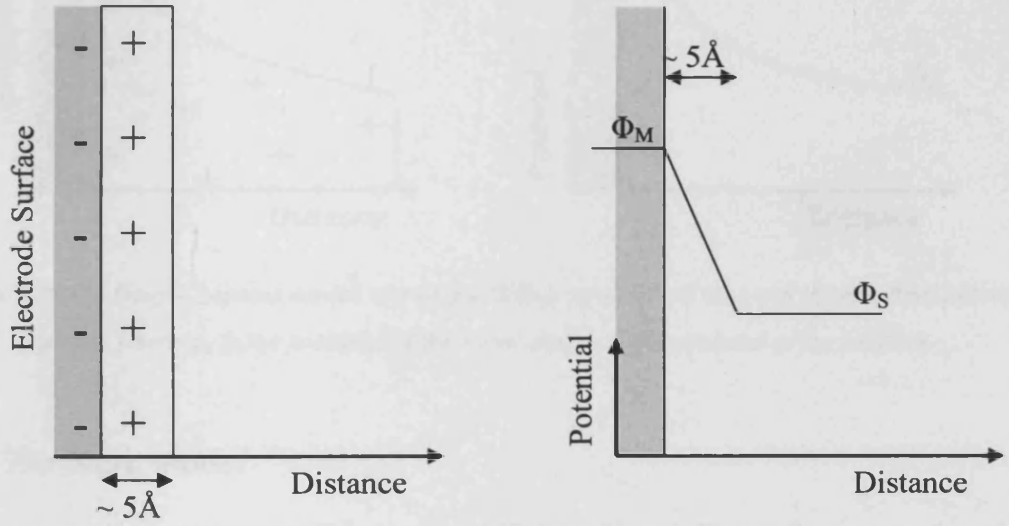

Figure A.1: The Helmholtz model, showing a rigid double layer of ions and the resultant potential profile where ϕ_M is the potential of the metal and ϕ_S is the potential of the solution.

A.1.3 The Gouy-Chapman model

The limitations of the Helmholtz model led to a new double layer model being proposed by Gouy in 1910 [4, 5] and by Chapman in 1913 [6]. This model is also known as the *diffuse double layer* model since and took into account the fact that potential and electrolyte concentration influence the capacitance. Instead of considering the electrode/electrolyte interface as a rigid structure, the electrolyte ions are considered as

point charges which are free to move and hence form a Boltzmann like distribution of varying thickness (dependent on applied potential and electrolyte composition) due to thermal motion disrupting the excess ions. In effect this model is a half-way house between the rigid Helmholtz model and random distribution of bulk electrolyte.

Figure A.2 shows the proposed model of electrode-electrolyte interface based on the Gouy-Chapman theory and the resultant potential curve. Experimentally it has been found from capacitance measurements that this model only holds for systems containing very weak electrolyte and at potentials close to the potential zero of charge (PZC) [7].

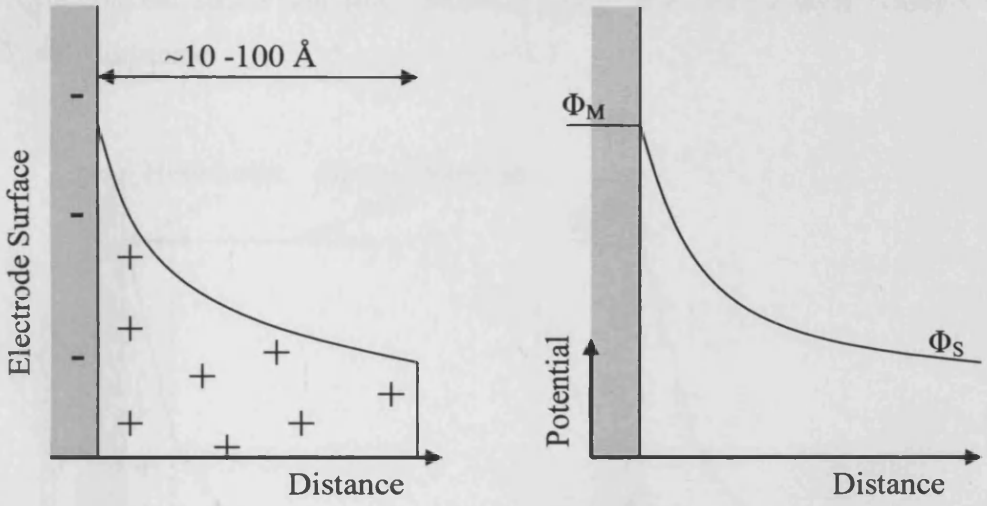

Figure A.2: The Gouy-Chapman model, showing a diffuse structure of ions and the resultant potential profile where ϕ_M is the potential of the metal and ϕ_S is the potential of the solution.

A.1.4 The Stern model

The Stern model was proposed in the 1920s and combines the concepts of the Helmholtz and Gouy-Chapman models [8]. The model envisages two areas, a rigid layer of ions next to the electrode surface as in the Helmholtz model and a diffuse layer further out similar to the Gouy-Chapman model. The model was based on the idea that the electrode charge would have a greater effect on ions that are closer to the electrode surface and that the effect would fade out with increasing distance. The presence of two distinct regions within the double layer meant that the total capacitance was a combination of the Helmholtz and Gouy-Chapman capacitances working in series, as shown by equation A.2.

$$\frac{1}{C_t} = \frac{1}{C_r} + \frac{1}{C_d} \qquad \textbf{(A.2)}$$

where:

C_t is the total capacitance, C_r is the capacitance of rigid Helmholtz layer and C_d is the capacitance of diffuse Gouy-Chapman layer.

From the above equation it is evident that the layer that gives the smallest capacitance contribution will have the largest effect on the total capacitance. As such at high electrolyte concentrations the rigid layer (Helmholtz model) will dominate but at low electrolyte concentrations and low electrode charge the diffuse layer (Gouy-Chapman model) will dominate.

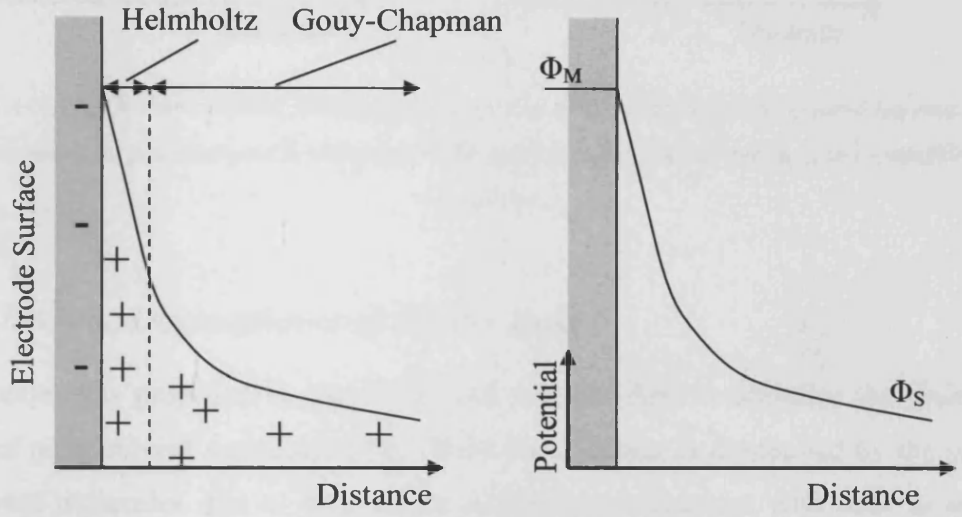

Figure A.3: The Stern model, showing a combination of the Helmholtz and Gouy-Chapman models and the resultant potential profile where ϕ_M is the potential of the metal and ϕ_S is the potential of the solution.

A.1.5 The Grahame model

This model was proposed in the 1940s and was the first to deal with the concept of specific adsorption [9]. An ion that is specifically adsorbed has lost its solvation layer and as such is able to approach closer to the electrode surface than a species which has not. Figure A.4 shows the three regions which arise from this theory, the new inner Helmholtz plane (IHP) which extends from the electrode surface to the loci of the specifically adsorbed ions, the outer Helmholtz plane (OHP) as proposed by Helmholtz which passes through the centre of hydrated ions at their closest position to the

electrode and the diffuse layer proposed by Gouy-Chapman which lies beyond the OHP. This model normally gives the best agreement between theory and experiment.

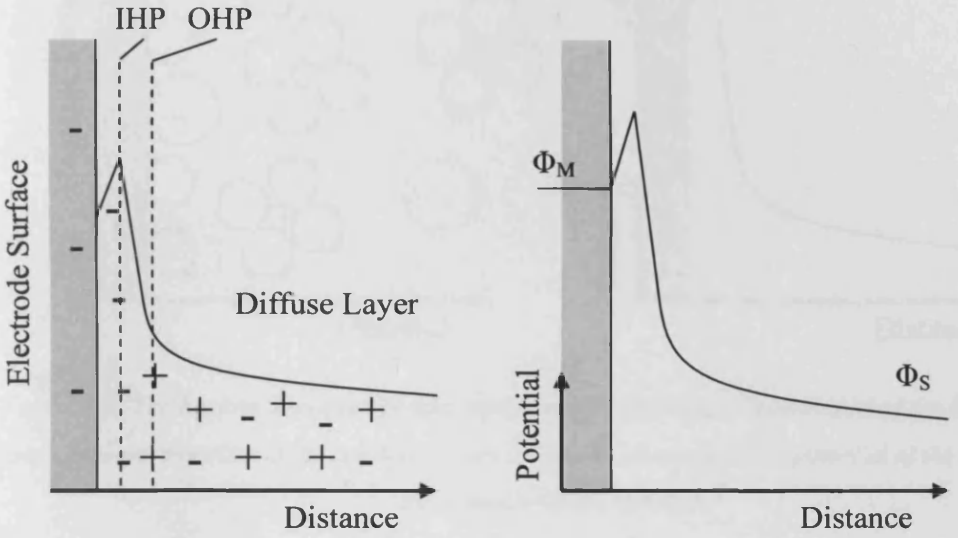

Figure A.4: The Grahame model, showing a combination of the Helmholtz and Gouy-Chapman models and the resultant potential profile where ϕ_M is the potential of the metal and ϕ_S is the potential of the solution.

A.1.6 Bockris, Devanathan and Muller model

This model was proposed in the 1960s and was the first to consider the dielectronic effect of polar solvent molecules [10]. Here the interface is dominated by the presence of solvent molecules due to their molar excess in comparison with ions in solution. They form a layer in the IHP with the specifically adsorbed ions and can be considered as the solvation layer for the electrode. They orientate depending on the charge of the electrode and the presence or absence of specifically adsorbed ions. This new addition to the model does not affect, in qualitative terms, the potential/distance graph proposed for the previous model.

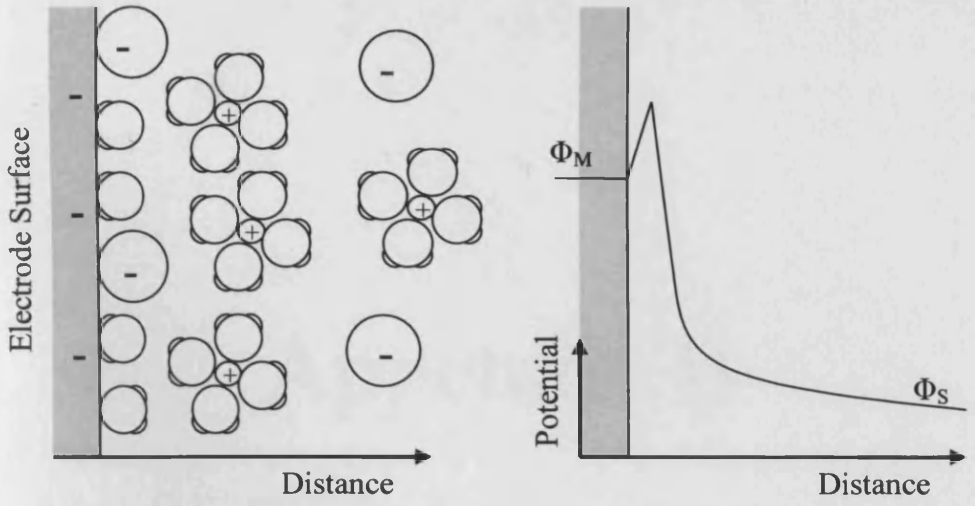

Figure A.5: The Bockris, Devanathan and Muller model, showing a combination of the Helmholtz and Gouy-Chapman models and the resultant potential profile where ϕ_M is the potential of the metal and ϕ_S is the potential of the solution.

A.2 References

1. H.L.F. von Helmholtz, *Ann. Physik*, **89** (1853) 211.
2. H.L.F. Von Helmholtz and W. Abhandl, *Physik Tech. Reichstaldt*, **1** (1879) 925.
3. H.L.F. von Helmholtz, *Ann. Physik*, **7** (1879) 337.
4. G. Gouy, *J. Phys. Radium*, **9** (1910) 457.
5. G. Gouy, *Compt. Rend.*, **149** (1910) 654.
6. D.L. Chapman, *Phil. Mag.*, **25** (1913) 475.
7. J.M. Czajkowski, T. Blaszczyk, *Electrochim. Acta*, **34** (1989) 405.
8. O. Stern, *Z. Electrochem.*, **30** (1924) 508.
9. D.C. Grahame, *Chem. Rev.*, **41** (1947) 441.
10. J.O'M. Bockris, M.A.V. Devanathan, K. Muller, *Proc. Roy. Soc.*, **A 274** (1963).

Appendix B

TEM Images

B.1 TEM images of the 2% Au/graphite catalyst

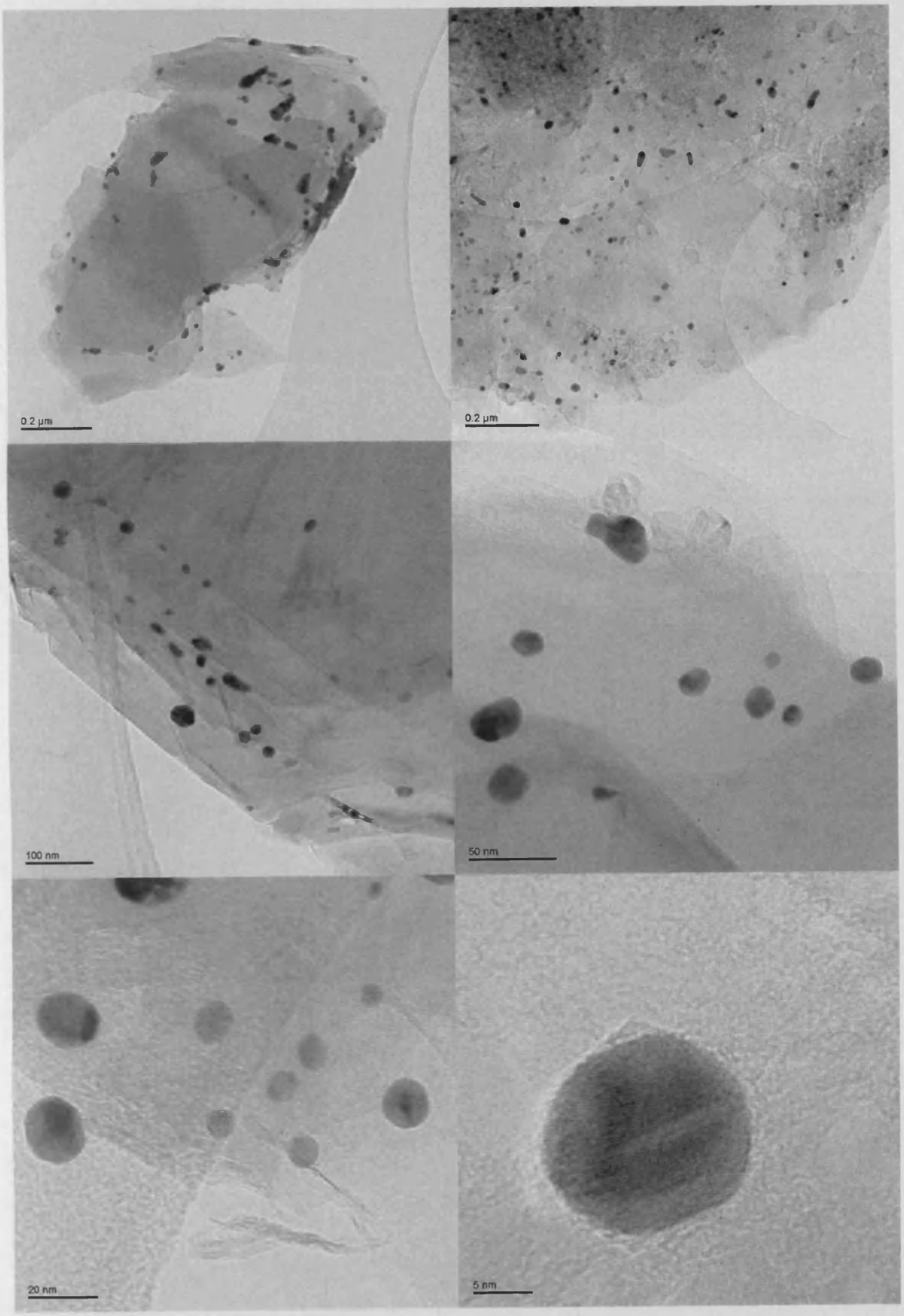

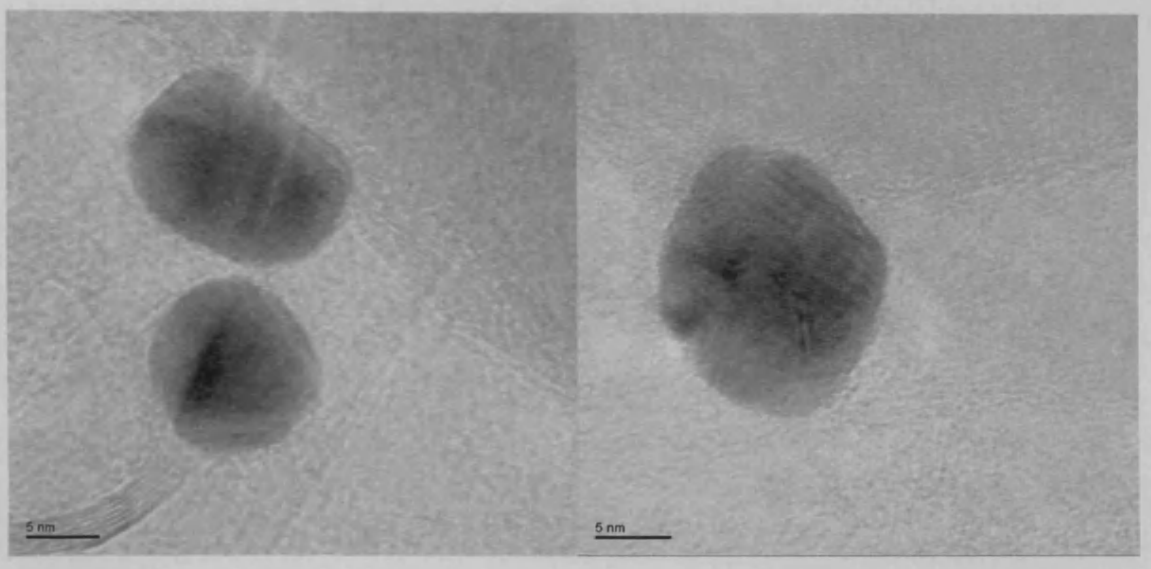

B.2 TEM images of the 2% Au/graphite catalyst (500K, Air)

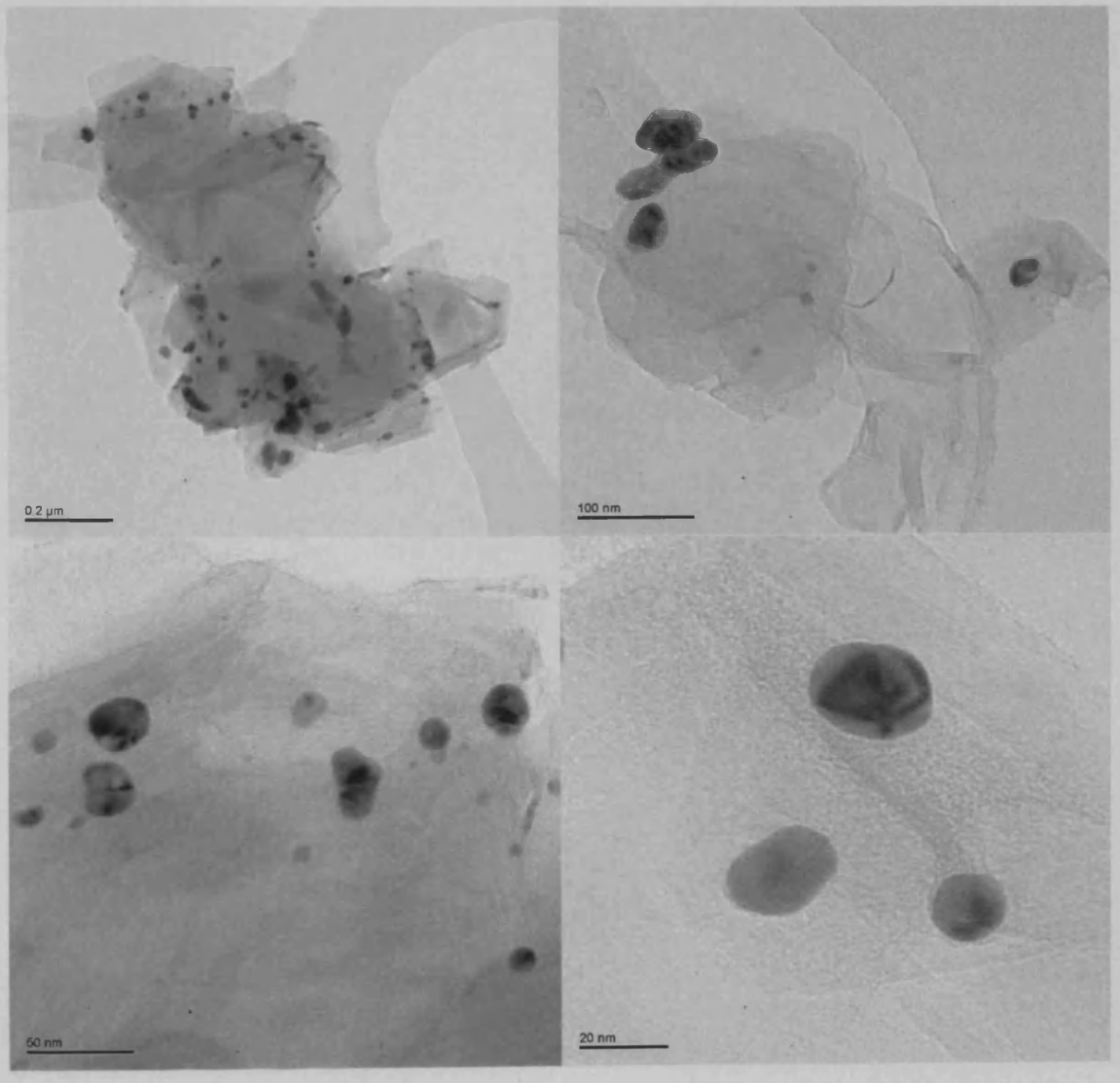

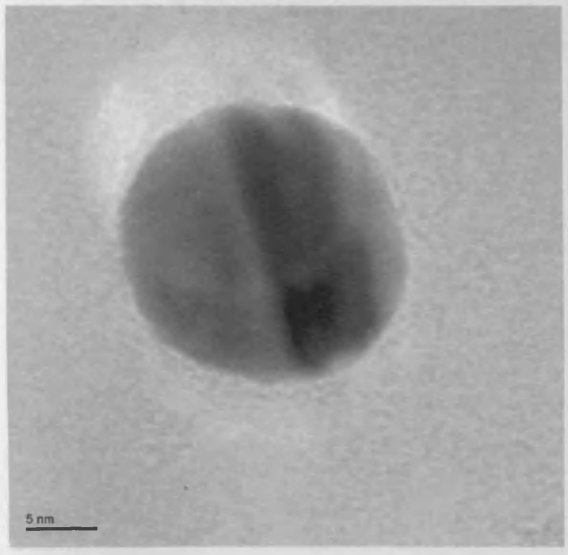

B.3 TEM images of the 2% Au/graphite catalyst (600K, Air)

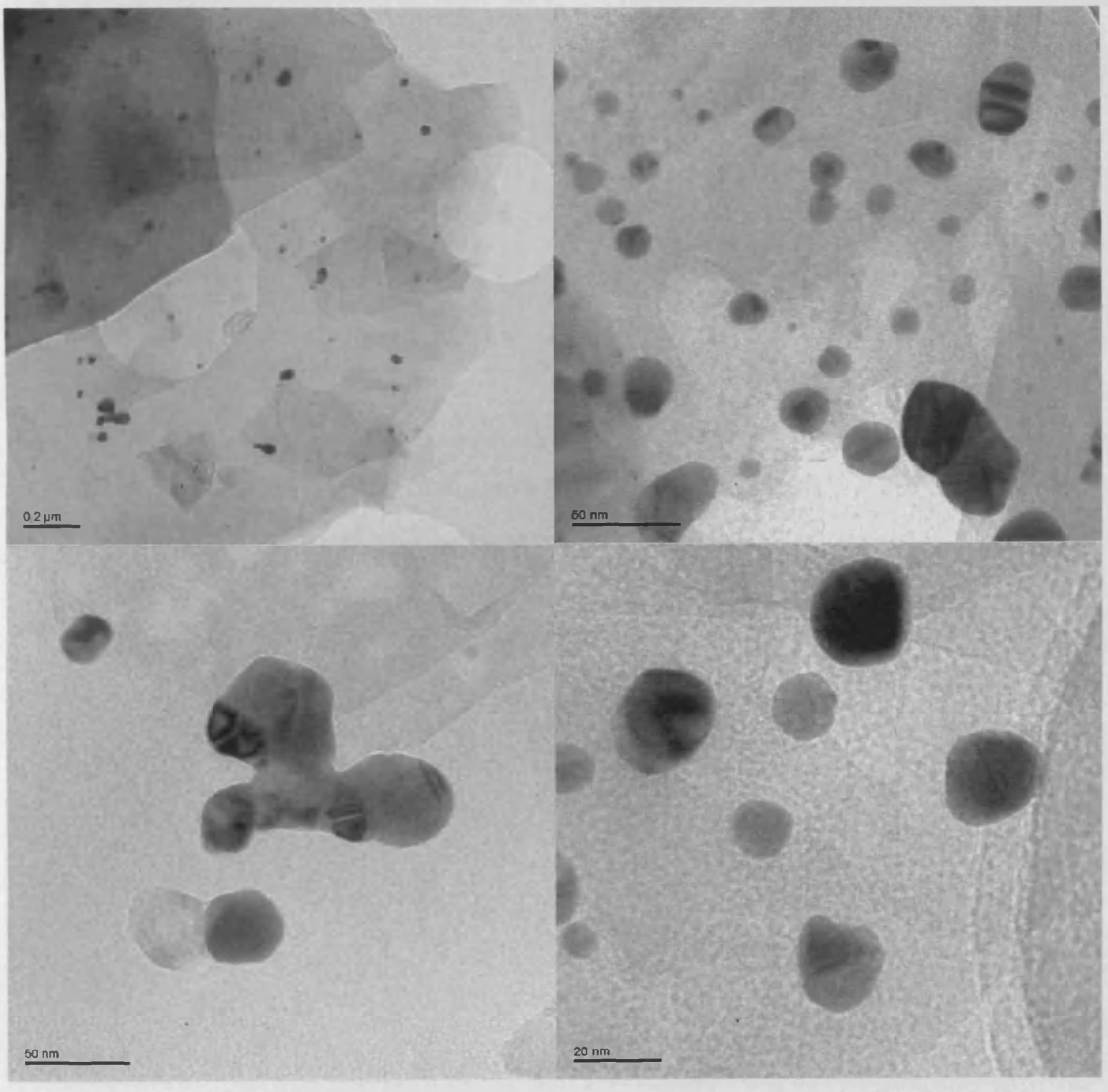

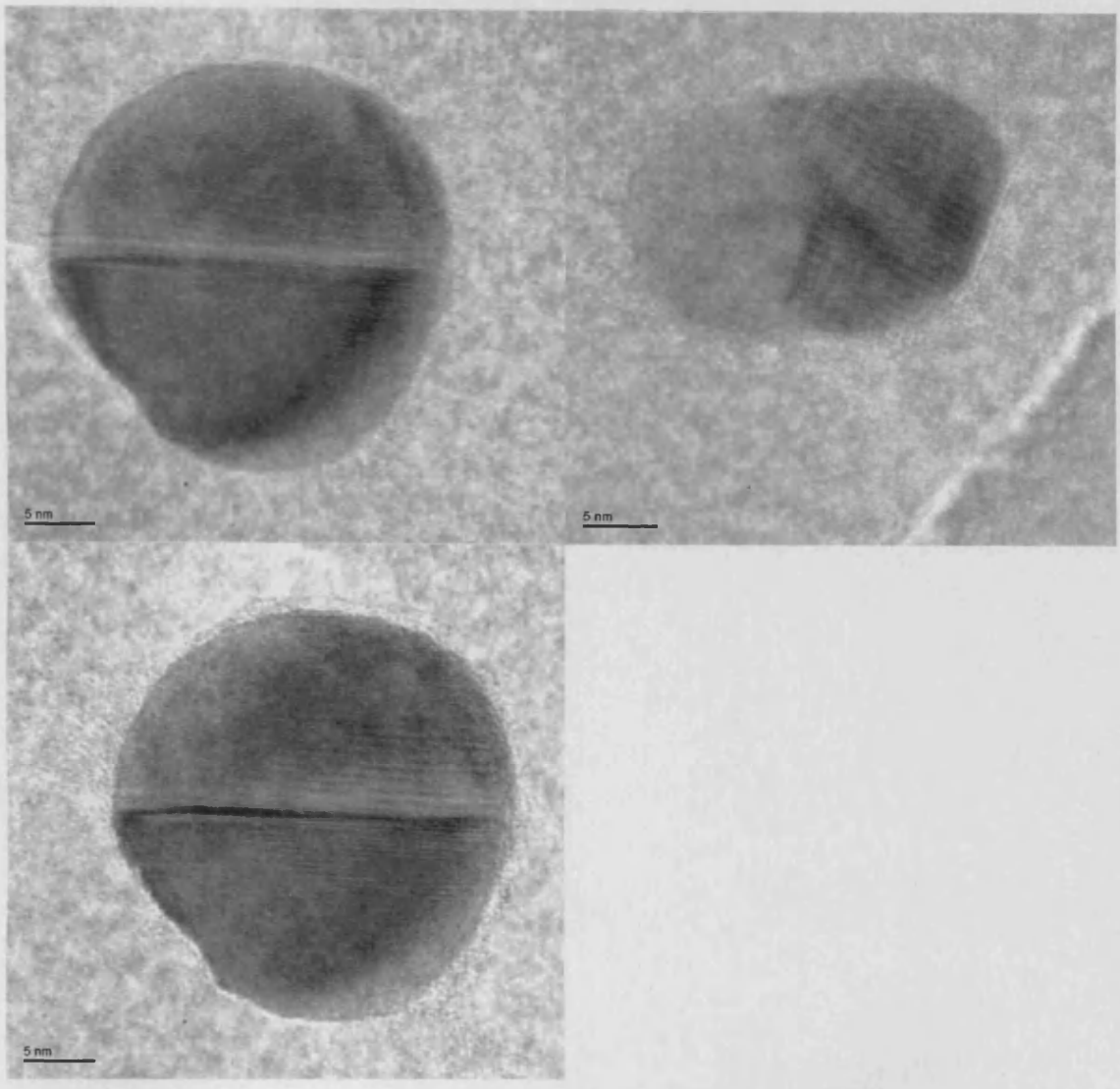

B.4 TEM images of the 2% Au/graphite catalyst (700K, Air)

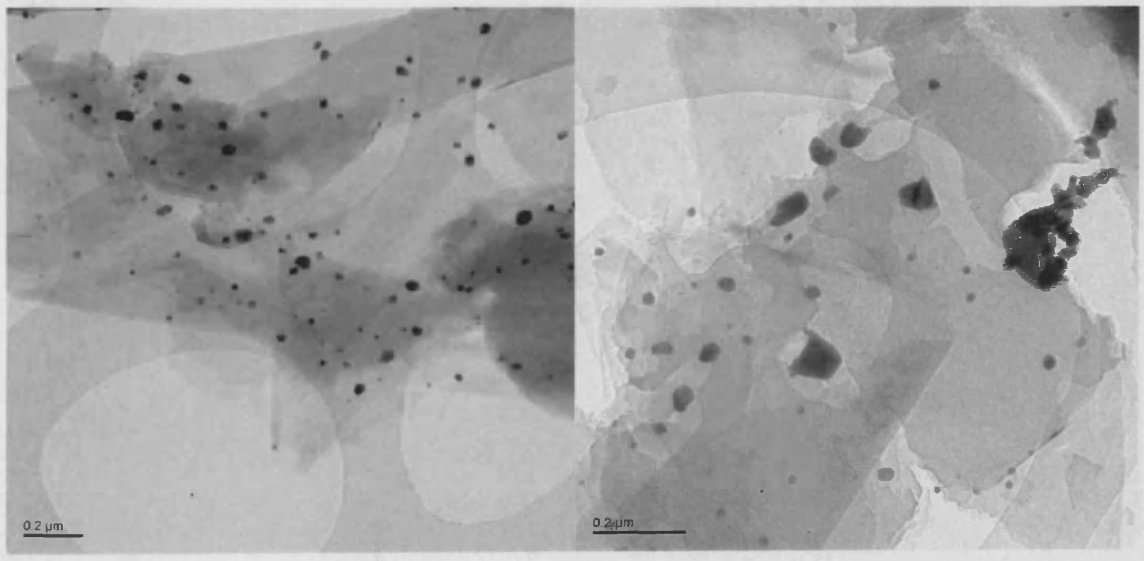

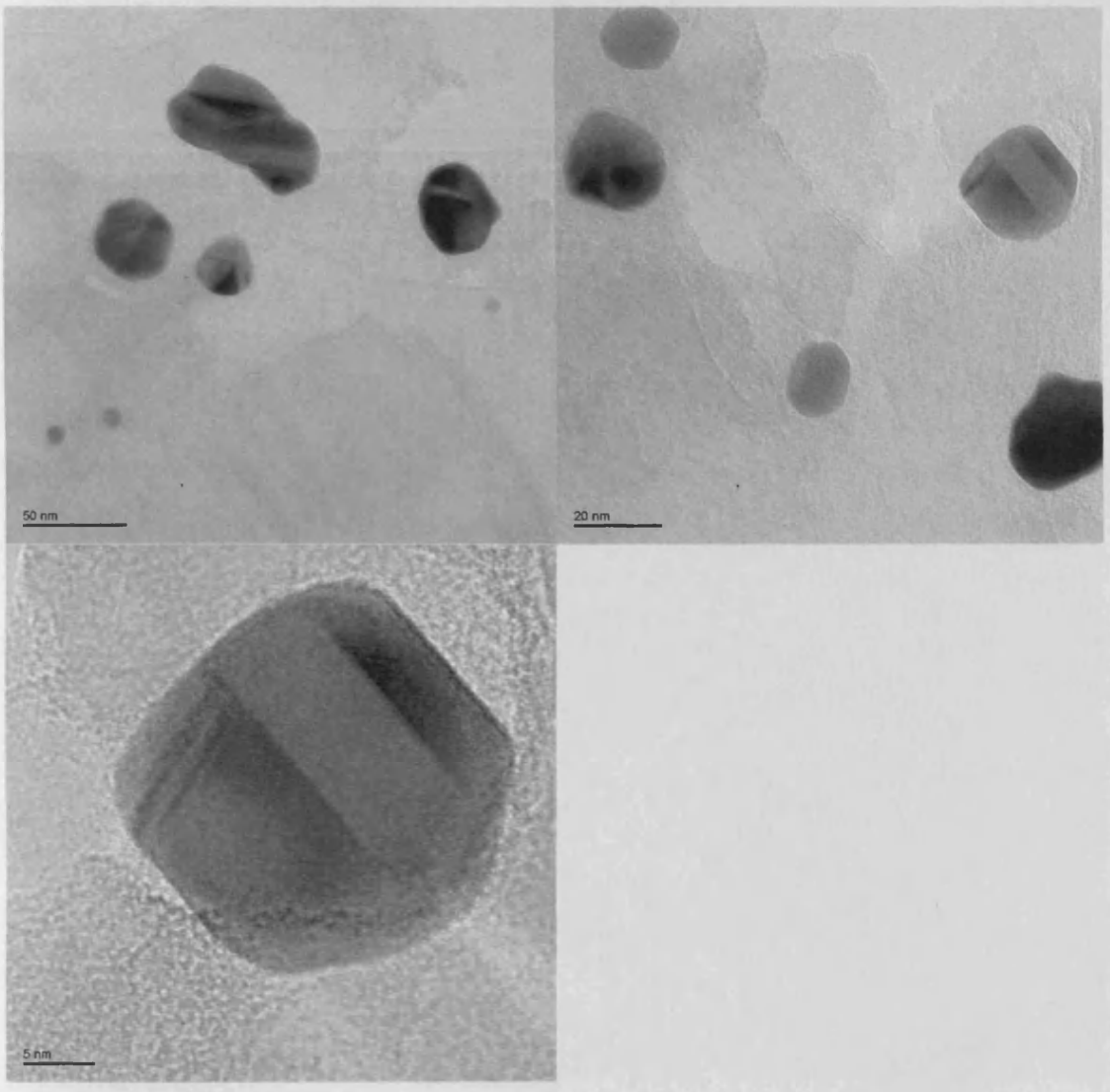

B.5 TEM images of the 2% Au/graphite catalyst (500K, H_2)

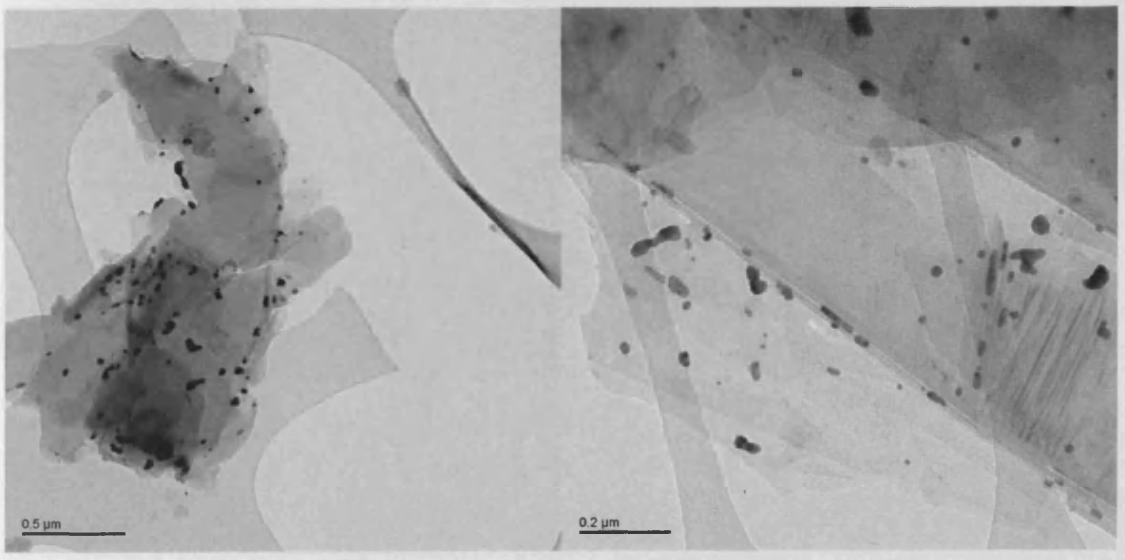

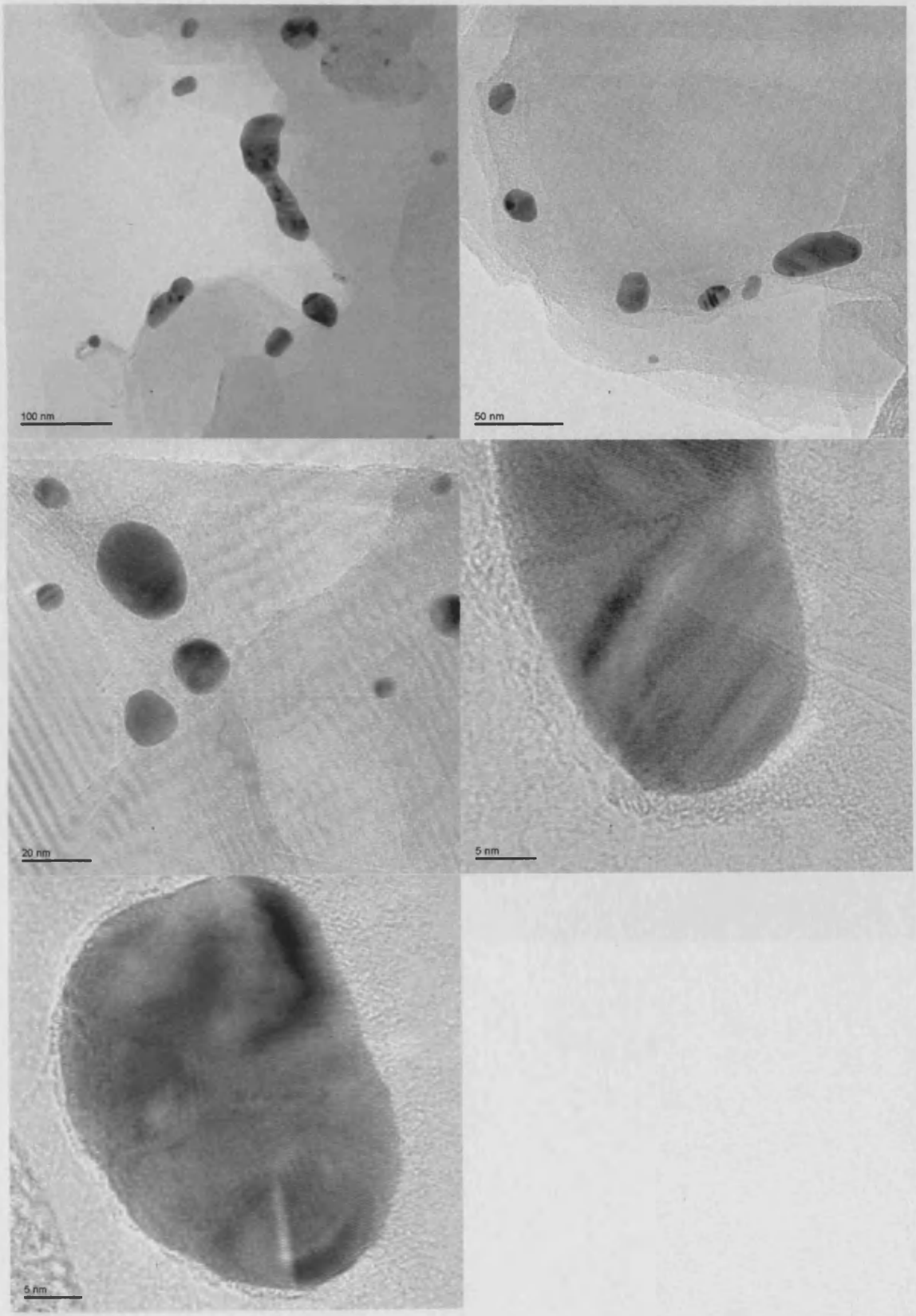
100 nm
50 nm
20 nm
5 nm
5 nm

B.6 TEM images of the 2% Au/graphite catalyst (600K, H_2)

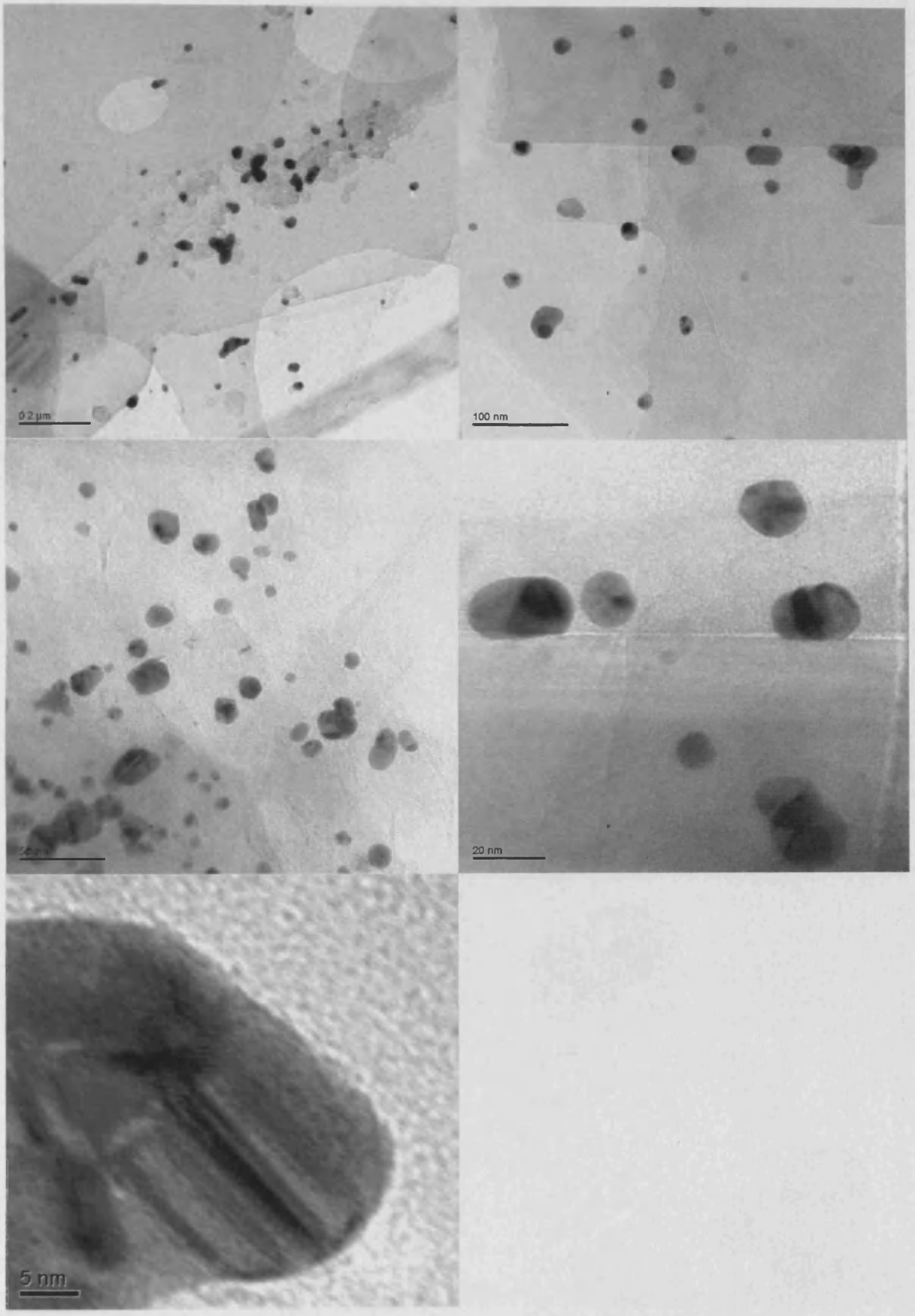

B.7 TEM images of the 2% Au/graphite catalyst (700K, H_2)

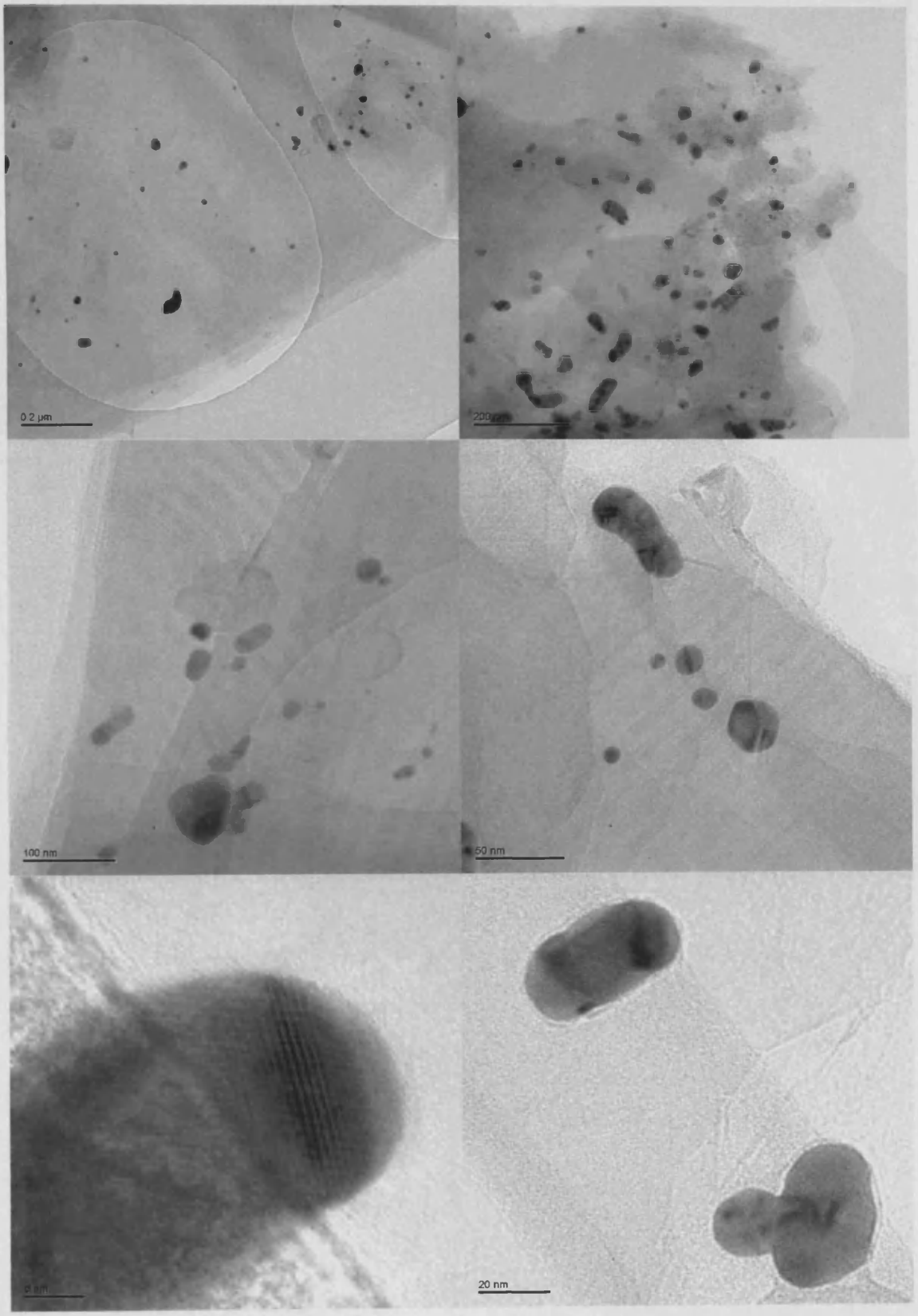

B.8 TEM images of the 1 ml Bi-2% Au/graphite catalyst

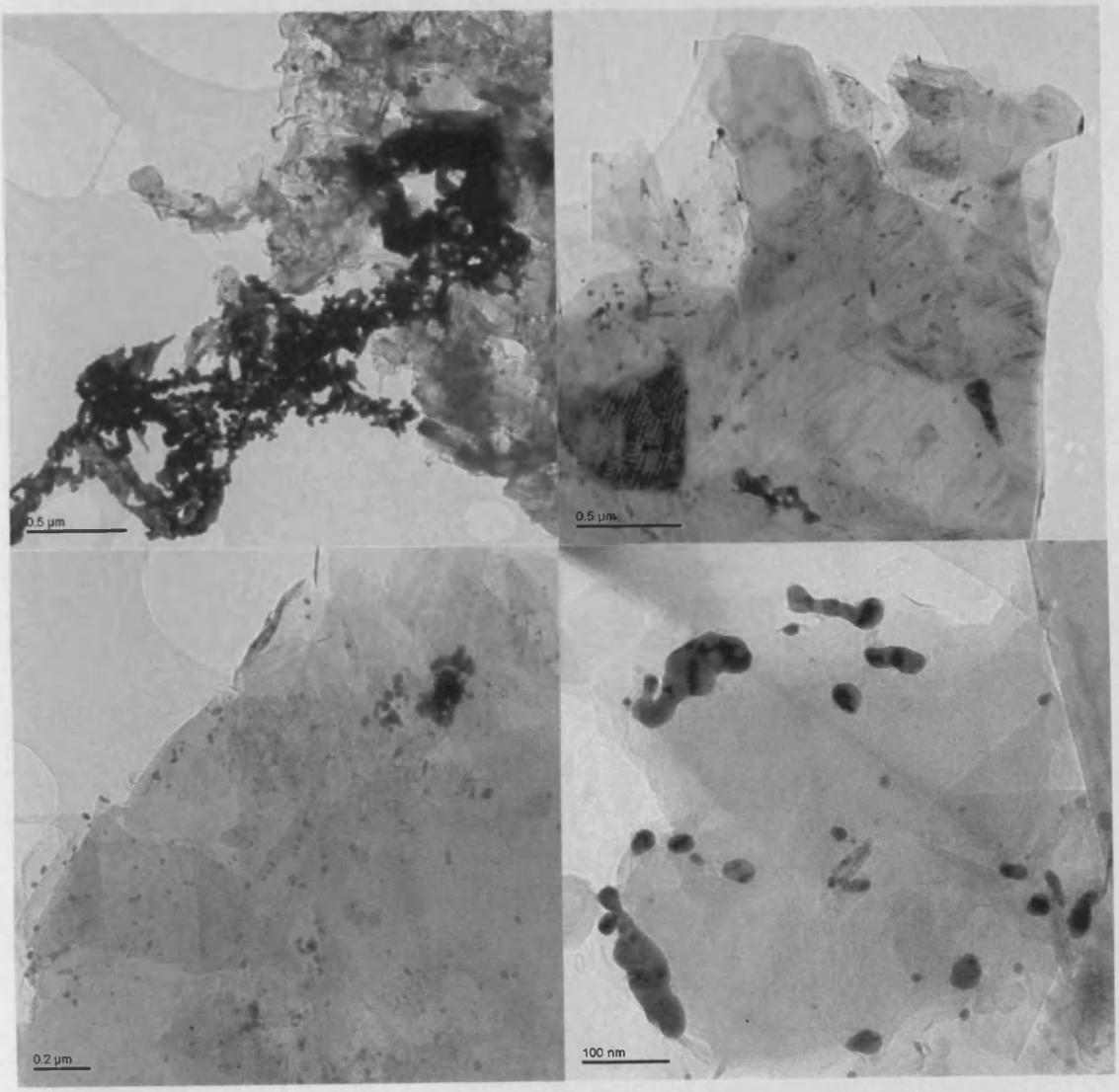

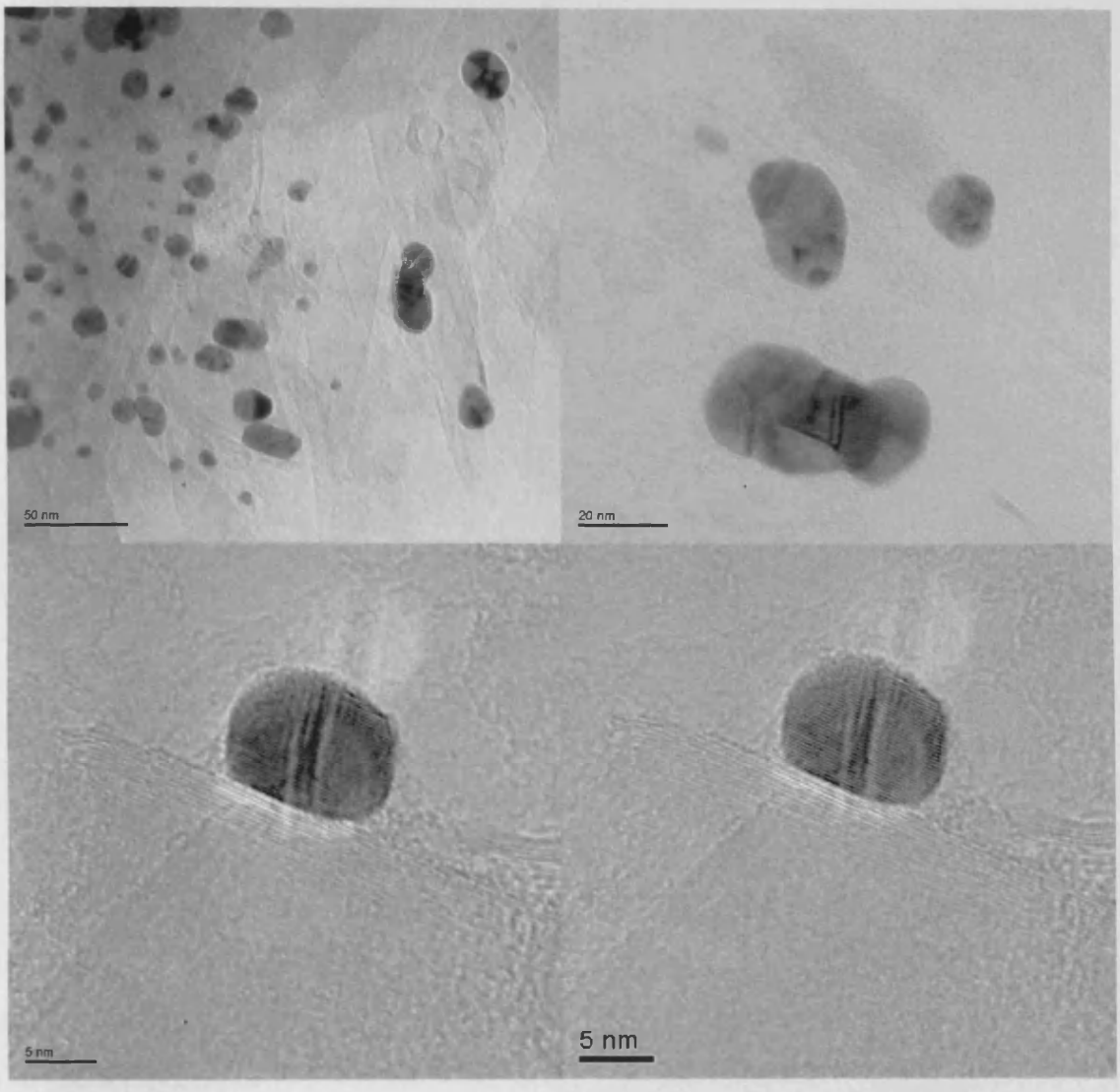

B.9 TEM images of the 10 ml Bi-2% Au/graphite catalyst

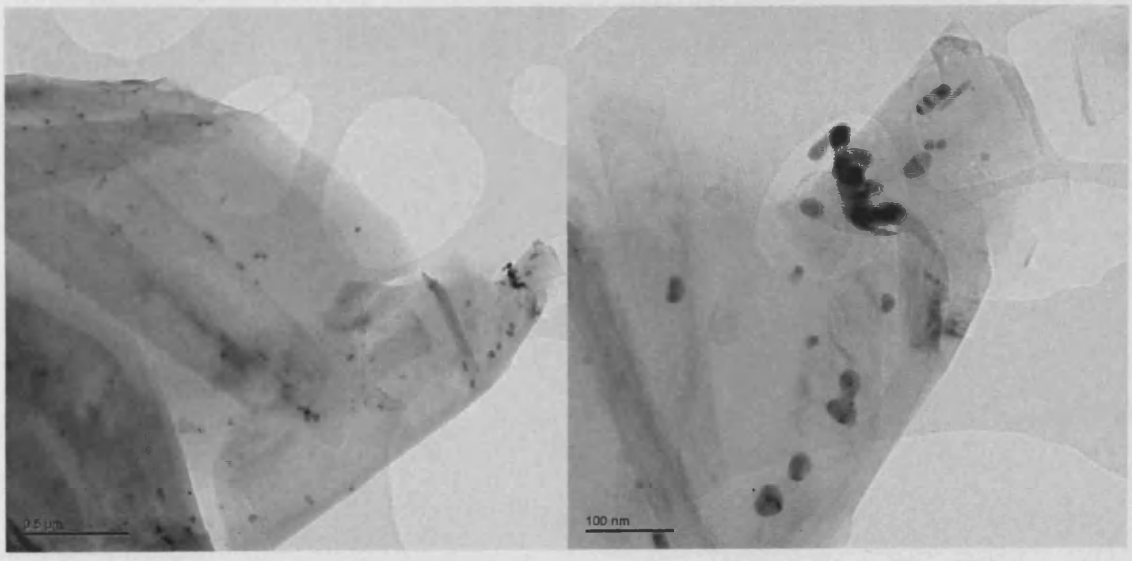

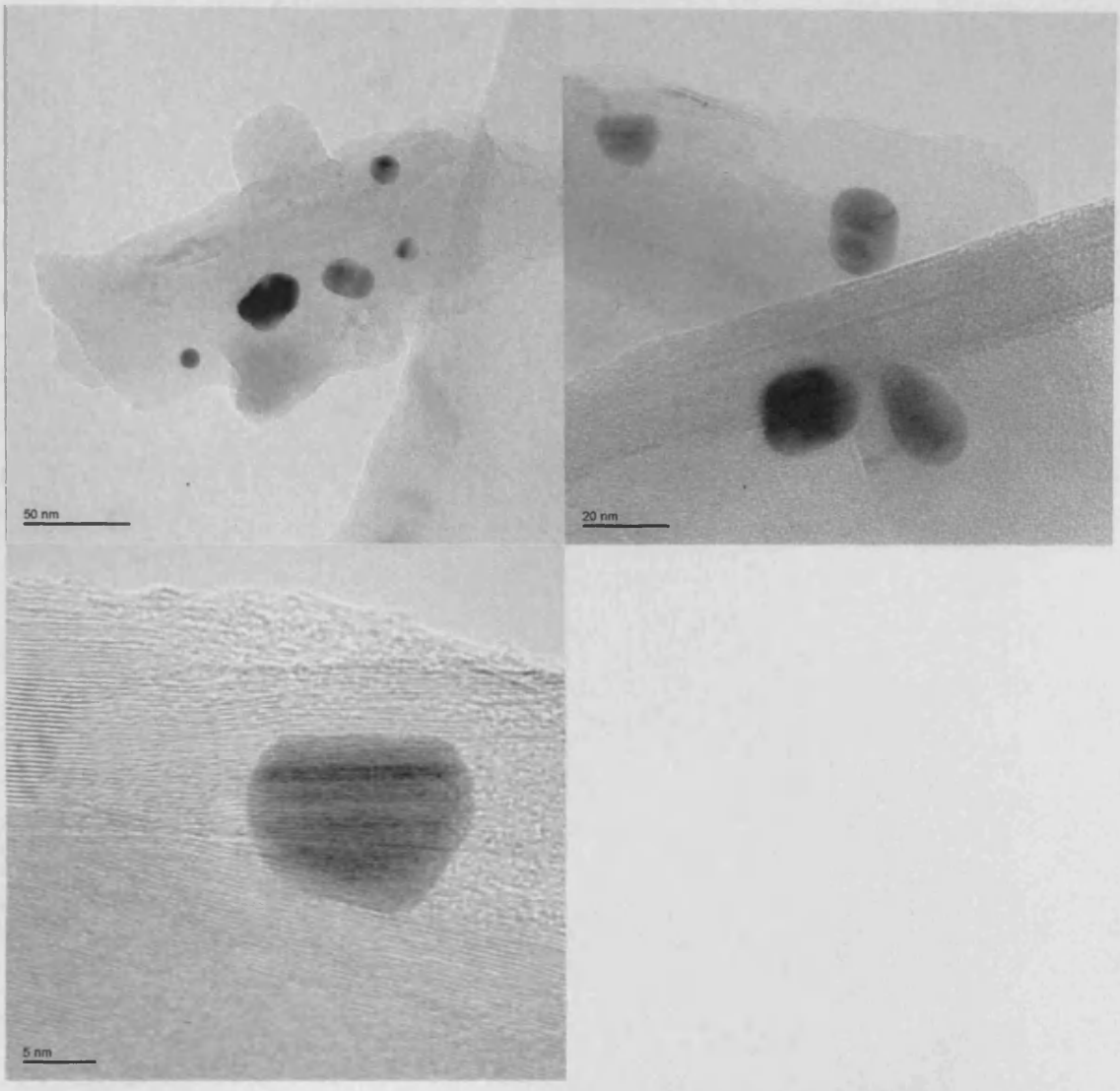

B.10 TEM images of the 30 ml Bi-2% Au/graphite catalyst